TERTIARY MAGMATISM IN NORTHERN SARDINIA

by

Michael John Rutter

A Thesis submitted for the Degree of
Doctor of Philosophy, University of London

Department of Geology,
Imperial College of Science & Technology,
Prince Consort Road,
LONDON SW7.

ABSTRACT

Tertiary magmatism in northern Sardinia is dominated by a temporal transition from subduction-related (29.9-13 Ma) to extensional (5-0.12 Ma) volcanism. Geochemical parameters of lavas, independent of any differentiation processes, have been used to constrain the changing chemical characteristics of magma-producing source mantle beneath Sardinia, during and after active subduction.

Late Oligocene and Miocene (29.9-13 Ma) basalt-andesite-dacite-rhyolite lavas were associated with active subduction, to the east of the Sardinia continental block. They are associated with contemporaneous extension, possibly in a back-arc environment, which facilitated passage of magmas to the surface, and high-T low-P fractionation of an anhydrous gabbroic mineral assemblage. Low K/Cs and high Ba/La ratios in Sardinian subduction-related magmas, may reflect the influx of fluids or melts, derived from the subducted slab, into their mantle source. Low Nb and Ta abundances can be explained by the retention of these elements in some residual phase, stable under the hydrous conditions which may exist in the mantle wedge, although this phase is probably not titaniferous. High LILE-HFSE ratios may represent the addition of LILE-enriched fluids or melts from the subducted oceanic lithosphere to MORB-source mantle, or to magma generation in OIB-source mantle.

Following a gap in magmatic activitiy, volcanism resumed in the Pliocene with the eruption of high-Al basalt, dacite and rhyolite lavas, which require the persistence of subduction-related source mantle beneath Sardinia at least 8 Ma after the cessation of active subduction. Hawaiites and basaltic andesites were erupted contemporaneously during the Plio-Pleistocene, although probably from separate vents or fissures. Basaltic andesites predominate in the lower part of the sequence. The hawaiites are LILE-enriched relative to most OIB, which can be explained by the mixing of OIB magmas with mantle which had been previously metasomatised by LILE-enriched fluids or melts, derived from the subducted slab.

The genesis of siliceous basaltic andesites and high-Mg andesites can be explained by relative shallow melting of hydrous mantle peridotite, possibly within the sub-continental mantle lithosphere. The heat input required for melting may have been supplied by the injection of mafic alkaline magmas derived from the asthenospheric mantle, and later to form hawaiite lava flows and pyroclastic eruptives. However, magma genesis by assimilation of time-integrated low Rb/Sr sialic crust during ascent of oceanic magmas to the surface cannot be excluded.

Mafic alkaline lavas contain abundant inclusions of mantle peridotite. These inclusions are predominantly porphyroclastic-textured spinel lherzolite and harzburgite, which have been depleted, relative to a model pyrolite composition, by about 20% partial fusion and loss of a basaltic melt. Equilibration temperatures, calculated using the two-pyroxene geothermometer, imply that the xenoliths were incorporated into rising mafic alkaline magmas, somewhere near the top of the lithospheric mantle.

ACKNOWLEDGEMENTS

I would like to thank Dr. Bob Thompson for his supervision of this research project. Field work in Sardinia was partly financed by the N.E.R.C. Special thanks are due to Dr. Jack Nolan and Peter Watkins, for their constant help and advice, regarding the analytical work undertaken during the course of this project. Analytical work also benefitted from the efforts of many other people. In particular, Paul Suddaby and Nick Royale, for help with the electron microprobe; Sue Parry and Ian Sinclair for their assistance with neutron activation analysis at Silwood Park, and Dr. C.T. Williams for making available, and helping with, neutron activation counting facilities at the British Museum. Strontium isotopic work was carried out at the University of Oxford, thanks to the co-operation and advice of Dr. S. Moorbath and Dr. P. Taylor. Day to day running of the mass spectrometer depended much on the labours of Roy Goodwin. Thanks are also due to all the technical staff at Imperial College.

Many friends and colleagues have helped (or hindered) the completion of this thesis, and I would like to thank all of them, for their advice and friendship. Lastly, special thanks to my Mum and Dad for constant encouragement, and to Sue Salter for her enthusiastic typing of an unintelligible thesis.

LIST OF CONTENTS

LIST OF FIGURES

LIST OF TABLES

LIST OF PLATES

CHAPTER 1

INTRODUCTION

In this study, attention is focussed on a sequence of Tertiary volcanic rocks which outcrop extensively in Northern Sardinia. These can be divided into two temporally distinct magmatic cycles. The earlier cycle consists of subduction-related lavas and pyroclastics of late Oligocene and Miocene age. Younger, Plio-Pleistocene lavas and cinder cone eruptives comprise a chemically transitional basaltic suite of contrasting alkaline and sub-alkaline composition. Plio-Pleistocene mafic alkaline lavas contain abundant inclusions of presumed upper mantle or deep crustal origin.

1.1 Geographical location of Sardinia

The island of Sardinia lies in the western Mediterranean between the latitudes of 39°N and 41°N, and some 275 km west of the Italian mainland (Figure 1.1). It is bounded to the east by the Tyrrhenian Sea Basin, and to the west by the Alghero-Balearic Basin. The relief is rugged, the land rising from the low-lying marshes of Oristano to the peaks of Gennargentu at over 1800 metres.

1.2 Geological structure of Sardinia

Sardinia, together with Corsica situated to the north, is thought to comprise a small continental microplate within the western Mediterranean Basin (Alvarez, 1972). Along the western part of the island, an important N-S trending graben began to subside by downfaulting of the crystalline basement, during the middle Oligocene (Cocozza and Jacobacci, 1975). This, so-called, Sardinia Trough is bounded to the west and east by Palaeozoic crystalline

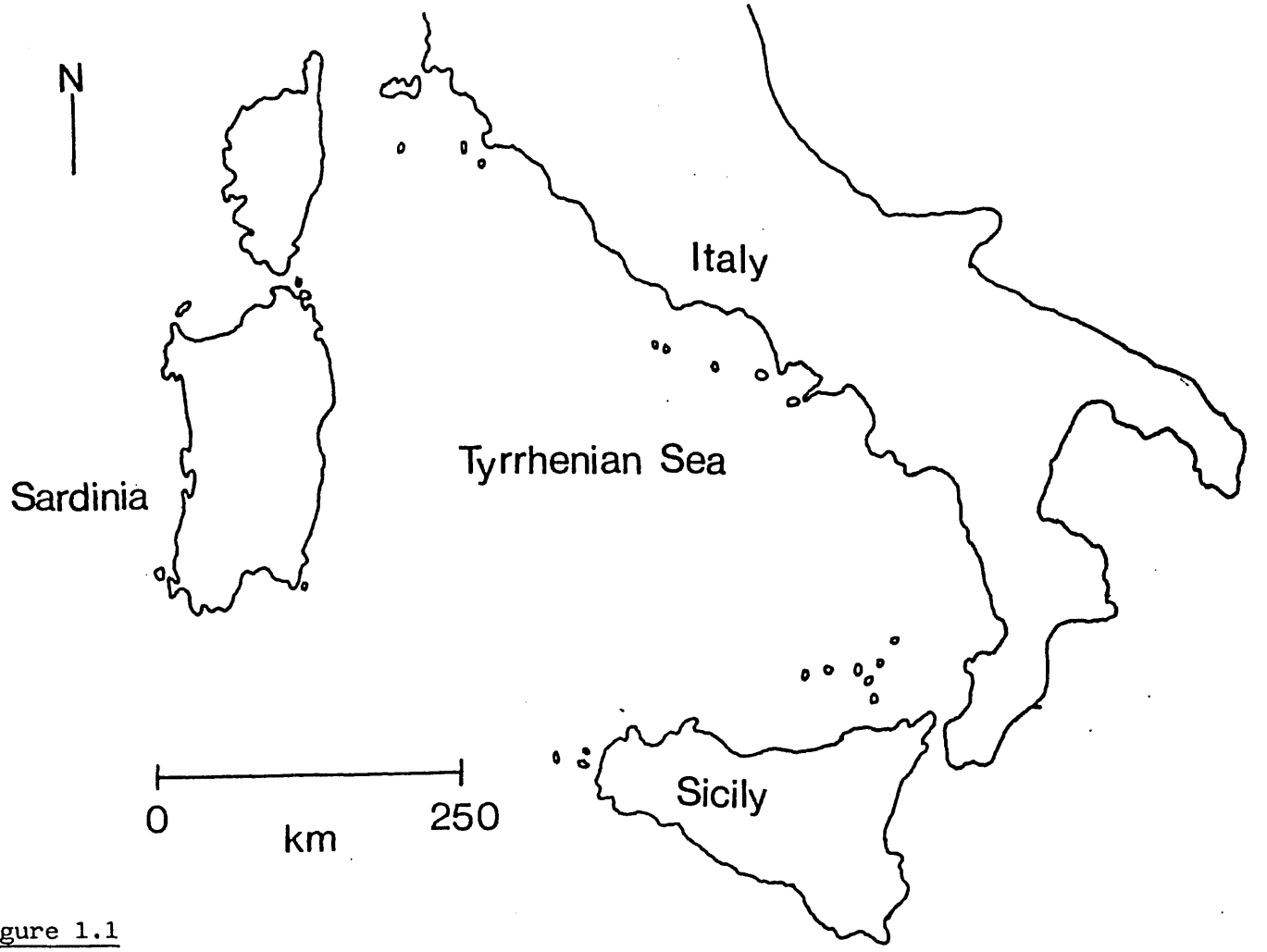

Figure 1.1

Location of Sardinia in the western Mediterranean

massifs (Figure 1.2). The much younger, NW-SE trending, Campidano Graben, subsided during the Plio-Pleistocene in south-central Sardinia (Cocozza and Schafer, 1974). Its subsidence may be related to Plio-Quaternary normal faulting in the Ligurian-Balearic Basin (Mauffret et al, 1973). Seismic data indicates a maximum crustal thickness of 30-35 km beneath the Sardinia-Corsica microplate (Morelli et al, 1967; Morelli, 1970; Hirn and Sapin, 1976).

1.3 Nature of the Sardinian crystalline basement

Lithologically, the Palaeozoic crystalline basement rocks of Sardinia consist predominantly of quartzo-feldspathic gneisses, mica schists and augen gneisses, which are interbanded with ortho-amphibolites and granitic gneisses. These metamorphic rocks are intruded by volumetrically abundant intermediate to acid plutons of Hercynian age. The metamorphic rocks show an increase in grade from greenschist-facies in the SW to amphibolite-facies in the NE (di Simplico et al, 1974). Rare retrogressed eclogite-facies rocks form lenses within amphibolite-facies gneisses (Ghezzo et al, 1982). The metamorphic rocks were intensely deformed during the Hercynian orogeny (Carmignani, 1982), and isotopic dates of 284-319 Ma probably reflect a Hercynian metamorphic event (Ferrara et al, 1978).

1.4 Late Oligocene and Miocene subduction-related volcanism

Calc-alkaline volcanic rocks are exposed in the Logudoro and Bosano districts of northwestern Sardinia (Figure 1.3), and have been the subject of much research interest. They consist of relatively scarce high-Al basalts (Dostal et al, 1976), abundant andesites (Coulon et al, 1973; Dupuy et al, 1979), dacites and rhyolites.

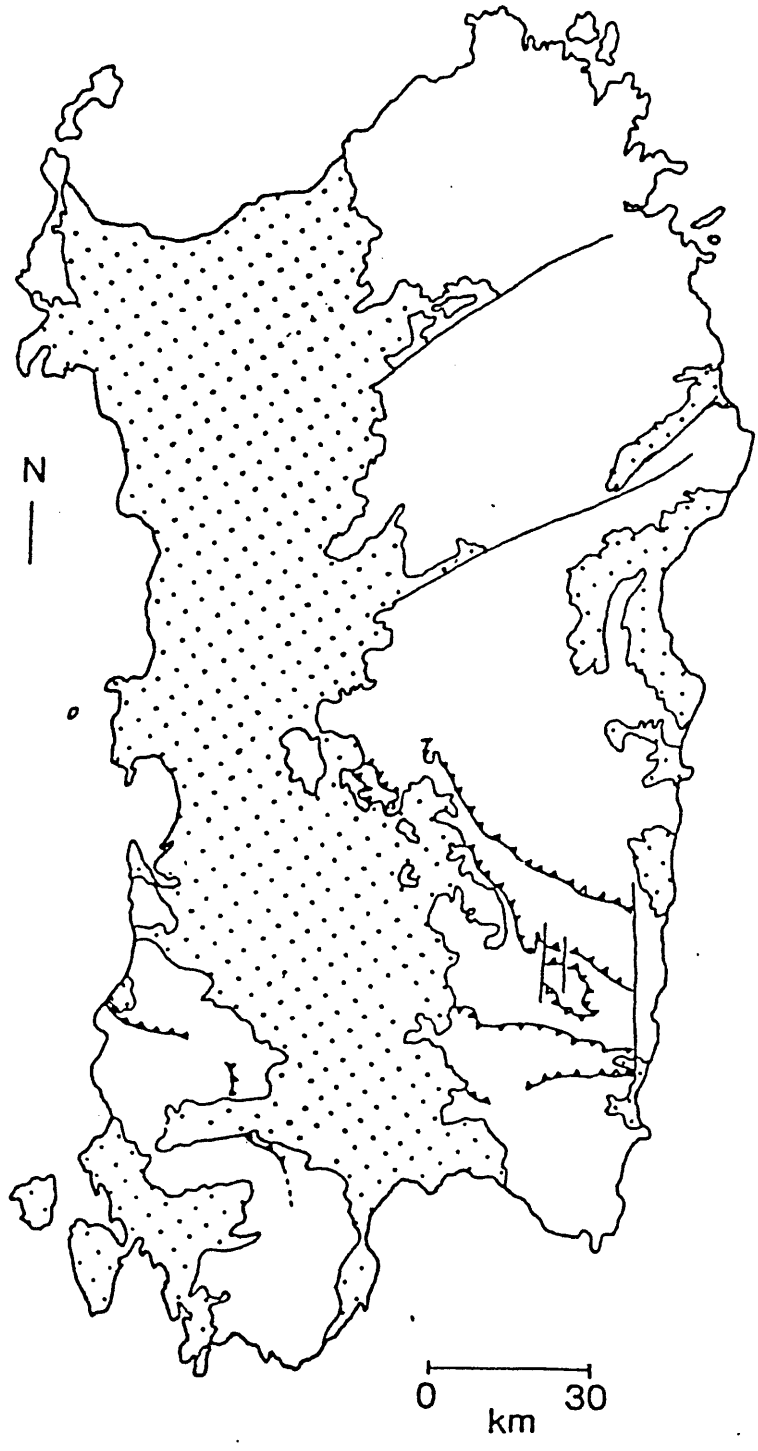

Figure 1.2

Simplified geological map of Sardinia (after Carmignani et al, 1982). Stippled areas represent post-Hercynian volcanics and sediments. Unshaded areas represent Palaeozoic metamorphic and plutonic rocks, with minor Mesozoic sediments. The more important thrusts and faults are also shown

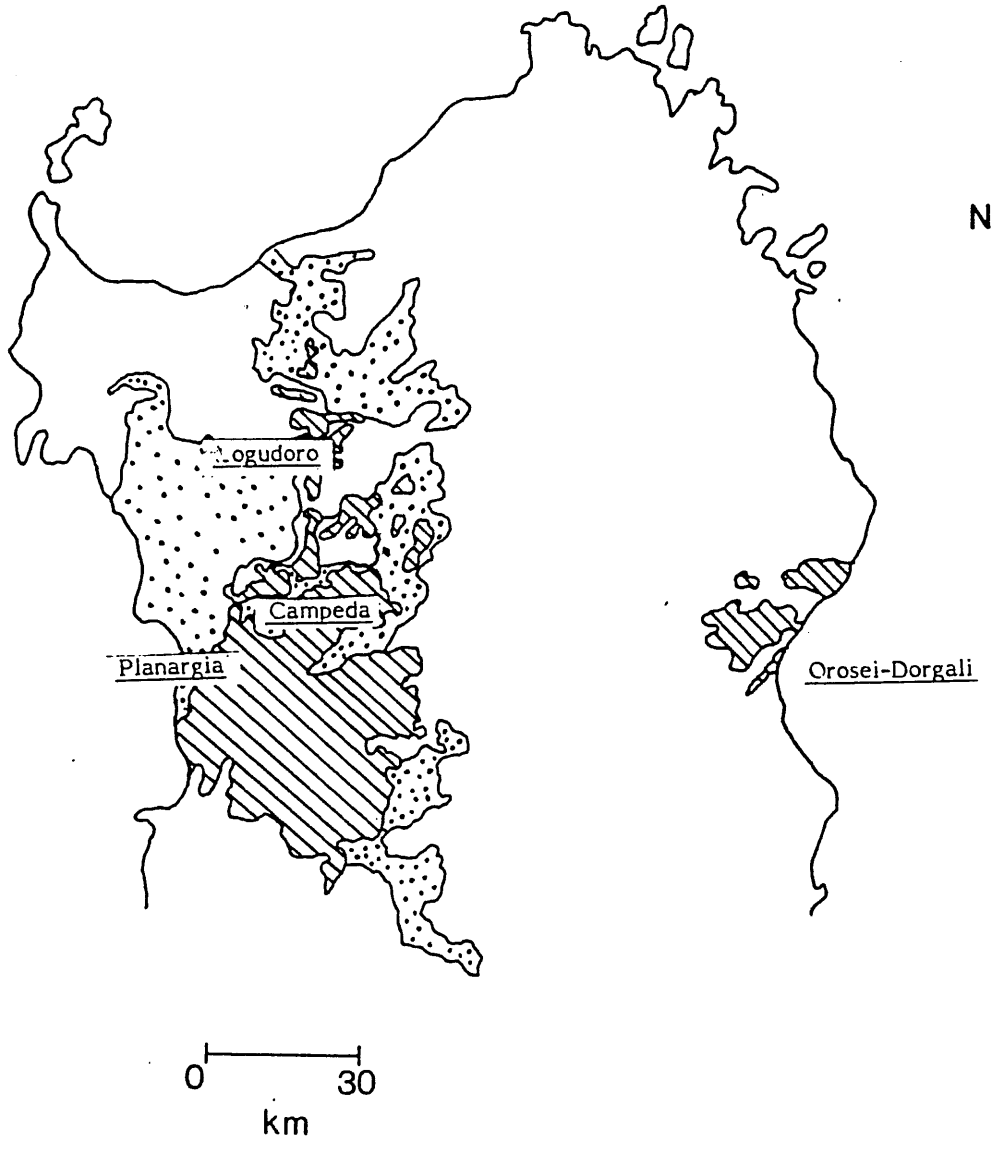

Figure 1.3

Sketch map of Northern Sardinia showing the outcrop of Tertiary volcanic rocks. Ruled diagonal lines = Plio-Pliestocene lavas and pyroclastics; stippled area = Oligo Miocene subduction related volcanics (after Beccaluva et al, 1977).

These lavas are associated with abundant intermediate to acid tuffs and ignimbrite flows (Coulon, 1974). Blocky, andesitic lahars have also been observed underlying younger hawaiite lavas near Pozzomaggoire. The lahars are unsorted, and contain angular blocks, up to several metres across, of predominantly andesitic and dacitic material, in a volcanic matrix of mud-sand grain size. K-Ar age dates obtained on the volcanics suggest that this volcanism was active from about 30 Ma to 13 Ma ago (Coulon et al, 1974; Savelli, 1975; Montigny et al, 1981). Calc-alkaline magmatism is probably related to a subduction zone, which was active to the east of the Sardinian continental block at this time (Boccaletti et al, 1971). Subduction-related lavas and pyroclastics are interbedded with continental and marine sediments, including fault-related breccias, fluviatile sandstones and shallow marine limestones. The sediments record a gradual deepening of the Sardinia Trough, and invasion by the sea, from the middle Oligocene onwards (Cherchi and Montadert, 1982). Subduction-related magmatism in northwestern Sardinia is typical of subduction-related continental margin orogenic volcanism, except that the magmas were erupted solely within a rift-related tectonic setting. It is suggested that subduction-related magmas only reached the surface within the Sardinia Trough, because extension and crustal thinning facilitated passage of magmas to the surface. A back-arc tectonic setting behind an easterly migrating trench-arc system may explain concurrent rifting and subduction-related magmatism (Boccaletti and Guazzone, 1974). Possibly Tertiary calc-alkaline plutons were emplaced within the crust, beneath the Palaeozoic crystalline basement, to the east of the rift.

1.5 Plio-Pleistocene extensional volcanism

The Plio-Pleistocene volcanic cycle consists of basaltic rocks of contrasting chemical composition:-

1. High-Al basalt;
2. Low-K basaltic andesite;
3. Mafic K-rich hawaiite and trachybasalt;
4. Analcite basanite.

Some authors have noted a marked increase in the alkalinity of the erupted products with time during the Plio-Pleistocene, both in Sardinia (Macciotta et al, 1977), and in the Tyrrhenian Sea Basin (Keller, 1981). Much of the Tyrrhenian Sea is underlain by oceanic crust (Hutchinson et al, 1985), which suggests that this transition is unrelated to sialic contamination during ascent of magma through the continental crust.

Volumetrically insignificant post-Miocene high-Al basalt and dacite were erupted at Monte Castanza and Monte Pizzinnu (Coulon, 1974). They herald the onset of Plio-Pleistocene magmatic activity. Rhyolite lavas have been observed at the base of the lava pile near Macomer, and pass upwards into hawaiite and basaltic andesite lavas. Air-fall lithic tuffs are spatially associated with these more silicic lavas. They are localised in outcrop, and consist predominantly of andesitic and dacitic material ($\leqslant$ 10 cm) in a sand-silt grain size volcanic matrix. The tuffs exhibit well-developed fining-upwards and thinning-upwards sequences, presumably reflecting decreasing explosiveness within, and between, successive eruptions. Rare cumulate xenoliths consisting of amphibole, calcic plagioclase and clinopyroxene were collected from a dacite at Monte Pizzinnu. Pliocene high-Al basalts are petrographically and geochemically indistinguisable from mafic lavas of the older, subduction-related volcanic cycle.

The earliest K-Ar date obtained on these volcanic rocks is 4.9-5.1 Ma, from a quartz-normative trachyte (Beccaluva et al, 1977). The available K-Ar dates for the Plio-Pleistocene rocks are summarised in Figure 1.4.

Plio-Pleistocene magmatism is associated with extensional tectonics in the Ligurian-Balearic Basin (Mauffret et al, 1973) and in the Tyrrhenian Sea Basin (Selli and Fabri, 1971). Much of the western Mediterranean was affected by an extensional tectonic regime at this time, following on from the Alpine and Apennine orogenies. The Campidano Graben in south-central Sardinia also began to subside during the Pliocene. Fault-related clastic deposits are interbedded with volcanic rocks at Montiferru (Brotzu et al, 1969), which suggests contemporaneous faulting and volcanic activity. Early flows of evolved alkaline composition at Montiferru, dated at 3.9-2.9 Ma, are cut by dykes of alkali basalt and basaltic andesite, which have been dated at 2.8 Ma (Beccaluva et al, 1977). To the south-east of Montiferru, Monte Arci was contemporaneously volcanically active. Magmatism at Monti Arci was probably related to normal faulting and the ascent of magmas along fissures, rather than to a central volcano. Interbedded rhyolites, dacites, basaltic andesites and alkali basalts have been described from Monte Arci (Cioni et al, 1982).

In this study, sampling of volcanic rocks belonging to this younger Plio-Pleistocene volcanic cycle was confined to two distinct regions of northern Sardinia (Figure 1.3):-

1. Logudoro and Bosano districts of northwestern Sardinia, where Plio-Pleistocene lavas and pyroclastics overlie Tertiary subduction-related volcanic rocks and Miocene sediments;

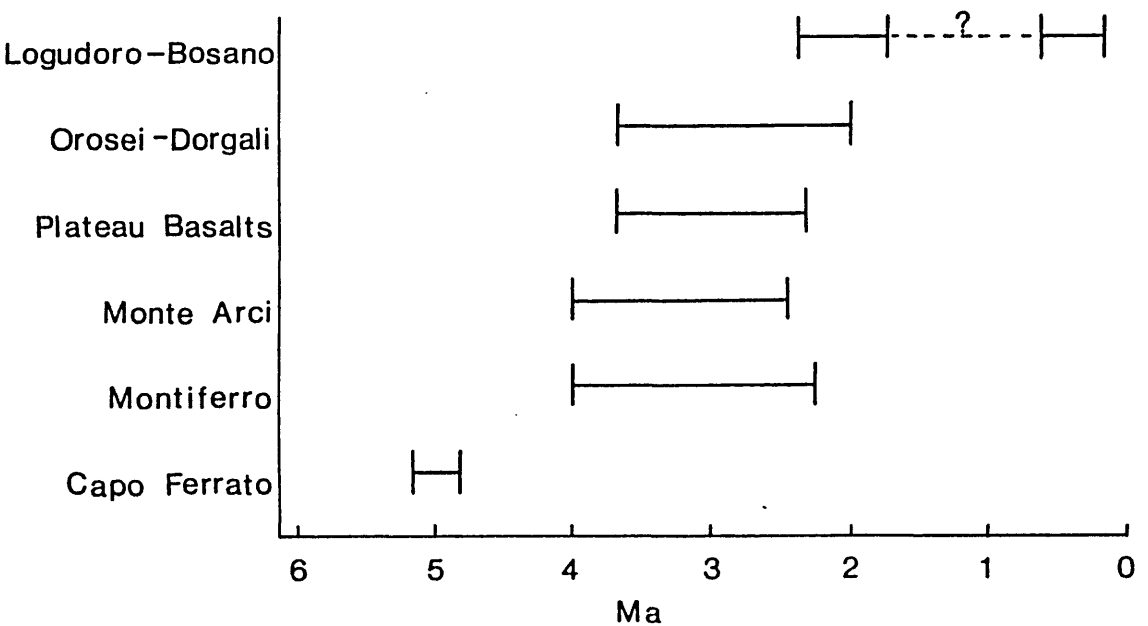

Figure 1.4

K-Ar dates obtained for the Plio-Pleistocene volcanic rocks (after Beccaluva et al, 1977)

2. Orosei-Dorgali region of eastern Sardinia, where Plio-Pleistocene lavas overlie predominantly Palaeozoic crystalline basement rocks.

These two areas encompass the diversity of basic volcanic rocks erupted during the Plio-Pleistocene.

Basaltic andesite lavas were erupted from predominantly N-S, and NE-SW, trending fissures, and built up areally extensive lava fields which were later strongly dissected by erosion. Less abundant hawaiite lavas form the distinct plateau of Monte Santo. Hawaiites and basaltic andesites generally form distinct geographic sub-provinces, and magmas of contrasting geochemical composition were probably erupted from separate vents or fissures. These plateau basalts have been dated at 3.7-2.5 Ma (Beccaluva et al, 1977).

The Orosei-Dorgali volcanic rocks are associated with NE-SW faults, which are related to subsidence in the Gulf of Orosei (Gandolfi, 1974), and have been dated at 3.6-2.0 Ma (Savelli and Pasini, 1973). Compositionally, they range from basaltic andesite to hawaiite. Ultrabasic xenoliths have been described from mafic alkalic rocks close to eruptive vents or fissures (Brotzu et al, 1969). Local pillow lavas imply a sub-aqueous environment of eruption for some of the magmas (Massari and Dieni, 1973).

The lava flows are blocky, sometimes showing a typical aa morphology. At Monte Pelao, near Theisi, successive lava flows ($\lesssim$ 7m thick) built up a small shield volume, with a low slope angle of 3-4^{o}. Small, parasitic vents on the slopes of this volcano are evidence of poorly exposed scoriaceous ejecta, probably the product of small-scale fire fountaining. Morphologically young cinder

cones were built up on the floor of the Sardinia Trough. They are composed of highly vesicular ejecta, and range in height from 30 to 280 metres. They have relatively steep slope angles of about 25^{o}. Cinder cones are the product of Strombolian-type eruptions (Williams, 1983). The scoria is predominantly loose, implying that it was solid before it hit the ground. Volcanic bombs are common. They may be spherical ($\lesssim$ 1m in diameter) or spindle-shaped. Spindle-shaped ejecta reflect either in-flight rotation, or stretching of the lava as it was thrown from the vent (Walker and Croasdale, 1972). Such cinder cones are generally built up in a few days, or possibly several years (Walker, 1973).

The cinder cones are frequently aligned along N-S, or NE-SW, directions where passage of magma to the surface was probably facilitated by pre-existing normal faults. Surficial eruptions in northern Sardinia are confined to areas of thinned continental crust, and magmas rising beneath and through those regions of greater lithospheric thickness may have solidified before they reached the surface.

1.6 Magmatism and tectonics in northern Sardinia

Many authors have noted a general correlation between tectonic settings and particular magma-types (Pearce and Cann, 1973). From the late Oligocene onwards, the Sardinian continental block was involved in complex plate motions which, although only poorly understood, are important to our understanding of the temporal evolution in magmatism observed in Sardinia from 30-0.14 Ma. The geodynamic evolution of the Sardinia-Corsica microplate during this period is briefly discussed below.

There is much evidence for the former proximity of the Sardinia-Corsica continental fragment to southern European coast:-

1. The good geometrical fit between Sardinia-Corsica, and the south coast of Europe (Argand, 1922);
2. The similarity in Palaeozoic geological structures between Sardinia-Corsica and southern Europe across the join when the continents are re-constructed along the 2000m isobath (Westphal et al, 1972);
3. Microfaunal evidence implies the former proximity of Sardinia to N.E. Spain (Cherchi and Schroeder, 1976);
4. The drainage pattern in southern France reversed during the late Oligocene, from north and west, to its present southerly direction.

In addition to Sardinia-Corsica, the Balearic Islands, Calabria and the Kabylie massifs of north Africa may originally have formed part of a continuous Alpine belt (Alvarez et al, 1974). It is envisaged that Sardinia-Corsica drifted away from the southern European landmass by anticlockwise rotation and eastward translation (Auzende et al, 1973; Alvarez et al, 1974). Recent palaeomagnetic and K-Ar dating results have constrained the timing of rotation to between 19 and 20.5 Ma (Montigny et al, 1981). Subduction was probably active to the east of Sardinia during the late Oligocene and Miocene. The eruption of predominantly andesitic volcanics in N.W. Sardinia at this time has been related to back-arc volcanism behind an easterly-migrating arc-trench system (Boccaletti et al, 1971). The Ligurian-Balearic Basin may have opened by sea-floor spreading processes as a marginal ocean basin behind this subduction zone (Boccaletti and Guazzone, 1974). Seismic and magnetic evidence is consistent

with an oceanic crustal structure (Burrus, 1984). The rifting event which led to the opening of the Ligurian-Balearic Basin during the Aquitainian may also be related to subsidence in the Gulf of Valencia and the Sardinia Trough (Auzende et al, 1973). The opening of the Balearic Sea ended with the collision of Sardinia-Corsica with the Adria plate, although coupled anti-clockwise rotation of about 30^{o} may have continued after collision (Reutter et al, 1978). During collision, the western edge of the Adria plate was underthrust by the Sardinia-Corsica continental fragment (Giese et al, 1978). The Tyrrhenian Sea Basin opened from 12-5 Ma (Hutchinson et al, 1985). Basaltic rocks with mid-ocean ridge basalt (MORB) affinities have been drilled from the floor of the Tyrrhenian Sea (Barberi et al, 1978), and heat flow studies are also consistent with opening by sea-floor spreading. A mechanism of opening by sea-floor spreading behind a migrating volcanic arc has been suggested (Hutchinson et al, 1985). The Aeolian Islands are located above a WNW-dipping subduction zone (Beccaluva et al, 1981), and calc-alkaline volcanism is associated with subduction of the Mesozoic crust of the Ionian Sea beneath Calabria. A schematic model for the geodynamic evolution of the western Mediterranean since the late Oligocene is shown in Figure 1.5. Sardinian Plio-Pleistocene magmatism is associated with the post-collisional regional extension which extended over much of the western Mediterranean following the Apennine and Alpine orogenies.

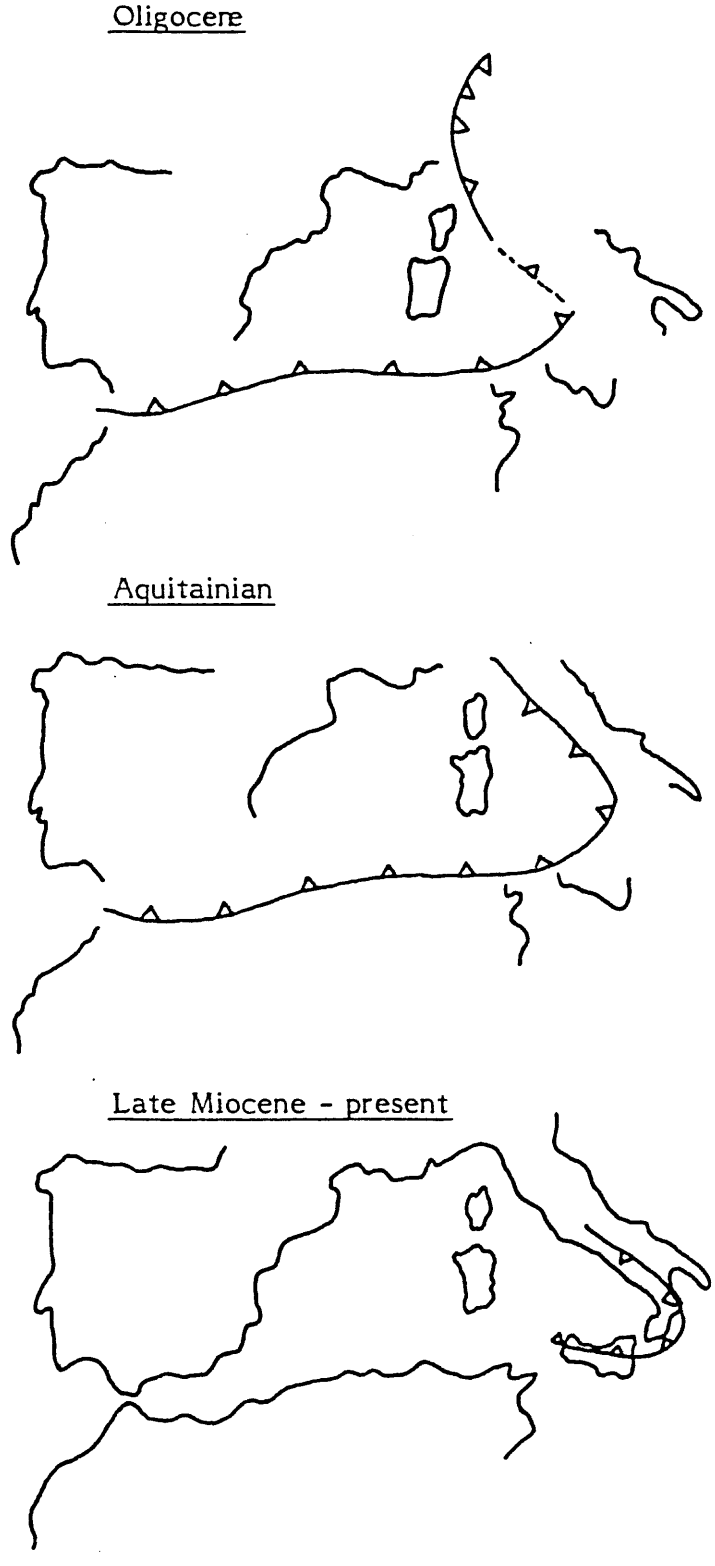

Figure 1.5

Possible plate tectonic evolution of the Western Mediterranean basin (Hutchinson et al, 1985). Not to scale. See text for details.

CHAPTER 2

PETROGRAPHY AND MINERAL CHEMISTRY OF SARDINIAN TERTIARY VOLCANIC ROCKS

Tertiary mafic lavas, dykes and pyroclastics fall into four main groups, which are distinguished largely on the basis of geochemical criteria (see Chapters 3 and 4), as well as by a number of petrological features. These groups include:- 1. high-Al basalt; 2. basaltic andesite and high-Mg andesite; 3. alkali basalt and hawaiite, and 4. analcite basanite. The petrography and mineral chemistry of each of these, plus more silicic subduction-related lavas, whose genesis is modelled in terms of crystal fractionation in Chapter 3, are briefly discussed below. Mineral compositions, obtained by electron probe microanalysis, are given in Appendix C. Typical probe analyses for the major rock-forming minerals in each group are given for easy comparison, in Table 2.1

2.1 High-Al basalts

These are strongly porphyritic with phenocrysts of plagioclase, olivine, clinopyroxene and titanomagnetite set in a holocrystalline groundmass of the same mineral assemblage. Plagioclase phenocryst compositions are shown in Figure 2.1. Euhedral to subhedral phenocrysts (0.5-2.0 mm) vary from strongly calcic (An86) in the least evolved lavas, to more Na-rich (An41) in the less magnesian samples. Very calcic plagioclase phenocrysts (An85-An95; Foden, 1983) are commonly observed in mafic island arc volcanic rocks. The range in phenocryst compositions shown by the high-Al basalts suggests

TABLE 2.1

"TYPICAL" PHENOCRYST COMPOSITIONS IN TERTIARY VOLCANIC ROCKS

(a) Plagioclase

	Basaltic andesite (K64)	Hawaiite (K104)	High-Al basalt (MR20)
SiO_2	54.30	55.08	46.16
Al_2O_3	27.83	27.59	33.84
FeO	0.63	0.75	0.34
CaO	11.16	10.18	17.94
Na_2O	4.93	5.33	1.60
K_2O	0.18	0.66	0.03
TOTAL	99.03	99.59	99.91

(b) Olivine

	Basaltic andesite (K83)	Hawaiite (N124)	High-Al basalt (MR20)
MgO	41.41	40.15	30.78
SiO_2	38.67	38.27	36.14
MnO	0.12	0.29	0.79
FeO	19.18	21.29	30.98
NiO	0.25	0.08	-
TOTAL	99.63	100.08	98.69

(c) Clinopyroxene

	Basaltic andesite (K85)	Hawaiite (K58)	High-Al basalt (MR20)	Basanite (MR23)
SiO_2	49.97	48.81	47.51	50.86
Al_2O_3	2.47	3.12	5.71	2.62
TiO_2	1.89	2.85	1.32	0.36
FeO	9.63	11.70	8.45	11.48
MnO	0.28	0.17	0.14	0.48
MgO	14.17	12.71	12.93	12.83
CaO	19.86	20.55	22.77	19.79
Na_2O	0.79	0.63	0.99	0.27
Cr_2O_3	-	0.11	-	0.06
TOTAL	99.06	100.65	99.82	98.75

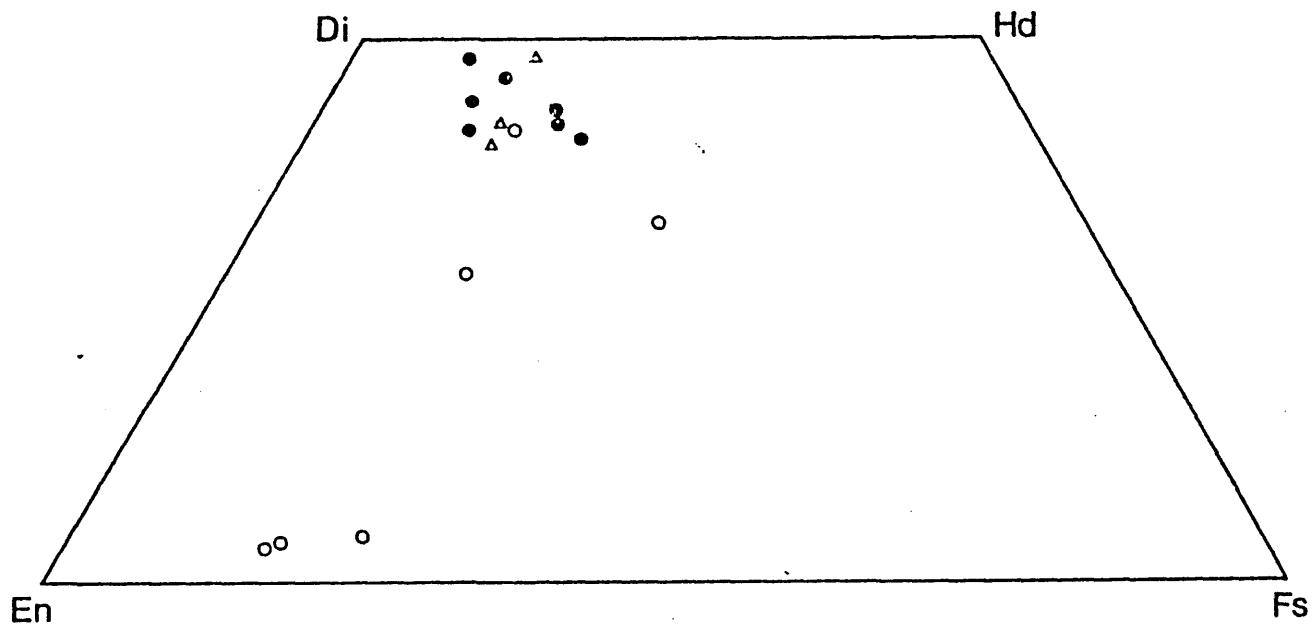

Figure 2.1

Pyroxene compositions projected onto Ca-Mg-Fe for all analysed tertiary mafic rocks in northern Sardinia. Open circles represent sub-alkaline rocks; filled circles represent alkaline rocks; and open triangles represent subduction-related lavas

Figure 2.2

Feldspars plotted in terms of end-member compositions
Symbols as in Figure 2.1

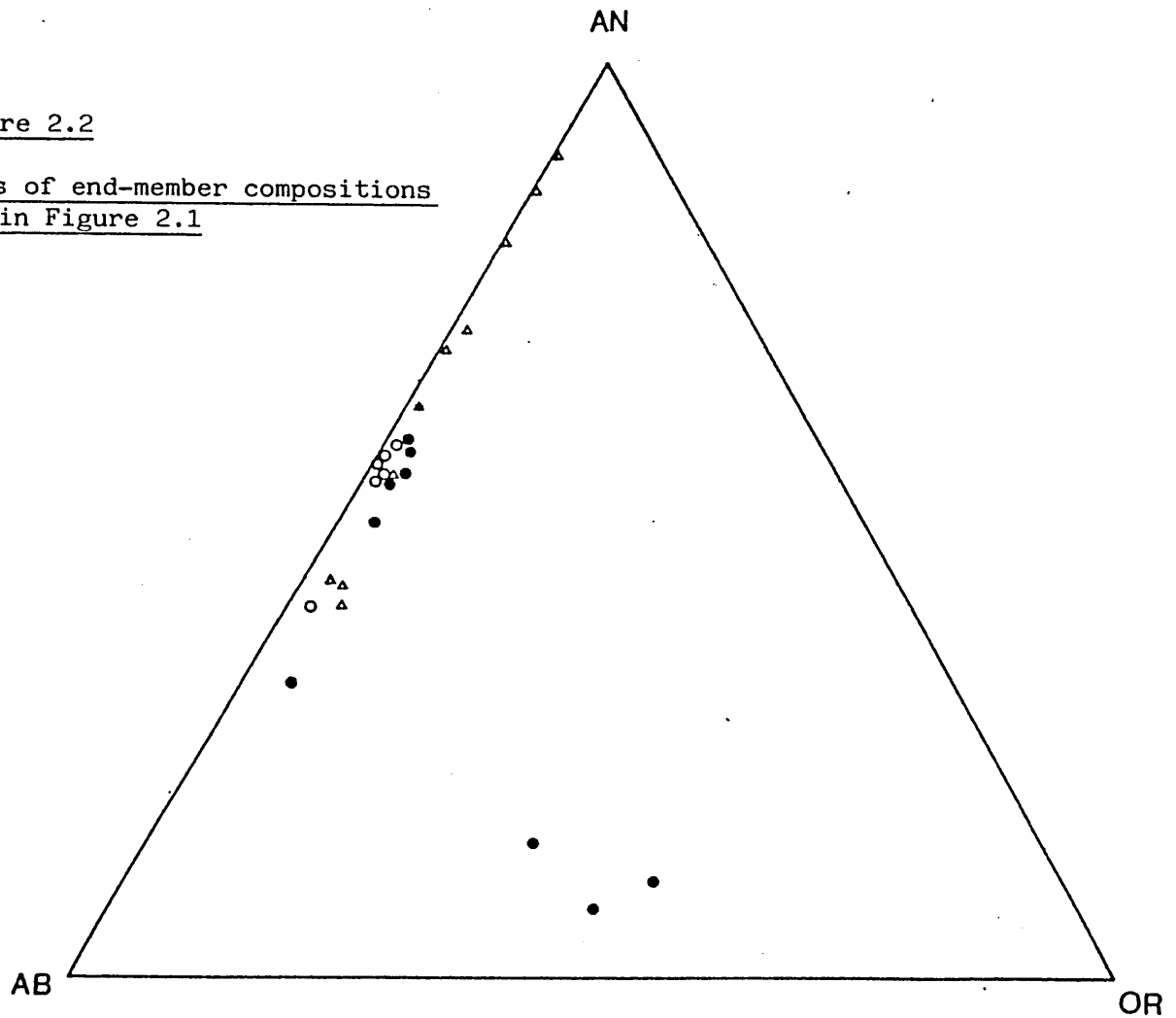

that crystal fractionation processes were important in their petrogenesis. The phenocrysts are, in general, normally-zoned towards a more sodic margin, and groundmass plagioclase is more sodic than phenocryst core compositions.
Subhedral olivine phenocrysts ($\lesssim$ 1 mm) are often variably altered to yellow-brown iddingsite, and when fresh are relatively Fe-rich, ranging from Fo_{63}-Fo_{69}. Pyroxene phenocryst compositions are shown plotted in terms of their Fe, Mg and Ca end-members in Figure 2.2. They are calcic augites, rich in Al(Al_2O_3 = 2.2-5.9 wt. %), with moderately low Ti(TiO_2 < 1.4 wt. %) and Na(Na_2O < 0.99 wt. %) contents, and are very similar to augitic pyroxenes described from calc-alkaline basalts in the Sunda arc (Foden, 1983).
Glomeroporphyritic aggregates of plagioclase, with subordinate augite and olivine are ubiquitous. Anhedral titanomagnetite phenocrysts (< 0.5 mm) contain 11 wt. % TiO_2 in the most magnesian basalt, which is within the range reported for high-Al basalts from the Sunda arc (Foden, 1983).

2.2 Basaltic andesites and high-Mg andesites

Basaltic andesites, with subordinate high-Mg andesites, were erupted during the Plio-Pleistocene in northern Sardinia. Andesitic rocks are characterised by a higher proportion of orthopyroxene relative to clinopyroxene.
The basaltic andesites are holocrystalline, generally fresh and fine grained. They frequently show a well-developed ophitic texture, with anhedral pyroxenes enclosing olivine and plagioclase. The plagioclase is generally labradorite, although andesine has been observed in some medium-K andesites

(Figure 2.1). Plagioclase occurs as bladed phenocrysts ($\lesssim$ 0.5 mm), and as sub-parallel oriented laths ($<$ 0.2 mm) which imparts a felted texture to much of the groundmass. Subhedral olivine phenocrysts ($\lesssim$ 0.5 mm) are variably altered to brown iddingsite, particularly along cracks and around their margins. They are more Mg-rich (Fo_{82}-FO_{78}) than olivines from both the high-Al basalts, and most of the hawaiites, which is consistent with their generally higher whole-rock MgO/MgO + FeOT ratios. The augitic pyroxenes are generally poorer in Ca (Figure 2.2) than clinopyroxenes from either the high-Al basalts or hawaiites. They sometimes show pervasive alteration to an ochre-coloured mineral. Subhedral, sometimes elongate, orthopyroxene phenocrysts ($\lesssim$ 1 mm) are enstatites (Figure 2.2) with an end-member composition of En_{79} Fs_{17} Wo_4. No whole-rock geochemical difference has been observed between enstatite-bearing and enstatite-free rocks.

2.3 Hawaiites and alkali basalts

These are generally fresh, fine grained and sparsely porphyritic, with phenocrysts of olivine, clinopyroxene and plagioclase, with or without biotite. Subhedral olivine ($<$ 0.5 mm), the dominant phenocryst phase, is usually mantled by a yellow-brown iddingsitic alteration product. The olivine shows a wide range in composition (Fo_{81}-Fo_{63}), which suggests that crystal fractionation may have played an important role in petrogenesis.

Pyroxene compositions are shown in Figure 2.2. They show a large range in FeO/MgO ratios, from 0.22 to 0.61, are aluminous (Al_2O_3 = 3.0-3.9 wt. %) and Ti-rich (TiO_2 = 0.9-3.1 wt. %). These subhedral augites become more Fe-rich with increasing differentiation, and range from $En_{44}\ Fs_{11}\ Wo_{45}$ in the most Mg-rich samples, to $En_{37}\ Fs_{22}\ Wo_{41}$ in more evolved rocks.

Euhedral plagioclase forms laths ($<$ 0.7 mm) and ranges from An_{59}-An_{32} (Figure 2.1). They show much more extensive ternary solid solution than feldspars from either the basaltic andesites or high-Al basalts (Figure 2.1), with a slightly greater proportion of the orthoclase component reflecting the higher whole-rock K content of the mafic alkaline rocks. High Or contents may also reflect higher eruptive temperatures for the hawaiites, because of the narrowing of the feldspar-plagioclase solvus curve at high temperatures (Carmichael et al, 1974).

Euhedral, pink and pleochroic biotite phenocrysts occur in some of the lavas. They contain a large amount of the Mg end-member, and are more properly termed phlogopites, ranging from $Ann_{15}\ Phlg_{85}$ to $Ann_{21}\ Phlg_{79}$.

The holocrystalline groundmass consists of the same mineral assemblage as the phenocrysts, together with alkali feldspar, and titanomagnetite octahedra. The opaque Fe-Ti oxides are too small for microprobe analysis. Alkali feldspar compositions are shown in Figure 2.1. Granular olivine and clinopyroxene, with abundant plagioclase microlites, make up the remainder of the groundmass. Quartz xenocrysts

have been observed in some of the lavas, as have glass-rich inclusions which may reflect silicic crustal melts (see Chapter 6).

2.4 Analcite basanites

These are characterised by the presence of pervasive groundmass analcite. Experimental work has shown that analcite cannot coexist with a silicate melt at temperatures above 650°C (Roux and Hamilton, 1976), which suggests that analcite forms by secondary alteration of some other primary magmatic phase. The most likely precursors are nepheline or leucite, neither of which has been observed as relics in any of the samples. In addition to groundmass analcite (and plagioclase in some of the samples), these rocks contain phenocrysts of clinopyroxene and olivine, with or without biotite. Subhedral augite ($\leq$ 0.3 mm) is often zoned from a colourless core to a pink, more Ti-rich, rim. Core compositions are relatively Fe-rich (En_{38} Fs_{20} Wo_{42}) which implies that the whole-rock major element chemistry may not represent the melt composition. The basanites contain abundant xenocrysts of Mg-rich olivine which will especially affect the whole-rock concentrations of Si, Mg and Ni.

2.5 Oligo-Miocene subduction-related silicic lavas

Although attention in this thesis is focussed on the comparative geochemistry of Tertiary mafic lavas, geochemical modelling of fractional crystallisation within the subduction-related rock suite (Chapter 3) requires a brief discussion of the important petrographic features of the more silicic lavas.

Andesites are the most abundant lava type erupted in northern Sardinia during the late Oligocene and Miocene. They are porphyritic, with phenocrysts of strongly zoned plagioclase and clinopyroxene, together with orthopyroxene and titanomagnetite (Dostal et al, 1982). Olivine only occurs in the more basic andesites, and is replaced as the dominant ferromagnesian phase by orthopyroxene.

Dacitic and rhyolitic rocks are porphyritic, with euhedral to subhedral phenocrysts of zoned plagioclase (An_{60}-An_{40}), augite and Fe-rich biotite (Ann_{60} $Phlg_{40}$). The groundmass consists of sub-parallel oriented plagioclase microlites, with minor augite and orthopyroxene, and titanomagnetite. Small rod-like (< 0.5 mm) apatites have also been observed. Glomeroporphyritic clots of plagioclase phenocrysts are relatively common. The biotites show a dark outer rim, which is probably related to exsolution of volatiles due to pressure release on eruption.

CHAPTER 3

MAJOR AND TRACE ELEMENT VARIATION WITHIN THE SUBDUCTION-RELATED ROCK SUITE

During the late Oligocene and Miocene the island of Sardinia formed a volcanic province with subduction of oceanic crust being active to the east of the Sardinia-Corsica continental block (Boccaletti and Guazzone, 1974). There are extensive exposures of calc-alkaline volcanic rocks in the Logudoro and Bosano districts of northwestern Sardinia (Coulon et al, 1974), which imply almost continuous subduction beneath Sardinia from 30-13 Ma, although magmatic activity may not always have been associated with active subduction, and vice versa.

A range of major and trace elements have been analysed for 18 lava samples which form a compositional range from basalt ($<$ 52 wt. % SiO_2) through to rhyolite ($>$ 70 wt. % SiO_2). Most of the lavas are of Oligo-Miocene age, although post-Miocene high-Al basalt (Monte Castanza), dacite (Monte Pizzinnu) and rhyolite (Macomer) lavas, which are geochemically similar to the older subduction-related volcanics, have also been included.

The relative ages and distribution of the rocks show clearly that the lavas are either too old or too young, or located too far away, to be derived from the same magma chamber. Nonetheless, their geochemical variation is consistent with their derivation from similar parent magmas. They have been divided into basalts ($<$ 52 wt. % SiO_2), andesites (56-63 wt. % SiO_2),

dacites (63-70 wt. % SiO_2) and rhyolites (> 70 wt. % SiO_2), and all the basaltic rocks are medium-K basalts (Figure 3.1; after Peccerillo and Taylor, 1976). Low Ti (TiO_2 < 1.5 wt. %) and high Al(Al_2O_3 > 18 wt. %) contents are characteristic of high-Al basalts (Carmichael et al, 1974), which are typical of many subduction-related volcanic rock associations (Mann 1983; Foden, 1983).

The data set does not accurately represent the exposure of the suite. Ignimbrites are four times more abundant at the surface than the lavas, and andesitic lavas are the predominant lava-type (Coulon et al, 1974). However, the geochemistry of mafic rocks more closely reflects the chemical composition of their mantle source region; chemical features relating to their source are dealt with in Chapter 5, and only within-suite chemical variations are described here.

The least evolved Sardinian high-Al basalts are unlikely to represent primary mantle-derived melts, unmodified by crystal fractionation processes. Low Ni (Ni $\leq$ 31 ppm) and Cr (Cr $\leq$ 33 ppm) contents, and high FeOT (total Fe as FeO)/MgO ratios of > 1.8 would not have been in equilibrium with mantle olivine of > Fo_{88}. The initial trends of rapidly decreasing Ni with decreasing MgO suggests that olivine may have been a significant fractionating phase. Cr-rich spinel, occurring as inclusions within Mg-rich olivines in the East Sunda arc (Foden, 1983), may have accompanied olivine as an early fractionating phase, and can explain low Cr abundances in Sardinian mafic lavas. Experimental constraints suggest that high-Al basalt is unlikely to be a primary mantle melt,

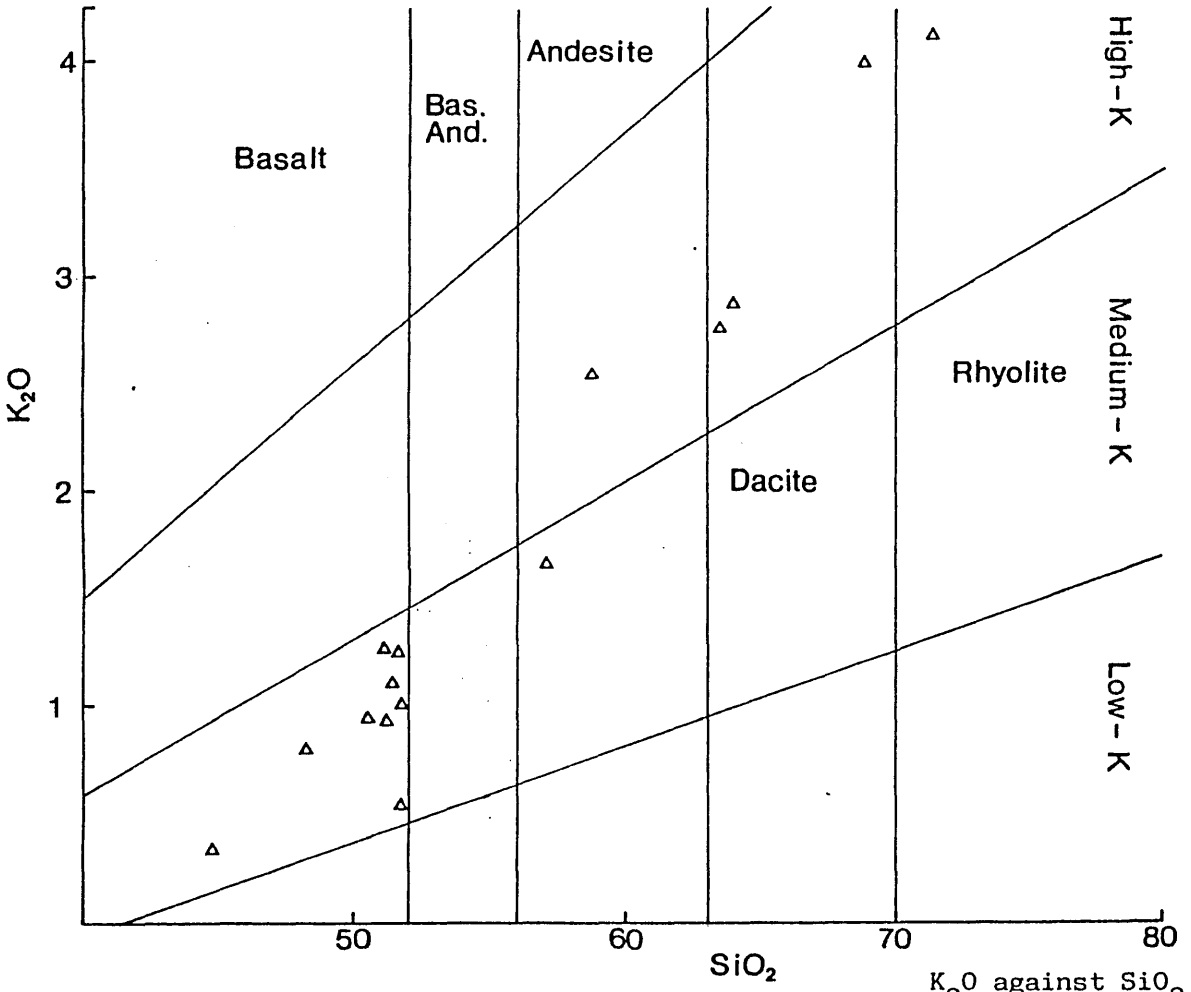

Figure 3.1

K_2O against SiO_2 in Sardinian subduction-related volcanic rocks. The fields for low-K, medium-K and high-K samples are from Peccerillo and Taylor (1976)
Values in weight % oxide

and has probably differentiated from a more picritic parent (Wyllie, 1984).

FeOT/MgO is shown plotted against SiO_2 in Figure 3.2. All the lavas lie to the right of the discriminant line which separates magmas showing broadly tholeiitic (right) and calc-alkaline (left) trends (Miyashiro, 1974). Some of the more silicic lavas show strong Fe-enrichment, which has been attributed in some Aleutian arc lavas to an absence of amphibole fractionation (Kay and Kay, 1982). Sardinian Oligo-Miocene subduction-related lavas contain phenocrysts of plagioclase, olivine, pyroxene and titanomagnetite, with biotite in the dacites. No amphibole has been observed. In contrast, post-Miocene dacites show only moderate Fe-enrichment, consistent with the removal of amphibole, which has been observed as a phenocryst phase in these lavas.

The observed major and trace element variation in all analysed Sardinian subduction-related lavas is discussed below in terms of plausible crystal/melt fractionation processes.

3.1 K_2O-SiO_2 trend

The variation of K_2O with SiO_2 is shown in Figure 3.1. K_2O abundances in the basalts are variable, ranging from 0.35-1.28 wt. %. The strong increase of K_2O with increasing SiO_2 implies that amphibole was not a significant fractionating phase. Kay and Kay (1982) have related such a trend to high-temperature, low-pressure fractionation of an anhydrous gabbroic mineral assemblage, in which K remains

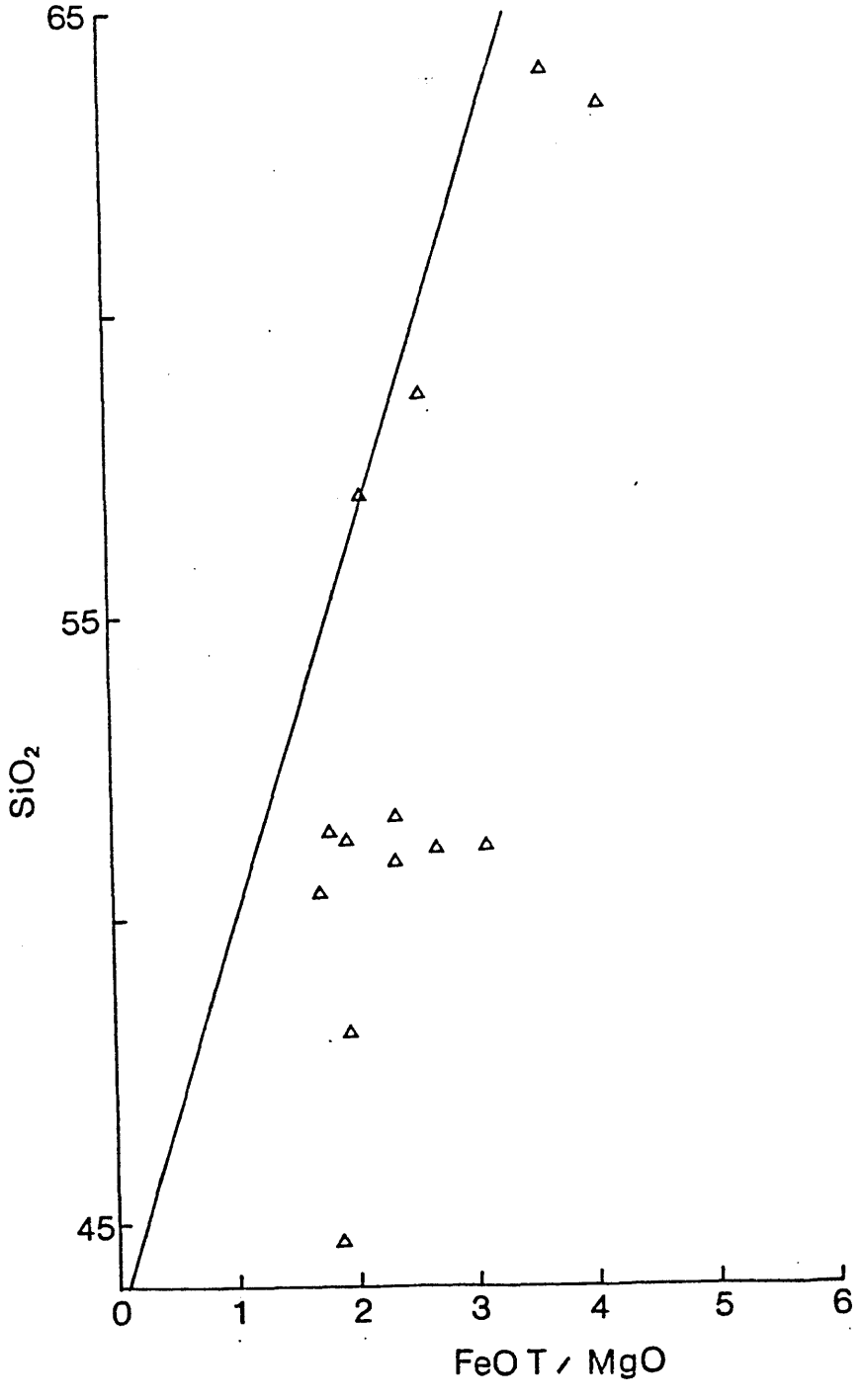

Figure 3.2

FeOT (total Fe as FeO)/MgO ratio against SiO_2 in Sardinian subduction-related volcanic rocks. The tholeiitic-calc-alkaline discriminant line is from Miyashiro (1974)

an incompatible element. The major element variation within the Sardinian mafic rock suite can be modelled in terms of the removal of variable amounts of plagioclase, olivine, clinopyroxene and titanomagnetite, all of which have been observed as phenocryst phases.

3.2 Major element variation

All major element concentrations have been plotted against MgO in a series of two-element variation diagrams in Figure 3.3. The negative correlations of Na, K and Si with decreasing MgO implies that fractional crystallisation is probably the dominant process in producing the observed major element variation. Inflection points in some of the major element trends mark the end or beginning of fractionating of a particular phase. Decreasing Ti, Fe, Ca and Mn with decreasing MgO is consistent with a fractionating assemblage consisting of olivine, clinopyroxene, plagioclase and titanomagnetite for the mafic lavas. Variably high Al_2O_3 contents in the basalts suggest that plagioclase was not a dominant fractionating phase. However, Al decreases rapidly with decreasing MgO in rocks with < 4 wt. % MgO, which suggests that plagioclase is a significant fractionating phase in andesites and dacites. SiO_2 shows considerable scatter, but it generally increases with decreasing MgO which is consistent with gabbro removal (and almost every other fractionating mechanism). Si and K compositional variability may be at least partly due to interaction with, and assimilation of, sialic material in

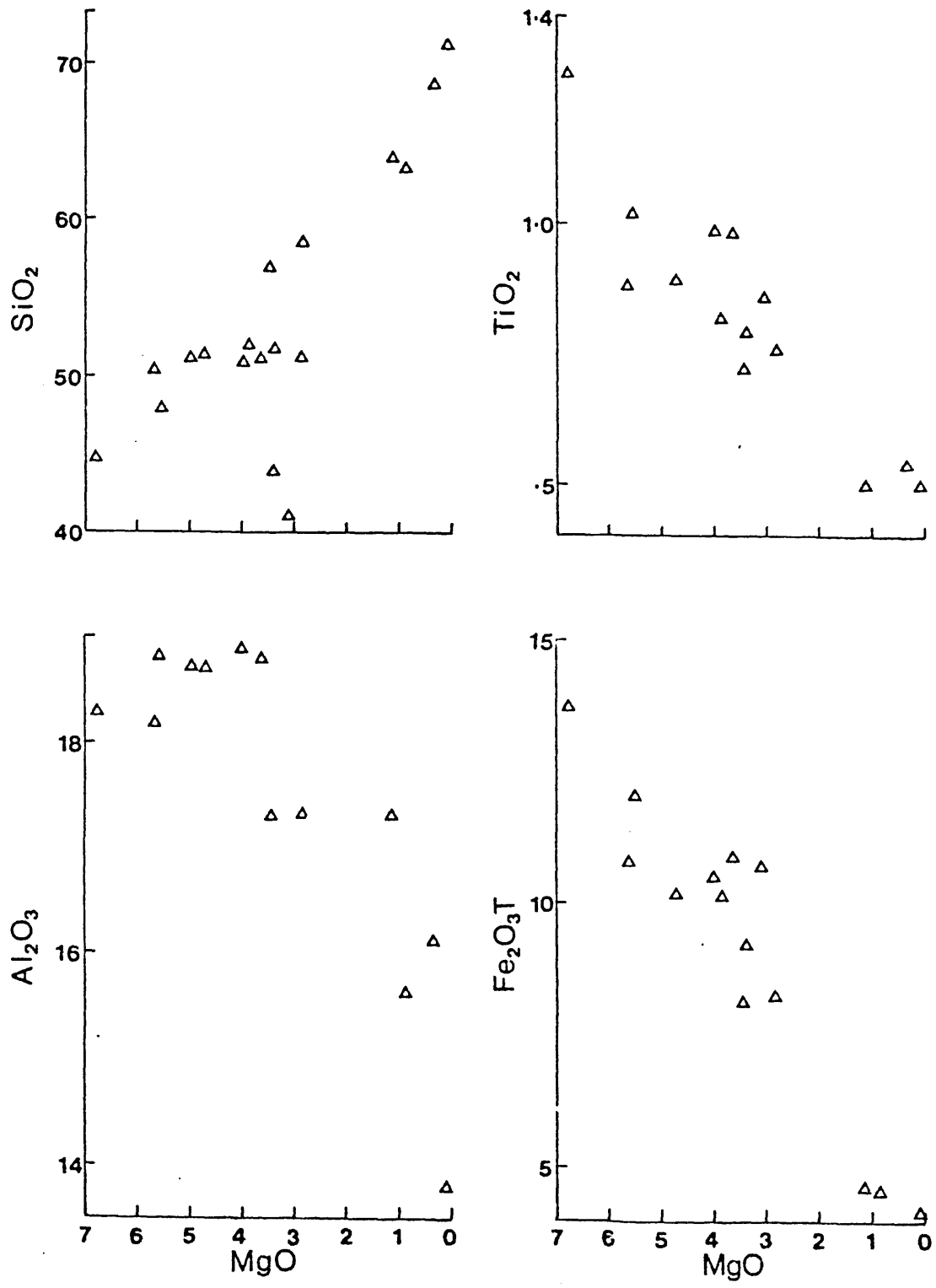

Figure 3.3

Major element chemical variation in Sardinian subduction-related lavas plotted against MgO

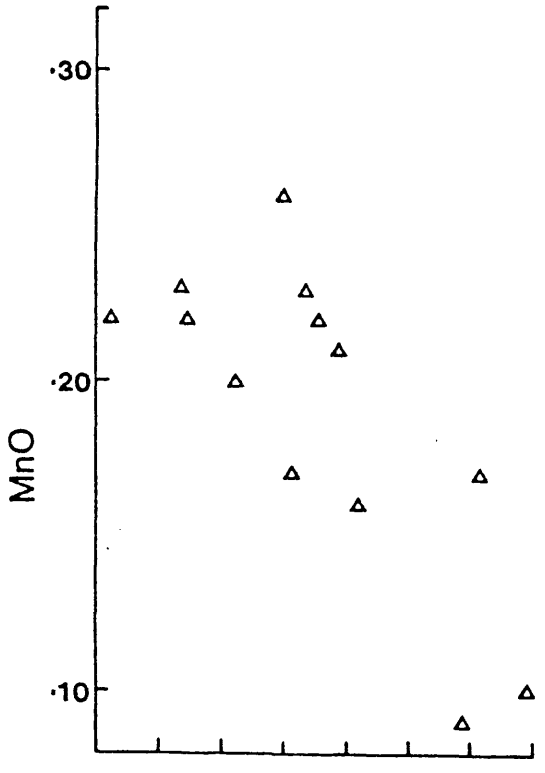
·30
·20
·10
MnO

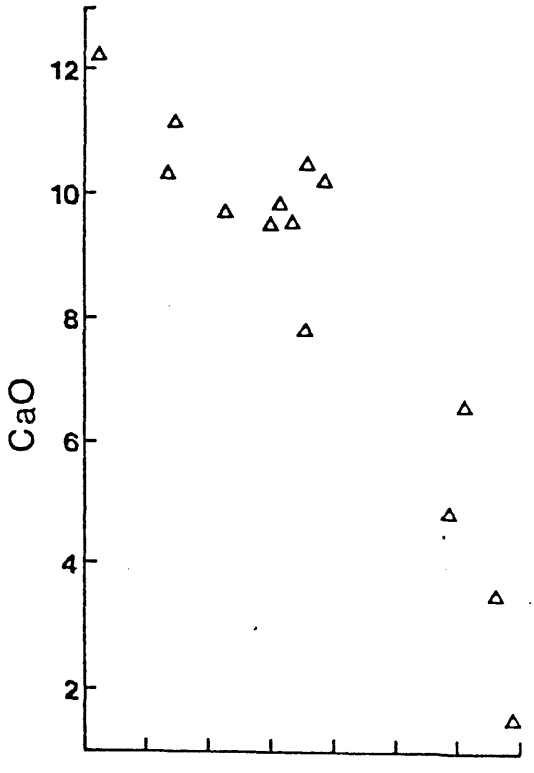
12
10
8
6
4
2
CaO

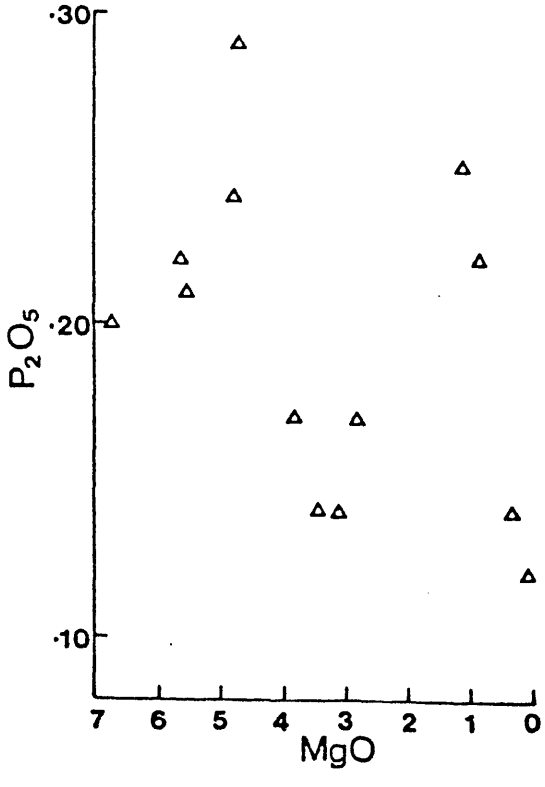
·30
·20
·10
P2O5
7 6 5 4 3 2 1 0
MgO

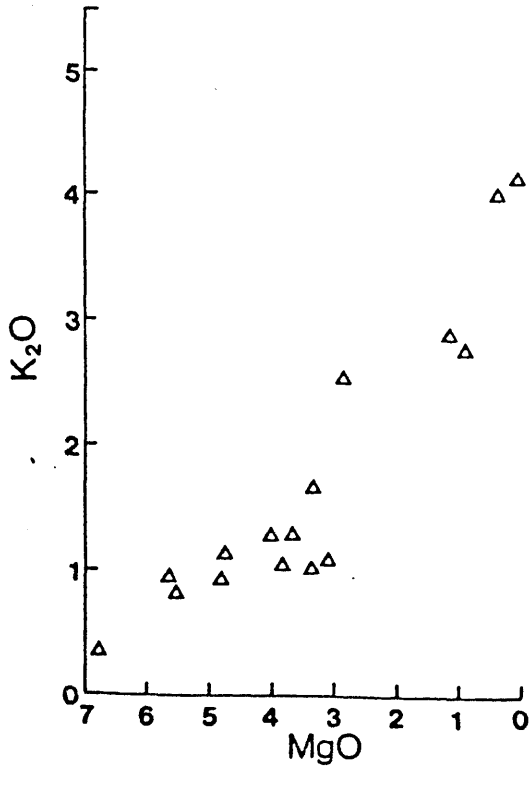
5
4
3
2
1
0
K2O
7 6 5 4 3 2 1 0
MgO

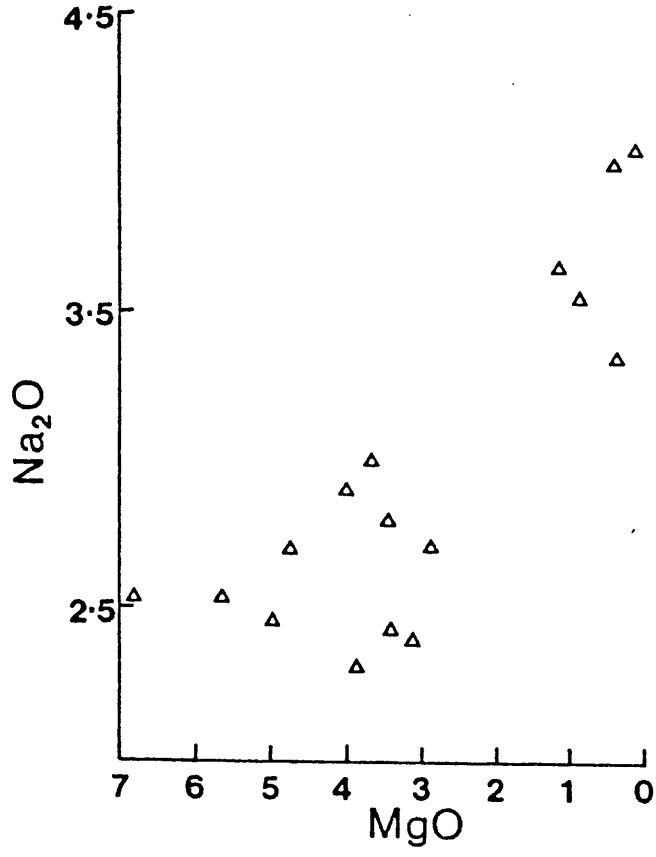
4·5
3·5
2·5
Na_2O
7
6
5
4
3
2
1
0
MgO

crustal magma chambers. P initially increases with decreasing MgO, since P is incompatible in a gabbroic solid assemblage, but then starts to a decrease at MgO = 4 wt. %. Presumably apatite is an important fractionating phase in magmas less magnesian than basalt. Apatite has been observed as a phenocryst phase in the dacites, but not in the basalts. Because of the high phenocryst content of the lavas it is improbable that their whole-rock chemical compositions reflect liquid compositions. This may explain the departure of the variation trends from single liquid lines of descent because of variable crystal accumulation. In calc-alkaline magmas the scatter may also be explained by magma mixing (Grove et al, 1982).

3.3 Geochemical modelling of the major element variation

A mass balance approach has been used to model the major element chemical variation within the subduction-related rock suite. A simple least squares fractionating model (Le Maitre, 1979) was used to calculate the proportion of each mineral which must be removed from a parent magma in order to produce a supposed derivative magma. Mineral compositions were generally obtained by electron micro-probe analysis of phenocryst cores in the lavas (orthopyroxene compositions were taken from Deer et al, 1978). P_2O_5 and K_2O were not included as components in the fractionation calculations, because of their low abundances in plagioclase, olivine and augite. Results of the modelling are shown in Table 3.1. An acceptable upper limit

TABLE 3.1

RESULTS OF FRACTIONAL CRYSTALLISATION CALCULATIONS

	Amounts	SiO_2	Fe_2O_3T	TiO_2	Al_2O_3	MgO	CaO	Na_2O	Total
Reactants used									
MR20	100.00	44.74	13.74	1.28	18.26	6.81	12.22	2.54	99.59
Products used									
MR17	57.91	48.18	12.04	1.02	18.82	5.55	11.13	2.53	99.27
CPX (MR14)	10.54	51.57	10.35	0.42	2.20	15.50	19.84	0.74	100.62
OL (MR14)	5.45	37.43	30.49	-	-	35.19	0.17	-	103.28
PLAG(MR20)	21.10	46.14	0.38	-	33.84	0.14	17.94	1.60	100.04
MGNT(MR20)	5.00	0.38	84.86	11.06	4.25	1.71	-	-	102.26
Estimated compositions									
Reactants		44.74	13.74	1.28	18.26	6.81	12.22	2.54	99.59
Products		45.13	14.05	1.19	18.48	6.88	12.33	1.88	99.94
Differences		-0.39	-0.31	0.09	-0.22	-0.07	-0.11	0.66	
Residual sum of squares			= 0.7581						
Distance between two estimated compositions			= 0.8707						
Reactants used									
MR17	100.00	48.18	12.04	1.02	18.82	5.55	11.13	2.53	99.27
Products used									
K1	70.35	51.32	10.22	.89	18.70	4.74	9.68	2.70	98.25
CPX (MR14)	7.29	51.57	10.35	.42	2.20	15.50	19.84	.74	100.62
OL (MR14)	2.79	37.43	30.49	0.00	0.00	35.19	.17	0.00	103.28
PLAG(MR20)	15.81	46.14	.38	0.00	33.84	.14	17.94	1.60	100.04
MGNT(MR20)	3.76	.38	84.86	11.06	4.25	1.71	0.00	0.00	102.26
Estimated compositions									
Reactants		48.18	12.04	1.02	18.82	5.55	11.13	2.53	99.27
Products		48.22	12.04	1.07	18.83	5.53	11.10	2.21	99.00
Differences		-.04	-.00	-.05	-.01	.02	.03	.32	
Residual sum of squares			= .1103						
Distance between two estimated compositions			= .3321						

TABLE 3.1 (Cont'd.)

	Amounts	SiO_2	Fe_2O_3T	TiO_2	Al_2O_3	MgO	CaO	Na_2O	Total
Reactants used									
MR17	100.00	48.18	12.04	1.02	18.82	5.55	11.13	2.53	99.27
Products used									
K40	12.45	58.71	8.19	.76	17.31	2.84	6.66	2.71	97.18
MGNT(MR20)	8.48	.38	84.86	11.06	4.25	1.71	0.00	0.00	102.26
CPX (K90)	19.14	48.57	7.83	.77	5.68	13.56	23.48	.38	100.27
PLAG(K100)	52.84	54.76	.37	0.00	28.72	0.00	11.04	4.85	99.74
OL (MR14)	7.09	37.43	30.49	0.00	0.00	35.19	.17	0.00	103.28
Estimated compositions									
Reactants		48.18	12.04	1.02	18.82	5.55	11.13	2.53	99.27
Products		48.23	12.07	1.18	18.78	5.59	11.17	2.97	99.99
Differences		-.05	-.03	-.16	.04	-.04	-.04	-.44	
Residual sum of squares			= .2296						
Distance between two estimated compositions			= .4792						

Reactants used									
K40	100.00	58.71	8.19	.76	17.31	2.84	6.66	2.71	97.18
Products used									
K90	74.00	64.05	4.66	.50	17.31	1.14	4.79	3.65	96.10
AMPH(K90)	8.66	43.41	14.14	2.09	11.60	13.59	11.87	1.97	98.67
CPX (K90)	4.01	48.57	7.83	.77	5.68	13.56	23.48	.38	100.27
PLAG(K100)	9.85	54.76	.37	0.00	28.72	0.00	11.04	4.85	99.74
MGNT(MR20)	3.49	.38	84.86	11.06	4.25	1.71	0.00	0.00	102.26
Estimated compositions									
Reactants		58.71	8.19	.76	17.31	2.84	6.66	2.71	97.18
Products		58.51	7.98	.97	17.02	2.62	6.60	3.36	97.06
Differences		.20	.21	-.21	.29	.22	.06	-.65	
Residual sum of squares			= .6915						
Distance between two estimated compositions			= .8315						

TABLE 3.1 (Cont'd.)

	Amounts	SiO_2	Fe_2O_3T	TiO_2	Al_2O_3	MgO	CaO	Na_2O	Total
Reactants used									
K94	100.00	50.99	10.47	.98	18.87	4.03	9.54	2.90	97.78
Products used									
K102	35.83	57.00	8.07	.72	17.34	3.46	7.81	2.78	97.18
CPX (M14)	11.07	51.57	10.35	.42	2.20	15.50	19.84	.74	100.62
PLAG(K100)	42.22	54.76	.37	0.00	28.72	0.00	11.04	4.85	99.74
MGNT(MR20)	7.16	.38	84.86	11.06	4.25	1.71	0.00	0.00	102.26
OPX	3.70	52.86	11.42	.33	4.15	30.04	1.36	.08	100.24
Estimated compositions									
Reactants		50.99	10.47	.98	18.87	4.03	9.54	2.90	97.78
Products		51.24	10.70	1.11	19.04	4.19	9.71	3.13	99.12
Differences		-.25	-.23	-.13	-.17	-.16	-.17	-.23	
Residual sum of squares			= .2684						
Distance between two estimated compositions			= .5181						

Reactants used									
K40	100.00	58.71	8.19	.76	17.31	2.84	6.66	2.71	97.18
Products used									
K100	54.27	68.77	3.43	.54	16.08	.36	3.49	3.36	96.03
PLAG(K100)	24.58	54.76	.37	0.00	28.72	0.00	11.04	4.85	99.74
MGNT(MR20)	3.02	.38	84.86	11.06	4.25	1.71	0.00	0.00	102.26
BIOT(K100)	7.92	31.65	30.93	5.22	11.83	10.30	.10	.91	90.94
CPX (MR14)	10.21	51.57	10.35	.42	2.20	15.50	19.84	.74	100.62
Estimated compositions									
Reactants		58.71	8.19	.76	17.31	2.84	6.66	2.71	97.18
Products		58.57	8.02	1.08	17.08	2.65	6.64	3.16	97.20
Differences		.14	.17	-.32	.23	.19	.02	-.45	
Residual sum of squares			= .4524						
Distance between two estimated compositions			= .6726						

of $\sum r^2 = 1$ (where $\sum r^2$ is the sum of the squares of the residuals) was arbitrarily taken for the calculations. A basalt with 5.6 wt. % MgO (MR17) can be generated from the least evolved basalt (MR20; MgO = 6.8 wt. %) by 42% crystallisation of the parental basalt, involving the removal of a crystal assemblage consisting of 50 wt. % calcic plagioclase, 25 wt. % augite, 13 wt. % olivine and 12 wt. % titanomagnetite. Andesites may be generated by 64% crystallisation of a parental basalt composition (MgO = 5.6 wt. %) by the removal of a solid assemblage consisting predominantly of calcic plagioclase (66 wt. %), with augite (17 wt. %), titanomagnetite (11 wt. %) and either olivine or orthopyroxene (6 wt. %). Dacite may be generated by 43% crystallisation of a parental andesite, where plagioclase is again the dominant fractionating phase (49 wt. %) with lesser amounts of augite (23 wt. %), titanomagnetite (6 wt. %) and biotite (22 wt. %). Biotite has been observed as a phenocryst phase in dacites and rhyolites. Amphibole has not been observed in any Oligo-Miocene subduction-related lavas, although amphibole phenocrysts are common in post-Miocene dacites at Monte Pizzinnu. Such dacites may be generated by 26% crystallisation from a parental andesite (MgO = 2.8 wt. %) of a solid assemblage consisting of 33 wt. % amphibole, 15 wt. % clinopyroxene, 38 wt. % plagioclase and 14 wt. % titanomagnetite.

Thus, the major element chemical variation from basalt to dacite in Sardinian subduction-related lavas can be generated by the removal of their observed phenocryst phases. The geochemical behaviour of some selected trace elements is discussed below.

3.4 Trace element variation

Rb increases with increasing fractionation in the magma series, showing, for example, a negative correlation with MgO and V (Figure 3.4). This is consistent with its incompatability in the proposed olivine, plagioclase and pyroxene fractionating assemblage, although it is probably partitioned into biotite in the most silicic rocks. Selected trace elements have been plotted against Rb in Figure 3.4. Although there is evidence for mobility of Rb during hydrothermal alteration (Wood et al, 1976), such a process has played a minimal role in the genesis of Sardinian volcanic rocks. Further, the good positive correlation of Rb with Zr (apparently residual here) reinforces the validity of the above observation.

The incompatible elements (Ba, La, Th, Be and Zr) show positive correlations with Rb, and are progressively enriched through the basalt to rhyolite series. Observed enrichment factors from the least evolved basalt to the most evolved silicic rock are: Zr x 3.4; Ba x 7.4; La x 4.6; Be x 2.9; Th x 19.0; Nb x 4.0; Hf x 4.8; Yb x 2.1. In contrast, the compatible trace elements, V and Sc, are progressively depleted, and show pronounced negative correlations with Rb,

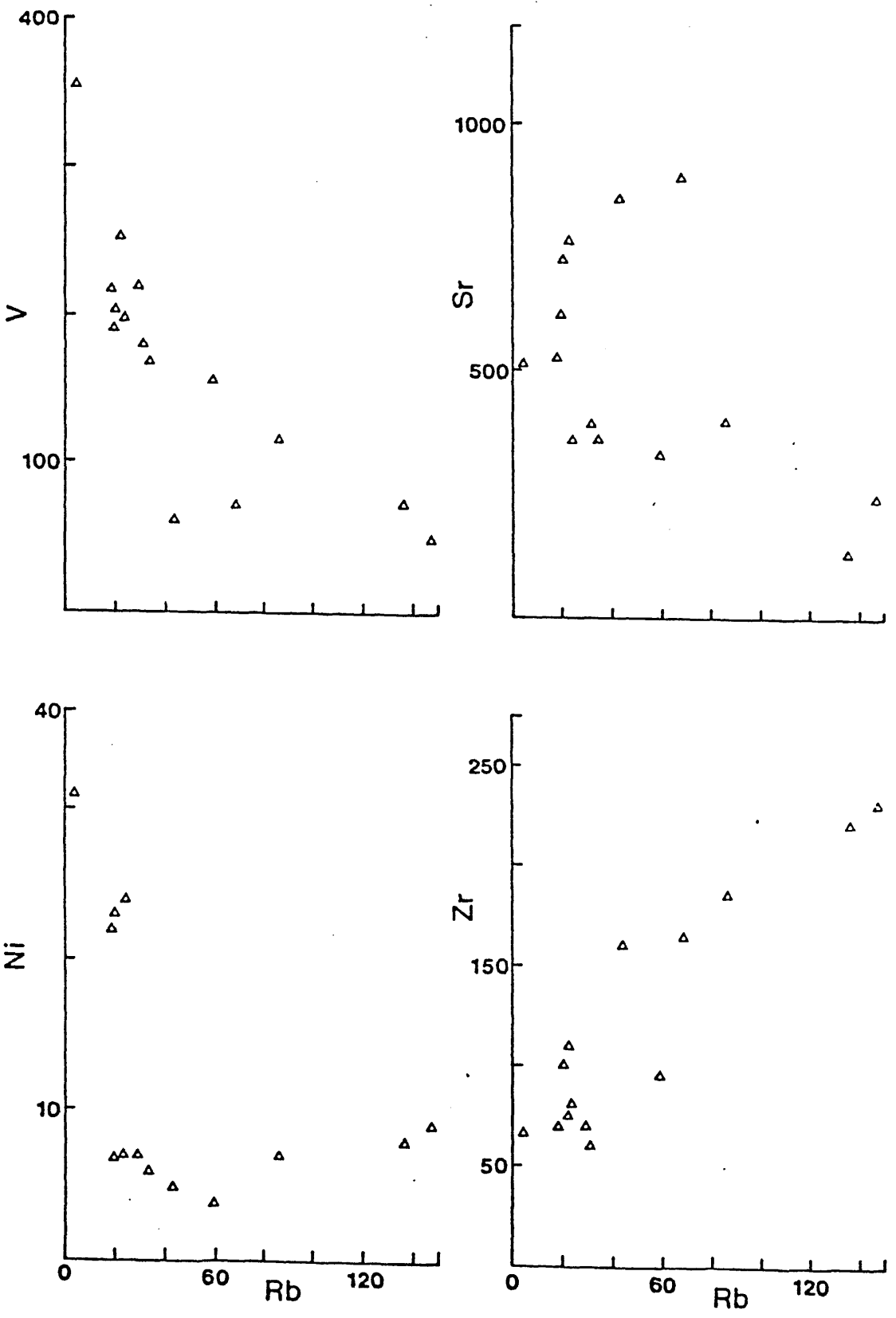

Figure 3.4

Trace element chemical variation in Sardinian subduction-related lavas plotted against Rb

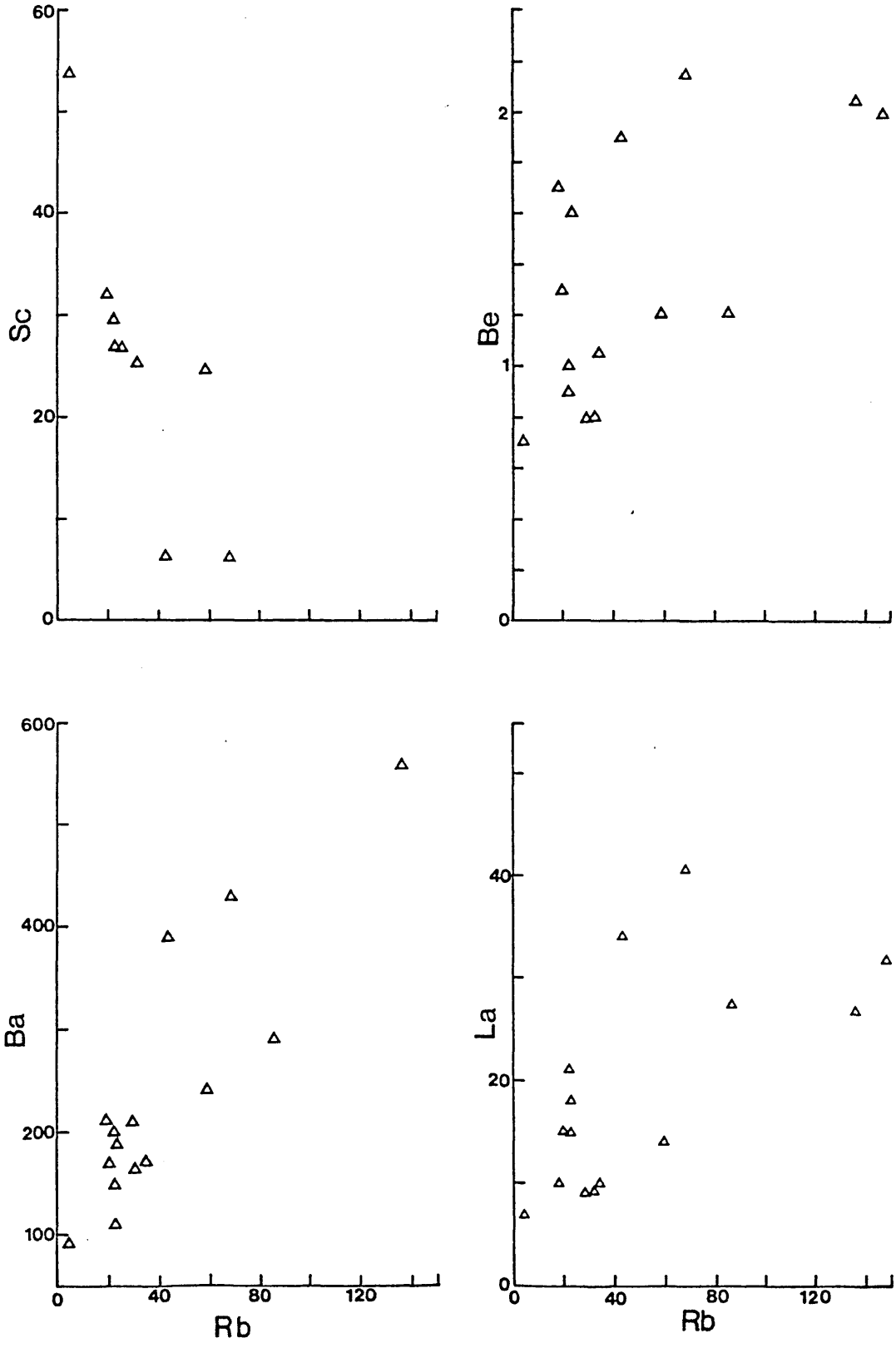
Sc
60
40
20
0
Be
2
1
0
Ba
600
400
200
100
0
40
80
120
Rb
La
40
20
0
0
40
80
120
Rb

consistent with titanomagnetite ($D_V^{mgnt/l}$ = 20; Irving, 1978) and clinopyroxene ($D_{Sc}^{cpx/l}$ = 2.7; Henderson, 1981) removal. Sr abundances are variable (Sr = 510-770 ppm) in the more mafic samples ($SiO_2 \leq$ 5.2 wt. %), but Sr decreases with increasing Rb in the andesites and dacites consistent with significant plagioclase fractionation. Ni shows a strong negative correlation with Rb, consistent with olivine ($D_{Ni}^{ol/l}$ = 14; Henderson, 1981) and/or titanomagnetite ($D_{Ni}^{mgnt/l}$ = 12; Irving, 1978) removal. There is a marked inflection in the Ni-Rb curve at about 60 ppm Rb, when Ni begins to increase with increasing Rb, Ni contents being about 3 ppm in the andesites and about 8 ppm in the rhyolites. There is no petrographic evidence for fayalite in the Sardinian rhyolites.

Large variations exist in incompatible element abundances within the more mafic ($<$ 5.2 wt. % SiO_2) Sardinian lavas, with a factor of 2 variation in Sr, La and Ba; a factor of 3 variation in Be and Th; and a factor of 5 variation in Rb. Such wide variation cannot be explained by plausible degrees of crystal fractionation, and implies multiple parentage for the volcanic rocks as a whole. This observation does not affect the validity of the major element modelling which is controlled by fractionation of the major rock-forming minerals.

The trace element abundances in parent and daughter magmas cannot be modelled using the weight fractions of residual liquids, calculated from the major element least squares fractionation modelling (Table 3.2), assuming simple Rayleigh fractionation. Such decoupling between major and trace elements has been observed by other authors in subduction-related rock suites (Luhr and Carmichael, 1981; Mann, 1983).

Although the major element least squares solution may be incorrect, the fit between model and observation cannot be improved by substituting in other non-phenocryst phases, such as amphibole (except for dacites from Monte Pizzinnu). There is some evidence for combined AFC processes in crustal magma chambers and the assumption of closed system behaviour may be incorrect. Possibly, the magma chamber operated under open system conditions (O'Hara and Matthews, 1981). Alternatively, trace element abundances may vary between lavas due to source heterogeneity, and this question is addressed in Chapter 5.

3.5 Rare earth elements (REE)

Representative samples of Sardinian subduction-related lavas are shown in Figures 3.5-3.7. The most important features of the REE patterns are summarised overleaf:

TABLE 3.2

TRACE ELEMENT ABUNDANCES CALCULATED ASSUMING 30% FRACTIONAL CRYSTALLISATION OF A STARTING COMPOSITION SIMILAR TO MR17. THE FRACTIONATING ASSEMBLAGE CONSISTS OF 25 wt. % AUGITE, 9 wt. % OLIVINE, 53 wt. % PLAGIOCLASE AND 13% TITANOMAGNETITE (CALCULATED USING LEAST SQUARES MAJOR ELEMENT MODELLING).
DISTRIBUTION CO-EFFICIENTS WERE TAKEN FROM HENDERSON (1981) MAJOR ELEMENT LEAST SQUARES CALCULATIONS MODELLED THE GENESIS OF K1 BY 30% FRACTIONAL CRYSTALLISATION OF A PARENTAL BASALT (MR17) BY THE REMOVAL OF THE ABOVE PHASES IN THESE PROPORTIONS

	MR17 (starting composition)	Model	K1
Th	1.14	1.62	2.34
Rb	18	26	22
Sc	31.9	31.8	26.7
Sr	526	531	619
V	217	71	192
Ni	22	7	23
K	0.81 wt. %	1.13 wt. %	1.11 wt. %
Ba	109	150	200
Yb	2.23	2.93	2.26
Cr	22	1	48
Ce	21	28.1	43

All values in ppm, except where stated

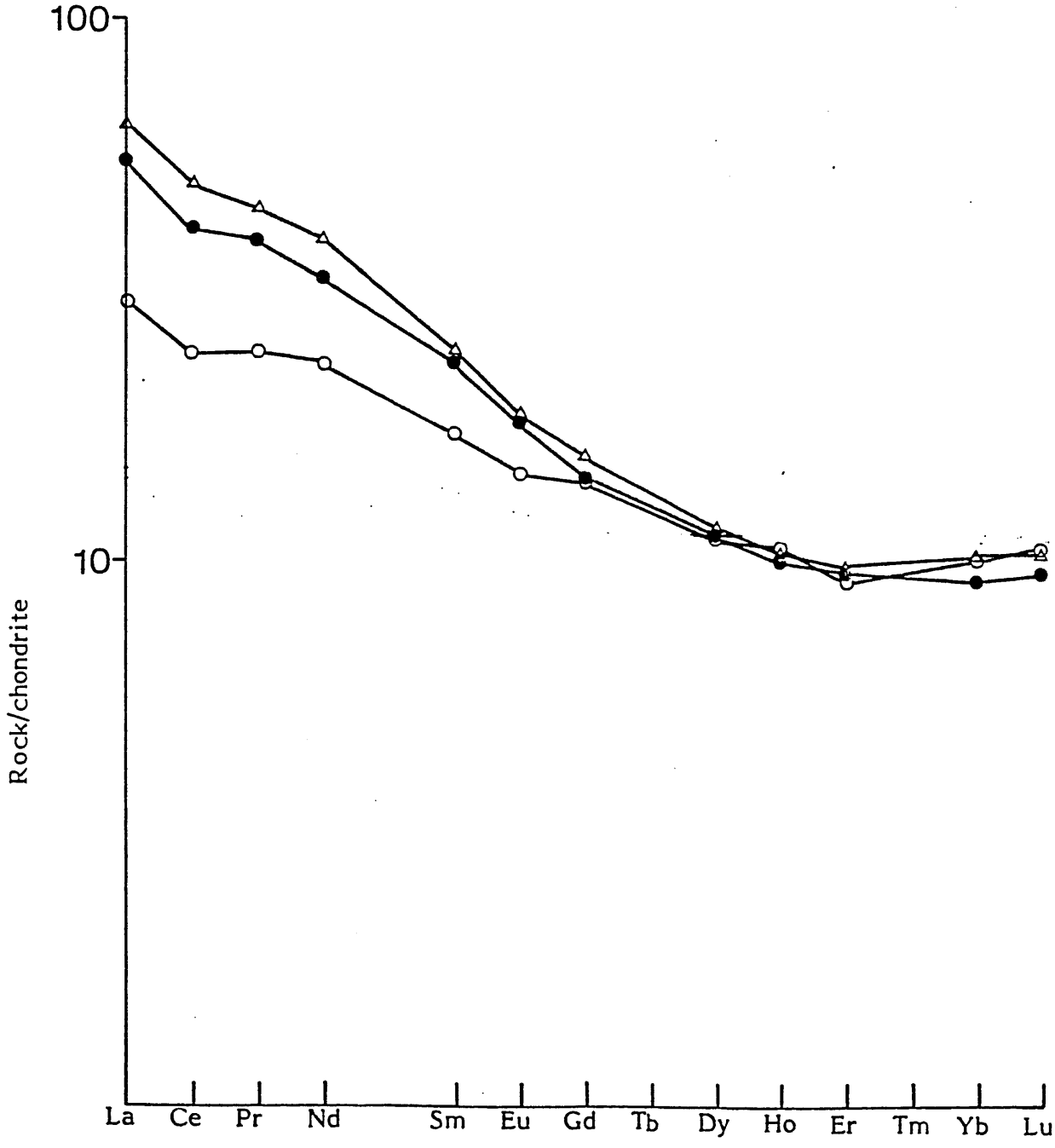

Figure 3.5

Chondrite-normalised REE data for some selected high-alumina basalts. Open triangles = K1; filled circles = K94; and open circles = MR17.

Figure 3.6

Chondrite-normalised REE data for two andesitic-rocks from N.W. Sardinia. Filled triangles = K40; open triangles = K102.

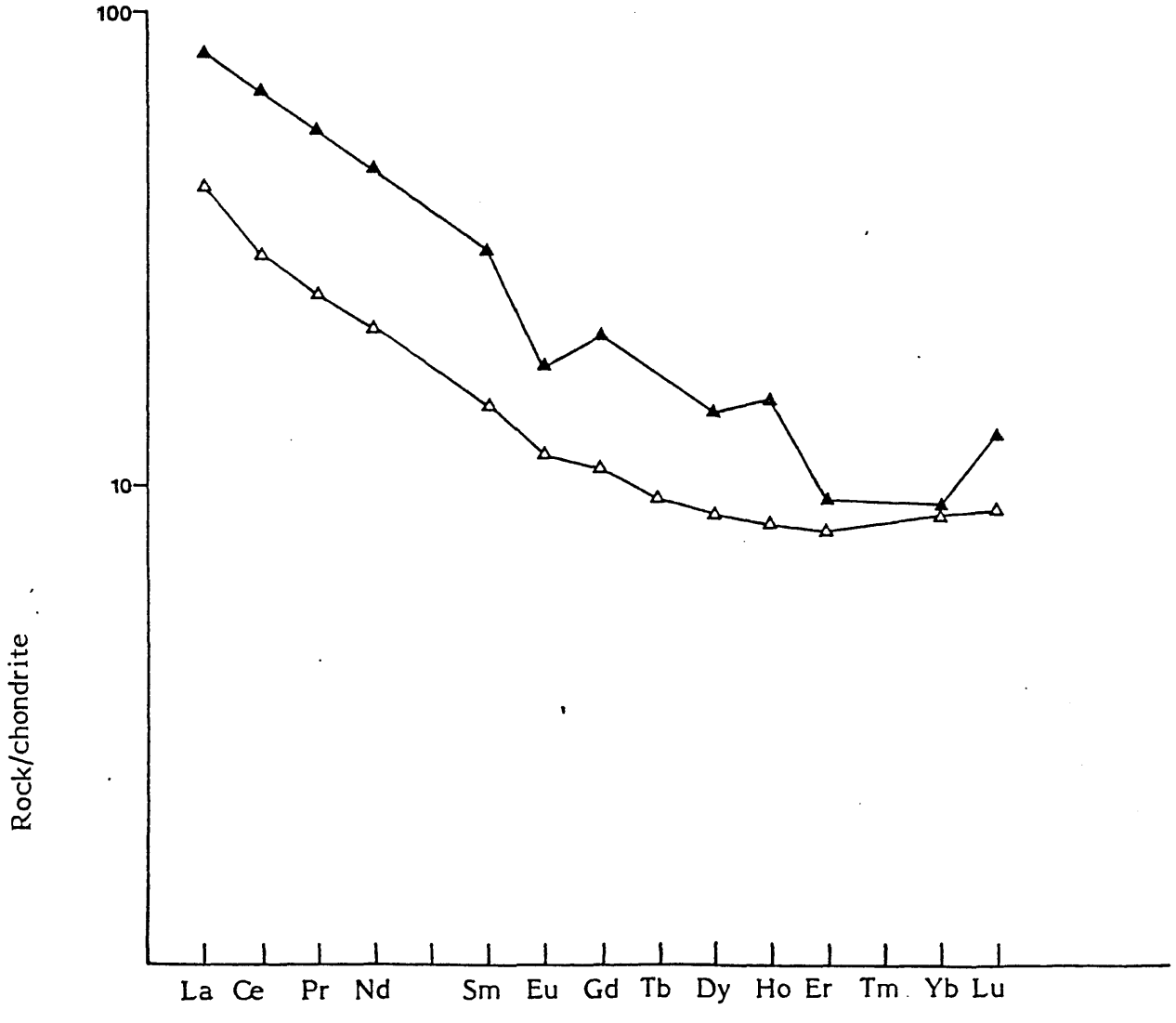

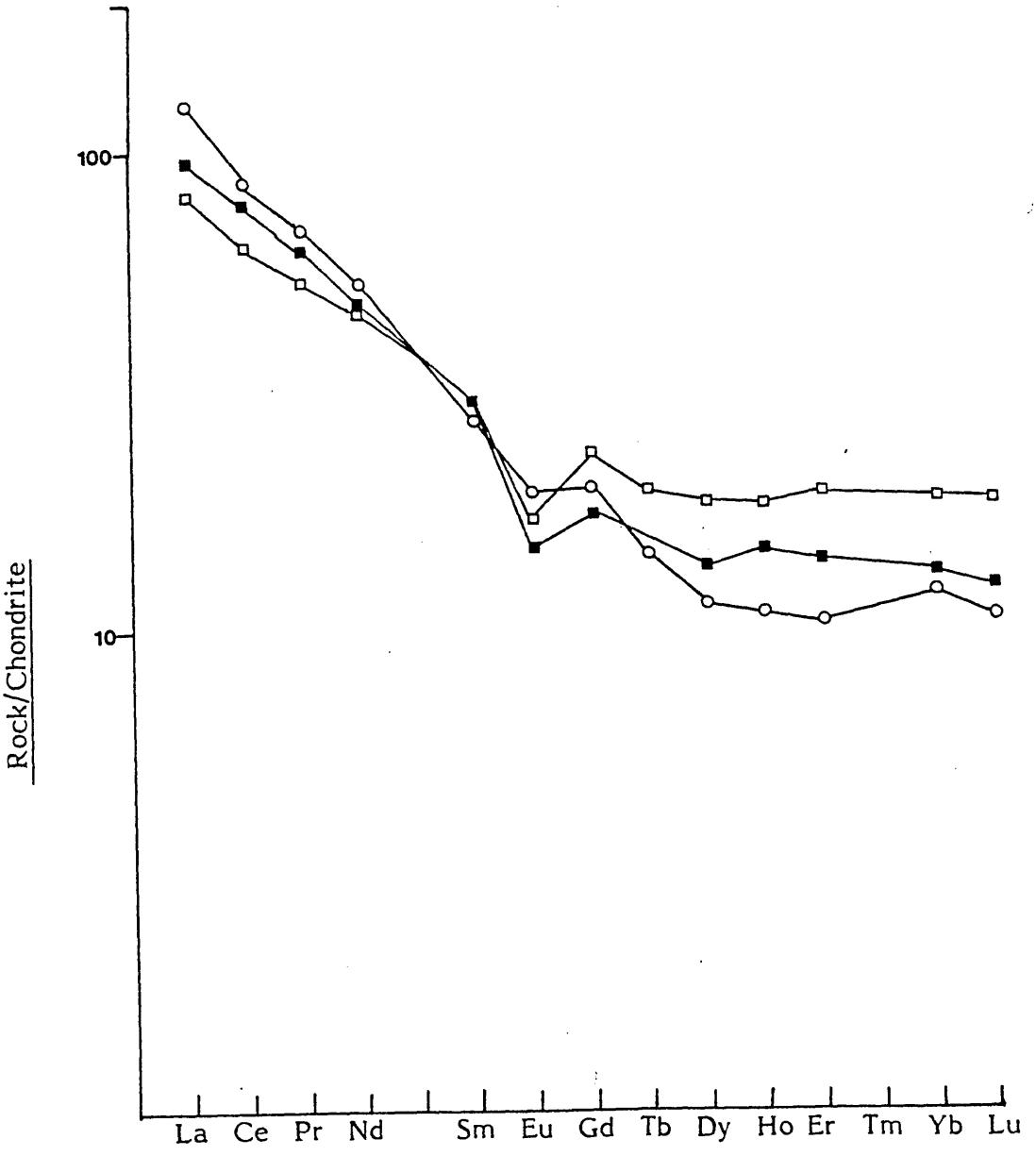

Figure 3.7

Chondrite-normalised REE data for some selected Sardinian dacite and rhyolite lavas. Open circles = K90; filled squares = K100; and open squares = C11.

1. Basaltic rocks are LREE-enriched relative to the HREE, and show a much wider range in LREE (Ce_N = 20-48) than HREE (Yb_N = 7.6-10.4) abundances.
2. Andesitic, dacitic and rhyolitic rocks are strongly LREE-enriched, and show small negative Eu anomalies.
3. Total REE abundances generally increase with increasing differentiation.
4. Basalts show a relatively flat REE pattern from Dy to Lu.
5. Some of the basalts show negative Ce anomalies.
6. The least evolved basalt (MR20) has a negative Eu anomaly.
7. Degree of LREE-enrichment increases from basalts (La/Yb_N = 2.7-6.1) to dacites (La/Yb_N = 7.8-10.3).
8. Rhyolite shows substantially higher HREE, but lower LREE, abundances than dacite.
9. There is a strong concave upwards curvature in the HREE end of the pattern for K90.

Increasing REE abundances (except Eu) with decreasing MgO is consistent with fractionation of a gabbroic mineral assemblage. Low HREE contents and the concave upwards HREE pattern for the post-Miocene dacite (K90) indicate amphibole removal, and hornblende has been observed as a phenocryst phase in this rock. Cumulate xenoliths, consisting of hornblende, calcic plagioclase and augite (Table 3.3), have been observed in these lavas. The co-existence of amphibole and Ca-rich plagioclase implies

TABLE 3.3

MINERAL COMPOSITIONS IN A CUMULATE XENOLITH FROM A DACITE LAVA FROM MONTE PIZZINNU

	Amphibole	Clinopyroxene	Plagioclase
SiO_2	40.47	48.29	44.30
Al_2O_3	14.17	5.81	34.54
TiO_2	1.92	1.11	-
MgO	14.07	13.30	-
MnO	0.03	0.21	-
CaO	12.43	22.33	19.24
K_2O	0.76	0.01	-
Na_2O	2.13	0.32	0.37
FeO	9.76	8.50	0.54
NiO	0.02	0.10	-
Cr_2O_3	0.09	0.04	-

All values given in wt. % oxide

the early precipitation of amphibole. Possibly the early products of the Plio-Pleistocene volcanic cycle fractionated at the base of the continental crust under higher pressure and lower temperature conditions than for the Oligo-Miocene lavas, prior to the establishment of crustal conduits to the surface.

Although the HREE are partitioned into clinopyroxene ($D_{Yb}^{cpx/l}$ = 1.3; Henderson, 1981) the strong LREE-enrichment shown by the more differentiated lavas cannot be modelled by plausible amounts of augite removal. Sr-isotope data indicate that assimilation and fractional crystallisation (AFC) processes were operating during differentiation in shallow crustal magma chambers. $^{87}Sr/^{86}Sr$ ratios show a poor positive correlation with Rb, and approximate negative correlations with both Ni and V (Figure 3.8). Thus, with increasing fractionation the lavas become enriched in radiogenic Sr. The latent heat of crystallisation of the magmas is believed to provide sufficient heat input to allow partial melting and assimilation of the country rock (De Paolo, 1981). The addition of LREE-enriched crustal melts can explain the observed relatively high LREE abundances in the more evolved lavas.

Negative Eu anomalies in the intermediate and acid lavas indicate significant plagioclase removal ($D_{Sr}^{plag/l}$ = 6; Henderson, 1981), which is consistent with the least squares major element modelling. Slight negative Eu anomalies in the REE patterns for the more mafic lavas are also consistent with fractionation of plagioclase, required by the major element modelling.

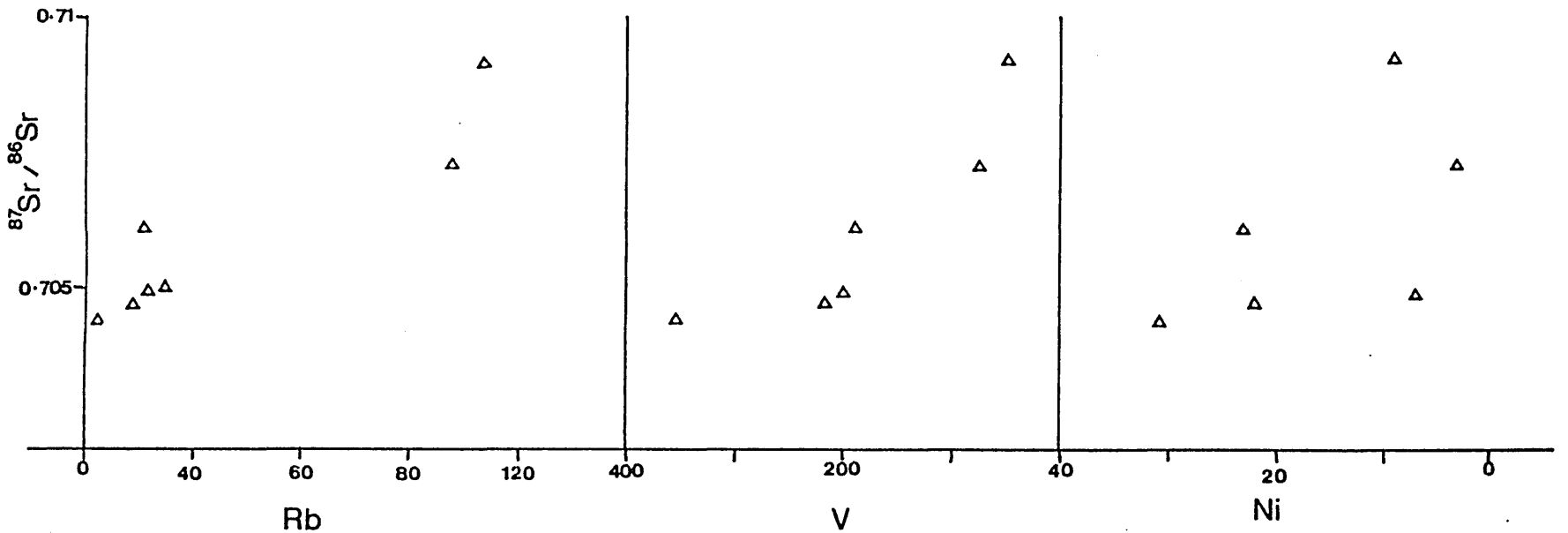

Figure 3.8

Rb, Ni and V plotted against $^{87}Sr/^{86}Sr$ in some subduction-related lavas from N.W. Sardinia.

The flat REE pattern from Dy to Lu shown in Figure 3.6 is consistent with at least some control of REE distribution by residual garnet during partial melting ($D_{Yb}^{gnt/l}$ = 30; Henderson, 1981). Isotopic constraints limit the amount of sialic crust involved in basic magma genesis to only a few percent, and such small amounts of crustal involvement cannot explain the observed REE variation. The wide range in LREE abundances observed in Sardinian basaltic rocks may be produced by any or a combination of the following:-

1. Varying degrees of partial melting of a garnet-bearing source mantle;
2. Addition of a silicic melt from the continental crust during magma ascent;
3. A heterogeneous mantle source, possibly due to the addition of a LREE-enriched component from the subducted slab.

Low K/Cs ratios relative to oceanic basalts and variations in highly incompatible element ratios (e.g. K/Ba = 32-57; Ba/Rb = 6-9) within the mafic rocks indicate that some of the chemical variation is due to mixing of at least two compositionally-distinct end-members, possibly one of which is derived from the subducted slab (see Chapter 5).

3.6 Synthesis

The dominance of fractional crystallisation processes in explaining the within-suite geochemical evolution of Oligo-Miocene subduction-related volcanic rocks is shown in Figure 3.9, in which the concentrations of selected elements are shown normalised to chondrites (except Rb, K and P; Thompson, 1982). Changing slopes within the patterns reflect variation in inter-element ratios, which can often be explained by fractionation of a particular phenocryst phase. The main chemical features relevant to the differentiation pathway from andesite through to rhyolite are discussed below:-

1. Increasing Y and HREE abundances indicate that amphibole was not a significant fractionating phase ($D_{Yb}^{amph/l}$ = 6.2; Henderson, 1981);
2. Decreasing Sr/Ce ratios imply the progressive removal of plagioclase;
3. Increasing Tb/Ti ratios correlated with decreasing V, reflects titanomagnetite fractionation.
   Thus, Tb/Ti ratios in Sardinian mafic rocks are probably related to titanomagnetite fractionating, and are not a mantle source characteristic;
4. Decreasing P/Nd with increasing fractionation indicates apatite removal;
5. Similar increases in Zr and Hf abundances and increasing HREE contents, indicate that zircon did not begin to fractionate;

Figure 3.9

Chondrite-normalised multi-element diagram showing the dominance of fractional crystallisation processes in producing the observed elemental variation from andesite through dacite to rhyolite.
Open circles = K102; filled circles = C11; and open squares = K100.

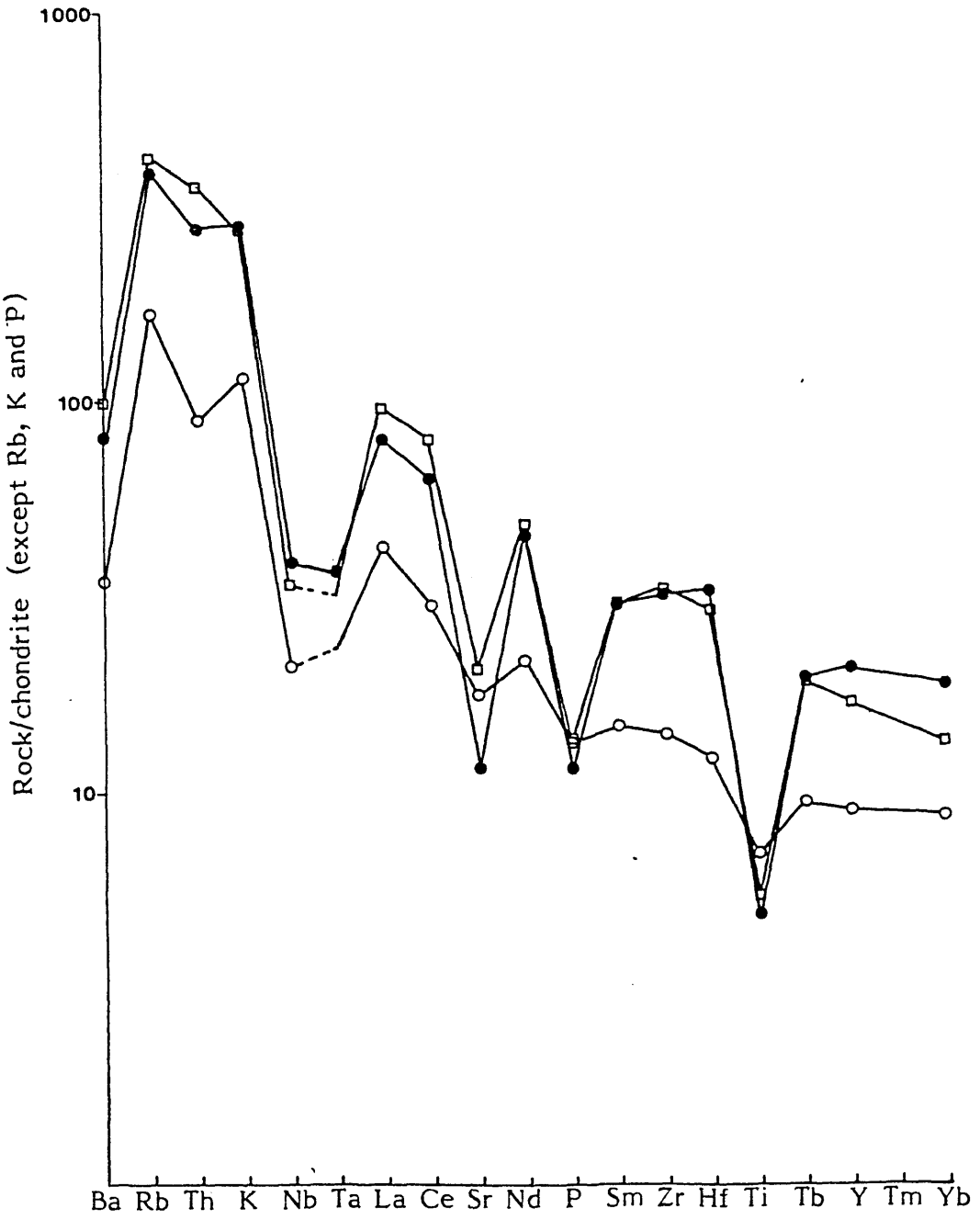

6. Decreasing Rb/Th and K/Th in the most evolved lava implies biotite removal ($D_{Rb}^{biot/l}$ = 3.4; Henderson, 1981);
7. Decreasing La/Nd from K100 to C11 may reflect the removal of a LREE-enriched phase, possibly allanite ($D_{La}^{all/l}$ = 820; Henderson, 1981), although this phase has not been observed petrographically.

CHAPTER 4

COMPARATIVE MAJOR AND TRACE ELEMENT VARIATION WITHIN THE PLIO-PLEISTOCENE MAGMA SUITE

Plio-Pleistocene mafic lavas and pyroclastics consist of the following chemically distinct rock types: high-Al basalt; basaltic andesite; high-Mg andesite; alkali basalt; hawaiite and basanite. Their petrographic features have been discussed in Chapter 2. Rock nomenclature is based on geochemical criteria, which are outlined below.

4.1 High-Al basalt

Post-Miocene high-Al basalts were erupted at Monte Castanza (Coulon et al, 1974), and are geochemically similar to the older Oligo-Miocene subduction-related basalts although no active subduction is envisaged during the Plio-Pleistocene. The geochemistry of post-Miocene high-Al basalts has been discussed in Chapter 3. Only their more important chemical features are summarised below:

(i) low Nb abundance (Nb = 5 ppm);

(ii) high Sr/Ce = 14.4;

(iii) high alumina content (Al_2O_3 = 18.7 wt. %);

(iv) moderately high La/Yb_N = 6.3;

(v) low Ti content (TiO_2 = 0.9 wt. %).

4.2 Alkali basalts, hawaiites, basaltic andesites and high-Mg andesites

These have been classified on the basis of their variation of K_2O with SiO_2 (after Cox et al, 1978; Figure 4.1). However, the chemical gradation between high-K hawaiites and low-K basaltic andesites is clear from Figure 4.1,

Figure 4.1

K20 against SiO_2 variation in all analysed Tertiary volcanic rocks. Open triangles = subduction lavas; filled circles = hawaiites, and open circles = basaltic andesites and high-Mg andesites.

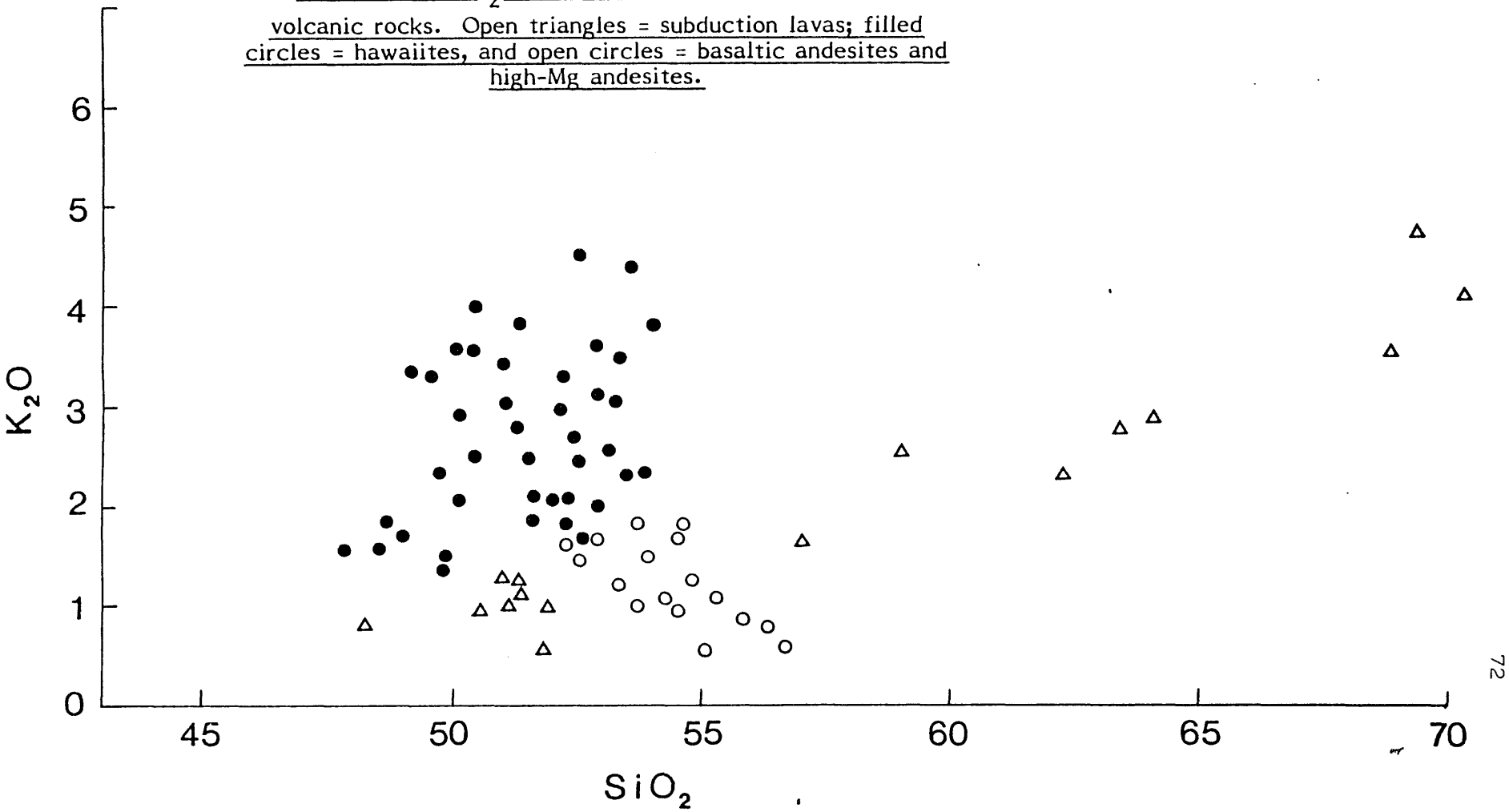

and has been observed at other localities (Cox, 1972). Consequently, an arbitrary upper limit to the basaltic andesites has been set at Ba = 700 ppm. Most of the rocks discussed in this Chapter contain >1 wt. % K_2O, and fall into the high-K group of Mahoney et al (1985). A few samples are andesites (Cox et al, 1978), but have been termed high-Mg andesites because of their relatively high Mg contents (MgO = 4.3-6.1 wt. %), although they have lower Mg and Si contents than high-Mg andesites from S.W. Japan

4.3 Basanites

Several samples fall into the basanite field on the basis of their K_2O and SiO_2 contents, and have been described as analcite basanites by some authors (Macciotta et al, 1977). However, their abundant xenocrystal Mg-rich olivines tend to decrease whole-rock SiO_2 (and increase MgO) contents. Further, low K abundances may be related to secondary replacement of an originally K-rich phase by analcite (see Chapter 2). The following chemical features imply that the basanites may in fact be more evolved than the associated hawaiites:

(i) Relatively Fe-rich augite phenocrysts;

(ii) Higher incompatible element (e.g. Ba, Sr, Rb, Zr, LREE, P and HREE) abundances;

(iii) Sub-parallel REE patterns, relative to the hawaiites.

4.4 Primary or differentiated magmas in northern Sardinia?

Frey et al (1978) established three criteria for recognising primary mantle-derived magmas, unmodified by crystal fractionation processes. These include:

(1) the presence of spinel lherzolite xenoliths in the lavas;

(2) $Mg/Mg + Fe^{2+}$ ratios of 68-75;

(3) Ni $\geq$ 320 ppm.

Although the occurrence of abundant xenoliths of mantle origin (see Chapter 8) implies rapid ascent of magma to the surface and minimal crystal fractionation within the continental crust, differentiation may have taken place within the lithospheric mantle prior to magma ascent. This can explain the low $Mg/Mg + Fe^{2+}$ ratios in all Plio-Pleistocene mafic lavas, which cannot have been in equilibrium with mantle olivine (hawaiite MR16 = 35.3; high-Mg andesite MR25 = 40.8, and basaltic andesite MR18 = 63.7). Similarly, Ni values in hawaiites lacking olivine xenocrysts are too low (Ni = 34-164 ppm) for the magmas to represent primary mantle melts. Ni abundances range from Ni = 57-93 ppm in the basaltic andesites, to Ni = 100-147 ppm in the high-Mg andesites, which again imply that the magmas have undergone crystal fractionation at some depth, probably involving olivine removal, during ascent to the surface.

4.5 CIPW normative compositions

The compositions of fresh Sardinian mafic rocks are plotted in terms of their CIPW normative olivine, diopside, hypersthene, nepheline and quartz contents in Figure 4.2, assuming $Fe^{3+}/Fe^{2+} = 0.15$. The cotectic curves for mafic melts in equilibrium with olivine, plagioclase and clinopyroxene at increasing pressures are from Thompson et al (1983). All the samples form a transitional volcanic suite, ranging from nepheline- to quartz-normative, although most are olivine- and hypersthene-normative.

The alkalic mafic lavas straddle the diopside-olivine join, which is a thermal divide at low pressures under anhydrous conditions (O'Hara, 1968). Therefore, magma generation or differentiation must have occurred either at higher pressures or under hydrous conditions, when this join is no longer a thermal barrier. All the rocks plot well below the 1 atmosphere cotectic, which is consistent with the above observation. Thompson et al (1983) have suggested that the 1 atmosphere cotectic is very sensitive to pressure and will migrate towards the hypersthene apex with increasing pressure. Most of the samples lie above the 9 ± 1.5 kb cotectic, and have probably reached equilibrium at a depth of about 20 km within the continental crust. Equilibration at this depth must have been relatively rapid, because the presence of abundant ultramafic xenoliths in the alkaline lavas implies rapid transfer of magma from the mantle lithosphere to the surface. This observation precludes

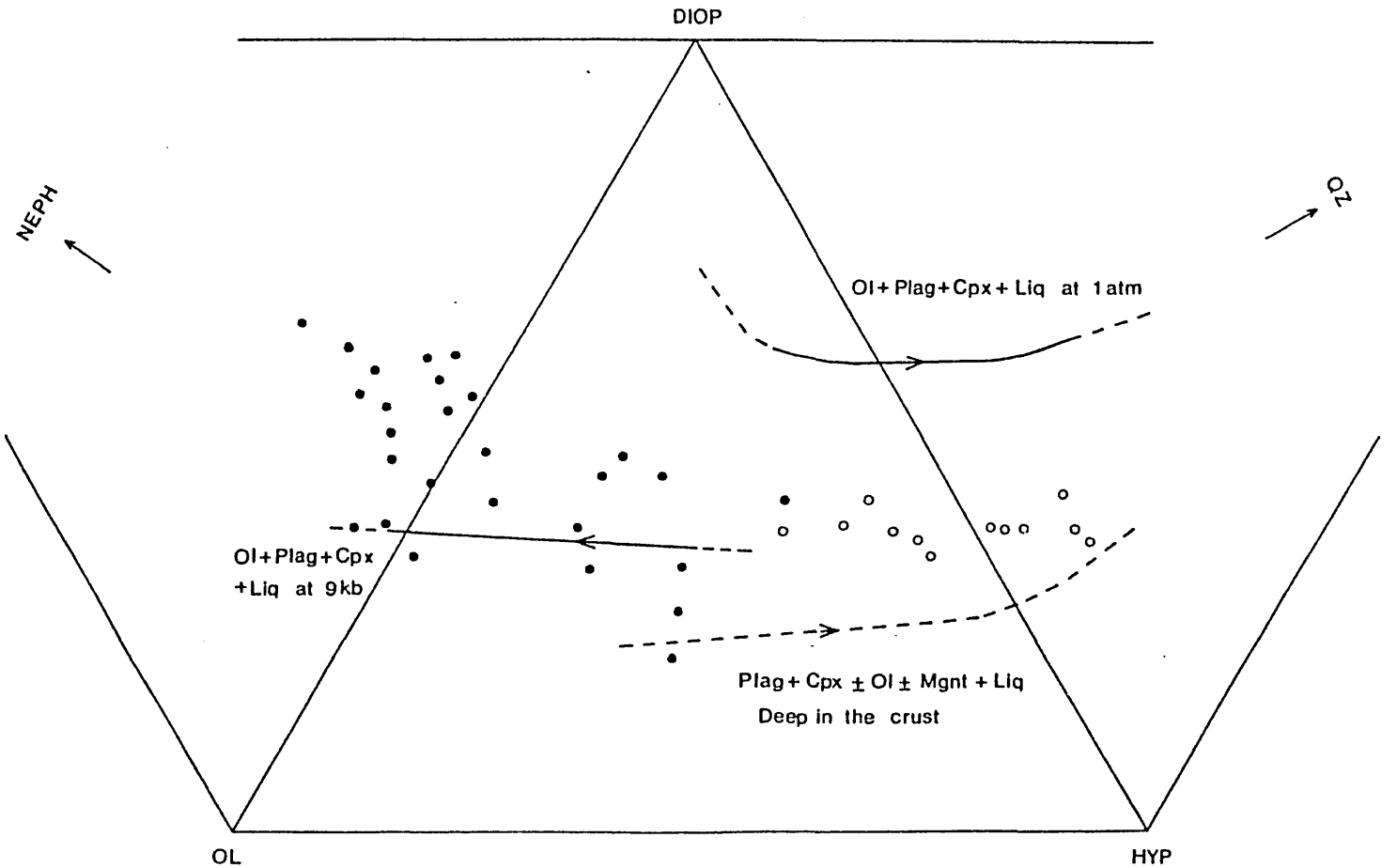

Figure 4.2

CIPW normative composition of selected Plio-Pleistocene volcanic rocks. See text for details. Symbols as in Figure 4.1.

significant interaction of the magmas with sialic material during magma ascent, unless heat transfer to the continental crust occurs rapidly by turbulent convection (Huppert and Sparks, 1985; see Chapter 6). The rocks do not show decreasing Ni, Cr or MgO in a down-temperature direction along any of the cotectic curves, which suggests that their chemical variation is not related to crystal fractionation at this depth. Varying degrees of melting and/or some higher pressure fractionation event may explain their geochemical variability.

4.6 Major element chemical variation

The variation of K_2O with SiO_2 for all analysed Tertiary volcanic rocks is shown in Figure 4.1. The basaltic andesites are generally characterised by lower K contents than the hawaiites, and are indistinguishable from the older subduction-related lavas using this discriminant. Hawaiites and basaltic andesites were erupted contemporaneously, although probably from separate vents or fissures. They tend to form geographic sub-provinces, and low-K basaltic andesites predominate in the lower part of the sequence. The hawaiites show a general increase of K_2O with increasing SiO_2, although the factor of 4 variation in K abundances suggests that K variability is not related to fractional crystallisation processes. The wide range in K abundance may be related to varying sialic contamination during magma ascent, or to magma genesis from a heterogeneous mantle source.

The major element chemical variation in selected Plio-Pleistocene volcanic rocks is shown plotted against MgO in Figure 4.3. All the alkalic rocks show an approximate negative correlation of P, Ti, Al, Na, Si and K with Mg, while Ca is progressively depleted, and Fe_2O_3T remains approximately constant. Such chemical variation is consistent with olivine and clinopyroxene fractionation. Both of these phases have been observed experimentally as near-liquidus minerals under hydrous conditions at moderate to high pressures in natural hawaiite magma (Knutson and Green, 1975). Further, high-P clinopyroxene megacrysts have been observed in many of the Sardinian hawaiites (see Chapter 8), and biotite phenocrysts imply that the magmas were relatively H_2O-rich. The presence of abundant mantle peridotite inclusions suggests that crystal fractionation occurred within the lithospheric mantle, followed by rapid upwards transport of magma to the surface.

The hawaiites are generally characterised by higher K, Ti and P abundances than the basaltic andesites. Since these elements behave incompatibly toward anhydrous mantle peridotite, this observation may reflect smaller degrees of partial melting for the basaltic andesites. Basaltic andesites and high-Mg andesites show a restricted compositional range with MgO = 4.3-6.8 wt. % and moderately high SiO_2 = 52-57 wt. %. High Si abundances may reflect sialic contamination during magma ascent, although high-Si, high-Mg lavas from S.W. Japan are thought to represent

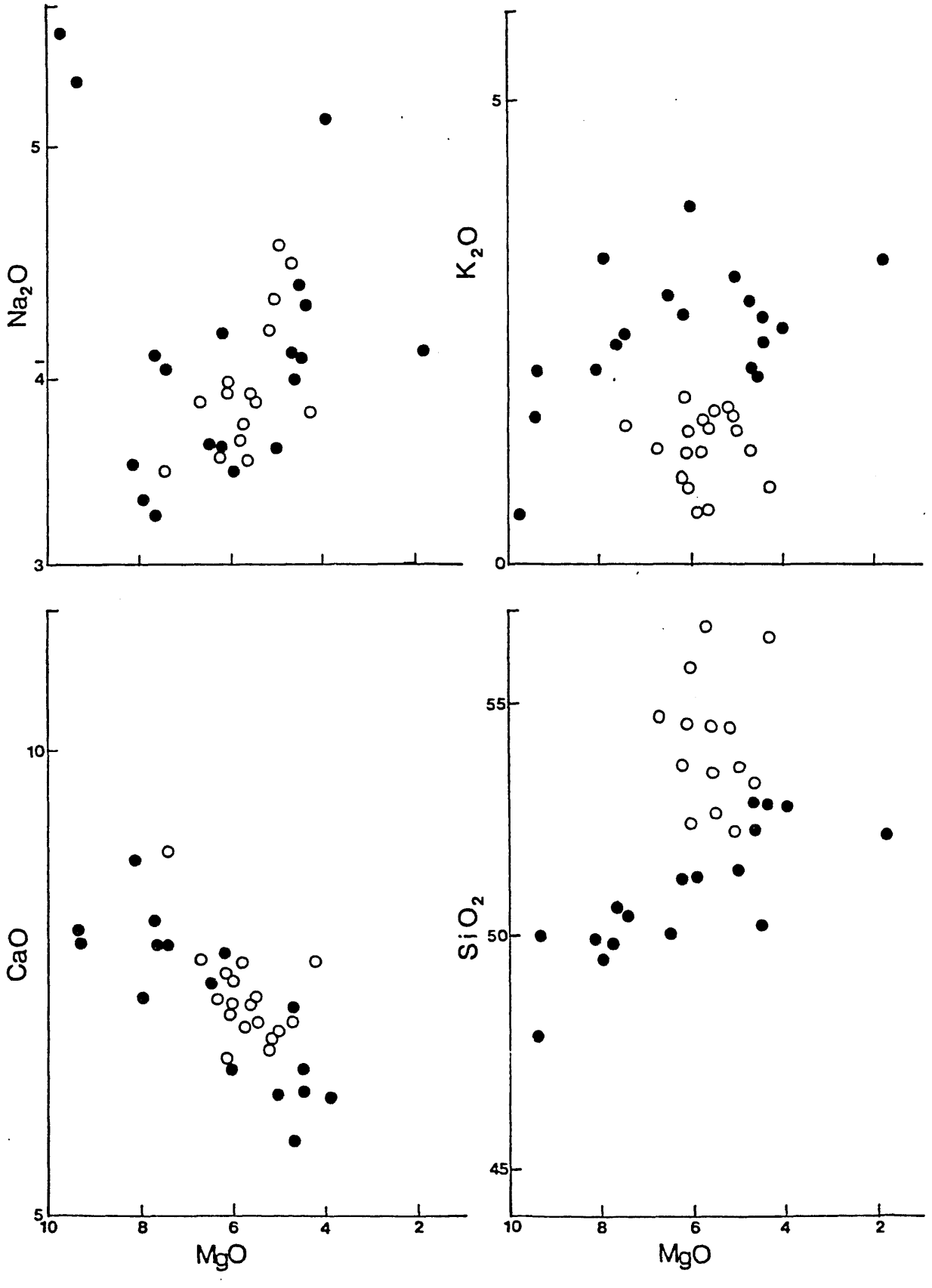

Figure 4.3

Major element chemical variation among selected Plio-Pleistocene volcanic rocks. Symbols as in Figure 4.1.

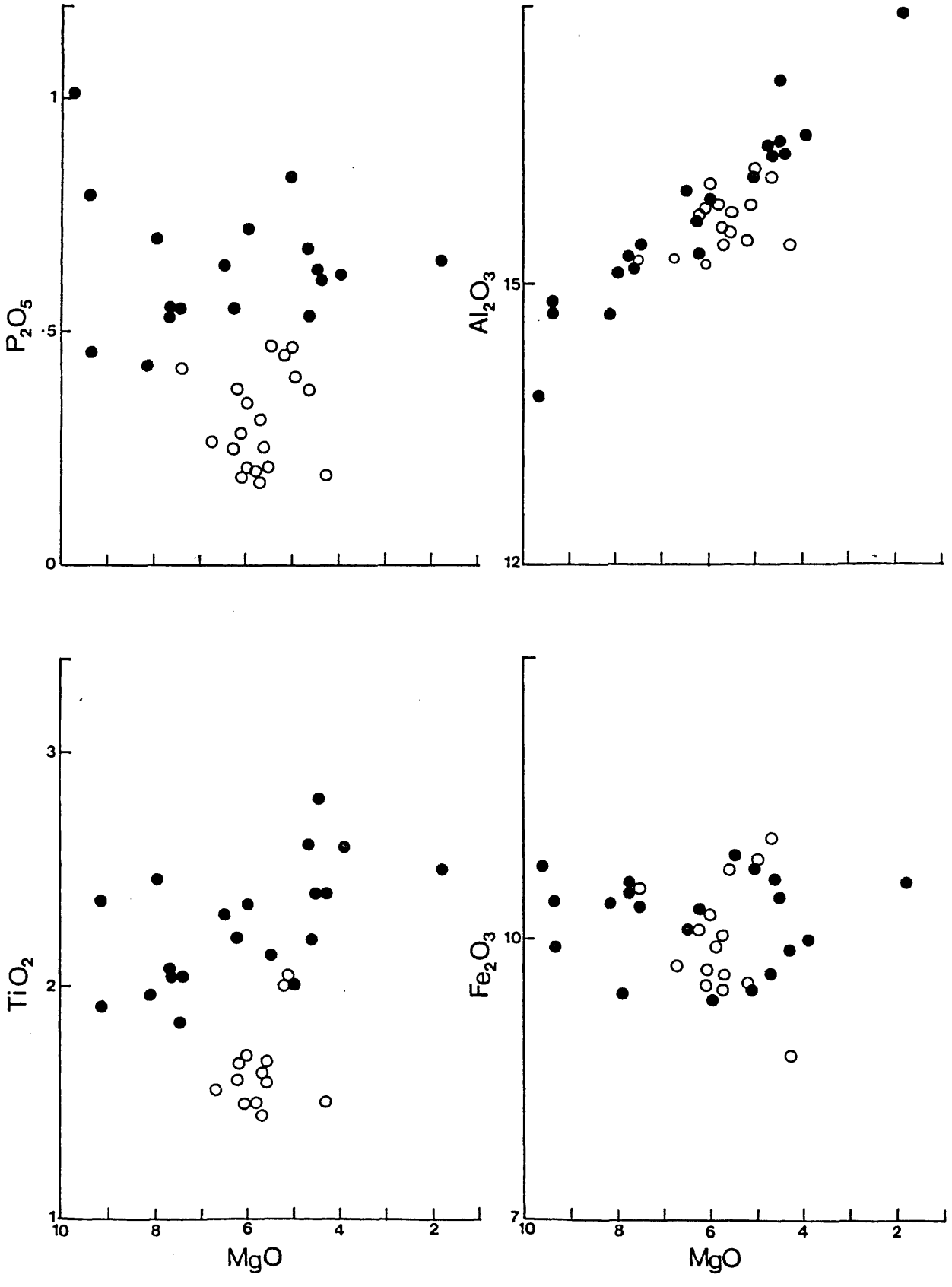
P_2O_5
1
.5
0
Al_2O_3
15
12
TiO_2
3
2
1
Fe_2O_3
10
7
10
8
6
4
2
MgO
MgO

primary mantle-derived melts (Tatsumi, 1981).

Lower K, P and Ti abundances in the high-Mg andesites relative to the basaltic andesites strongly argues against a genetic relationship by fractional crystallisation since such elements are enriched with progressive fractionation assuming apatite, Fe-Ti oxide or sphene are not crystallising. Basaltic andesites and high-Mg andesites may be related by varying degrees of melting of chemically heterogeneous source, or by different amounts of sialic assimilation during magma ascent (see Chapter 7).

4.7 Trace element chemical variation

The chemical variation of some selected trace elements is shown in Figure 4.4, also plotted against MgO. The positive correlation of Ni and Sc, with decreasing MgO, implies that olivine ($D_{Ni}^{ol/l}$ = 14, Henderson, 1981), and clinopyroxene ($D_{Sc}^{cpx/l}$ = 2.7, Henderson, 1981) were important fractionating phases. Constant V abundances preclude significant titanomagnetite removal, which is consistent with observed increase of Ti with decreasing MgO.

Incompatible elements, such as La, Zr, Rb, Th, Be, Rb, Th, Ba, Nb and Sr, do not show good negative correlations with MgO, which suggests that their variation is not directly controlled by fractional crystallisation processes. Their abundances vary by up to a factor of 2, which is too large to be accounted for by the small degrees of fractionation allowed by major element constraints. Sardinian hawaiites are characterised by much higher incompatible element

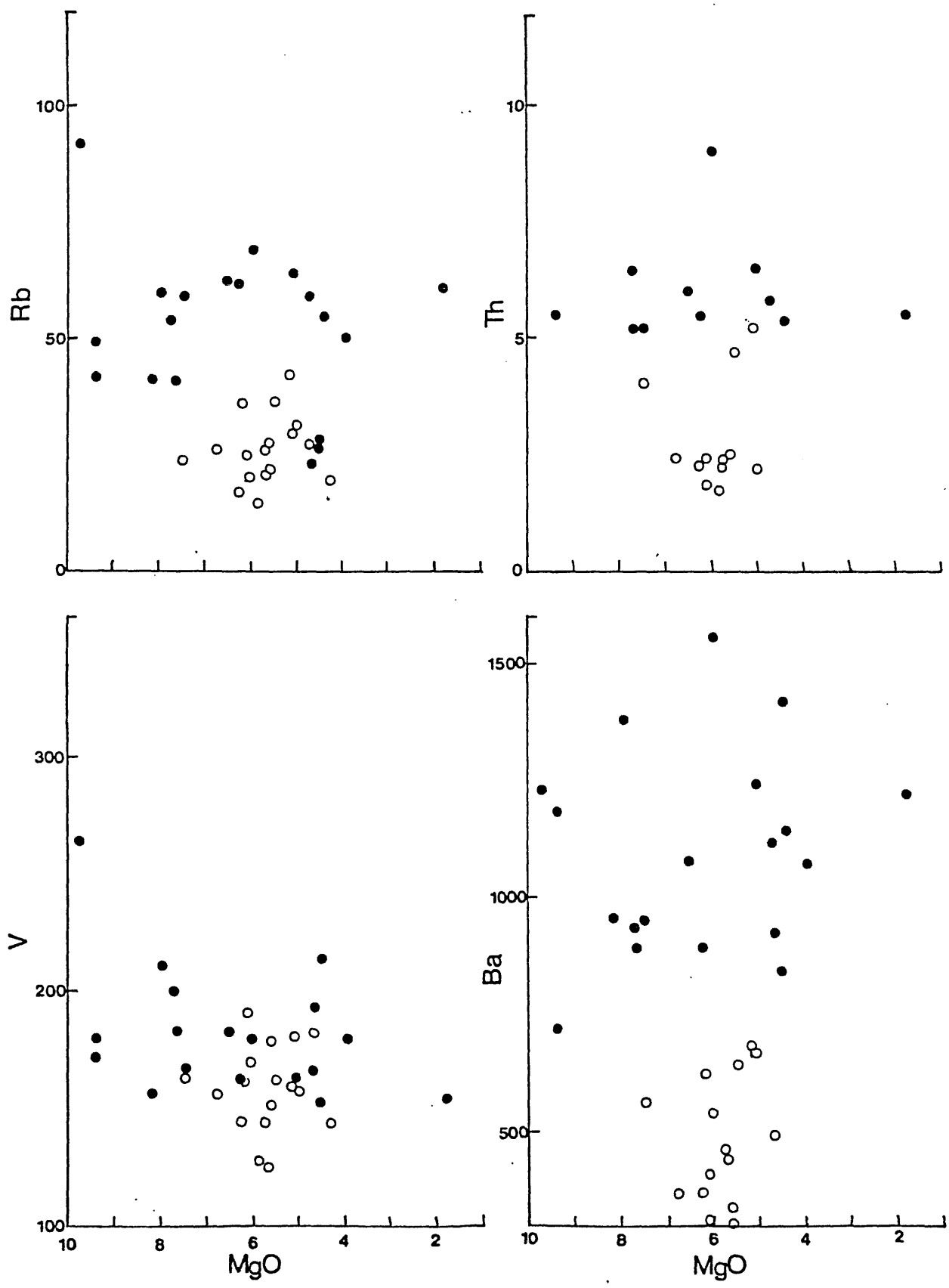

Figure 4.4.

Trace element variation among selected Plio-Pleistocene volcanic rocks. Symbols as in Figure 4.1.

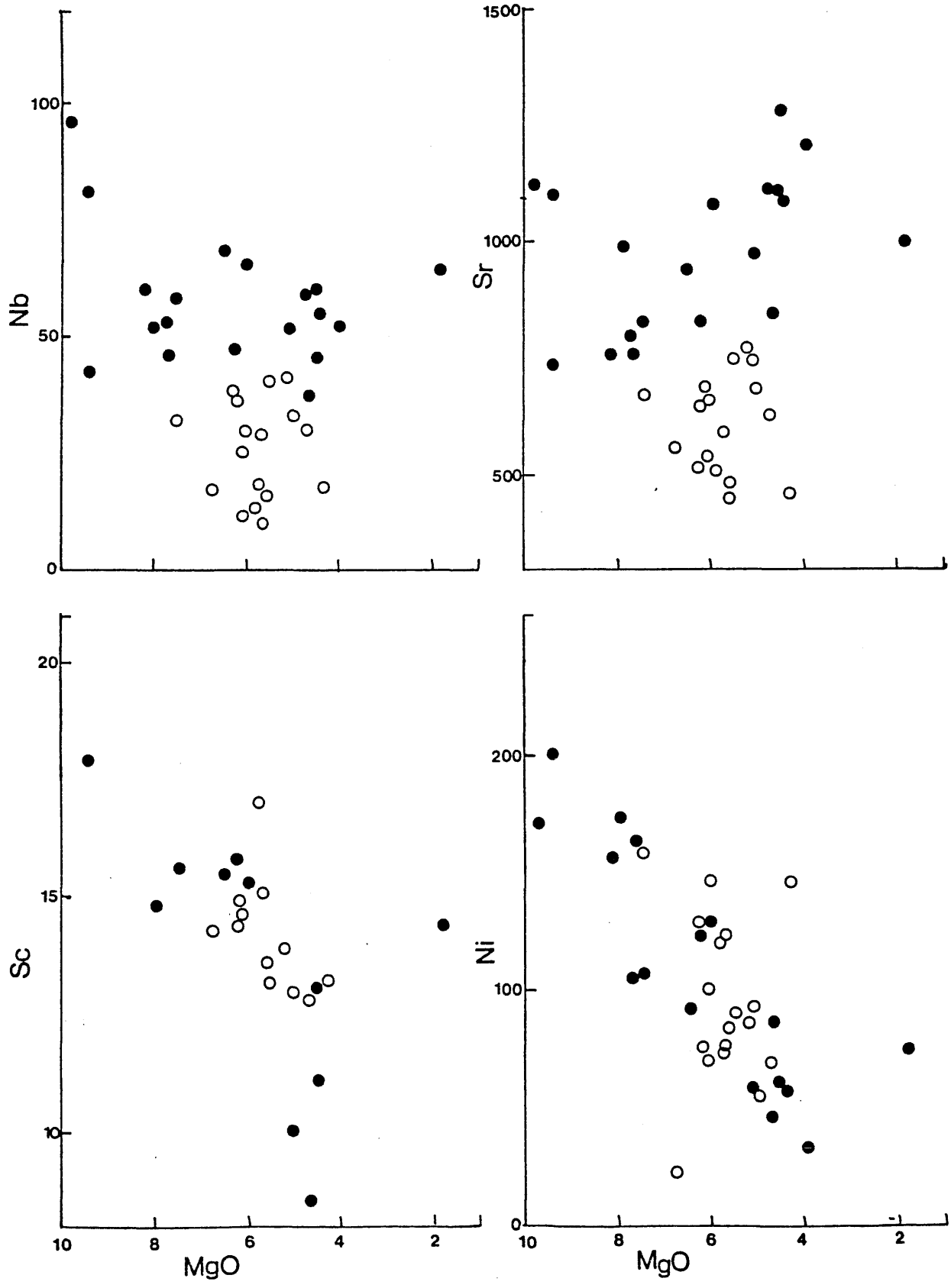
Nb
100
50
0
Sr
1500
1000
500
Sc
20
15
10
MgO
10
8
6
4
2
Ni
200
100
0
MgO
10
8
6
4
2

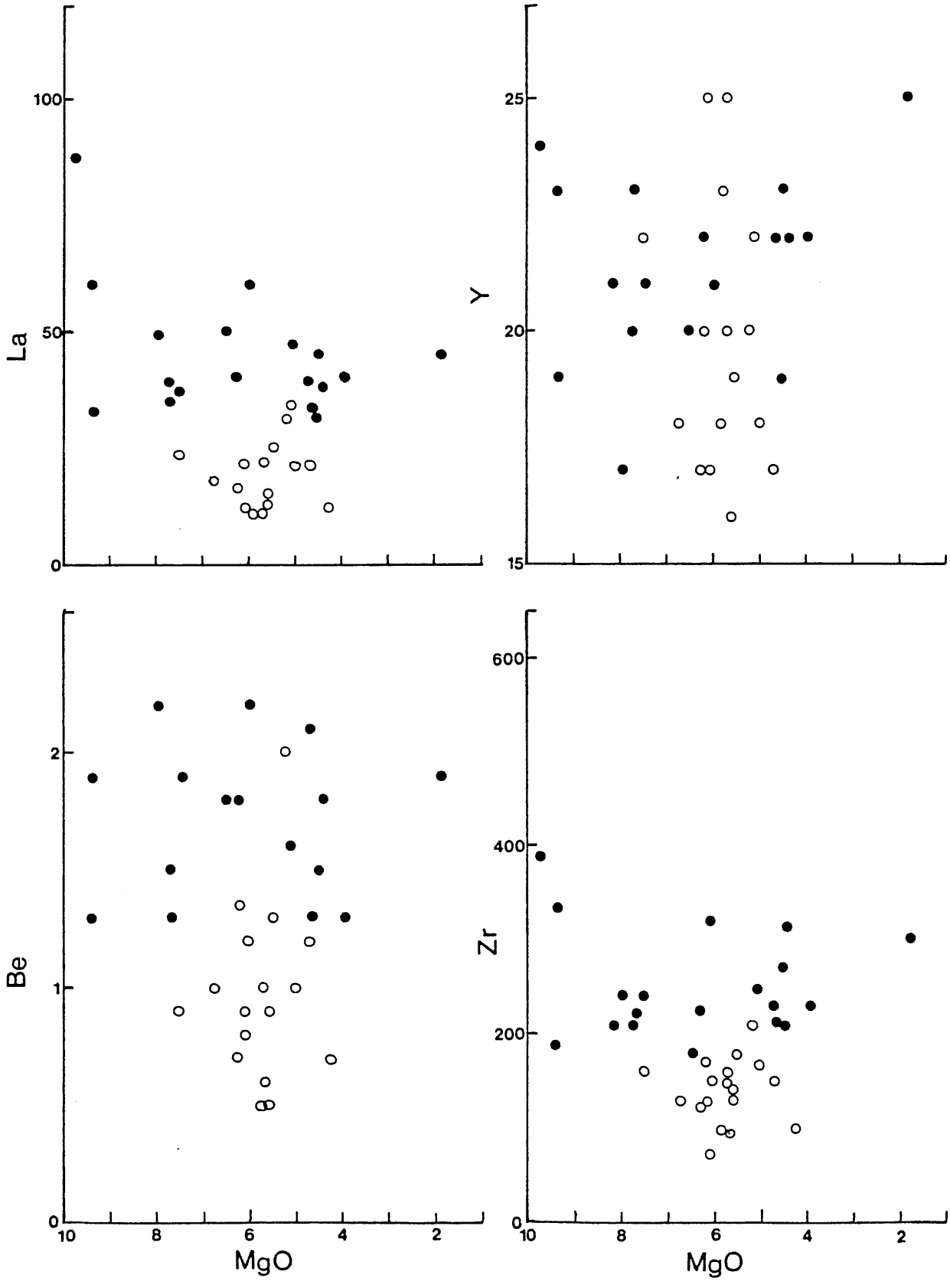
La
100
50
0
Y
25
20
15
Be
2
1
0
Zr
600
400
200
0
10
8
6
4
2
MgO
MgO

abundances than the more siliceous basaltic andesites, which strongly implies that the latter cannot be derived from the former by plausible fractional crystallisation mechanisms, since no probable fractionating assemblage can simultaneously deplete the liquid in Nb, Sr, Rb, Th, Ba, La, Be and Zr while increasing its silica saturation.

More likely, they are derived from different source(s), as envisaged for contemporaneously erupted basanites and sub-alkaline basalts from the Colima Volcanic Complex, Mexico (Luhr and Carmichael, 1982), although the transition from nepheline- to hypersthene-normative lavas at Crater Flat, Nevada, has been successfully modelled by removal of Si-poor amphibole (Vaniman et al, 1982). However, Sardinian hawaiites do not show decreasing Ti and increasing La/Sm with decreasing normative-nepheline (and then increasing normative-hypersthene) and are more likely to be related by varying degrees of partial melting.

4.8 Sr-isotope variation

The Sr isotopic composition of all analysed Plio-Pleistocene volcanic rocks is shown in histogram form in Figure 4.5. The high value of $^{87}Sr/^{86}Sr = 0.70610$ was obtained on a high-Al basalt from Monte Castanza. The remainder of the rocks range from 0.70437 to 0.70558, and such ratios lie well within the field for ocean-island basalts (Figure 4.6). $^{87}Sr/^{86}Sr$ does not show any systematic variation with compatible elements, such as Ni and Cr, which implies that the magmas underwent minimal combined assimilation and

Figure 4.5

Initial Sr-isotope ratios is all analysed Plio-Pleistocene volcanic rocks.

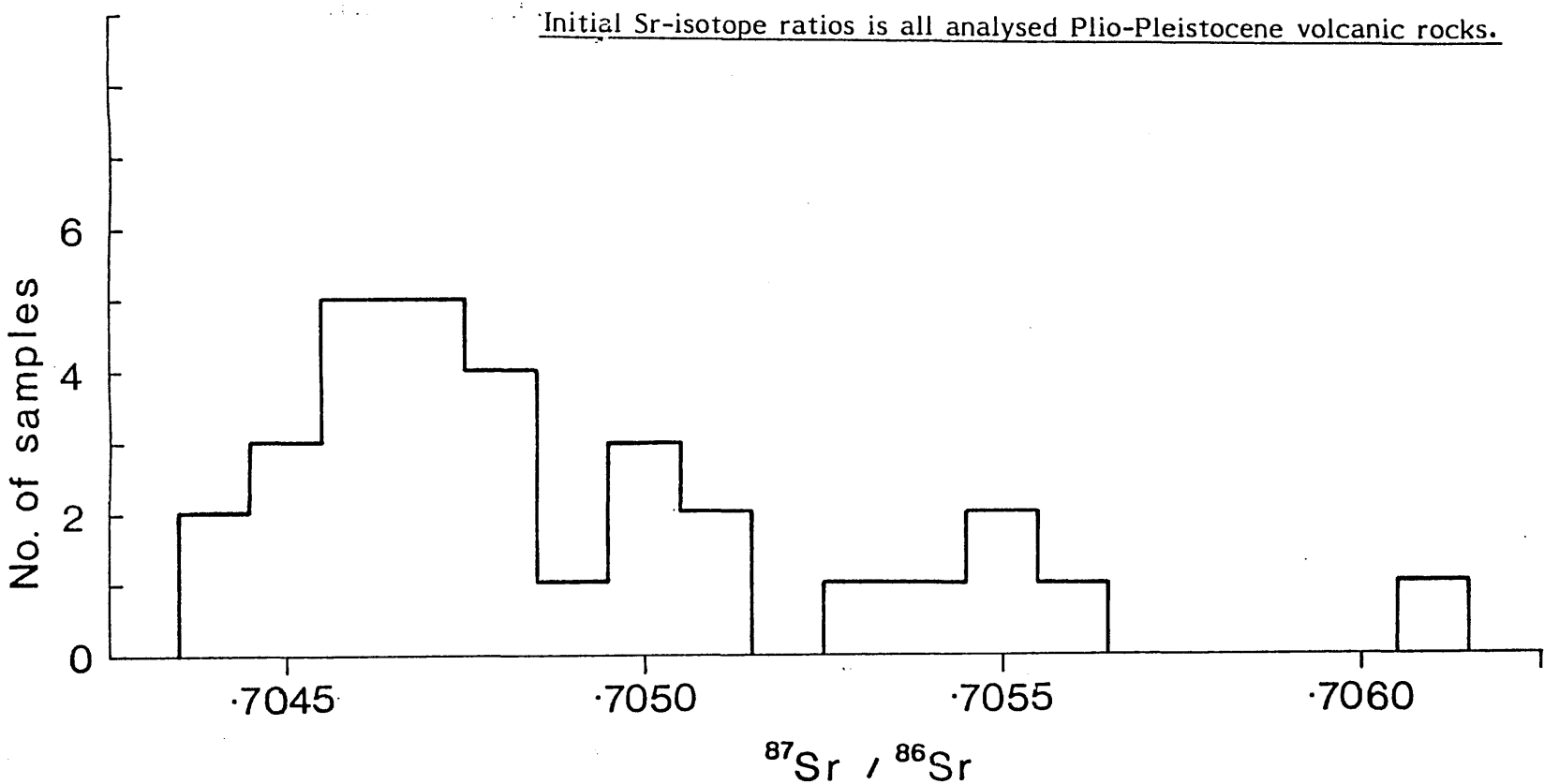

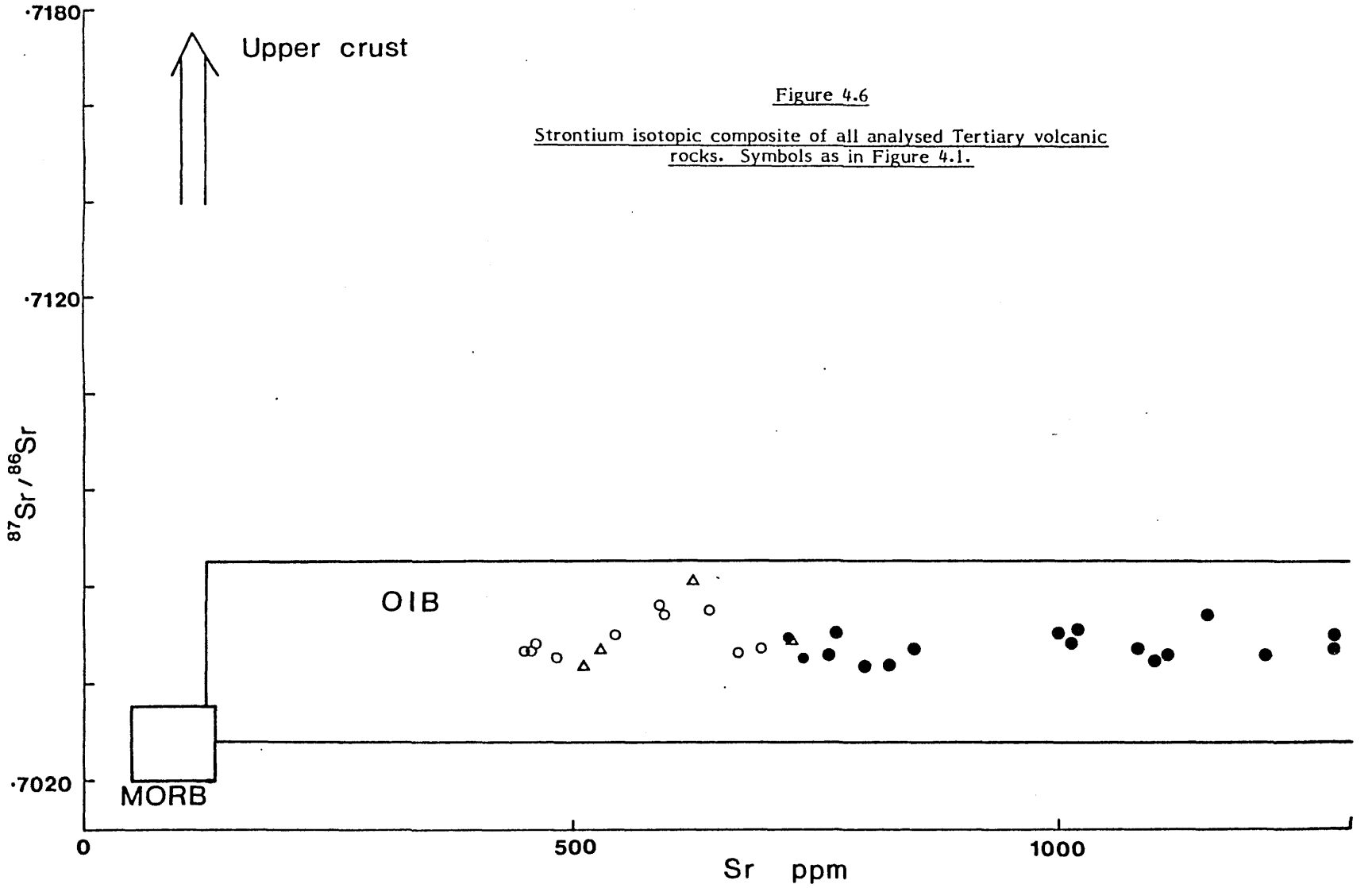

Figure 4.6

Strontium isotopic composite of all analysed Tertiary volcanic rocks. Symbols as in Figure 4.1.

fractional crystallisation within the continental crust. The overlap in Sr isotopic composition between low-K and high-K samples indicates that sialic contamination by high $^{87}Sr/^{86}Sr$ upper crustal rocks was not the dominant processes in generating the observed geochemical variation. However, this does not preclude the possibility of assimilation of time-integrated, low Rb/Sr granulite-facies rocks by mantle-derived magmas.

4.9 REE abundances in Plio-Pleistocene lavas

Selected analyses of Sardinian Plio-Pleistocene volcanic rocks are shown plotted on chondrite-normalised REE diagrams in Figure 4.7 and 4.8. The most important features of their REE patterns are discussed below.

1. Hawaiites and analcite basanites

   Mafic alkaline lavas are strongly enriched in the LREE relative to the HREE, which results in high La/Yb_N = 18.3-42.3. Their sub-parallel REE profiles suggests that they are related by fractional crytallisation processes, possibly involving clinopyroxene and olivine removal (see above). The slight negative Eu anomaly in the pattern for MR23 implies minor plagioclase fractionation. High LREE/HREE ratios are consistent with the presence of residual garnet during partial melting.

Figure 4.7

Chondrite-normalised REE data for selected Plio-Pleistocene hawaiite and basanite lavas. Filled squares = MR23; open squares = K138; filled triangles = K68; and open triangles = K33.

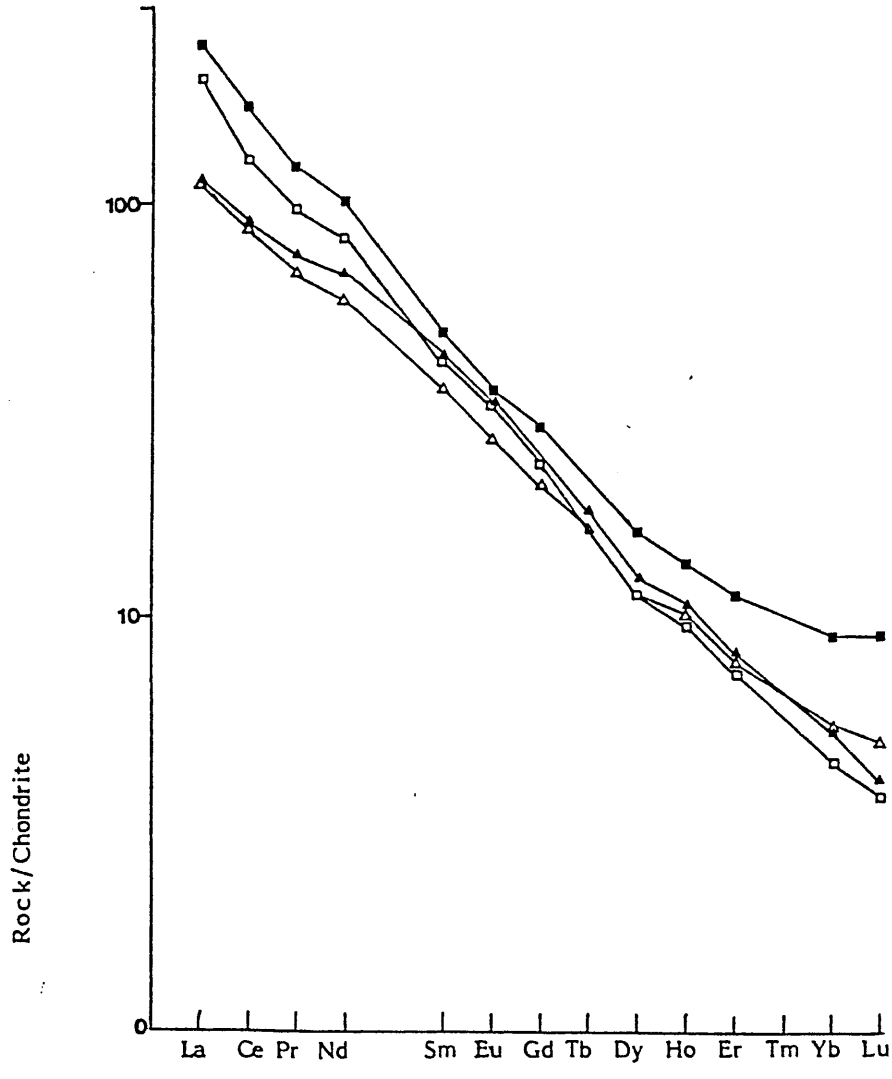

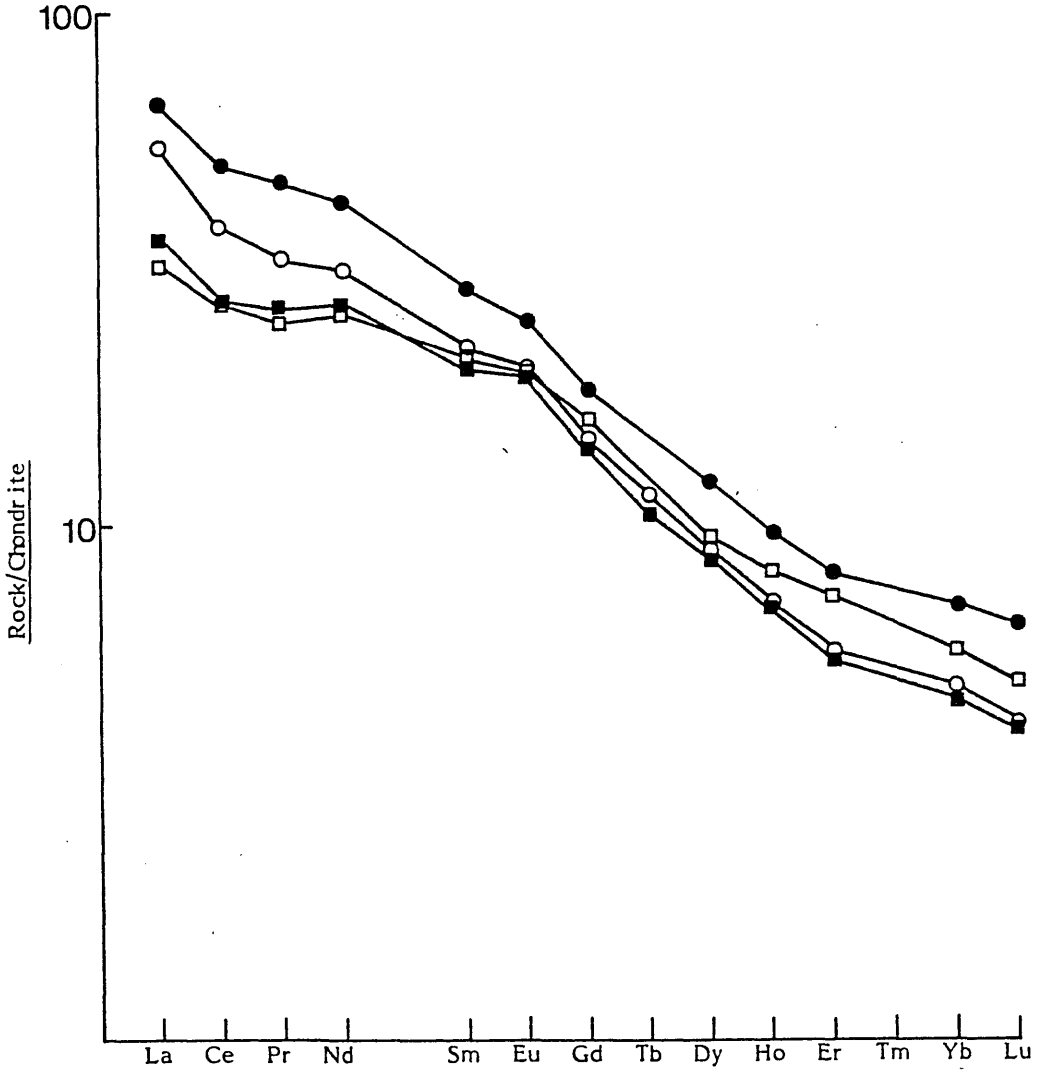

Figure 4.8

Chondrite-normalised REE data for some selected Plio-Pleistocene basaltic andesite and high-Mg andesite lavas. Open squares = PS7; filled squares = K43; open circles = K85; and filled circles = K110.

2. Basaltic andesites and high-Mg andesites

These are characterised by lower LREE/HREE ratios than the hawaiites, with La/Yb_N = 7.1-16.6. The most noteworthy feature of their REE profile is a concave-upwards pattern at the left-hand side of the diagram. Separate REE analyses on the same samples by both I.N.A.A. and ICP imply that this curvature is indeed real, and not an artefact of the analytical proceedure. The origin of the pattern is unclear. It may reflect retention of Ce and Pr in some residual phase during partial melting, or possibly to mixing of 2 compositionally-distinct end-members, one of which is LREE-enriched, and the other LREE-depleted. Many samples show a minor positive Eu anomaly, which may be due to the accumulation of plagioclase phenocrysts in the magma because of the preference of Eu for the Eu^{2+} state and its substitution in the plagioclase lattice.

CHAPTER 5

ELEMENTAL AND ISOTOPIC EVIDENCE RELATING TO THE SOURCE OF SARDINIAN SUBDUCTION-RELATED MAGMAS

Major and trace element variation within the subduction-related mafic rocks (< 52 wt. % SiO_2) of N.W. Sardinia has been shown to reflect low pressure fractionation of an anhydrous mineral assemblage consisting of plagioclase, olivine, clinopyroxene and titanomagnetite (see Chapter 3). High FeOT/MgO ratios of >1.8 indicate that the least evolved basalts could not have been in equilibrium with mantle olivine (FeOT/MgO = 0.7 in primary mantle-derived magmas; Irvine, 1971). Sardinian high-Al basalts have possibly differentiated from Mg-rich precursors by olivine and Cr-spinel removal (see also Reid and Nye, 1981).

Geochemical parameters of lavas, independent of any differentiation processes, can be used to infer some chemical characteristics relating to the composition of their magma source. Ratios of strongly incompatible elements are generally thought to be differentiation-independent (Kay, 1984), except for very small degrees of melting when matrix/melt fractionation becomes important (McKenzie, 1984).

Incompatible element ratios, and the strontium isotopic composition (another differentiation-independent characteristic) of magmas can be modified by interaction with sialic material during the ascent of mantle-derived magmas through the continental crust. It is consequently difficult, in regions of continental margin orogenic volcanism, to distinguish the effects of crustal contamination during magma ascent, from the re-cycling

of sedimentary material back into the mantle source of calc-alkaline magmas via subduction zones.

5.1 Magma generation in subduction-related tectonic settings

The generation of subduction-related mafic magmas during the Tertiary in northwestern Sardinia involves contributions from a variety of source rocks, which may include:-

1. Mantle peridotite in the asthenospheric mantle wedge above the subducted slab;
2. Subducted oceanic lithosphere, which consists of:
   (a) Variably metamorphosed (up to eclogite facies) ocean-floor basalts and gabbro;
   (b) Serpentinite;
   (c) Pelagic sediments, including calcareous nannofossil oozes, deep sea clays and siliceous radiolarian oozes;
   (d) Continent-derived clastic sediments.
3. Sea water via hydrothermal circulation at mid-ocean ridges, and concomitant alteration of ocean-floor basalts;
4. Sub-continental mantle lithosphere;
5. Assimilation of sialic material during the ascent of magmas through the continental crust.

5.2 Mantle peridotite source for subduction-related magmas

Partial melting of eclogite within the subducted oceanic crust is constrained by the results of experimental petrology to melts of basaltic andesite composition, although higher temperatures than normally envisaged within the mantle wedge are required to induce melting (Wyllie, 1984). Kay and Kay (1982) note the similarity between primitive melts in subduction-related

tectonic settings, and experimentally-determined melts of spinel lherzolite. They conclude that primitive Aleutian arc basalts can be derived from mid-ocean ridge basalt (MORB)-source mantle. The major element data, however, are also consistent with partial melting of a garnet lherzolite source, similar to the source of ocean-island basalts (OIB). The addition of water from the subducted slab to the mantle source of subduction-related magmas will cause an increase in the silica-saturation of the derivative melts (Wyllie, 1984), and may account for some of the differences between oceanic and subduction-related magmas.
The elemental composition of Sardinian subduction-related basalts is discussed below in terms of those chemical features which are characteristic of their possible source components.

5.3 Elemental characteristics of Sardinian subduction-related basalts

Major element geochemistry cannot unambiguously distinguish between an OIB or MORB source in the genesis of subduction-related magmas. Minor and trace elements, however, are more sensitive indicators of magma genesis. Selected analyses of Sardinian subduction-related mafic rocks are shown in the form of chondrite-normalised plots in Figure 5.1. Details of the normalisation proceedure are given in Appendix F. The elements are arranged in a general order of increasing incompatability from right to left of the diagram. Comparative multi-element patterns for representative subduction-related basalts from the Marianas Islands (Hole et al,1984),

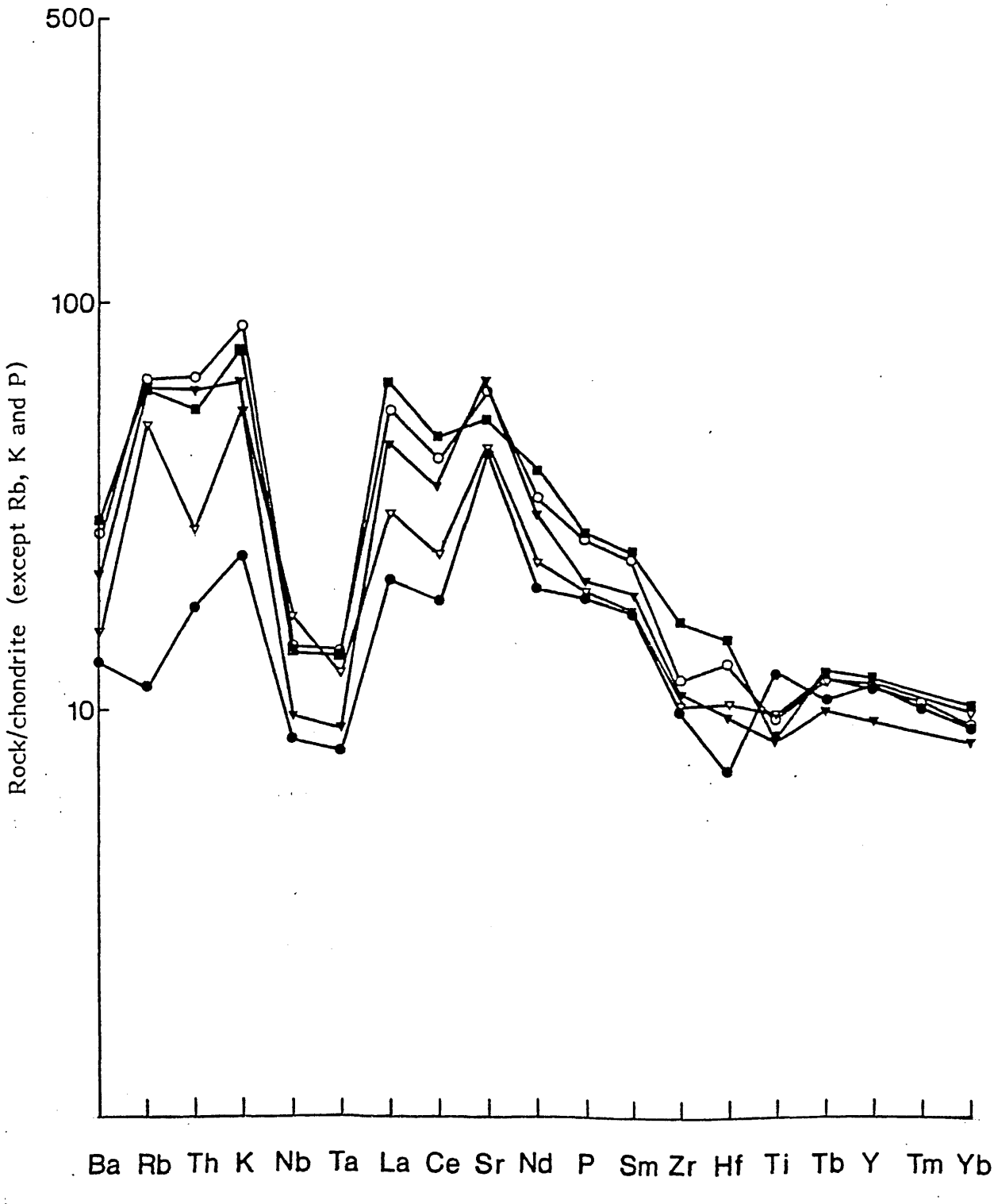

Figure 5.1

Chondrite-normalised multi-elements diagram for Sardinia subduction-related lavas. Open circles = K94; filled squares = K1; filled triangles = MR14; open triangles = MR17; and filled circles = MR20

and the Lesser Antilles (Baker, 1984) are shown in Figure 5.2. All the patterns in Figures 5.1 and 5.2 are remarkably similar. All the samples in Figure 5.1 are enriched in the large-ion lithophile elements (LILE), mostly those elements on the left-hand side of the diagram, relative to the small and highly-charged high-field strength elements (HFSE) such as Y, Nb, Ta, Zr, P, Ti and HREE. This is a characteristic feature of all calc-alkaline mafic rocks (Pearce, 1982; Figure 5.2). Although most of the elements in Figure 5.1 are incompatible, decreasing Ti/Tb and Sr/Ce ratios with increasing La abundance (which reflects evolution of the melt by crystal fractionation processes) indicate progressive titanomagnetite and plagioclase fractionation, respectively. Vanadium is a good indicator of titanomagnetite fractionation, and shows a strong negative correlation with Rb, which behaves incompatibly throughout the differentiation of this rock suite (see Chapter 3).
A further noteworthy feature of the basalts in Figure 5.1 are the low abundances of Nb and Ta, which result in a prominent trough on their chondrite-normalised patterns. The chondrite-normalised pattern for MR20 (Figure 5.1) shows a trough at Zr and Hf relative to the adjacent elements, which would be expected if zircon was a residual phase during magma genesis (Saunders et al, 1980). Because of the high mineral/matrix partition coefficient for Th in zircon, however, residual zircon in the mantle source should produce a trough at Th in the chondrite-normalised pattern, which it does not.

Figure 5.2

Chondrite-normalized multi-element diagram for representative subduction-related rocks. Open squares = Lesser Antilles (Baker, 1984); filled triangles = Marianas arc (Hole et al, 1984); and filled squares = Warner flow, California (Thompson et al, 1984)

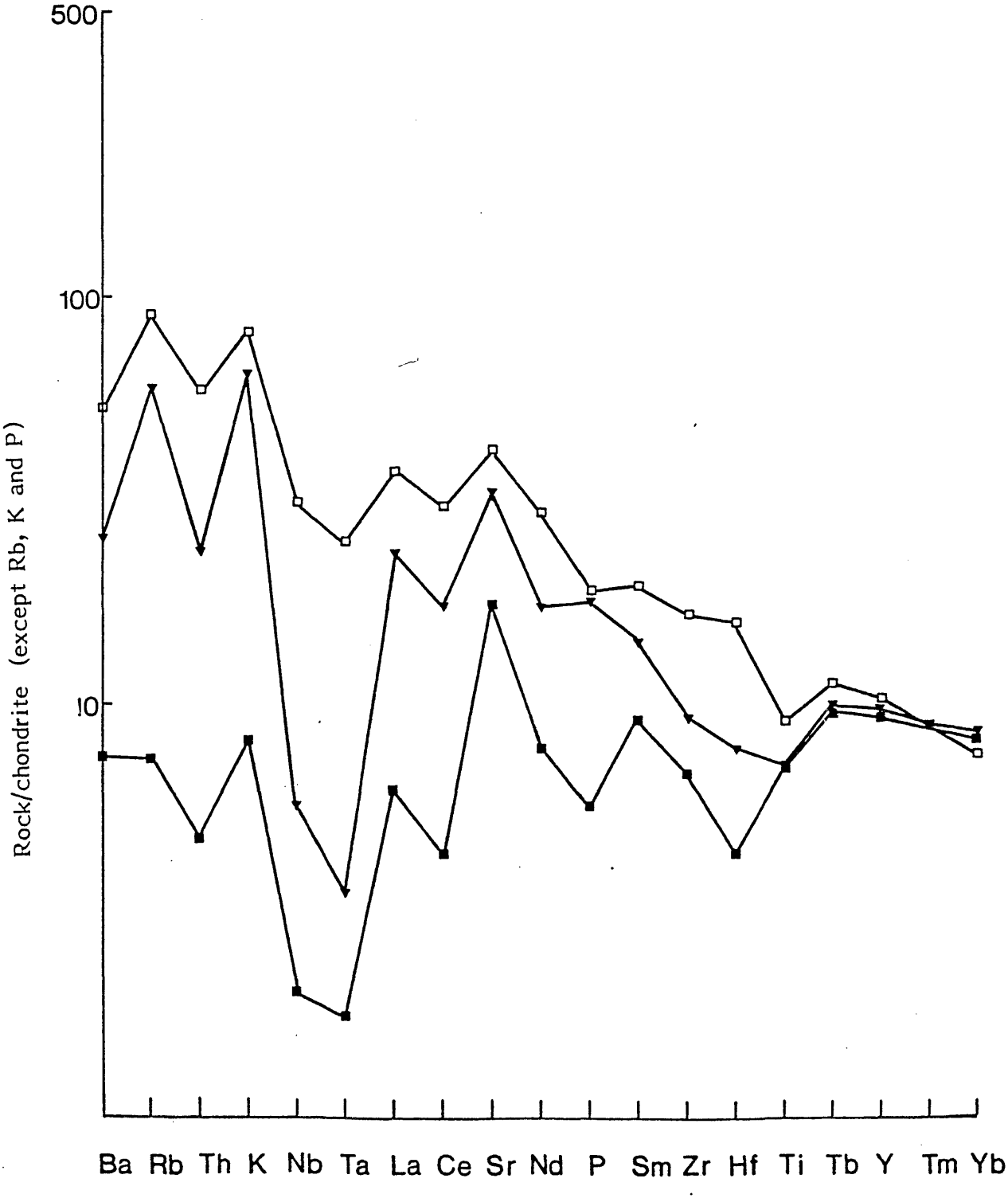

The similarity in their chondrite-normalised patterns between Sardinian subduction-related basalts in Figure 5.1, and mafic rocks from island arcs, such as the Lesser Antilles and the Marianas, in Figure 5.2, indicates that the typically subduction-related geochemical signature of Sardinian high-Al basalts is inherited not from any significant interaction with crystalline basement rocks during ascent of magma through the continental crust, but from their upper mantle source region.

Low abundances of Nb and Ta are a ubiquitous feature of subduction-related mafic rocks (Saunders and Tarney, 1982). Chondrite-normalised La/Nb (La/Nb_N) ratios of 3.9-4.6 in basaltic rocks from northwestern Sardinia are substantially higher than in either MORB or OIB, and within the range for island arc volcanic rocks (Thompson et al, 1983),

Strong relative Nb and Ta depletion in island arc volcanics has been explained by the retention of these elements in some residual Ti-rich mineral, such as perovskite, sphene or rutile, which is stable under hydrous conditions during partial melting of the source of subduction-related magmas (Saunders et al, 1980). Thompson et al (1984) have pointed out that since Ti does not always correlate with Ta and Nb (see also MR20, this work), this phase is not necessarily titaniferous. Perovskite will also act as a host for the REE (Carmichael, 1967), and should effect significant fractionation of LREE from HREE, which is not observed.

Pelagic sediments, which may, or may not be recycled into the upper mantle at subduction zones, are characterised by low abundances of Nb and Ta. Kay (1984) suggested that high La/Nb(Ta) ratios in subduction-related basalts may be related to the addition of a small component of subducted pelagic sediment to their upper mantle source. There is a considerable amount of isotopic evidence supporting the involvement of recycled subducted sediment in magma genesis at subduction zones.

5.4 Isotopic evidence for the recycling of pelagic sediment via subduction zones

High $^{208}Pb/^{204}Pb$ and $^{207}Pb/^{204}Pb$ in island arc volcanics (IAV) relative to most oceanic basalts implies a component of subducted sediment in the genesis of calc-alkaline rocks (Barreiro, 1984), although the magnitude of sediment involvement has been constrained to only a few percent (Meijer, 1976). High abundances of cosmogenically-produced ^{10}Be in some IAV, relative to fresh oceanic basalts, provides convincing evidence for sediment subduction (Brown et al, 1982). Further, some IAV are enriched in isotopically-light carbon relative to MORB and Hawaiian basalts, which implies the incorporation of an organic component, possibly derived from subducted pelagic material, into their mantle source (Mattey et al, 1984). High $^{87}Sr/^{86}Sr$ ratios in IAV relative to MORB have also been interpreted in terms of the addition to MORB-source mantle of a radiogenic-Sr enriched component from subducted oceanic lithosphere (Hawkesworth and Powell, 1980). However, $^{87}Sr/^{86}Sr$ ratios in IAV overlap with

the field defined by OIB, and an OIB (not MORB) source for JAV has been proposed by some authors (e.g. Morris and Hart, 1983). Such a model is discussed later.

Thus, there is sufficient isotopic evidence to suggest that sediments are recycled via subduction zones, although such recycling may be limited to only a few percent. The composition of sediments subducted beneath Sardinia during the Oligo-Miocene is unknown, and therefore, models of magma genesis involving subducted sedimentary material are poorly constrained. However, some of the more important geochemical features of pelagic sediments, relevant to magma genesis, are discussed below.

5.5 Geochemistry of pelagic sediments

Chondrite-normalised multi-element patterns for a Pacific pelagic calcareous nannofossil ooze (U120, this work), and a deep sea clay (compiled from the literature) are shown in Figure 5.3. U120 was dredged from the Pacific ocean floor, and represents the homogenised top 10 cm of the sediment column (Hodkinson, pers. comm.). Both the patterns are characterised by strong relative depletions of Nb, Ta and Ti, which results in high La/Ta = 630-794 and Y/Ti = 0.03-0.16 ratios. The chondrite-normalised pattern for U120 shows a prominent peak at Sr, which reflects the high carbonate content of the sediment. All the carbonate is in the form of calcite, and Sr^{2+} substitutes for Ca^{2+} in the calcite structure. Sr-barytes is not a host for Sr in U120 because separate aliquots of U120 dissolved up separately using both HF (which does not attack barytes) and $LiBO_4$ (which does) dissolution

Figure 5.3

Chondrite-normalized multi-element diagram for a Pacific nannofossil ooze (U120; filled triangles); and a 'typical' Pacific deep sea clay (filled squares).

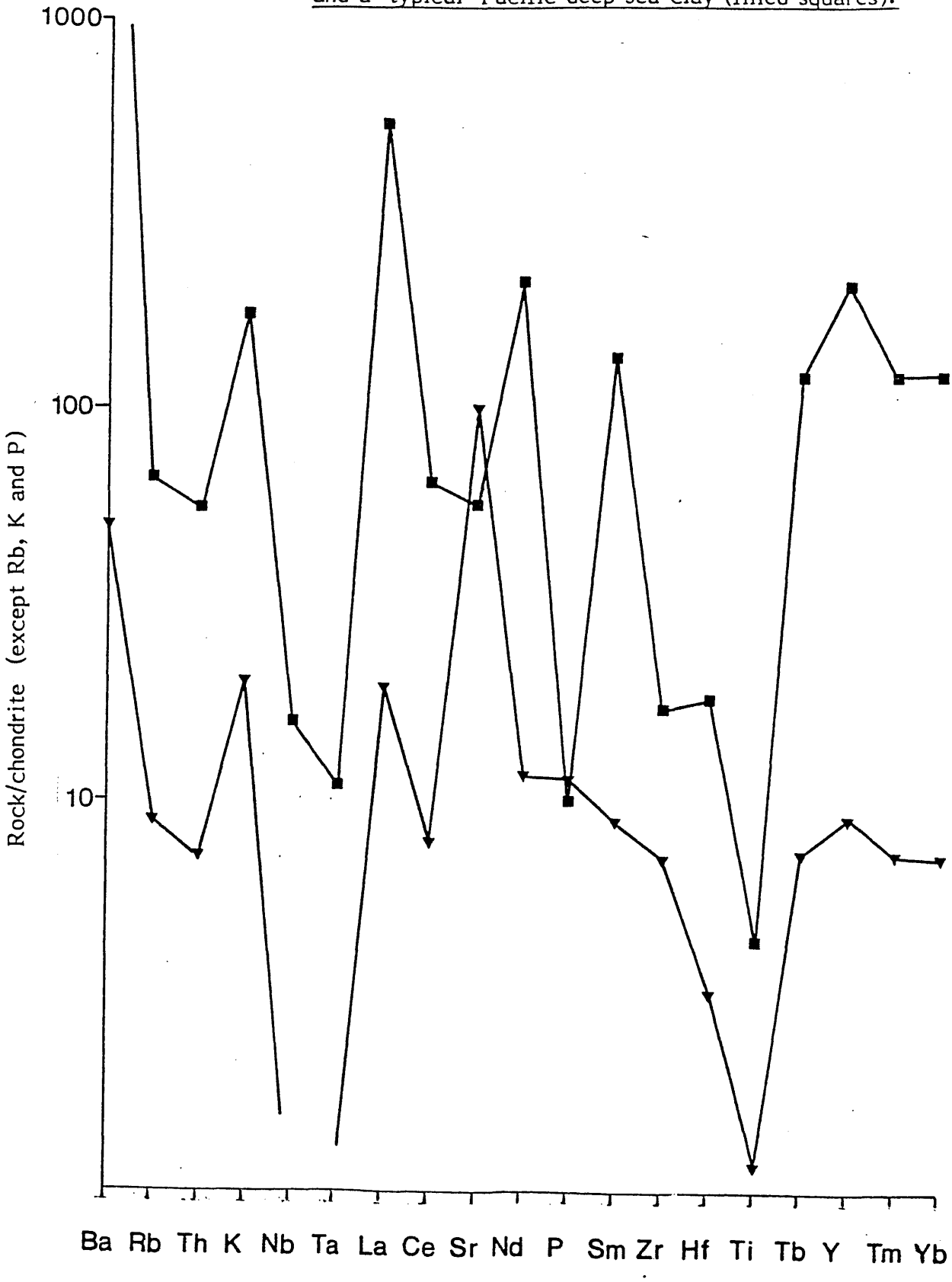

proceedures, give similar Sr abundances when analysed by ICP.

Ba is enriched relative to the other LILE, resulting in high ratios of Ba/Rb > 111, Ba/Th > 1236 and Ba/K > 0.14. Ba occurs predominantly in the form of barytes in pelagic carbonate oozes, which is precipitated from hydrothermal fluids on the sea floor. The deep sea clay in Figure 5.3 is characterised by much higher absolute abundances of all the elements, except Sr. The HREE, for example, are enriched by about 100x chondrite in the deep sea clay. Kay (1984) has analysed a variety of sediments for some important trace elements. He reports low Ba/La and high Cs/Ba ratios in zeolite-bearing clays, and notes that such ratios do not resemble those found in 1AV. Deep sea clays contain variably high Ba and Cs abundances, and siliceous radiolarian oozes show high Ba/La ratios (Kay, 1984).

The REE patterns of some selected Pacific calcareous nannofossil oozes (this work) are shown in Figure 5.4. Also shown are the REE patterns of some deep sea clays (Kay, 1984). All the analysed sediments show a pronounced negative cerium anomaly, resulting in low Ce/Ce* ratios of 0.38-0.57 in the nannofossil oozes ($Ce^* = (La_N + Pr_N)/2 \times 0.865$). They are also variably depleted in Eu, which results in high Sm/Eu_N ratios of 1.2-2.2. Ce is unique among the otherwise trivalent REE cations in having a preference for the Ce^{4+} state in sea water. Ce^{4+} is generally more readily incorporated into ferromanganese nodules relative to the other REE, which may explain its relative depletion in pelagic sediments (Murphy and Dymond, 1984).

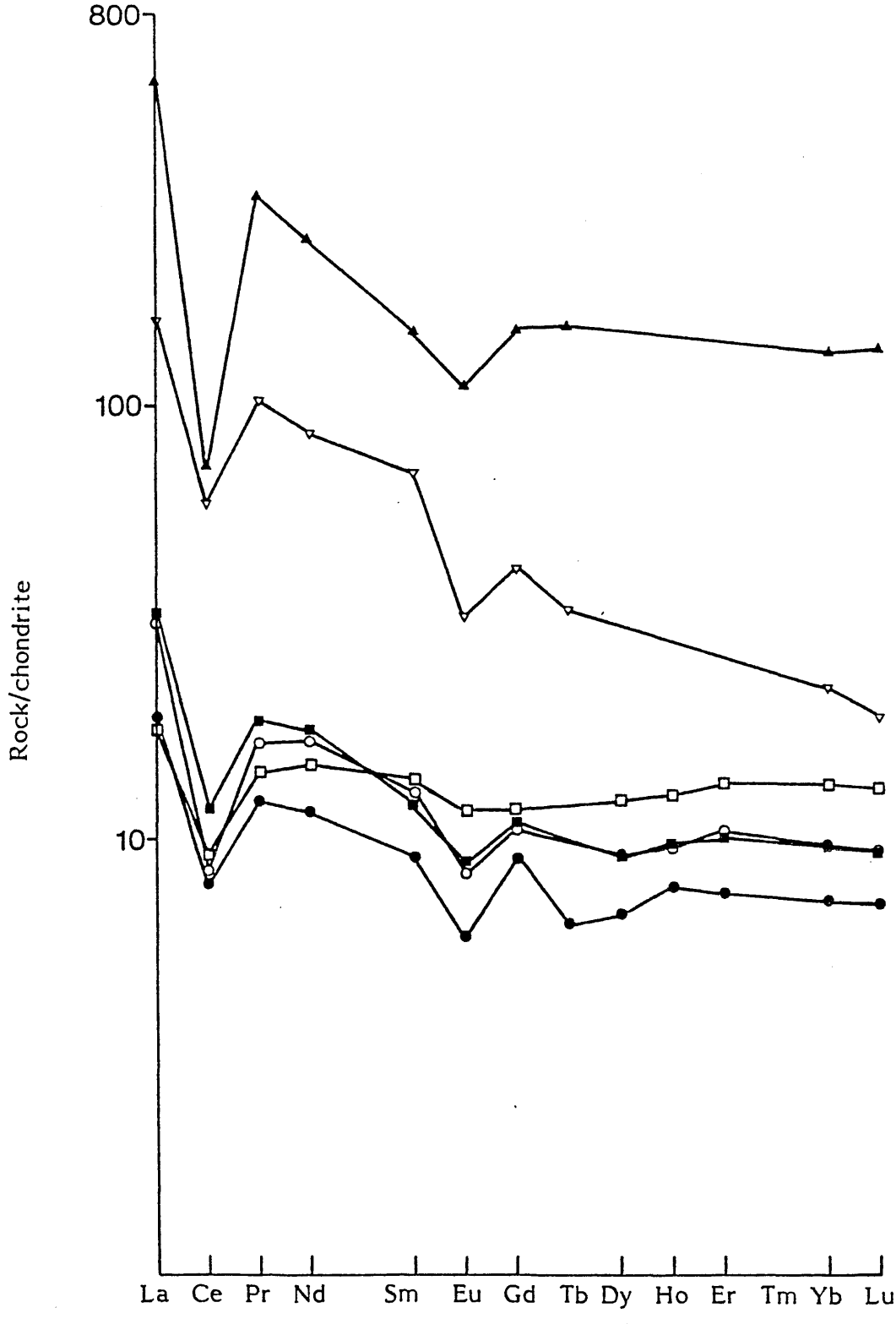

Figure 5.4

Chondrite-normalized REE patterns for some pelagic sediments from the Pacific. Filled squares = U69; open squares = U64; Open circles = U66; and filled circles = U120 (all this work); open triangles = 170; and filled triangles = 319 (Kay,1984)

The REE geochemistry of Sardinian basaltic rocks is discussed below in terms of the possible input of a sedimentary component into their mantle source.

5.6 REE geochemistry of Sardinian mafic rocks

Negative Ce anomalies in some IAV may indicate the input of a pelagic sedimentary component into the mantle source of subduction-related magmas (Dixon and Batiza, 1979). However, Ce depletions are not always associated with subduction-related basalts (White and Patchett, 1984), and neither have they been observed in fresh oceanic basalts.

The REE patterns of some high-Al basalts from N.W. Sardinia are shown in Figure 5.5. Most, but not all, of the analysed samples show a negative Ce anomaly, with $Ce/Ce^* = 0.9$, which is consistent with the addition of a small amount of subducted pelagic sediment to their mantle source. The Ce depletion can be modelled in terms of the addition of $< 1\%$ of pelagic sediment to a MORB-source mantle, which is consistent with the amount suggested by Hole et al (1984) for the Mariana arc lavas. However, addition of pelagic sediment to the mantle source of subduction-related magmas should produce a negative Eu anomaly, in addition to the observed Ce depletion, because of the high Sm/Eu ratios of deep sea clays and calcareous oozes. Such a large Eu depletion has not been observed in Sardinian basaltic rocks (except for sample MR20). White and Patchett (1984) invoke oxidising conditions within the subducted slab to explain negative Ce anomalies in calc-alkaline basalts by retention of Ce^{4+}, relative to the other trivalent REE cations, within subducted oceanic lithosphere.

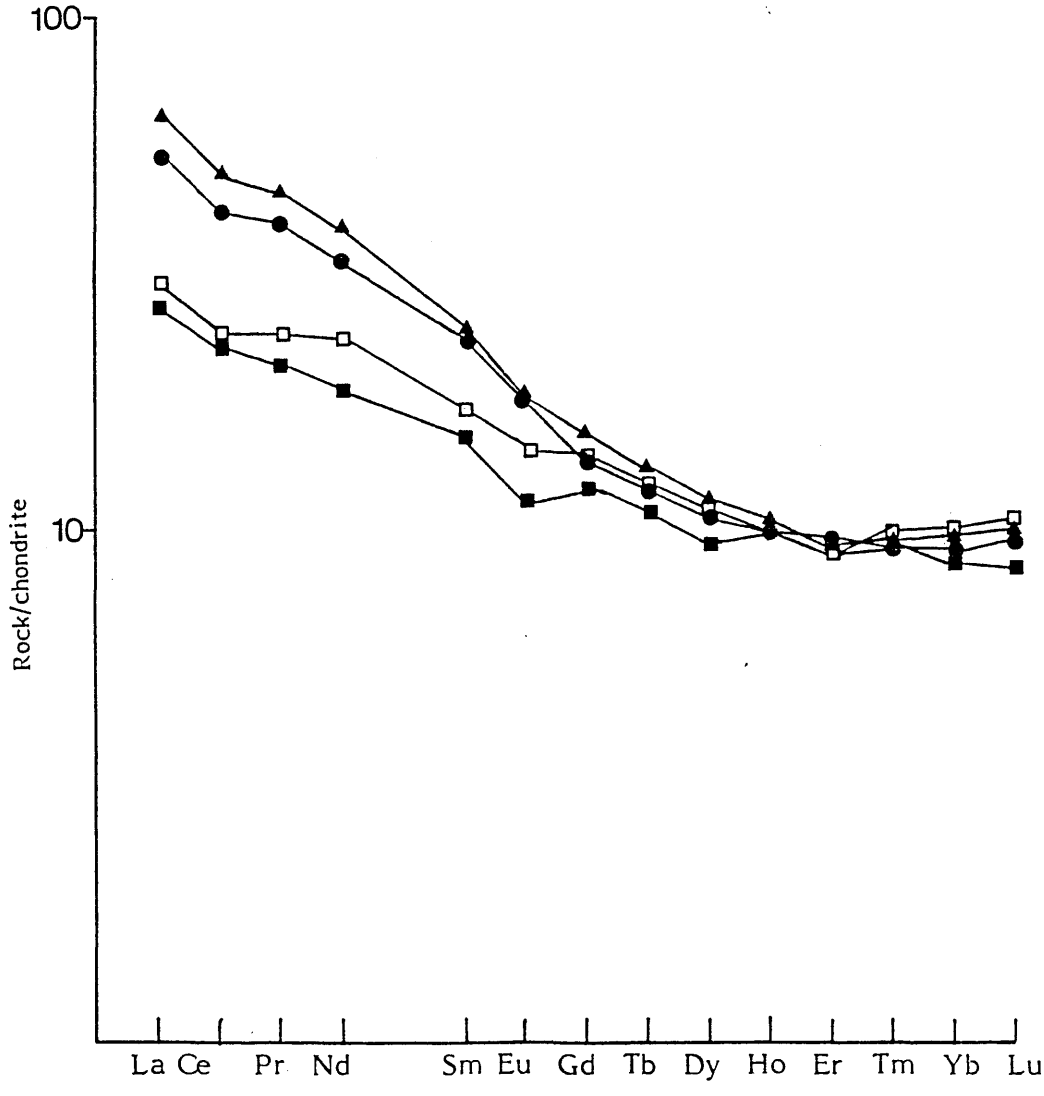

Figure 5.5

Chondrite-normalized REE patterns for some selected Sardinian high-Al basalts. Filled triangles = K1; filled circles = K94; open squares = MR17; and filled squares = K101.

The Sr-isotopic composition of Sardinian magmas has been shown to reflect AFC processes within upper crustal magmas chambers, and is not a mantle source characteristic (see Chapter 3). However, there is some isotopic evidence for the involvement of subducted pelagic sediment in magma genesis at island arc subduction zones (see above), where there is no possibility of sialic contamination during magma ascent. It is the purpose of the following section to assess how far the elemental signature of Sardinian basaltic rocks can be explained by the involvement of oceanic lithosphere in magma genesis.

5.7 MORB plus subducted sediment source for Sardinian basalts?

Basaltic rocks with MORB-like affinities have been drilled from the floor of the Tyrrhenian Sea Basin (Barberi et al, 1978; Deitrich et al, 1978). Chondrite-normalised multi-element patterns for two of these rocks are shown in Figure 5.6, and they show a LILE-depleted profile, similar to Icelandic E-type MORB (Wood et al, 1979). In Figure 5.7 a Sardinian high-Al basalt (MR17) has been normalised to a Tyrrhenian E-type MORB. MR17 is enriched in Ba, Rb, Th, K, Sr, La, Ce, Nd, P and Sm, but depleted in Nb, Ta, Ti, Y and the HREE, relative to this Tyrrhenian basalt.

Ba, Rb, Th, K and Sr are all elements of low ionic potential, and are readily soluble as chlorides in aqueous fluids. Their relative enrichment in subduction-related magmas may result from the addition to mantle peridotite of aqueous fluids enriched in these elements, released from clays,

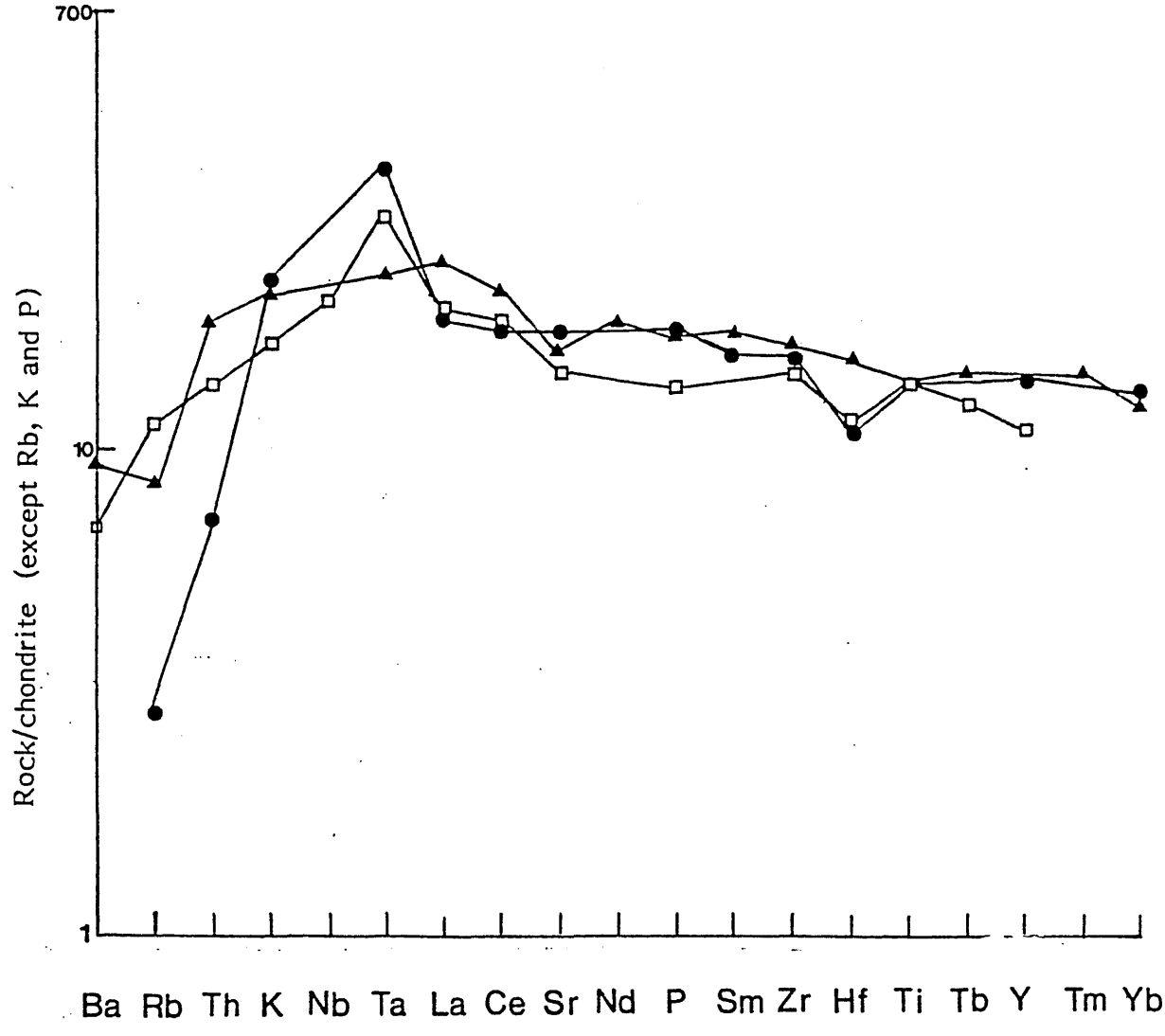

Figure 5.6

Chondrite-normalized multi-element diagram for some oceanic basalts. Filled circles = 6CC (Barber, et al, 1978); filled triangles = 2.1 (Dietrich et al, 1978); open squares = ISL 28 (Wood et al, 1979). 6CC and 2-1 are from Tyrrhenian Sea Basin.

FIGURE 5.7

ELEMENTAL COMPOSITION OF A HIGH-AL BASALT (MR17)
NORMALISED TO A TYRRHENIAN SEA BASALT
(BARBERI ET AL, 1977)

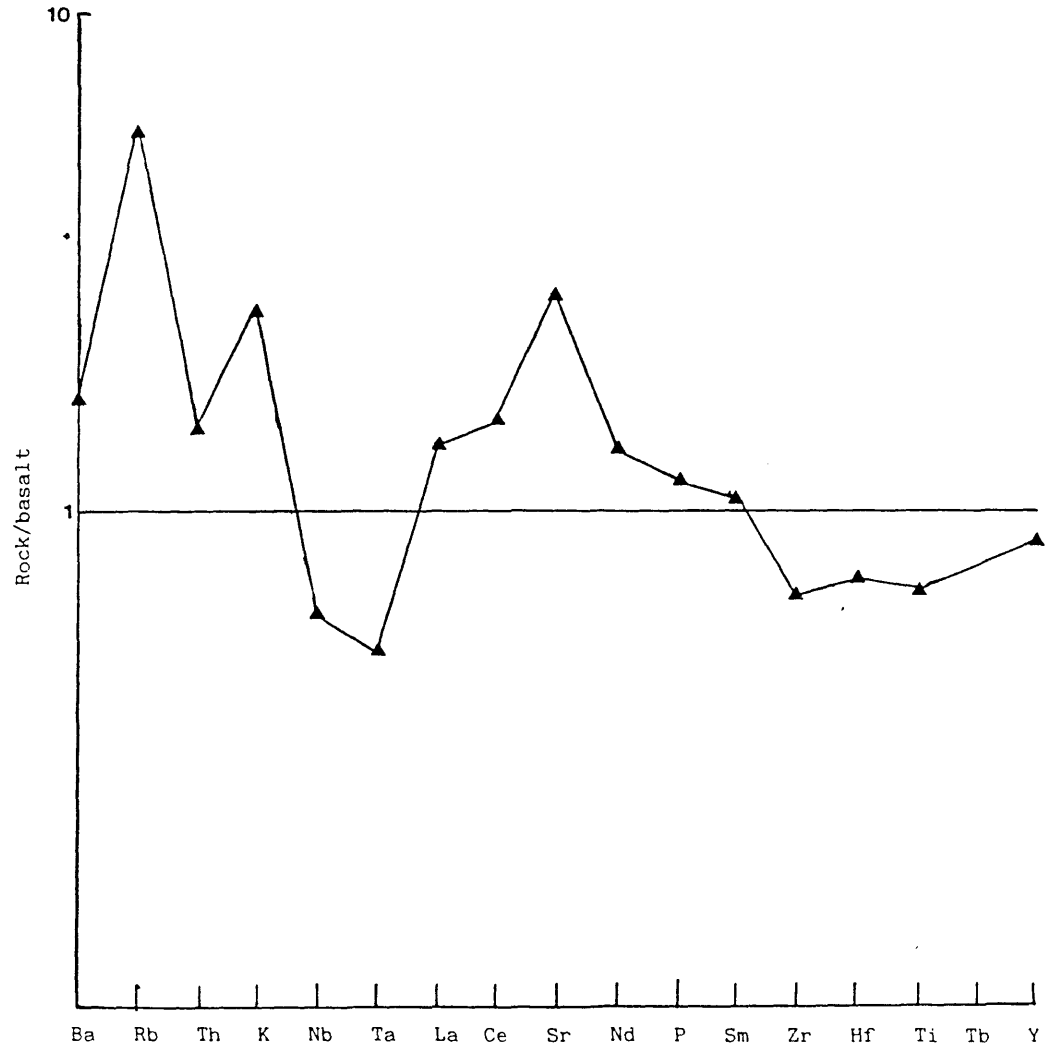

during subduction of oceanic lithosphere (Saunders and Tarney, 1979). These elements would be released as a result of dehydration reactions occurring within the slab during subduction, provided that the breakdown products of the clays are not a suitable host for such LILE. The relatively insoluble HFSE remain locked within the subducted slab.

Addition of a melt, rather than a fluid, to mantle peridotite, can also explain the enrichment in LREE and P shown in Figure 5.7. Wyllie (1982) suggested that reactions within the sinking slab at high pressures could lead to a range of SiO_2-rich fluids and hydrous partial melts. Sekine and Wyllie (1983) experimentally simulated the hybridisation of a hydrous silicic melt rising from the subducted slab into mantle peridotite at 30 kb. They found that reactions within the zone of hybridisation produced regions of phlogopite-pyroxenite, which cannot yield high-Mg picrites on melting. Inter-HFSE ratios among Sardinian basaltic rocks of Zr/Y = 2.9, Zr/Hf = 41, Ti/Zr = 101 and Ti/Y = 295 are MORB-like, although Nb and Ta abundances are too low. High La/Nb, La/Ta and Sr/Ce ratios have been successfully modelled by the addition of 5% of a deep sea clay-calcareous ooze mixture to MORB-source mantle (Figure 5.8). However, there are significant discrepancies between the model and a typical Sardinian basalt (MR17) which include:

(1) high K/Rb; (2) high Ba/Th; (3) low Ce*, in the model.

Although Hole et al (1984) modelled the generation of Marianas arc basalts by the addition of $\lesssim$ 1% of Pacific oceanic

FIGURE 5.8

GEOCHEMICAL MODELLING OF HIGH-AL BASALT GENESIS BY THE ADDITION TO MORB-SOURCE MANTLE (WOOD ET AL, 1979) OF 4.9 WT. % U120 AND 0.1 WT. % DEEP SEA CLAY. THE MODEL COMPOSITION (FILLED SQUARES) HAS BEEN MULTIPLIED BY 10 IN AN ATTEMPT TO ACCOUNT FOR TRACE ELEMENT ENRICHMENT DURING CRYSTAL FRACTIONATION PROCESSES. A SARDINIAN HIGH-AL BASALT (MR17) IS SHOWN FOR COMPARISON (FILLED CIRCLES)

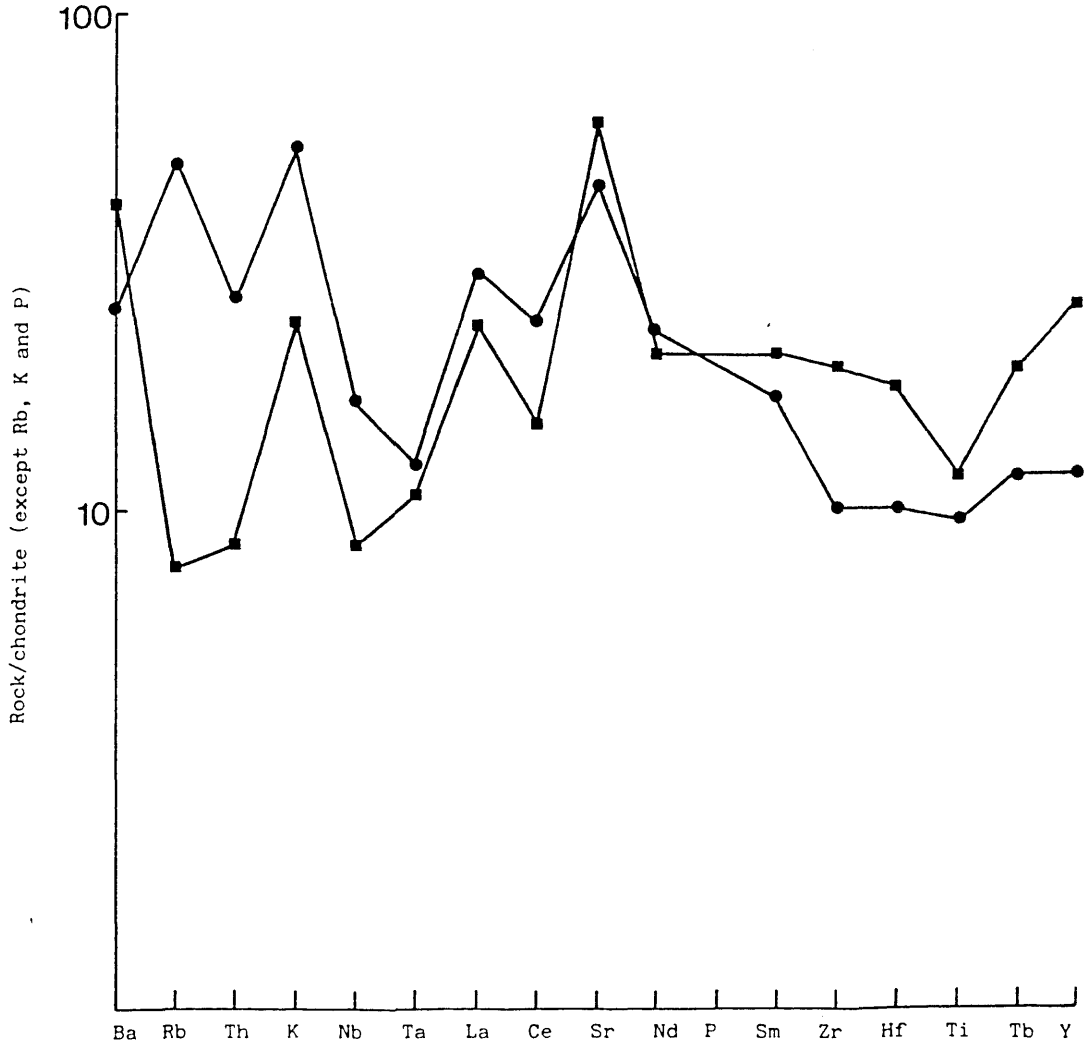

lithosphere to MORB-source mantle, they emphasised that low $^{87}Sr/^{86}Sr$ in the lavas precluded significant involvement of high-Sr carbonate material to explain high Sr/Ce ratios.

Low Nb and Ta can also be explained by the retention of these elements in some residual phase which is stable during partial melting in the mantle wedge. Such a phase may be stable under the hydrous conditions that exist in the mantle wedge above the subducted slab. However, most mineral hosts for Nb and Ta contain significant amounts of Ti, which does not always positively correlate with low Nb and Ta. This precludes sphene, perovskite and rutile as residual phases; perovskite will also produce a significant LREE-depletion relative to the HREE which has not been observed.

5.8 OIB plus subducted sediment source for Sardinian basalts?

Generation of IAV from OIB-source mantle has been suggested because of the isotopic similarity between IAV and OIB, rather than MORB (Morris and Hart, 1983). Thompson et al (1984) envisage the generation of island-arc tholeiites from shallow MORB-source mantle, which overlies the deeper OIB-source of calc-alkaline and shoshonitic basalts. Gill (1984) suggested that pods or dykes of OIB-source mantle may be present within a MORB-source host beneath Fiji, and Morris and Hart (1983) envisage "blebs" of OIB-mantle suspended within MORB-source mantle. Smaller degrees of melting may selectively tap OIB-source mantle (Gill, 1984).

The elemental characteristics of Sardinian mafic rocks are discussed below in terms of their possible generation in OIB-source mantle. Inter-LILE ratios among Sardinian basaltic rocks are shown in Figure 5.9, and compared to IAV and OIB (data for IAV and OIB is from Morris and Hart, 1983). The similarity in K/Rb, K/Sr and K/Ba ratios between OIB and IAV implies a similar mantle source. K/Sr and K/Rb ratios in Sardinian lavas overlap with both IAV and OIB, but K/Ba ratios are higher; high K/Ba ratios may reflect assimilation of sialic material during magma ascent through the continental crust.

High Ba/La ratios in calc-alkaline basalts have been noted by many authors (e.g. Kay,1984). Higher Ba/La ratios in Sardinian mafic lavas relative to OIB may reflect either addition of Ba (via high Ba/La subducted pelagic sediment) or removal of La (presumably in some residual LREE-bearing phase such as apatite or perovskite). Low La/Be ratios in Sardinian basalts, relative to OIB, cannot be explained by the subduction of Pacific-type pelagic oozes, because La/Be ratios in calcareous sediments are usually high (U120, La/Be = 22). La/Be ratios in some terrigeneous slates range from 8 to 36 (Thompson et al, 1984), which are again too high to explain low La/Be in the Sardinian samples. Therefore, either Be-enriched material was subducted beneath Sardinia during the Tertiary, or La was retained in the mantle source during partial melting.

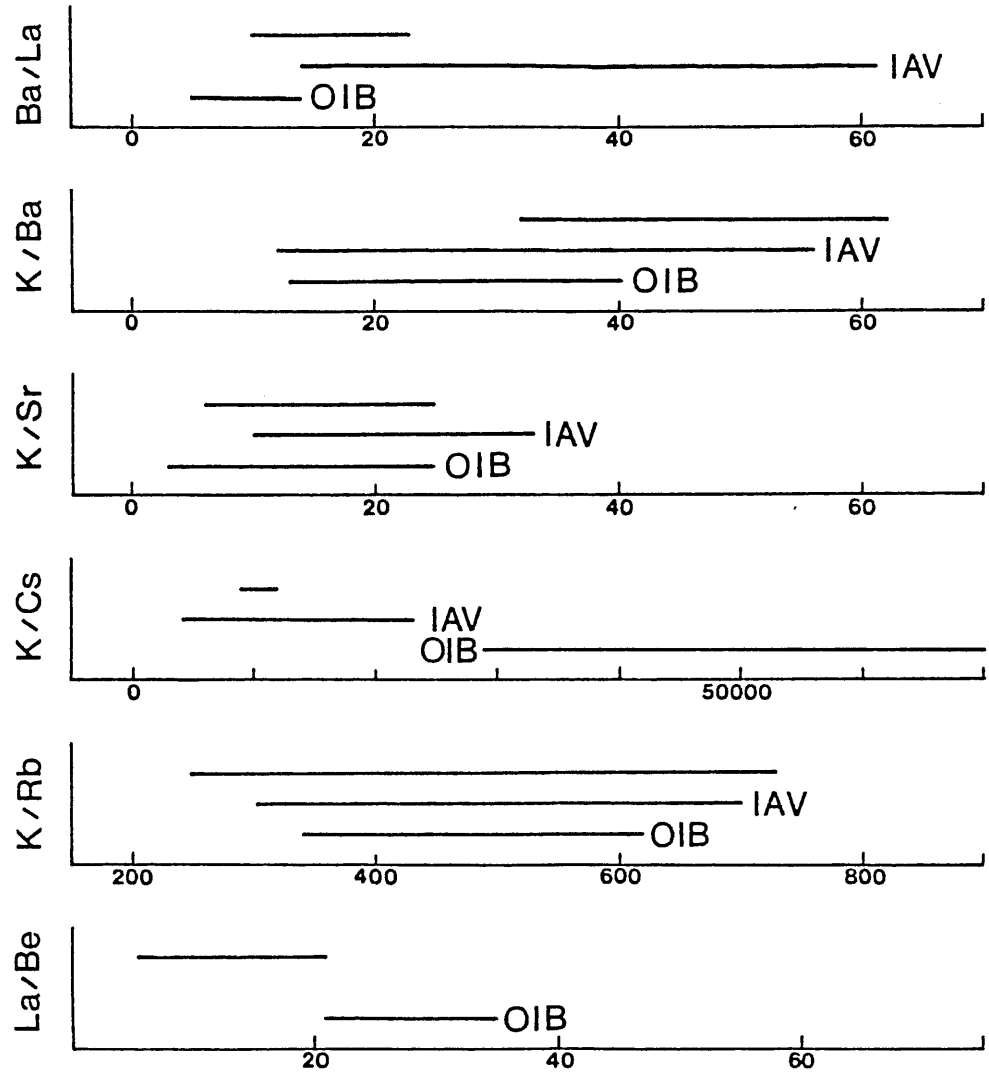

Figure 5.9

Comparative incompatible element ratios among island arc volcanics (IAV), ocean island basalts (OIB) and Sardinian basalts (upper range in each plot). Data for IAV and OIB from Morris and Hart (1983) and Thompson et al (1984).

Low K/Cs ratios relative to OIB in IAV and Sardinian subduction-related volcanics can be explained by the addition of Cs-enriched pelagic sediment via subduction zones. Kay (1984) has reported variably high Ba and Cs abundances in pelagic clays, and explains the high Cs/Rb ratios in IAV by the addition of pelagic sediments to mantle peridotite by subduction.

High Sr/Ce in most subduction-related mafic rocks cannot be explained by the retention of Ce in apatite, because the presence of residual apatite would produce a prominent negative P anomaly, which is not observed. Similarly, plagioclase accumulation could explain high Sr/Ce ratios, but the major element modelling (see Chapter 3) requires plagioclase removal.

5.9 Summary

Thus, the characteristic geochemical features of Sardinian subduction-related magmas require either, or both, of a net addition or net depletion of individual elements to, or from, their mantle source. Addition of melts or fluids to a MORB-source mantle can explain the relative enrichment in K, Rb, Th, Ba, LREE and P, although geochemical modelling was unable to accurately reproduce all the incompatible element ratios in Sardinian rocks. Generation of LREE-enriched subduction-related magmas from OIB-source mantle requires the addition of Cs (and Ba?), presumably from subducted pelagic sediment. Low Nb and Ta, and sometimes

Zr and Hf, requires the retention of these elements in residual mantle phases during partial melting. But the lack of covariance of Ti with Nb and Ta, and Th with Zr and Hf, make both (a) residual rutile, perovskite or sphene, and (b) residual zircon, difficult to explain.

CHAPTER 6

LILE-ENRICHED MAFIC ALKALINE MAGMAS IN NORTHERN SARDINIA

In this Chapter, a comparative approach has been adopted in order to compare and contrast the geochemical features of Sardinian mafic alkaline lavas, which were erupted 8 Ma and more after the end of active subduction, with alkalic rocks erupted in other continental anorogenic and ocean-island tectonic settings.

Volcanic rocks of hawaiite and basanite composition were erupted during the Plio-Pleistocene in northern Sardinia. Mafic rocks ($>$ 4 wt. % MgO) range in normative composition from under-saturated nepheline-normative to olivine and hypersthene-normative types. It has been shown in Chapter 4 that the hawaiites are not primary mantle-derived magmas, but have probably evolved by crystal fractionation from more Mg-rich parental magmas at depths of $>$ 30 km within the mantle lithosphere.

Plio-Pleistocene magmatic activity in Sardinia was associated with the regional extensional tectonic regime, which affected much of the western Mediterranean following the end of orogeny in the Alps and Apennines. Alkali basalts were erupted in the Tyrrhenian Sea Basin (Keller, 1981), and in eastern Spain, southern France and the Balearic Islands (Bellon and Brousse, 1977), at this time. This widespread distribution strongly implies that alkaline magmatism in northern Sardinia is not related to a deep mantle plume, as has been envisaged from volcanic activity in Hawaii,

Tristan da Cunha and Iceland (Hoffman and White, 1982), since myriads of hot spots would be required.

Extensional volcanism in northern Sardinia may be the result of varying degrees of melting of a variety of source rocks, including the following:-

1. Continental crust;
2. Sub-continental mantle lithosphere;
3. Asthenospheric upper mantle.

6.1 Continental crustal source

Seismic data indicate a maximum crustal thickness of about 30 km beneath the Sardinia-Corsica continental fragment (Hirn and Sapin, 1976). Direct derivation of magmas by melting of continental crustal rocks should therefore be constrained by results from experimental petrology with temperatures and pressures appropriate to this maximum depth. Melts of continental crustal gneisses, at depths of less than 30 km in the presence of water, will be granitic in composition (Wyllie, 1984). Generation of mafic magmas by in situ partial melting of crustal rocks is unlikely, if not impossible. However, this does not preclude the possibility of a crustal source through assimilation of sialic material by mantle-derived magmas during their ascent to the surface. Johannes (1984) has shown experimentally that extensive melting in the system QZ-AB-OR-AN can be induced by the availability of only small amounts (< 1%) of water. The presence of silicic glass as inclusions in Sardinian mafic alkaline lavas is interpreted in terms of wet melting of quartzo-feldspathic gneisses (see later).

Further, isotopic heterogeneity in some continental flood basalts may be the result of variable interaction with rocks of the continental crust (Carlson et al, 1981).

6.2 Sub-continental mantle lithospheric source

Some authors envisage a source within the sub-continental mantle lithosphere for all continental anorogenic volcanism (Hawkesworth et al, 1984). Melting may be induced by the metasomatism of mantle peridotite by a free volatile-rich phase (Bailey, 1982). They point to the chemical heterogeneity of lithospheric mantle, evidenced by the presence of amphibole, apatite and mica in some mantle xenoliths (Menzies, 1983). Some recent mantle enrichment event ($\ll$ 0.2 Ga) can explain the LILE-enrichment in time-integrated low Rb/Sr, high Sm/Nd mafic magmas. Although there is no petrographic evidence for any hydrous phases in Sardinian mantle peridotite xenoliths, it will be shown in Chapter 8 that these xenoliths have apparently been transported only from a restricted portion of the upper mantle, somewhere near the top of the mantle lithosphere. However, magma generation probably occurred at deeper levels, and there is no direct evidence of the nature and composition of the deep lithosphere beneath Sardinia.

6.3 Asthenospheric upper mantle source

The isotopic (Allègre et al, 1981), and elemental (Thompson et al, 1984), similarity between OIB and continental mafic alkalic lavas has been emphasised by some authors. Thompson et al (1983) suggest a source within the convecting asthenospheric upper mantle for all continental basaltic rocks, combined with variable interaction with either, or both, of the sub-continental mantle lithosphere and the continental sialic crust.

Alkali basaltic rocks from the Cameroon Line, West Africa, are elementally and isotopically indistinguishable, whether they were erupted through oceanic or continental crust (Fitton and Dunlop, 1985). These authors suggest that there has been negligible involvement of the sub-continental mantle lithosphere in magma genesis, and that the source for all continental and oceanic mafic alkaline magmas, is within the asthenospheric mantle. Partial melting of old sub-continental lithospheric mantle may still explain the generation of large volumes of continental flood basalts (Hawkesworth et al, 1983).

Fitton and Dunlop (1985) suggest that MORB and OIB source mantle may be one and the same. They explain the LILE-enrichment in OIB by the leaching of K, Rb, Cs, Ba and Th from along grain boundaries during the upwards percolation of melt through the mantle. Thompson et al (1984) invoke very small degrees of partial melting of an isotopically-distinct source to explain the LILE-enrichment in mafic alkaline lavas.

6.4 Elemental composition of hawaiites from northern Sardinia

Selected analyses of hawaiite lavas and pyroclastics from northern Sardinia are shown in the form of chondrite-normalised multi-element diagrams in Figures 6.1 and 6.2. Comparative trace element data for some mafic alkaline rocks from Hawaii (Chen and Frey, 1983), the Cameroon line (Fitton and Dunlop, 1985) and Tristan da Cunha (Thompson et al, 1984) are given in Figure 6.3. The patterns are generally similar but have several important differences.

The Sardinian samples show a moderately steep downward slope from K to Yb in Figures 6.1 and 6.2, which results in relatively high chondrite-normalised La/Y(La/Yn) ratios of 9.3-11.0. The right-hand segments of all the patterns in Figures 6.1 to 6.3 are similar, although the slope from Nb to Yb for the Hawaiian alkali basalt is slightly less steep. This feature probably reflects a higher degree of partial melting of a similar mantle source in the genesis of the Hawaiian sample. Ratios of La/Nb = 0.70-0.76 and Zr/Nb = 4.8 in Sardinian hawaiites are lower than in MORB, but similar to ratios observed in alkali basalts from the Cameroon line and Tristan da Cunha.

Thompson et al (1984) noted that a characteristic feature of all OIB chondrite-normalised patterns was a peak at Nb(Ta), which is also true of most continental anorogenic mafic alkalic rocks (Thompson, 1985; Fitton and Dunlop, 1985), and is reflected in Figure 6.3. All those for Sardinian hawaiites, however, peak at K and show a slight downward

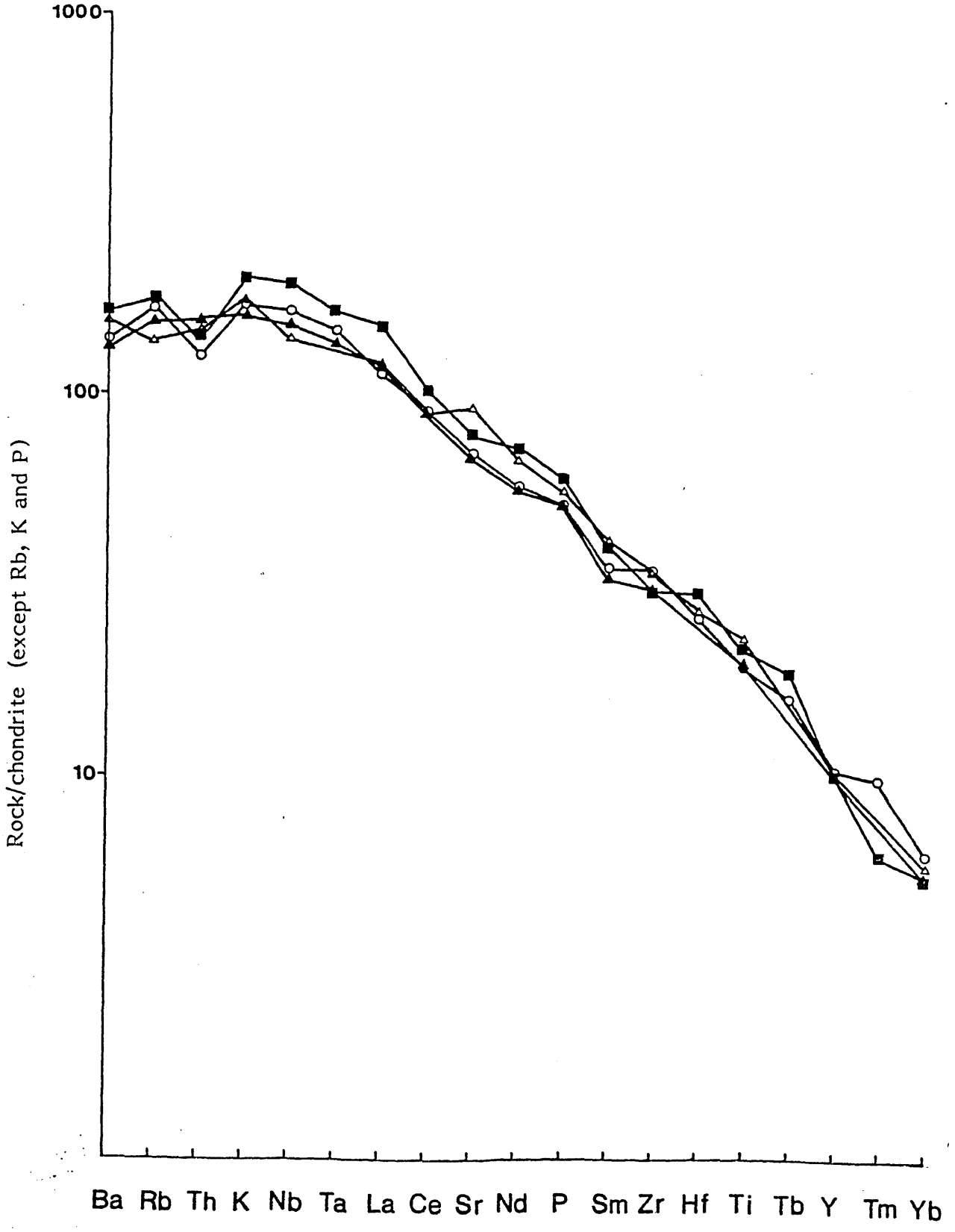

Figure 6.1

Chondrite-normalised multi-element diagram for Sardinian cinder cone pyroclastics. Filled squares = K59; open circles = K33; open triangles = K126 and filled triangles = MR1

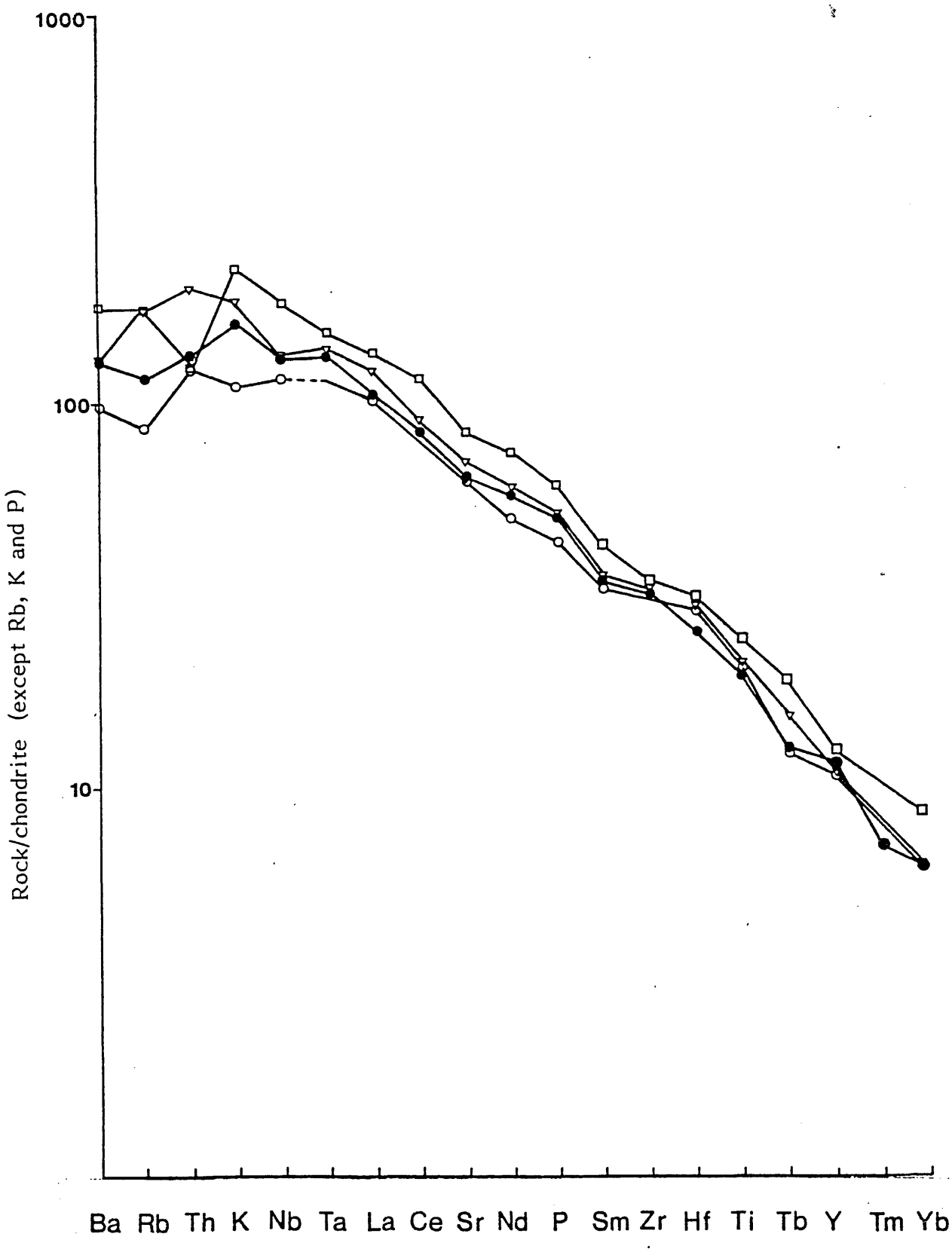

Figure 6.2

Chondrite-normalised multi-element diagram for Sardinian hawaiite lavas. Open squares = K107; open triangles = K106; filled circles = C15 and open circles = MR21

Figure 6.3

Chondrite-normalised multi-element diagram for representative mafic alkaline lavas. Open squares = ocean island basalt from Cameroon line (Fitton and Dunlop, 1985); open circles = continental alkali basalts from Cameroon line (Fitton and Dunlop, 1985); filled circles = trachybasalt from Tristan da Cunha (Thompson et al, 1984); and filled triangles = alkali basalt from Hawaii (Chen and Frey, 1983)

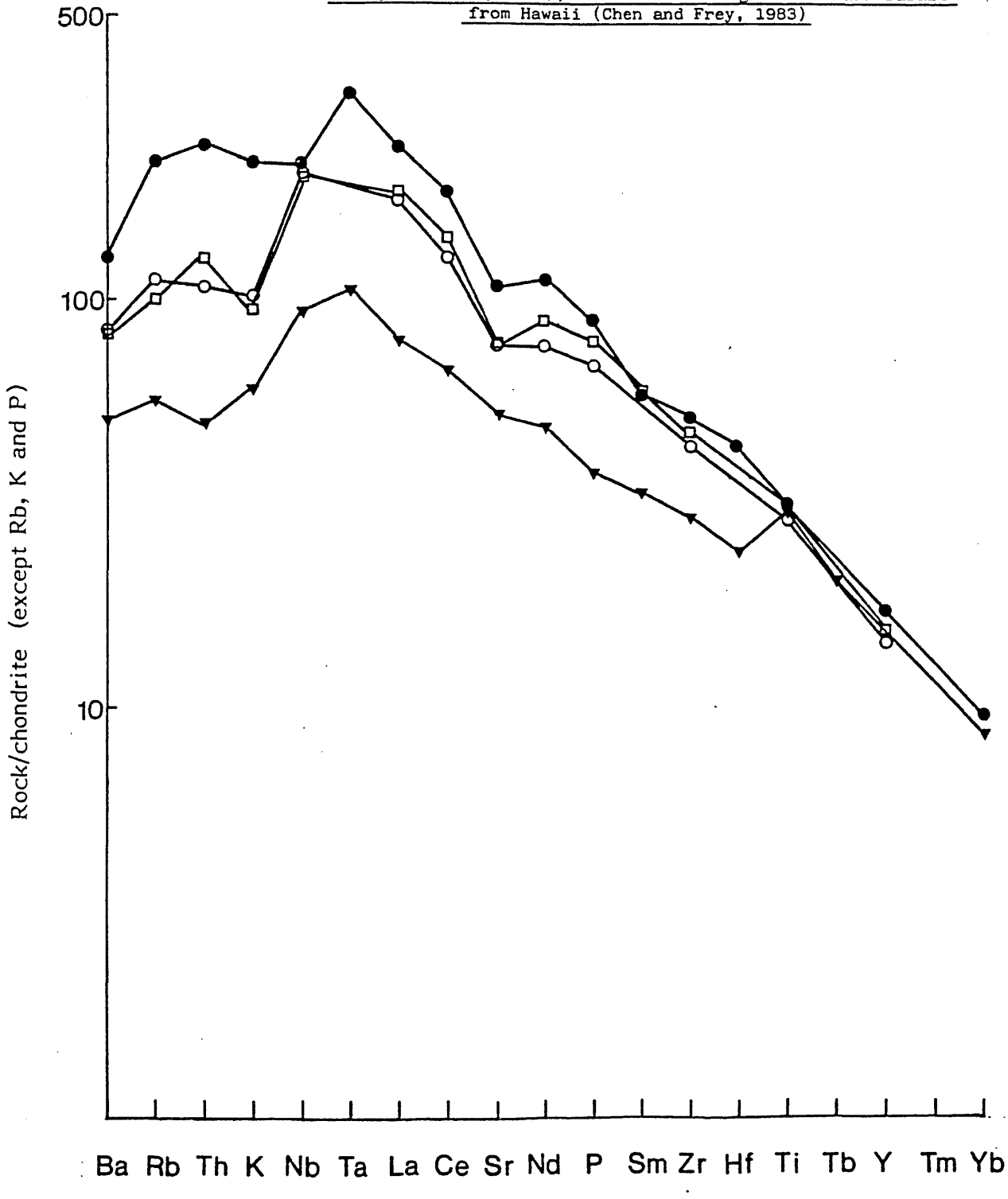

curvature from K to Ba. In contrast, the patterns for rocks from the Cameroon line and Hawaii slope down much more steeply from Ta to Ba. This results in low LILE/Nb ratios, such as Rb/Nb = 0.5, Ba/Nb = 9, Th/Nb = 0.07 and K/Nb = 159-217. LILE/Nb ratios in Sardinian hawaiites (Figures 6.1 and 6.2) are substantially higher, with K/Nb = 360, Th/Nb = 0.09, Ba/Nb = 16.4 and Rb/Nb = 1.0. The small trough at Sr in some Sardinian hawaiites (and Cameroon line volcanic rocks) probably reflects minor plagioclase fractionation, possibly during final re-equilibration of the magmas at mid-crustal depths. Alternatively Sr depletion can also be explained by the bulk assimilation of Sr-poor upper crustal crystalline basement rocks by mafic mantle-derived magmas, during their ascent to the surface, whose ability to generate the overall enrichment in LILE depicted in Figures 6.1-6.3, therefore deserves some attention.

However, Thompson (1985) has shown that lavas from Tristan da Cunha are enriched in LILE relative to oceanic basalts from the North Atlantic. Kay (1984) reports Cs and Ta data for an alkali basalt from Gough Island, which shows a Cs/Ta ratio an order of magnitude higher than in an alkali basalt from St. Helena. Since Tristan and Gough are sited entirely on oceanic crust, such general LILE enrichment cannot be due to interaction with sialic material during magma ascent through the continental crust.

Inter-element ratios in a trachybasalt from Tristan da Cunha (Thompson et al, 1984), such as K/Nb = 350, Ba/Nb = 11.6, Rb/Nb = 1.0 and Th/Nb = 0.13, are similar to those observed in hawaiites from northern Sardinia, although Ba/Nb and Th/Nb ratios in the latter are somewhat higher and lower, respectively. Cs/Ta ratios of 0.13-0.23 in Sardinian hawaiites are substantially higher than a Cs/Ta = 0.047 ratio in an alkali basalt from St. Helena, but not as high as the Cs/Ta = 0.42 ratio reported for Gough Island (Kay, 1984).

The upper mantle source beneath the oceanic islands of Tristan and Gough is enriched in K, Rb, Cs, Ba and Th relative to most OIB, and has been related to the isotopically-defined Dupal anomaly of the southern hemisphere (Thompson, 1985). High $^{87}Sr/^{86}Sr$ ratios in mafic alkaline lavas from Tristan have led to the suggestion that the magmas may be derived from old subducted oceanic lithosphere (O'Nions, 1984), possibly stagnant at the proposed 650 km seismic discontinuity (Ringwood, 1982). Thus, LILE enrichment in hawaiite magmas erupted during the Plio-Pleistocene in northern Sardinia may result from one or a combination of the following sources/processes:-

1. The presence of an enriched asthenospheric upper mantle beneath Sardinia;
2. Interaction of OIB with enriched sub-continental mantle lithosphere;

3. Partial melting and assimilation of sialic material by mantle-derived magmas during ascent through the continental crust.

6.5 LILE-enriched basanites in northwestern Sardinia

Chondrite-normalised multi-element patterns for two representative basanites from N.W. Sardinia are shown in Figure 6.4. The patterns are very similar to those shown in Figure 6.1 and 6.2 for Sardinian hawaiites, except that the basanites are characterised by:-

1. A slightly steeper right-hand part to the pattern, from Nb to Yb, resulting in higher La/Yn ratios of about 22;
2. A marked trough at K, which results in high Rb/K = 0.021 and Ba/K = 0.274 ratios.

Comparative multi-element patterns for rocks of basanite composition from Hawaii and Tenerife (Thompson et al, 1984) and Western Australia (Frey et al, 1978) are shown in Figure 6.5. All the samples show a strong downward curvature from Ta(Nb) to Ba. In contrast, Sardinian basanites are characterised by a much shallower slope from Nb to Ba with Ba/Nb $\sim$ 12.8, Rb/Nb $\sim$ 0.96 and Th/Nb $\sim$ 0.115 - remarkably similar to those mafic alkaline lavas from Tristan da Cunha, and to ratios reported above for Sardinian hawaiites.

A trough at K in the chondrite-normalised pattern for a Tenerife basanite in Figure 5.5 may reflect the presence of a residual K-rich phase in its mantle source during partial

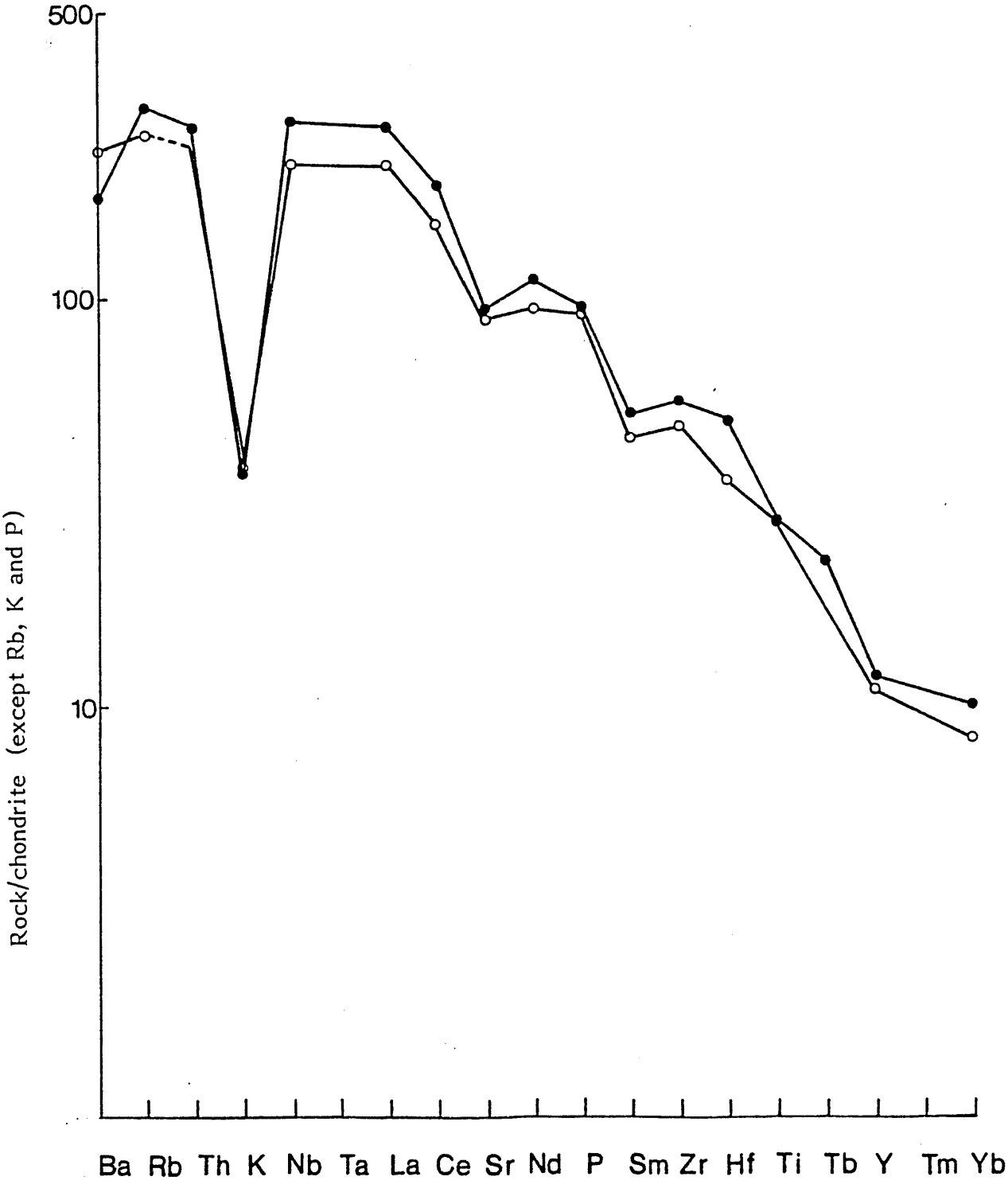

Figure 6.4

Chondrite-normalised multi-element diagram for Sardinian anacite basanites.
Filled circles = MR24 and open circles = K52

Figure 6.5

Chondrite-normalised multi-element diagrams for representative basanites. Open squares = basanite from Tenerife (Thompson et al, 1984); open circles = basanite from Western Victoria (Frey et al, 1978); filled triangles = basanite from Hawaii (Thompson et al, 1984) and filled squares = basanite from (Western Victoria (Frey et al, 1978)

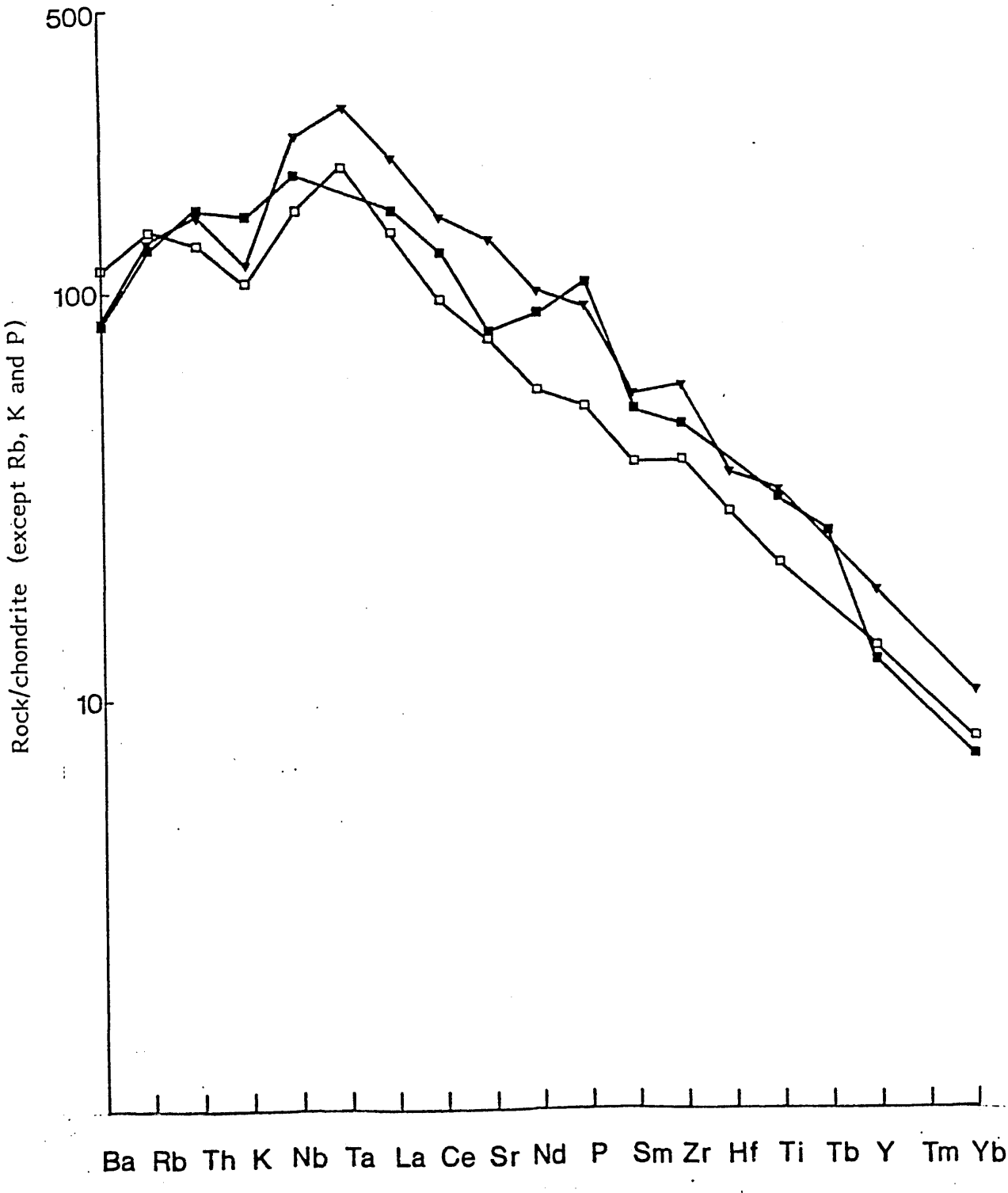

melting. Fitton and Dunlop (1985) attributea relative K, but not Rb and Ba, depletion in Cameroon line alkaline basalts to the presence of a residual K-bearing amphibole. However, low K abundances in Sardinian basanites reflect the presence of groundmass analcite. Experimental data in simple systems suggests that primary igneous analcite cannot crystallise from a silicate melt at temperatures of greater than about 650^{o}C (Boettcher and Wyllie, 1969; Roux and Hamilton, 1976). Analcite in Sardinian basanitic rocks is therefore likely to be of secondary origin, related to the deuteric alteration of an originally K-rich groundmass phase (possibly leucite?). Thus the K-troughs may also be of secondary origin.

6.6 Sr-isotope composition of hawaiite lavas in northern Sardinia

The occurrence of spinel peridotite xenoliths in mafic alkalic lavas has often been used as evidence for only negligible interaction of mantle-derived magmas with continental sialic crust (Frey et al, 1978; Fitton and Dunlop, 1985). If so, the Sr-isotopic composition of lavas should reflect the composition of their mantle source.

The hawaiite lavas range in $^{87}Sr/^{86}Sr$ from 0.70437-0.70514, and plot within the field defined by OIB in Figure 4 .6. Barberi et al (1969) report $^{87}Sr/^{86}Sr$ ratios of 0.7016-0.7067 for some recent volcanic rocks from the southern Tyrrhenian Sea Basin, in the genesis of which

crustal contamination probably played a negligible role. Thus, in the absence of significant crustal contamination $^{87}SR/^{86}Sr$ ratios for Sardinian mafic alkaline rocks are consistent with a heterogeneous OIB mantle source beneath Sardinia.

However, crustal contamination has been invoked to explain the elemental and isotopic characteristics of magmas erupted in some continental anorogenic regions (Cox and Hawkesworth, 1984). Therefore, the possibility, magnitude and importance of crustal sialic contamination in developing the distinctive geochemical features of Sardinian mafic alkalic rocks should also be discussed.

6.7 Evidence for partial melting within the Sardinian upper continental crust

Contamination of mantle-derived magmas by interaction with continental crust, during ascent to the surface, can occur by several processes, which include:-

1. Dehydration reactions, and the release of aqueous fluids (Dicken, 1980). This will cause enrichment of the magma in those elements of low ionic potential which are enriched in the fluid phase. It will be difficult to distinguish from K, Rb, Th, Ba and Cs-enrichment related to the former presence of a subduction zone;
2. Assimilation and fractional crystallisation (AFC) processes in crustal magma chambers (De Paolo, 1981). In AFC, the latent heat of crystallisation of the magma provides the heat input sufficient to cause melting of the country rock;

3. Partial melting and assimilation of wall-rock during the ascent of turbulently-convecting magma (Huppert and Sparks, 1985).

Rapid ascent of magmas through the continental crust is implied by the occurrence of spinel peridotite xenoliths in relatively phenocryst-poor Sardinian mafic lavas. Given a short residence time for magmas within sialic crust, it is unlikely that either crustal magma chambers became established, or that heat transfer by conduction was sufficiently fast to cause melting of the conduit walls. Although dehydration reactions may have taken place immediately adjacent to the conduit walls, it is improbable that these were ever extensive enough to generate the observed high LILE abundances in the lavas.

Much more rapid heat transfer from the magma to the wall-rock will occur if heat is transferred by convection, rather than by conduction (Huppert and Sparks, 1985). Theoretical calculations suggest that convective heat transfer will occur in turbulently-convecting magma. This may be sufficient to cause melting of the wall-rock, and such a contamination mechanism can explain the apparently anomalous duality of crustal assimilation in mantle xenolith-bearing magmas.

Two fresh glass-rich inclusions were collected from pyroclastic rocks in northwestern Sardinia, probably formed by melting of crustal rocks by a mechanism similar to that described above. Their major element chemical composition (Table 6.1) was

TABLE 6.1

MAJOR ELEMENT AND NORMATIVE COMPOSITION OF GLASSES FROM CRUSTAL XENOLITHS

	QF-D[1]	N12[2]
SiO_2	71.96	72.47
TiO_2	0.45	0.94
Al_2O_3	14.87	11.45
Fe_2O_3T	3.71	0.79
MnO	0.11	-
MgO	0.27	0.31
CaO	1.21	0.65
Na_2O	2.80	2.42
K_2O	4.41	6.64
P_2O_5	0.12	-
LoI	0.99	-
TOTAL	100.89	95.67
QZ	34.99	36.43
OR	26.03	36.88
AB	23.69	17.43
AN	5.27	3.19
HY	0.67	1.57
CO	3.56	-
IL	0.24	0.30
HE	3.71	1.32
SP	3.72	2.69
AP	0.30	-

All major element values given in wt. % oxide

1. Major elements determined by XRF.

2. Electron probe microanalysis.

obtained by XRF and electron probe microanalysis, and probably reflect liquid compositions, although the vesicular nature of the glass inclusions implies loss of volatiles on eruption.

The QZ-AB-OR ternary diagram (Figure 6.6) shows the glass compositions and two liquidae: the experimentally-determined H_2O-saturated liquidus at 1 kb (Luth et al, 1964), and the estimated dry liquidus at 5 kb (Wyllie, 1977). The glass compositions plot close to the former, which implies wet melting of crustal rocks at depths of less than 5 km. Biotite phenocrysts in some of the lavas imply a relatively high magmatic P H_2O.

Major and trace element data for one of the glasses (QF-D) is given in Appendix B, and its chondrite-normalised multi-element pattern is shown in Figure 6.7. The most noteworthy geochemical features are the low abundances of Ni, Cr, Sr, P and Ti, and the high contents of Ba, Th, U, K and Rb. This results in high ratios of Ba/Ta = 528, Rb/Ta = 134 and Th/Ta = 9.4. The LILE are also strongly enriched relative to the LREE. Ba is depleted relative to the other LILE, which results in a low Ba/Rb ratio of 3.9. Troughs in the chondrite-normalised pattern at Sr, P and Ti produce high ratios of Ce/Sr_N = 7.6, Nd/P_N = 3.4 and Tb/Ti_N = 3.8.

The REE pattern is shown in Figure 6.8, and is characterised by moderate LREE/HREE enrichment (resulting in a La/Yb_N ratio of 3.95) and a significant negative Eu anomaly. These elemental features, combined with the high alumina (Al_2O_3 = 14.9 wt. %), silica (SiO_2 = 72.0 wt. %) and total

Figure 6.6

Normative compositions of silicic glasses, formed by partial melting of the Sardinian upper crust, shown projected onto AB-OR-QZ. They are compared to liquidus phase relations at 1kb (H_2O-saturated; Luth et al, 1964) and 5kb (dry; Wyllie, 1977)

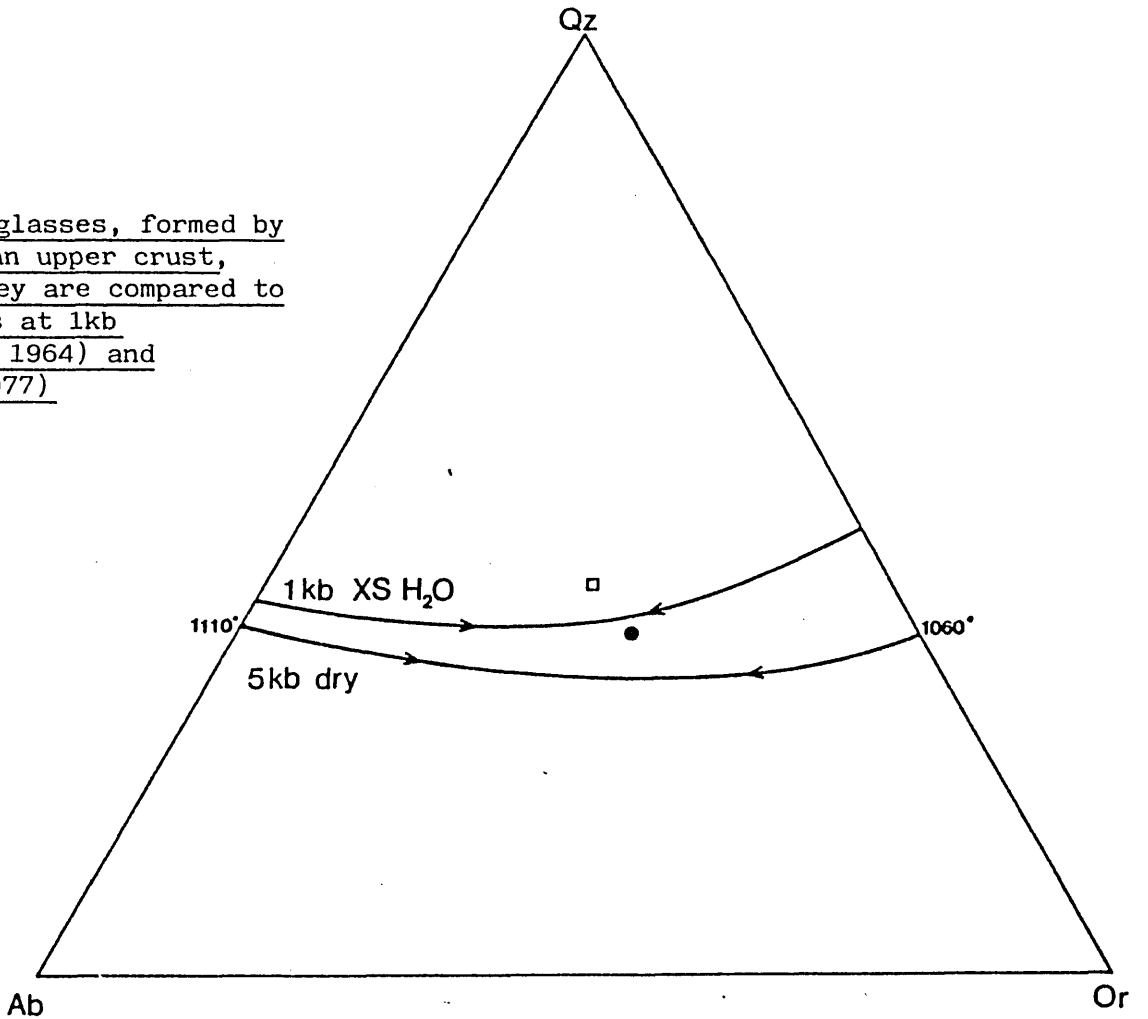

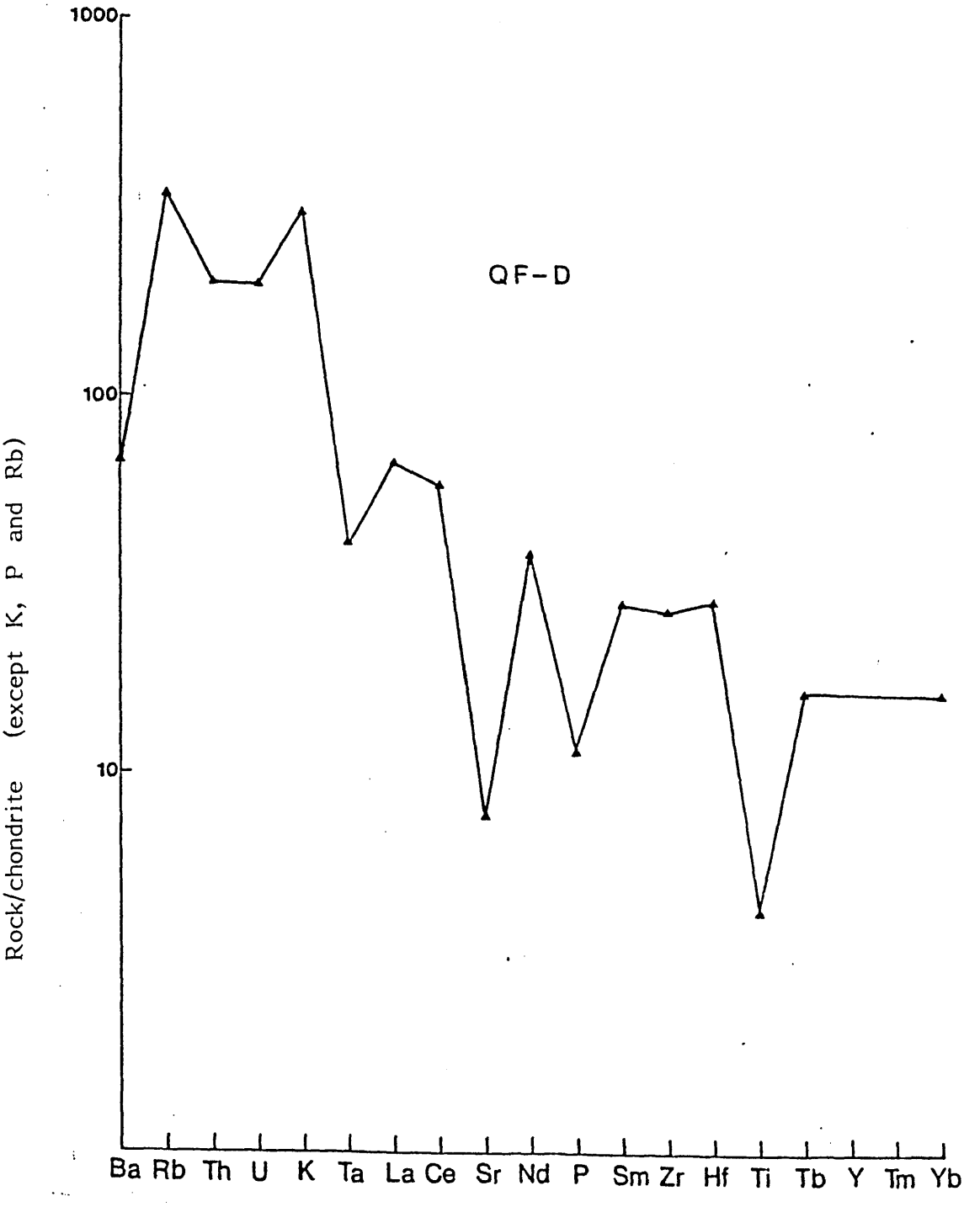

Figure 6.7

Chondrite-normalised multi-element diagram for a silicic glass (QF-D), formed by melting of Sardinian upper crustal quartzo-feldspathic gneisses

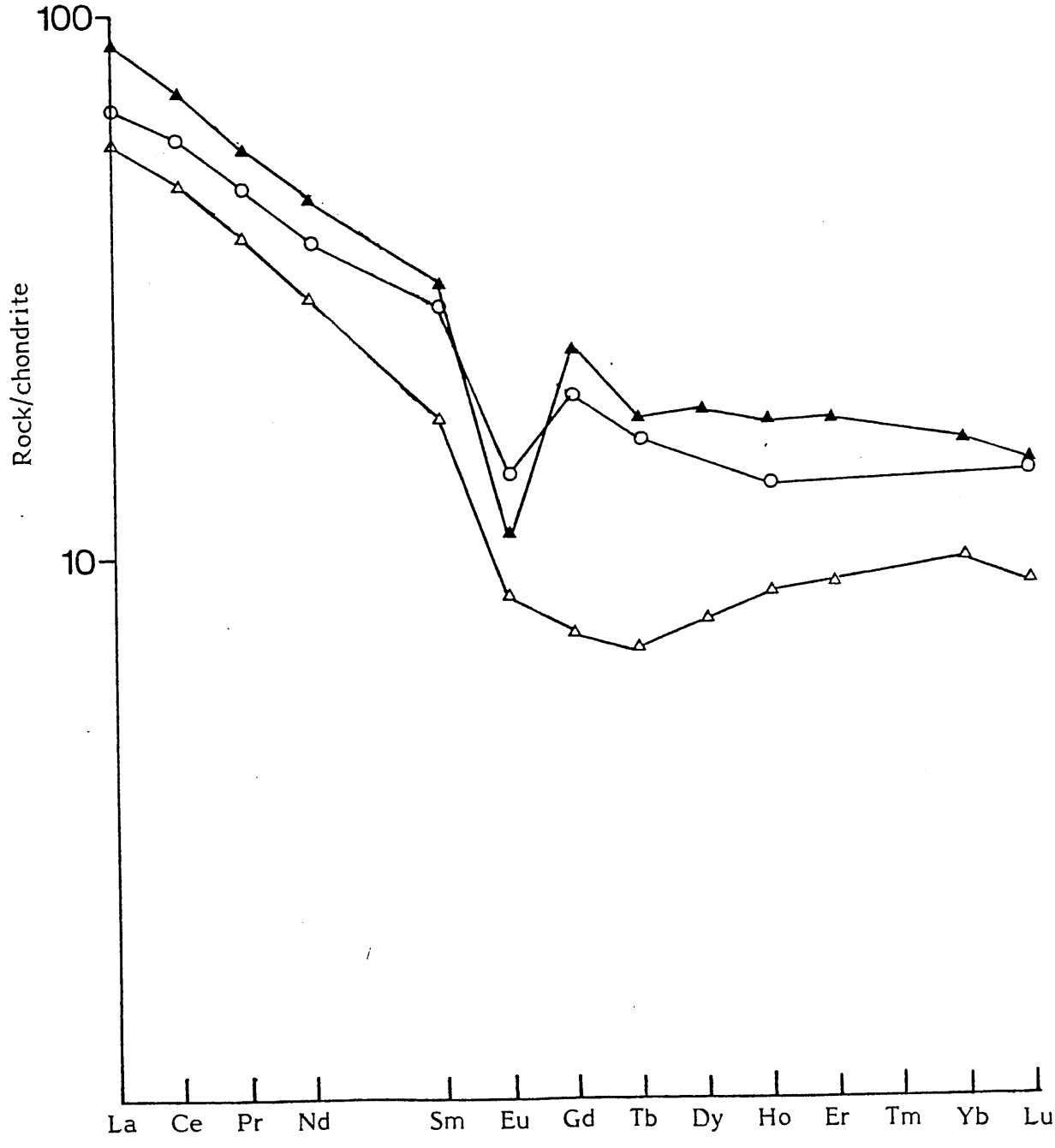

Figure 6.8

Chondrite-normalised REE patterns for a silicic glass (QF-D; open circles), a quartzo-feldspathic gneiss (C1; filled triangles) and a mica schist (C19; open triangles).

alkali (Na_2O + K_2O = 7.2 wt. %) contents are consistent with an originally sedimentary composition (see sample S33e, Thompson et al, 1983), which should therefore be represented in the basement complex.

6.8 Geochemical nature of the Sardinian crystalline basement rocks

The Palaeozoic crystalline basement of Sardinia consists predominantly of greenschist-amphibolite facies meta-sediments, interbanded with subordinate meta-igneous rocks, all of which have been intruded by Hercynian intermediate-acid plutons. Chondrite-normalised multi-element patterns for representative Sardinia meta-sediments are shown in Figure 6.9. C1 is a quartzo-feldspathic gneiss, and C19 a mica schist. The most important features of the patterns are the high abundances of Rb, Th, U, K and Ba, but the low abundances of Nb, Sr, P and Ti. This results in obvious troughs in their chondrite normalised patterns at Nb, Sr, P and Ti. C1 is characterised by depletions in U and Ba relative to the other LILE, which results in relatively low ratios of Ba/Rb = 4.3, Ba/Th = 51.4, Ba/K = 0.016 and U/Th = 0.1. Very high Zr, Th and Hf abundances in C19 probably reflect residual zircon, although this phase has not been observed optically.

The geochemical similarity between the chondrite-normalised patterns for C1 and the glass, QF-D, in Figure 6.7 is obvious. C1 also plots close to the H_2O-saturated minimum in the projection on to QZ-AB-OR in Figure 6.6. REE data for C1 and C19 are also shown in Figure 6.8. C1 resembles QF-D in being moderately LREE-enriched with La/Yb_N = 5.5, showing a

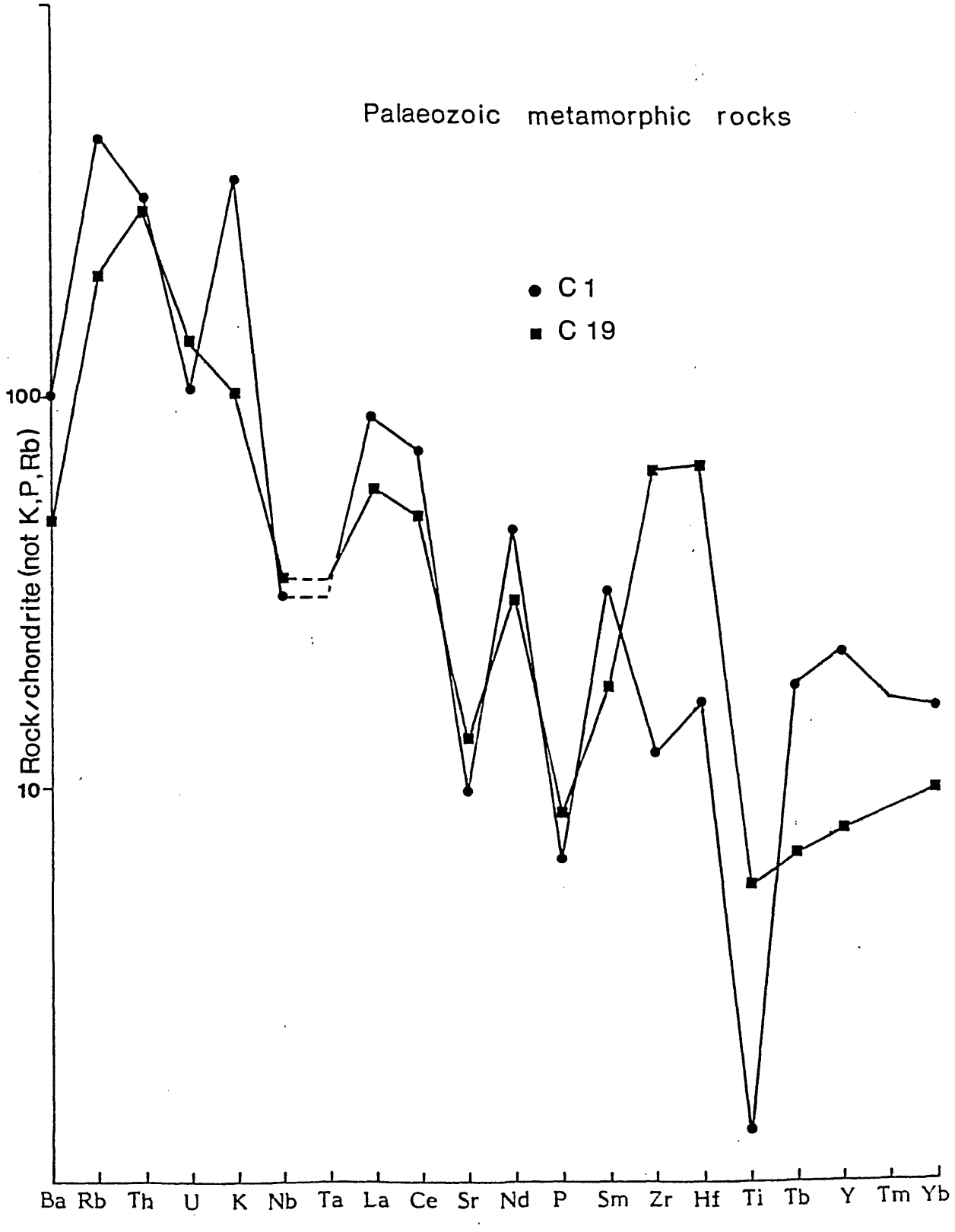

Figure 6.9

Chondrite-normalised multi-element diagram for two upper crustal Sardinian metamorphic rocks. The pattern for C1 is remarkably similar to that shown for the silicic glass in Figure 6.7.

prominent negative europium anomaly.

Chondrite-normalised multi-element patterns for representative silicic plutonic rocks from northern Sardinia are shown in Figure 6.10. The most noteworthy geochemical features are the variably low Sr, P and Ti abundances, and the high Rb/Ba ratios. Rb/Ba increases with fractionation due to removal of Ba in alkali feldspar. Progressively deepening Sr, P and Ti troughs reflect the dominance of plagioclase, apatite and titanomagnetite fractionation, respectively. All these phases have been observed petrographically.

It is envisaged that metamorphic rocks of quartzo-feldspathic composition, similar to C1, are the most fusible components within the Sardinian upper crust. Selective melting of only these most fusible crustal rock types may have occurred, to produce silicic melts similar in composition to QF-D.

6.9 High LILE abundances in Sardinian mafic alkalic magmas - a crustal signature

It has been shown that alkalic mafic magmas erupted during the Plio-Pleistocene in northern Sardinia are enriched in K, Rb, Th, Ba and Cs relative to OIB from Tenerife, Hawaii, St. Helena and the Cameroon line. They are also enriched in these elements relative to many continental anorogenic alkali basaltic rocks.

Further, Sardinian Tertiary alkalic melts ascended through, and interacted with, the crystalline basement, which is

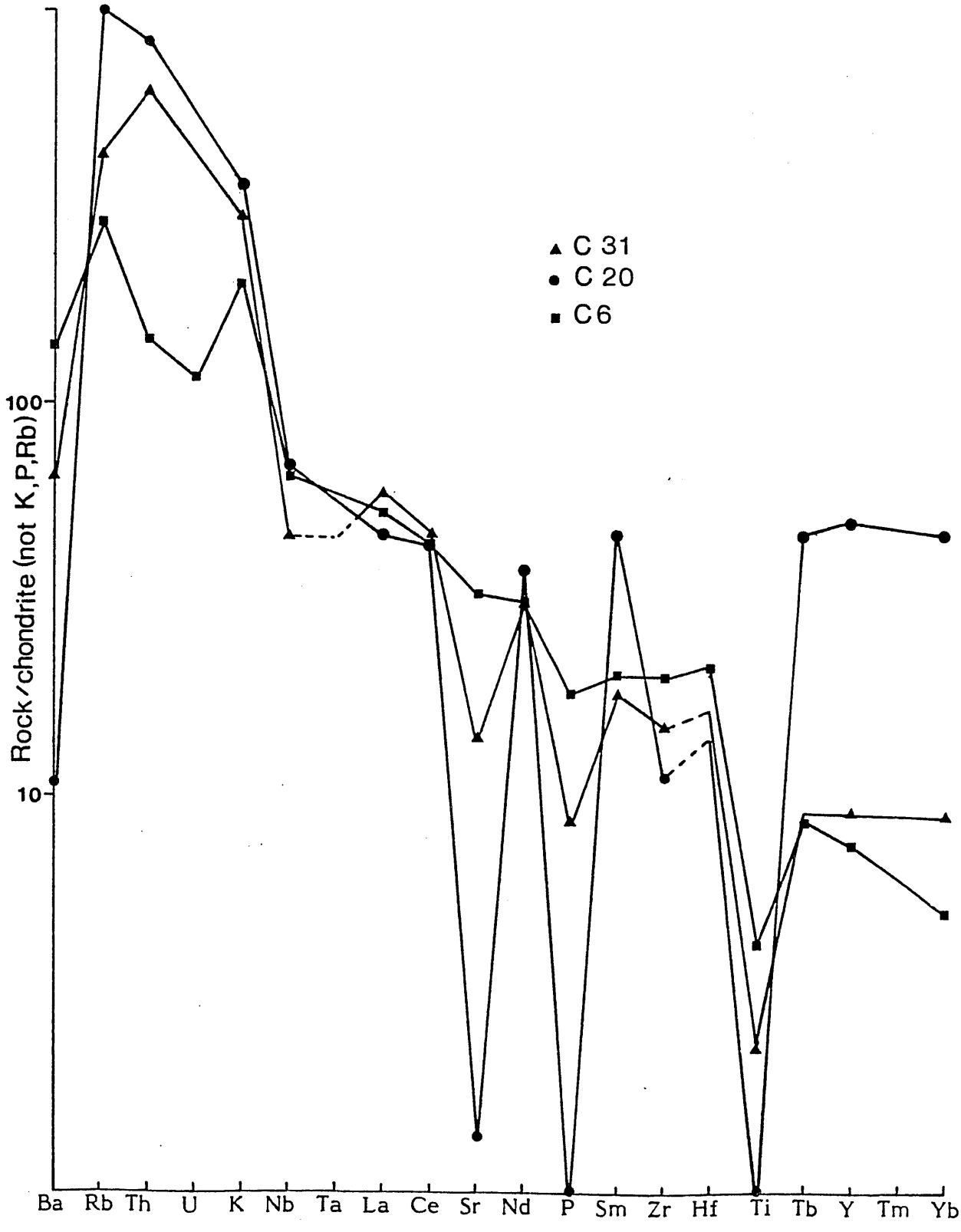

Figure 6.10

Chondrite-normalised multi-element patterns for some Hercynian intrusive rocks.

characterised by high LILE contents relative to the LREE. This observation immediately suggests that melting and assimilation of crustal rocks by mantle-derived OIB magmas, outlined above, may provide a suitable mechanism to explain the LILE-enrichment of Sardinian alkalic lavas. Accordingly, a simple bulk assimilation model of the geochemical features of Sardinian lavas has been constructed. It is only intended to show whether crustal contamination could have occurred, not whether it did. Choice of a crustal end-member composition was constrained by the composition of the glass inclusions. Since no Sr isotope data is available for QF-D, a geochemically similar quartzo-feldspathic gneiss (C1) was used to represent the most fusible crustal component. An average oceanic alkali basalt from the Cameroon line (Fitton and Dunlop, 1985) was used as the OIB end-member composition. Although its high $Fe_OT/MgO = 1.4$, and a Sr-trough in the chondrite-normalised pattern, indicate that this alkali basalt is probably not a primary magma, the overall shape of the pattern ought not to have changed during fractionation of olivine, clinopyroxene and plagioclase (except for Sr).

Many models of crustal contamination via bulk assimilation ignore constraints imposed by the major elements. Here, a simple least squares mixing calculation (Le Maitre, 1979), was used. Bulk assimilation of about 20% of C1 by an OIB most closely reproduces the geochemical composition of K33. K33 was chosen to represent Sardinian hawaiite magmas, because its chemistry has been most closely constrained by multiple

analysis. The results of the mixing calculation are shown in Table 6.2. Given the uncertainties in the end-member compositions, the model composition gives a close chemical fit to K33, and is consistent with the preferential melting of the most fusible part of the Sardinian upper crust by turbulently-convecting magma.

The incompatible elements have also been modelled in terms of the bulk mixing between C1 and an OIB in Figure 6.11. The overall shape of the multi-element pattern for K33 can again be reproduced by the addition of 20% of C1 to the OIB. The most significant discrepancies between the model and K33, however, are the much lower Ba/LILE ratio in the model, and its Sr isotope ratio of $^{87}Sr/^{86}Sr = 0.70760$ which is much too high (cf. K33, $^{87}Sr/^{86}Sr = 0.70442$). Further, a strong positive correlation exists between Ba/La and $^{87}Sr/^{86}Sr$ in Sardinian hawaiites (Figure 6.12) but all plausible end-member crustal compositions have Ba/La ratios which are too low to explain it. There can be no fractionation of Ba from La in bulk assimilation crustal contamination models.

Thus, although crustal contamination appears at first sight to be a suitable mechanism to explain the geochemical characteristics of Sardinian basic alkalic magmas, there are important discrepancies between the model and the geochemical composition of the lavas.

TABLE 6.2

SIMPLE LEAST SQUARES BULK ASSIMILATION MODEL USED TO TEST THE FEASABILITY OF PRODUCING THE OBSERVED MAJOR ELEMENT COMPOSITION OF SARDINIAN HAWAIITE MAGMAS BY ASSIMILATION OF UPPER CRUSTAL ROCKS BY OCEAN ISLAND BASALT (OIB) MAGMAS

	Amounts	SiO_2	Al_2O_3	Fe_2O_3T	MgO	CaO	Na_2O	K_2O	TiO_2	MnO	P_2O_5	TOTAL
Reactants used												
K33[1]	100.00	50.44	15.38	10.36	7.47	7.91	4.04	2.50	2.05	.18	.55	100.88
Products used												
OIB[2]	79.86	44.57	13.32	13.11	8.49	10.48	3.02	1.36	3.36	.18	.84	98.73
C1[3]	20.14	75.29	14.00	1.63	.19	.25	2.97	5.16	.14	.01	.07	99.71
Estimated compositions												
Reactants		50.44	15.38	10.36	7.47	7.91	4.04	2.50	2.05	.18	.55	100.88
Products		50.76	13.46	10.80	6.82	8.42	3.01	2.13	2.71	.15	.68	98.93
Differences		-.32	1.92	-.44	.65	-.51	1.03	.37	-.66	.03	-.13	

Residual sum of squares = 6 3331
Distance between two estimated compositions = 2.5166

1 Sardinian hawaiite lava.

2 Ocean island basalt from the Cameroon line (Fitton and Dunlop, 1985).

3 Sardinian upper crustal quartzo-feldspathic gneiss.

All values in wt. % oxide.

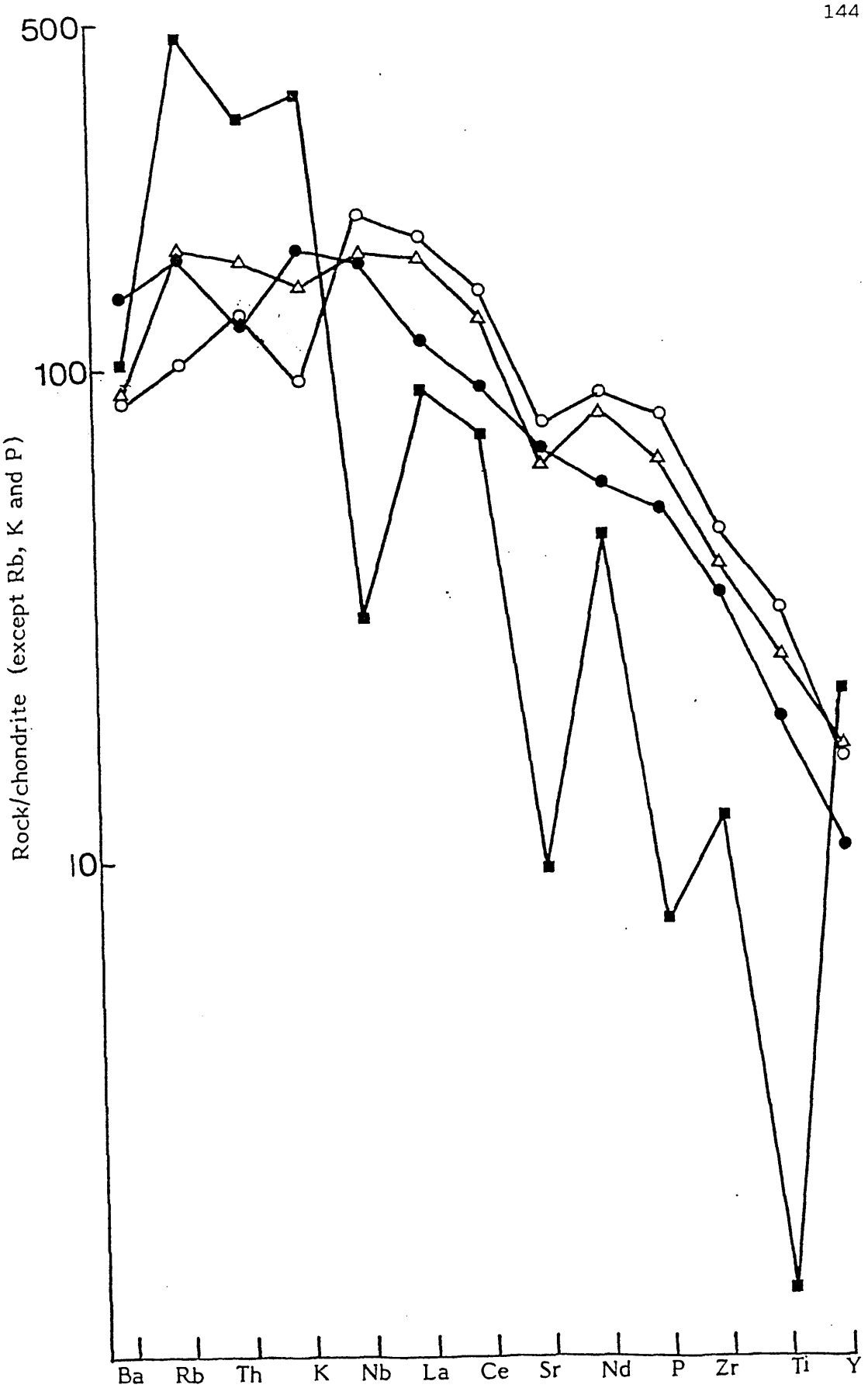

Figure 6.11

Genesis of Sardinian hawaiites by contamination of OIB by sialic crust. (See text for details). Filled squares = quartzo-feldspathic gneiss (C1); open circules = OIB (Fitton and Dunlop, 1985); open triangles = model composition, and filled circles = hawaiite (K33).

Figure 6.12

Ba/La against $^{87}Sr/^{86}Sr$ in Sardinian hawaiites.

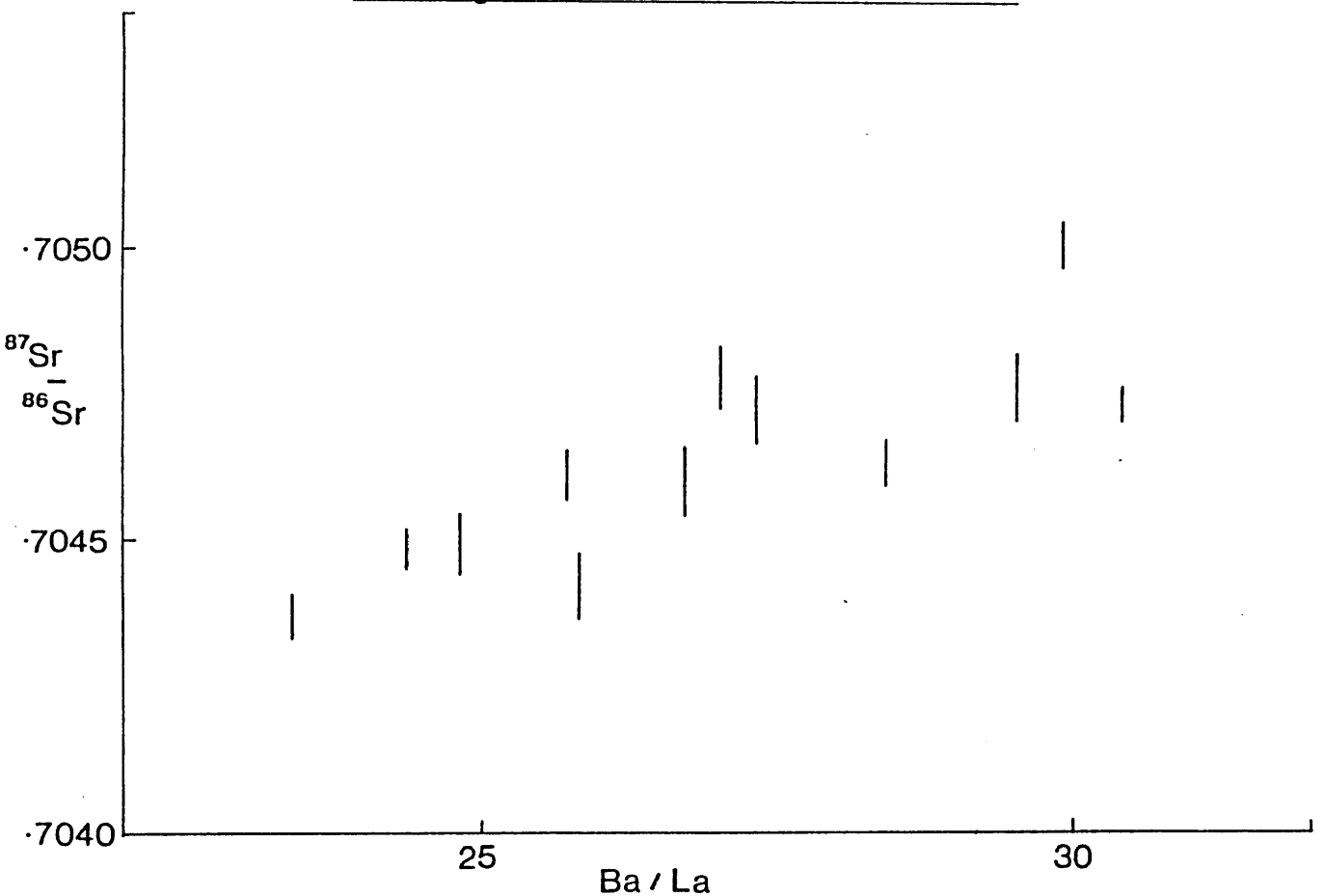

6.10 Fractionation of LILE from LREE - a subduction zone component in Sardinian alkalic magma genesis?

K, Rb, Th, Cs and Ba all have low ionic potential and are readily soluble in aqueous fluids (Pearce, 1982). The former presence of a subduction zone beneath Sardinia provides a means of fractionating such elements from the REE, by transport in H_2O-rich fluids emanating from the subducted slab, as it sinks through the mantle. The mantle wedge and the base of the continental lithosphere would therefore become enriched in LILE.

It is improbable that hydrous minerals can persist to the depth of generation of alkali basalts (Wyllie, 1984). More likely, contamination of mafic alkalic magmas occurred either in the mantle wedge or in the sub-continental lithosphere during ascent. Magmas probably rise through the mantle along grain boundaries (Ahren and Turcotte, 1978). There is some evidence that Sr is concentrated at grain boundaries in peridotites (Fraser et al, 1984), and therefore, possibly also the other LILE. Scavenging of these elements, which have been previously enriched by subduction zone processes, by rising alkalic melts could explain the LILE-enrichment of Sardinian alkaline lavas, which defy explanation by sialic contamination, provided that the subduction-enriched mantle could persist until alkali magma genesis began.

Heterogeneities can persist for long periods, even within the convecting asthenospheric upper mantle. Olson et al (1984) have shown that convective mixing in the mantle wedge will produce thin streaks of contaminated mantle sub-parallel to

the direction of flow. Thus, mixing of OIB with these enriched streaks can explain the observed positive correlation of Ba/La with $^{87}Sr/^{86}Sr$, and K/La with Ba/La (Figure 6.13). Lead isotopic evidence suggests the involvement of subducted pelagic sediment in the genesis of alkali basalts from N.E.. Japan, where subduction of the Pacific plate beneath Japan is currently active (Nakamura et al, 1985).

Reutter et al (1978) have suggested that Sardinia and the Adria plate underwent a post-collisional anticlockwise rotation of 30^{o}. A flip in the direction of subduction during the Miocene has been suggested by some authors (Boccaletti et al, 1971). This implies that much of the mantle beneath the western Mediterranean may have been metasomatised by the influx of LILE enriched fluids. High-K basic magmatism in the Roman and Campanian igneous provinces of Italy (Holm and Munksgaard, 1982; Rogers et al, 1985), may also be related to a palaeo-subduction zone. Metasomatised sub-continental mantle lithosphere is presumably coupled to the rotation, and in the absence of areally-extensive metasomatism of the asthenospheric mantle is a suitable enriched-source to explain the high abundances of some elements in Sardinian hawaiites and basanites. It is possible that the geochemical signature of subduction can be deciphered at least 13 Ma after the end of active subduction.

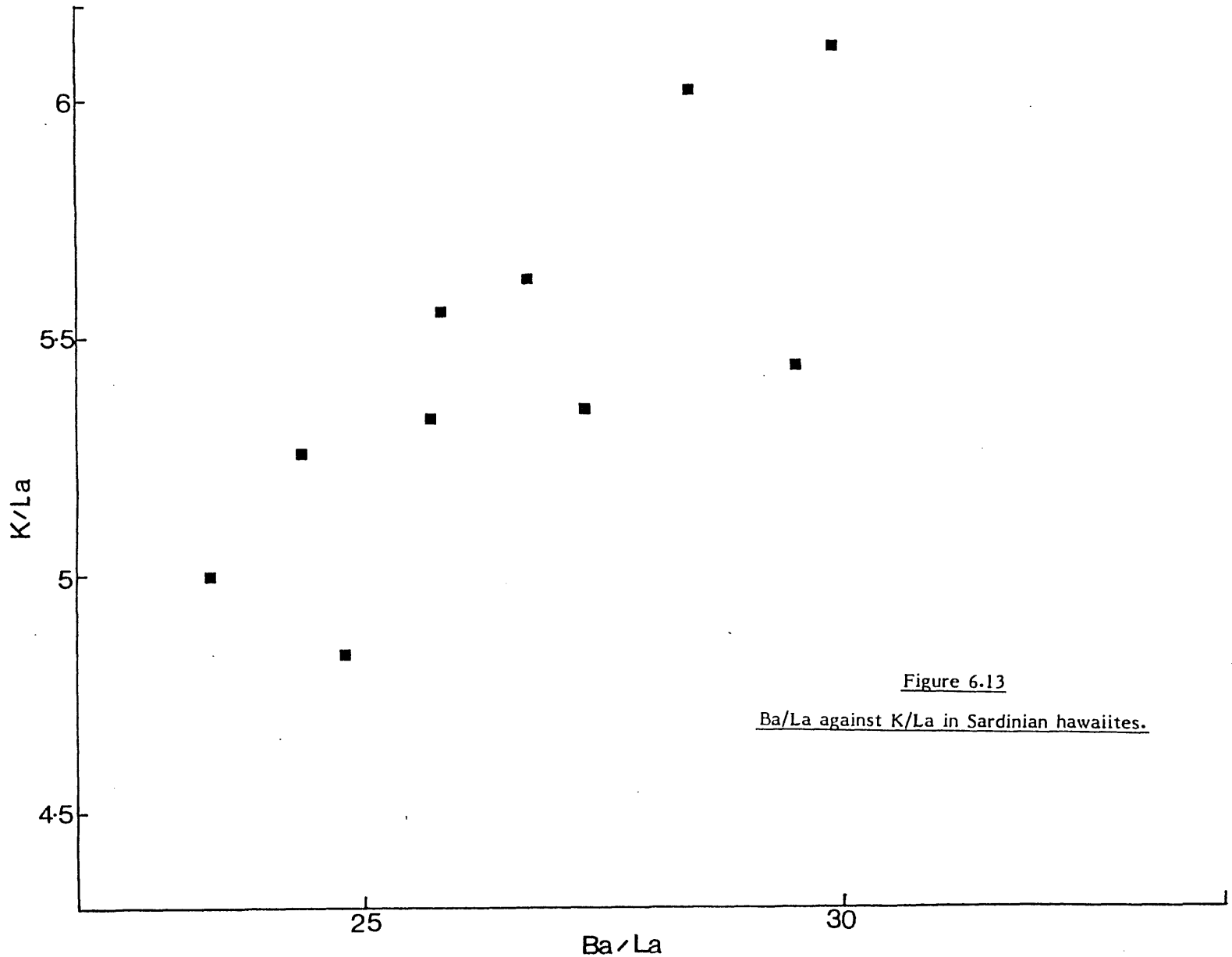

Figure 6.13

Ba/La against K/La in Sardinian hawaiites.

CHAPTER 7

THE TRANSITION FROM SUBDUCTION-RELATED TO EXTENSIONAL MAGMATISM - GEOCHEMISTRY OF PLIO-PLEISTOCENE HIGH-MG ANDESITES AND BASALTIC ANDESITES

The lower part of the Plio-Pleistocene volcanic sequence is dominated by basaltic andesite and high-Mg andesite lavas, which now outcrop as areally extensive lava fields, strongly dissected by erosion. Following Thompson et al, (1983), they are typical of continental flood basalts (CFB). Possible source rocks for Sardinian basaltic andesites and high-Mg andesites include the following:-

1. Heterogeneous lithospheric mantle (Menzies et al, 1984);
2. Assimilation of fusible sialic material by oceanic magmas during magma ascent through the continental crust (Thompson et al, 1983);
3. Input of previously subducted material into the mantle source of oceanic magmas.

The geochemistry of high-Mg andesites and basaltic andesites is discussed below in terms of the relative contributions of these various source components to magma genesis.

7.1 Geochemistry of basaltic andesites and high-Mg andesites

Chondrite-normalised multi-element patterns for some selected Sardinian basaltic andesites and high-Mg andesites are shown in Figures 7.1 and 7.2. Also shown is the comparative pattern for a basalt from the Rio Grande rift (US11; Thompson et al, 1983).

Figure 7.1

Chondrite-normalised multi-element patterns for selected Plio-Pleistocene basaltic andesites. Filled triangles = K85; filled circles = K111; and comparative data for US11 (Thompson et al, 1983; open circles).

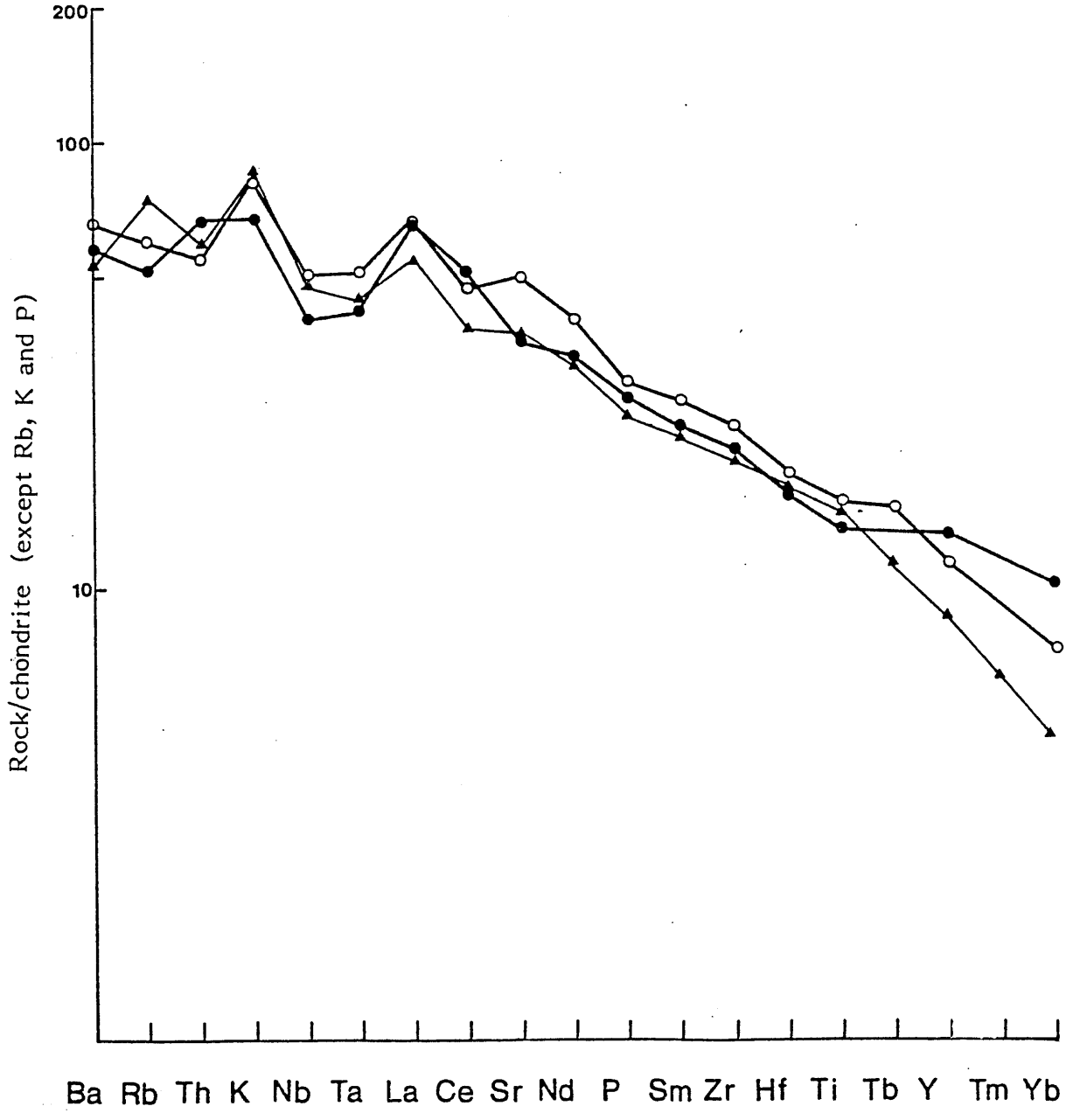

Figure 7.2

Chondrite-normalised multi-element patterns for selected Plio-Pleistocene basaltic andesites. Filled circles = K58; open circles = K110; and filled triangles = K64.

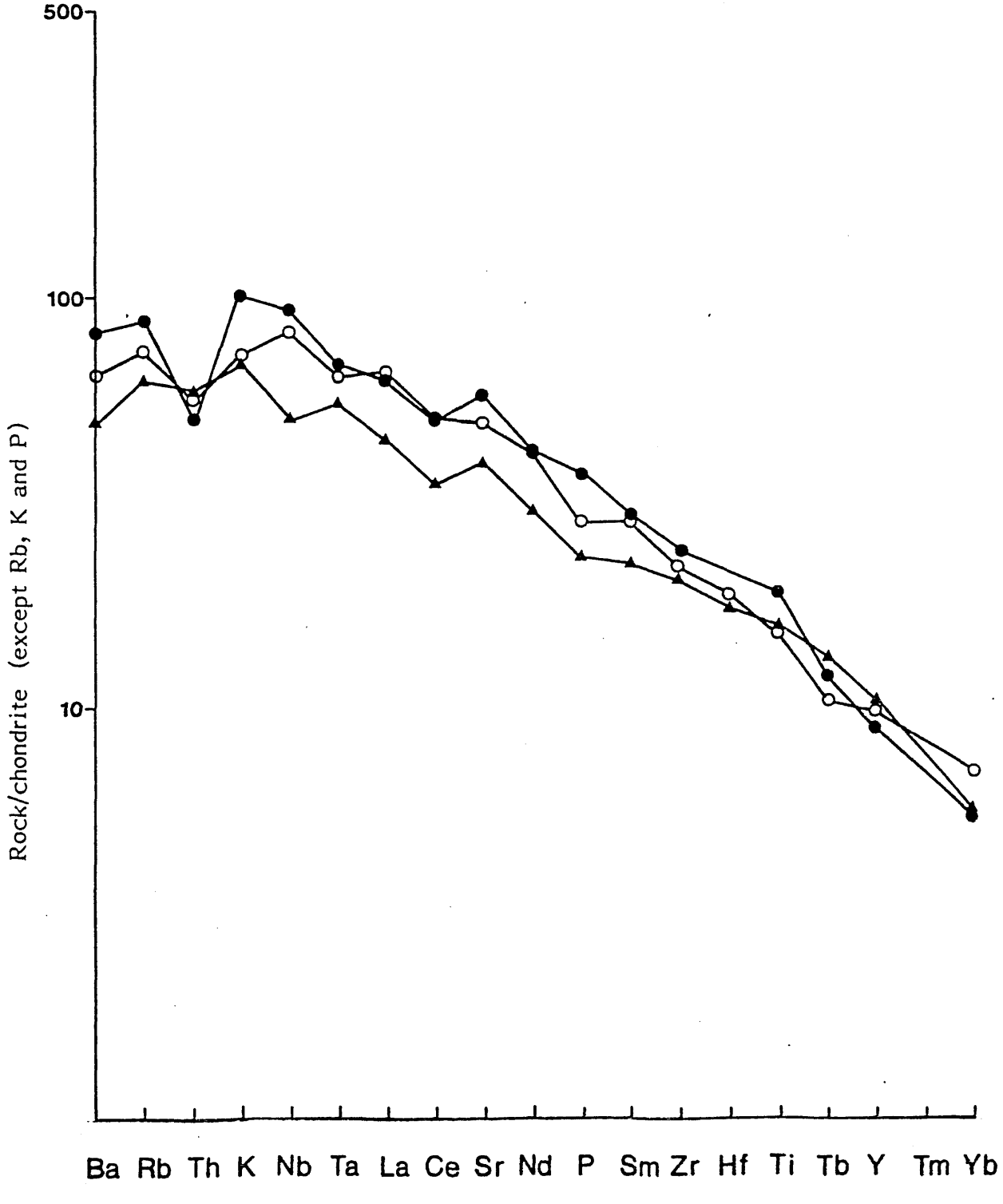

All the patterns in Figures 7.1 and 7.2 peak at K, and except for irregularities at Nb, Ta and Sr in some samples, slope downwards toward Yb. La/Y_N = 7-12 ratios, are moderately high, although lower than observed in contemporaneously-erupted hawaiites. The left-hand parts of the patterns are similar, and show a downward curvature from K to Rb. Ba/Rb_N = 0.7-1.3, Rb/Th_N = 1.1-1.3 and K/Th_N = 1.3-1.5 are similar to those ratios observed in Sardinian hawaiites. The samples in Figure 7.1 show a small trough at Nb and Ta, which results in moderately high La/Nb = 1.2 ratios. Relative Nb and Ta depletions have been observed in subduction-related volcanic rocks (see Chapter 5), and in CFB (Thompson et al, 1983). In the latter, they may reflect assimilation of low Nb and Ta crustal rocks by oceanic magmas, whereas low Nb and Ta abundances in IAV have been related either to the addition of small amounts of pelagic sediment to the mantle source of magmas, or to the retention of these elements in some residual mantle phase (Chapter 5).

La/Nb ratios in all analysed Sardinian Tertiary volcanic rocks are compared to La/Nb ratios of magmas erupted in several distinct tectono-magmatic settings in Figure 7.3. La/Nb ratios in Sardinian basaltic andesites and high-Mg andesites (sub-alkaline rocks) are within the range defined by OIB, but also overlap with the ranges for CFB and IAV (data from Thompson et al, 1983). It is therefore clear that La/Nb ratios cannot be used as a discriminant, separating magmas erupted in different tectonic settings (see also Thompson et al, 1983).

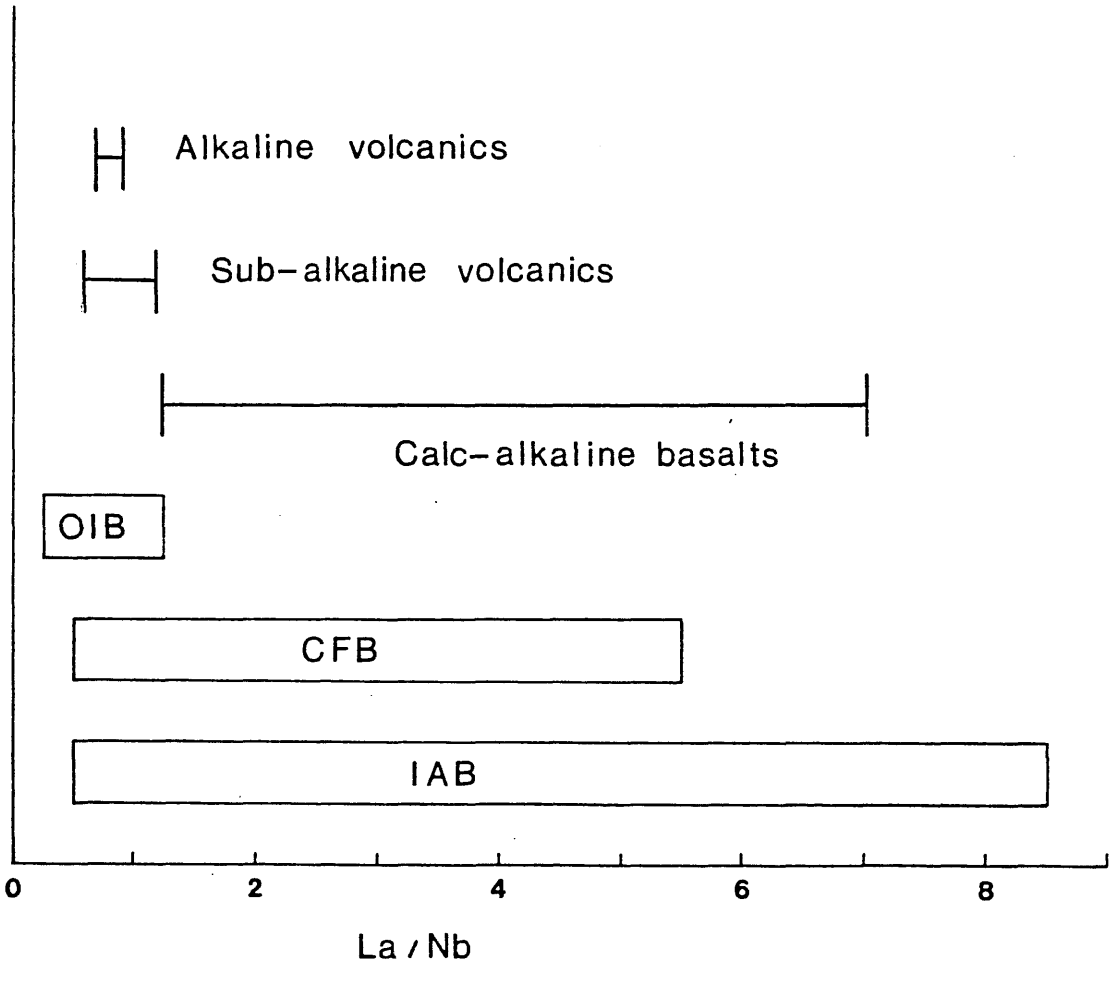

Figure 7.3

La/Nb ratios in Sardinian basaltic andesites and high-Mg andesites, with comparative data for other rock groups. IAB, CFB and OIB ranges are from Thompson et al 1983. Ranges for Sardinian alkaline volcanics and calc-alkaline basalts are from this work.

Some of the samples in Figure 7.1 and 7.2 peak at Sr, resulting in high Sr/Ce ratios (Sr/Ce = 28; MR25), which are typical of many calc-alkaline volcanic rocks (Pearce, 1982). However, relatively high Sr abundances in Sardinian basaltic andesites and high-Mg andesites are associated with a positive europium anomaly (see Chapter 4), which implies that the observed Sr peak may be related to the flotation of plagioclase phenocrysts. Relatively high Sr contents in Oligo-Miocene subduction-related volcanics are not associated with a positive Eu anomaly, which may reflect a high fO_2 (with Eu in the Eu^{3+} state), or the addition of high-Sr carbonate material to their mantle source (see Chapter 5).

Basaltic andesites and high-Mg andesites are characterised by generally lower La/Cs ratios than OIB and Sardinian hawaiites (Figure 7.4). This observation can be explained by the addition of a Cs-enriched component (possibly derived from subducted oceanic lithosphere) to their mantle source, or to a relative La depletion (residual perovskite?), much as envisaged for the genesis of Oligo-Miocene subduction-related lavas (see Chapter 5). The upper mantle beneath Sardinia may have been previously enriched in Cs (and the other LILE?) by earlier subduction-zone processes, presumably during the Oligocene and Miocene.

Lower La/Y_N ratios , relative to hawaiites, may reflect larger degree partial melting of a garnet-bearing mantle source. Such a model is discussed below.

Figure 7.4

La/Cs against Ba/La is same Tertiary volcanic rocks. Open triangles = subduction-ralted basalts; open circles = basaltic andesites, and filled circles = hawaiites. Open stars = OIB from Hawaii, Ascension and St. Helena (all from Kay, 1984)

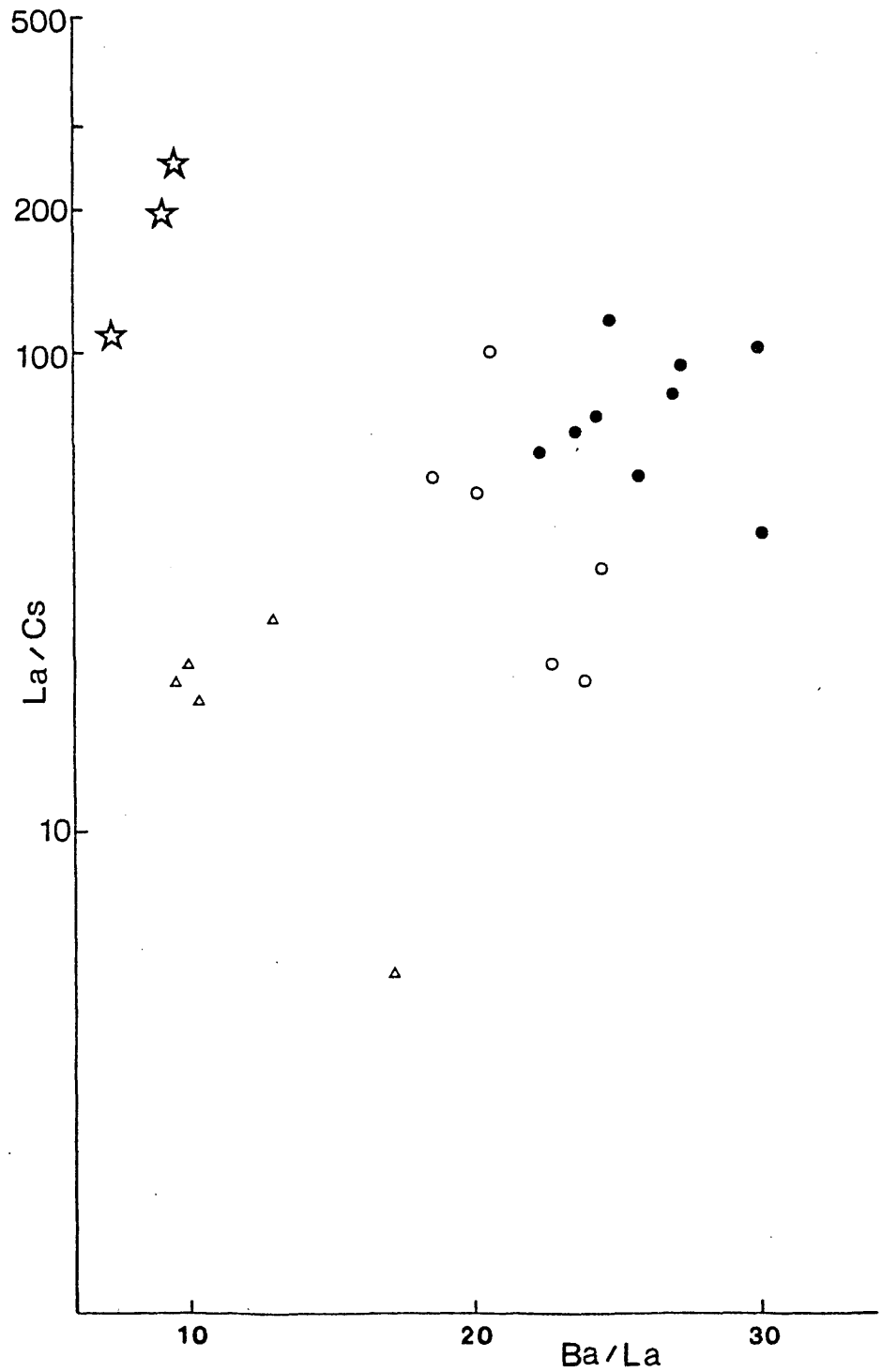

7.2 Role of varying degrees of melting of mantle peridotite in the genesis of Sardinian Plio-Pleistocene magmas

Chondrite-normalised multi-element patterns for a nepheline-normative hawaiite (K72), an olivine and hypersthene-normative hawaiite (K141), a quartz-normative basaltic andesite (K85) and a quartz-normative high-Mg andesite (PS7) are shown in Figure 7.5. Excepting the high La/Nb and Sr/Ce ratios in the more silica-saturated samples, the overall shape of the patterns is similar. The most noteworthy feature is the progressively steepening right-hand part of the pattern from K85 to K72, which results in increasing La/Yn from 5.7 to 29.7, respectively. This increase is consistent with a smaller degree of melting of garnet-bearing peridotite in the genesis of the more nepheline-normative basalts. Yb_N remains relatively constant, because of high $D_{Yb}^{gat/l} = 30$ (Henderson, 1981), while the LREE range in abundance by a factor 3. However, varying degrees of partial melting cannot explain the high La/Nb ratios observed in some basaltic andesites and high-Mg andesites (Figure 7.1). The possible role of crustal contamination, during magma ascent, in producing such ratios is discussed below.

7.3 The role of crustal contamination in the genesis of basaltic andesites and high-Mg andesites

Thompson et al(1983) suggest that most CFB are the product of the assimilation of crustal rocks by OIB-like magmas during magma ascent. They envisage a source for most continental anorogenic magmas within the convecting asthenospheric mantle.

Figure 7.5

Chondrite-normalised multi-element patterns for selected Plio-Pleistocene Sardinian lavas. Filled squares = K72; open squares = K141; filled triangles = K85; and filled circles = PS7.

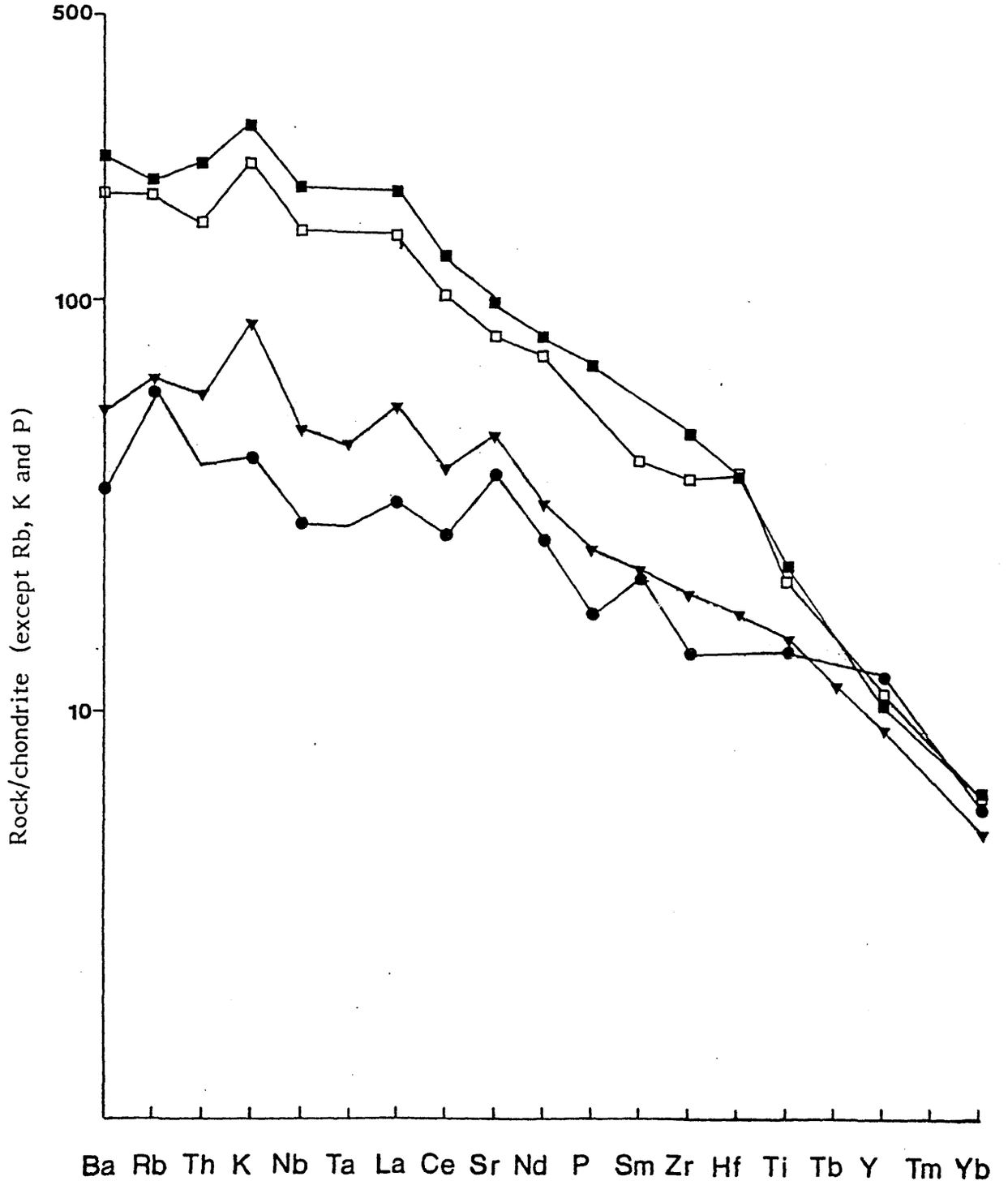

Similarly, Carson et al (1981), on the basis of Sr and Nd isotopic systematics, suggest that mafic lavas from the Columbia River Plateau evolved by the interaction of oceanic magmas with Precambrian sialic basement rocks.

Major element constraints require the addition of 20-30 wt. % of a possible sialic contaminant (in this case, a Sardinian quartzo-feldspathic gneiss; C1) to OIB magmas to explain the major element chemistry of Sardinian basaltic andesites and high-Mg andesites. However, Sardinian upper crustal silicic gneisses are characterised by high $^{87}Sr/^{86}Sr$ ratios ($^{87}Sr/^{86}Sr$ = 0.725; C1). Such ratios are too high to explain the genesis of these lavas by the required amounts of sialic assimilation. Further, all plausible contaminants are characterised by low Ba/Rb ratios (see Chapter 6), which cannot explain the high Ba/Rb ratios observed in Sardinian volcanic rocks. Although the genesis of rocks similar to US11 (Figure 7.1) have been explained by the assimilation of sialic crust (Carlson et al, 1981), this sample also shows a high Ba/Rb ratio (Ba/Rb = 22) which is difficult to explain by crustal contamination.

The isotopic evidence presented above does not preclude the addition of time-integrated low Rb/Sr lower crustal rocks to OIB-magmas as envisaged for the Skye Main Lava Series (Thompson et al, 1983). However, no lower crustal granulite-facies rocks are exposed in Sardinia, and although such a model can explain the high Ba/Rb of Sardinian lavas, it also produces high K/Th and K/Rb ratios, which have not been observed in these lavas. Because of the absence of lower crustal silicic rocks in Sardinia, no detailed geochemical modelling has been attempted.

Thus, crustal assimilation cannot explain all the geochemical variability observed in Sardinian basaltic andesites and high-Mg andesites. The similarity in inter-LILE ratios between these lavas and younger hawaiites may imply the involvement of a similar asthenospheric source, although they cannot be related by plausible crystal fractionation processes (see Chapter 4). However, high-Mg andesites from the Setouchi volcanic belt in S.W. Japan are thought to be primary mantle-derived magmas (Tatsumi, 1981), and the possible generation of Sardinian sub-alkaline magmas from hydrous sub-continental lithospheric mantle is discussed below.

7.4 The role of water in magma genesis

High-Mg andesites form an important constituent of the Setouchi volcanic belt in S.W. Japan, and have been shown using both petrographic and elemental evidence, and by high-P melting experiments, to represent primary mantle melts, produced by melting of hydrous peridotite within the mantle lithosphere (Tatsumi, 1981; Tatsumi and Ishizaka, 1981). Comparative major, and some trace, element data for Sardinian and Japanese samples are shown in Table 7.1. The Sardinian examples are characterised by lower MgO, Ni, Cr, SiO_2 (and generally K_2O), but higher TiO_2, than the Japanese lavas. High FeOT/MgO ratios (FeOT/MgO $\geq$ 1.39) and low Ni (Ni $\leq$ 147 ppm) make it unlikely that the Sardinian lavas represent primary mantle melts. Neither can they be derived from parental magmas similar to the Japanese samples, since no probable fractionating assemblage can simultaneously deplete the

TABLE 7.1

COMPARATIVE MAJOR ELEMENT, AND Ni AND Cr, DATA FOR HIGH-Mg ANDESITES FROM THE SETOUCHI VOLCANIC BELT, AND HIGH-Mg ANDESITES AND BASALTIC ANDESITES FROM NORTHERN SARDINIA

	TG1	SO-261	MR25	K83	K80	PS7
SiO_2	59.59	57.13	55.75	54.76	52.45	56.65
TiO_2	0.44	0.73	1.49	1.51	1.73	1.46
Al_2O_3	13.55	15.83	15.18	15.78	16.06	15.39
FeOT	6.32	6.33	8.69	8.52	9.23	8.51
MnO	0.12	0.13	0.14	0.13	0.14	0.10
MgO	9.65	7.39	6.11	6.11	6.04	5.70
CaO	6.24	7.19	7.15	7.26	7.50	7.23
Na_2O	2.66	2.89	3.95	3.98	3.98	3.65
K_2O	1.30	2.27	0.84	1.19	1.46	0.60
P_2O_5	0.13	0.14	0.19	0.28	0.34	0.18
Ni (ppm)	184	216	100	70	147	124
Cr (ppm)	472	324	214	181	234	210
FeOT/MgO	0.65	0.86	1.42	1.39	1.53	1.49

All values in wt. % oxide, except where stated
TG1 and SD-261 are high-Mg andesites from the Setouchi volcanic belt (Tatsumi, 1981)
MR25 and PS7 are Sardinian high-Mg andesites (this work)
K83 and K80 are Sardinian basaltic andesites (this work)

magma in Si, Mg, Ni, K and P while increasing Ti and Fe. However, this is not to say that Sardinian high-Mg andesites could not have differentiated from primary more Mg-rich basic andesites (although not the contemporaneously-erupted basaltic andesites; see Chapter 4) which formed by partial melting of the sub-continental lithospheric mantle.
The presence of water increases the silica-saturation of derivative melts (Wyllie, 1984), and water is almost certainly added to the upper mantle by subduction zone processes. The eruption of typical subduction-related high-Al basalt, dacite and rhyolite lavas at the base of the Plio-Pleistocene lava pile implies the longevity of subduction-related (hydrous?) magma-producing mantle. Indeed, the generation of Plio-Pleistocene LILE-enriched mafic alkaline magmas in Sardinia, has been explained by the mixing of OIB magmas with mantle peridotite previously metasomatised by aqueous fluids or melts (Chapter 6).
The available evidence strongly suggests that water was still available for magma generation during the Plio-Pleistocene, even though water is strongly partitioned into the magma during partial melting. Low Nb and Ta abundances in some basaltic andesites and high-Mg andesites can then be explained by the retention of these elements in some residual mantle phase during partial melting (see also Chapter 5). Again such a phase cannot be Ti-bearing because of the absence of a Ti-trough in their chondrite-normalised patterns.

The presence of mica and amphibole in mantle xenoliths (Menzies, 1983) shows that parts of the sub-continental mantle are both sufficiently enriched in LILE and hydrous (melting to produce high-Mg andesites can occur even under water undersaturated conditions; Tatsumi, 1981) to account for the generation of the precursors of Sardinian sub-alkaline magmas by partial melting. The absence of such hydrous phases in Sardinian spinel peridotites, brought to the surface by Plio-Pleistocene hawaiites (see Chapter 8), is not significant because it will be shown in the following chapter that they are derived from a restricted part of the upper mantle, somewhere near the top of the mantle lithosphere. The nature of the deeper lithosphere is therefore unknown.

Thus, the mantle source of high-Mg andesites and basaltic andesites may have been previously metasomatised by hydrous fluids or melts from the subducted slab. Relatively low K/Cs ratios (K/Cs = 20510; MR25) and high $^{87}Sr/^{86}Sr$ ratios in these rocks can be explained by mixing of subducted pelagic sediment ($^{87}Sr/^{86}Sr$ = 0.710) and mantle peridotite. The heat input required for melting of the mantle lithosphere may have been derived from the injection of hot mafic alkaline magmas (of deeper asthenospheric origin), which later formed the Plio-Pleistocene hawaiite lavas. Possible source rocks for Sardinian Plio-Pleistocene magmas are shown in Figure 7.6.

Figure 7.6

Possible source rocks for Sardinian Plio-Pleistocene volcanics. BA = basaltic andesites; HMA = high-Mg andesites; AB = alkali basalt; HAW = hawaiite. See text for details.

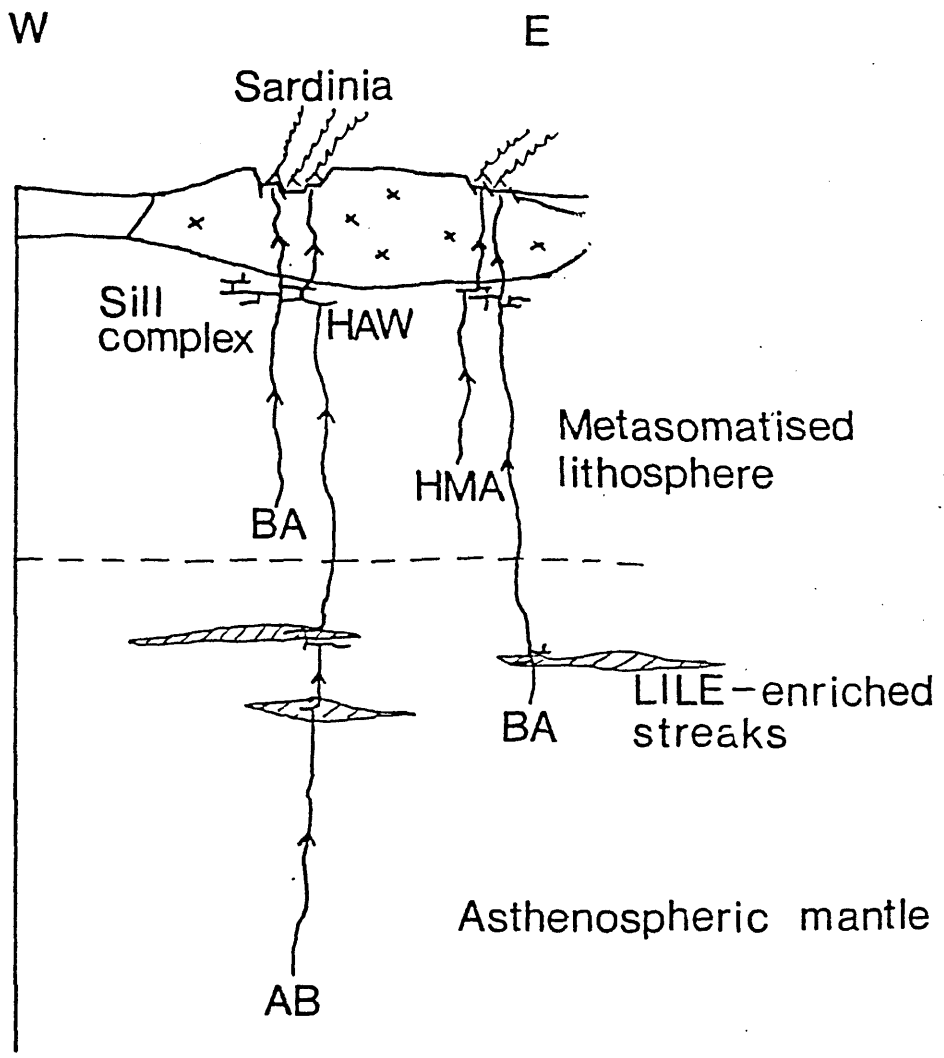

Thus, post-collisional magmatism in northern Sardinia was tapping a subduction-related mantle source (to produce the Pliocene high Al-basalt, dacite and rhyolite lavas), although active subduction had ceased at least 8 Ma previously. Gill (1976) has also shown that post-subduction lavas in Fiji are geochemically similar to earlier calc-alkaline magmas, associated with active subduction. Following continental collision in the Aquitainian, subduction migrated towards the south-east, with sea-floor spreading processes operating in the Tyrrhenian Sea, leaving Sardinia stranded as a remnant arc. LILE-enrichment in Plio-Pleistocene mafic alkaline lavas has been attributed to the mixing of OIB-magmas with mantle peridotite, variably metasomatised by fluids or melts from the subducted slab. Recent alkaline magma generation beneath Italy may involve melting of source mantle which has been previously metasomatised by subduction-related fluids or melts (Rogers et al, 1985). Sardinian basaltic andesites and high-Mg andesites may have formed by wet melting of mantle lithosphere, the water having been derived from previous subduction-zone processes.

7.5 Mantle dynamics during the transition from subduction-related to extensional magmatism

During the late Oligocene and Miocene subduction-related processes, probably involving the influx of LILE-enriched fluids or melts from the subducted slab into the mantle wedge, were active beneath Sardinia. Convection probably occurred within the asthenospheric mantle above the subducted slab, due to the sinking of relatively cold oceanic lithosphere into hotter asthenosphere. Within the asthenosphere, pods of LILE-enriched mantle may have been streaked out sub-parallel to the direction of this convective flow. Thinning of the lithosphere, during subsidence of the Sardinia Trough, may have facilitated passage of magmas to the surface.

The relationship between magmatism and mantle processes during the Plio-Pleistocene is unclear. After the cessation of active subduction (13 Ma) there may have been a continuous trickle of melts rising from the asthenosphere, which were unable to penetrate to the surface. However, following renewed extension (6 Ma), magmas may have been able to rise to the surface because of either or both of:-

1. Lithospheric thinning;
2. Reactivation of normal faults, which acted as conduits to the surface.

Therefore, possibly extensional tectonics accompanied surficial volcanism simply by allowing the passage of magmas to the surface. However, it is difficult to explain the sub-alkaline to alkaline transition using this model.

A second possible model suggests that extensional tectonics is causally related to Plio-Pleistocene volcanism, and that lithospheric extension triggered magmatism. In this model, lithospheric thinning causes rising of hot asthenosphere, and induces convection within the asthenosphere (Stecker, 1985). Upwelling asthenosphere may melt by decompression melting, eventually to form the younger hawaiite lavas. Heat would be transferred to the lower lithosphere because of two factors:-

1. Influx of hot alkaline magmas into, and through, the lithosphere;
2. Heat transfer from rising hot asthenosphere to cooler lithosphere.

This heat input may be sufficient to produce melting of metasomatised mantle lithosphere, and eventually form basaltic andesite and high-Mg andesite magmas. As the lithosphere cools, and as conduits to the surface for alkalic magmas become established, heat transfer to the lithosphere is reduced and lithospheric melting may cease. Erupted products will then be predominantly alkalic in composition.

CHAPTER 8

THE NATURE OF THE DEEP CRUST AND UPPER MANTLE BENEATH SARDINIA - EVIDENCE FROM INCLUSIONS IN ALKALINE MAGMAS

Ultrabasic and basic rocks and megacrysts are abundant as inclusions in Plio-Pleistocene hawaiite and basanite lavas and pyroclastics in northwestern Sardinia. They provide an important "window" into the nature of the lithosphere beneath the Sardinian continental block.

8.1 Field occurrence

Relatively dense ultrabasic xenoliths often occur as gravity-settled masses at the base of lava flows in northwestern Sardinia (cf. Frey and Prinz, 1978). In the lower part of an approximately 10m thick basanite, about 2 km S.W. of Padria, ultrabasic inclusions comprise over fifty volume percent of the flow. Such ponding of xenoliths implies a sudden decrease in flow velocity, possibly because of topographic irregularites. The rounded to sub-angular xenoliths range from 2 to 20 cm across. Some are banded, on a centimetre scale, with alternating olivine-rich and orthopyroxene-rich bands. Olivine and orthopyroxene xenocrysts are more common in scoriaceous material, and probably reflect the disaggregation of peridotite xenoliths during eruption.

Discrete, black clinopyroxene megacrysts ($\leq$ 2 cm), occurring both in the hawaiite lavas, and in a volcanic plug of hawaiite composition near Bonorva, have been the subject of preliminary study. Rare basic granulite-facies gneisses occur in some lavas.

The inclusions can be allocated to one of four distinct groups (after Upton et al, 1983):-

1. Magnesian peridotites;
2. Anhydrous pyroxenites;
3. Basic granulites;
4. Megacrysts.

The essential petrographic features of these four groups will now be discussed.

8.2 Petrography

1. Magnesian peridotites

Spinel peridotites are by far the most common type of inclusion in the Plio-Pleistocene mafic alkaline rocks. Modal compositions are shown in Figure 8.1, from which it is clear that all the xenoliths are spinel lherzolites or spinel harzburgites.

In hand specimen pale green olivine forms over seventy volume percent of the rock, with grey orthopyroxene predominating over emerald-green clinopyroxene. Black, metallic-lustred spinel generally forms less than three volume percent.

The peridotites contain no hydrous phases. Olivine and orthopyroxene range from 1-5 mm. Clinopyroxenes are generally less than 2 mm across, and accessory spinel grains less than 1 mm.

Spinel peridotite inclusions are generally thought to have retained the texture and fabric of their upper mantle source region (Mercier and Nicolas, 1975). Most studied here have a porphyroclastic texture (after the classification of Mercier and Nicolas, 1975). but a few have a mosaic texture (Harte, 1977; e.g. N6).

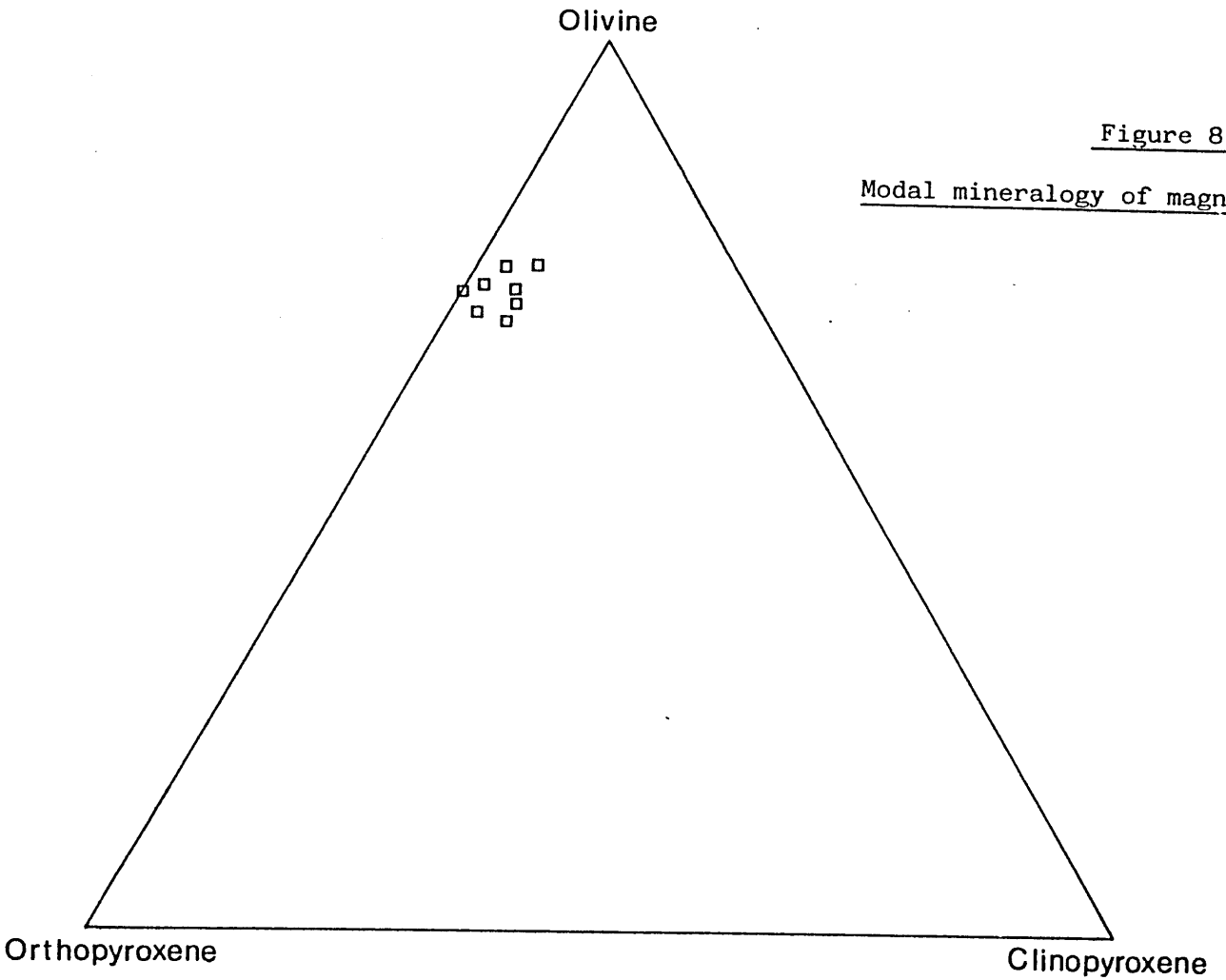

Figure 8.1

Modal mineralogy of magnesian peridotites

The porphyroclastic-textured peridotites consist of large (2-5 mm), strained porphyroclasts of olivine and orthopyroxene in a finer grained ($<$ 2 mm) re-crystallised matrix. Spinel and clinopyroxene occur solely within the matrix, which also contains olivine and orthopyroxene as unstrained neoblasts. Large, inequidimensional relict olivines, showing undulose extinction and kink-band boundaries, provide evidence for deformation within the upper mantle. The smaller, unstrained, rounded or polygonal olivines ($\lesssim$ 2 mm) sometimes possess a very close extinction position. This is good evidence for the effects of sub-grain rotation during deformation and re-crystallisation on an originally coarser grained peridotite ($>$ 5 mm), since grain size reduction accompanies re-crystallisation during deformation (Mercier and Nicolas, 1975). Grain-boundary equilibrium in the matrix is evidenced by 120^{o} triple junctions (Plate 8.1).

Impingement structures are common in the large ($>$ 3 mm) inequidimensional orthopyroxene porphyroclasts (Plate 8.2). It is mechanically easier for olivine to deform by inter-crystalline gliding than orthopyroxene (Nicolas et al, 1971), and thus orthopyroxenes appear to have deformed by the development of brittle fractures concentric to the impinging grains (usually olivine).

Small ($<$ 0.2 mm) spherical spinels are sometimes included within relict olivines or orthopyroxenes. More frequently, irregular or lobate spinels occur at grain boundaries. Sometimes they develop a "holly-leaf" form (Mercier, 1971); (Plate 8.1), and in some peridotites vermicular spinel is

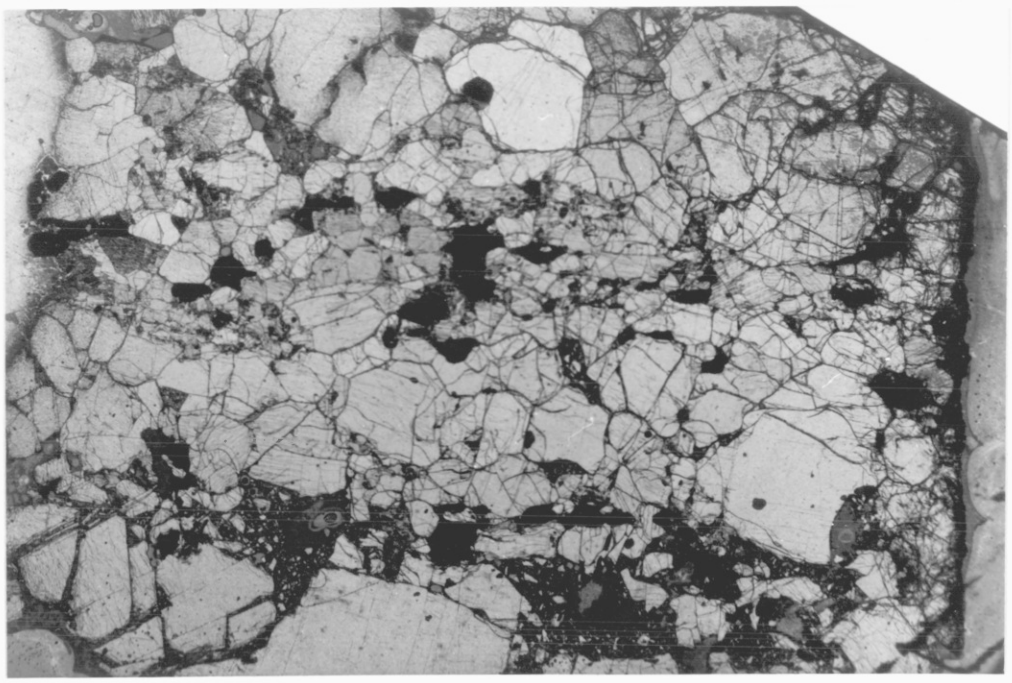

Plate 8.1

Porphyroclastic-textured spinel peridotite (T1)
A weak fabric is defined by parallel-aligned 'holly-leaf' spinel (opaque). Some of the matrix grains show well-developed 120° triple junctions.
Field of view represents 8.5 cm

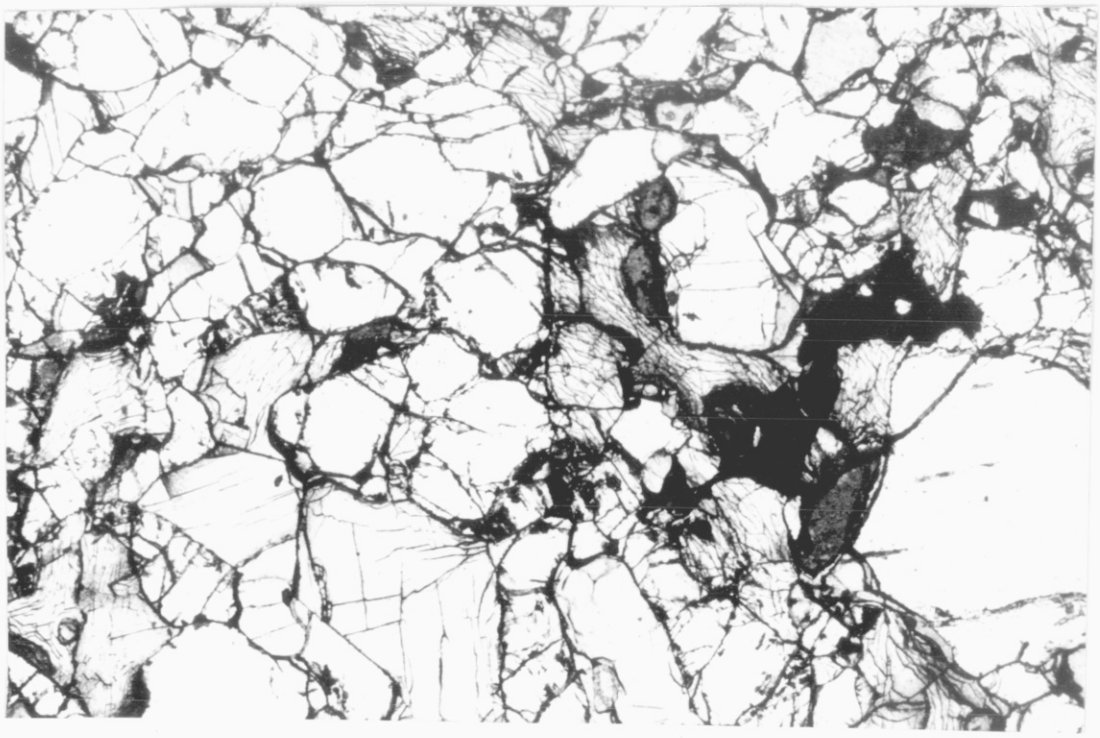

Plate 8.2

Impingement structures in orthopyroxene porphyroclasts. Note the concentric fractures which have developed adjacent to impinging olivine grains. Vermicular spinel is associated with orthopyroxene (bottom right)
Field of view represents 7cm.

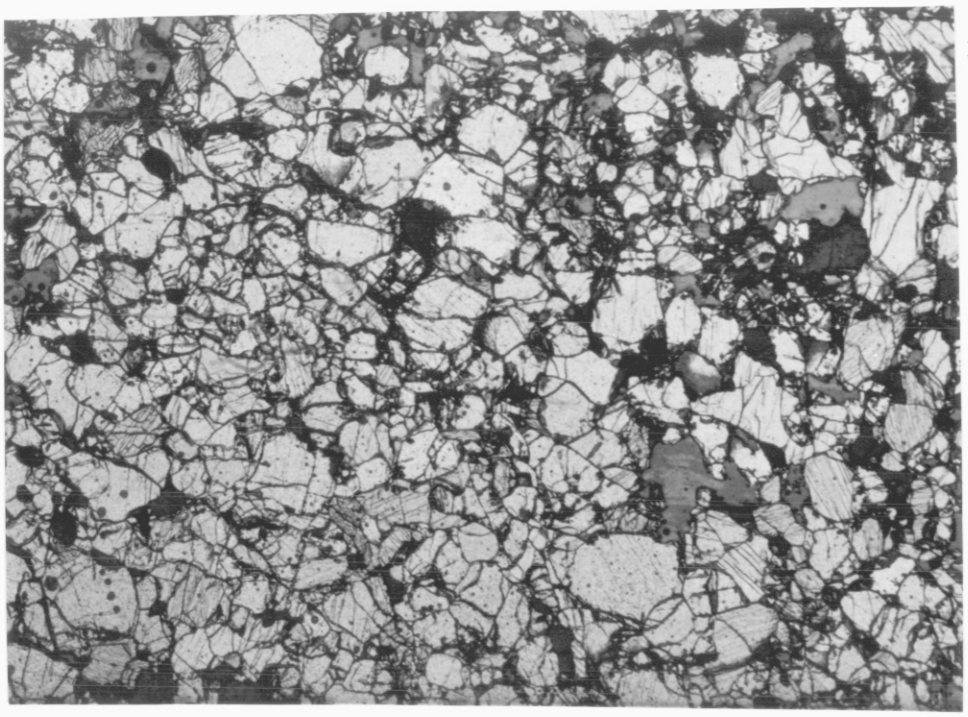

Plate 8.3

Mosaic texture in a spinel peridotite (N6)
Field of view represents 7.5 cm.

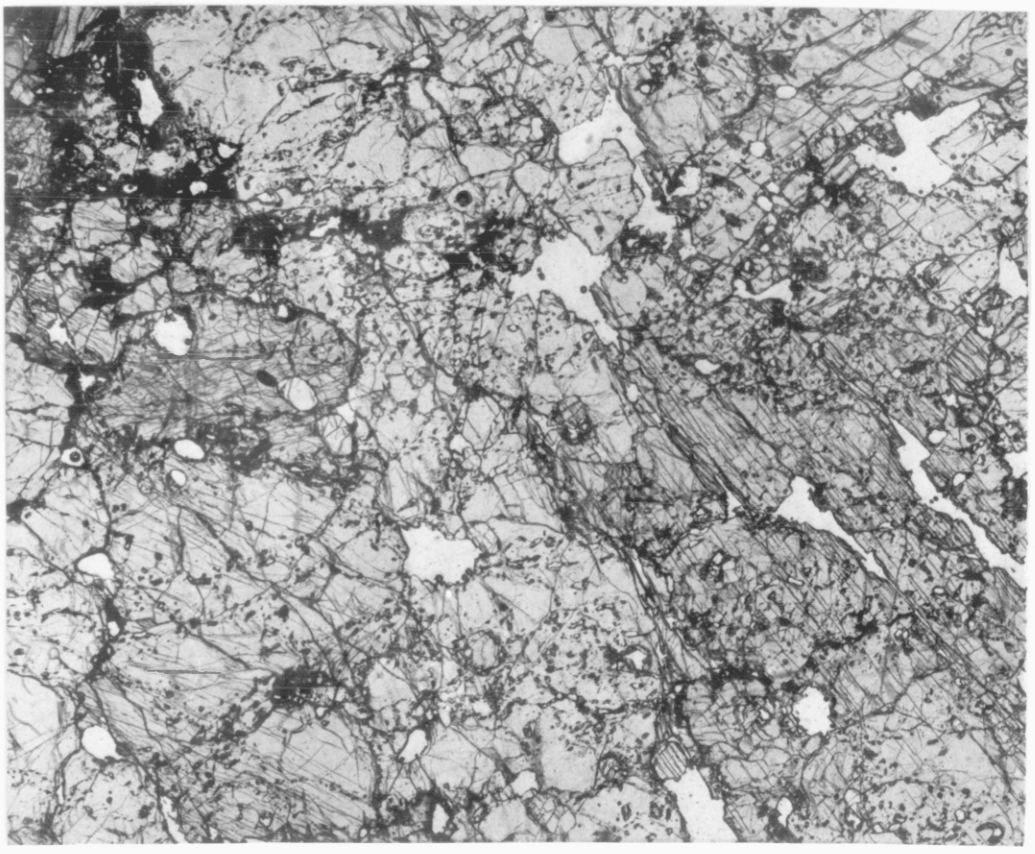

Plate 8.4

Exsolution of Ca-poor pyroxene from an augite host in a pyroxenite (TI-1). The exsolved grains trend NW-SE, and can be recognised by their slight relief differences. Field of view represents 5 cm.

associated with orthopyroxene (Plate 8.2).

Although no detailed petrofabric analysis has been attempted, a weak fabric is defined by a combination of the following:

(i) Sub-parallel preferred orientation of inequidimensional olivine and orthopyroxene porphyroclasts (Plate 8.1);

(ii) Discontinuous parallel-aligned strings of spinel (Plate 8.1);

(iii) Flattening of olivine grains.

Orthopyroxenite bands are sometimes interlayered with the spinel peridotites. These are up to 2 cm thick, with sharp plane-parallel contacts with the adjacent peridotite.

Mosaic-textured peridotites consist of small ($<$ 0.8 mm) grains of olivine and orthopyroxene, often with curved boundary segments (Plate 8.3). Most of the grains are equant, with only rare development of a weak fabric in some samples. Small, spherical spinels are sometimes included within olivine, and also occur at grain triple junctions, which show abundant evidence for grain-boundary equilibrium (i.e. 120^{o} triple junctions). Spinel and diopside grains are evenly distributed throughout the rock.

2. Anhydrous pyroxenites

Clinopyroxene-rich inclusions are found with magnesian peridotites at some localities. They consist of pale green clinopyroxene ($\sim$2 mm), with subordinate pink orthopyroxene ($\sim$1 mm). They have a xenomorphic-granular texture, with many of the grains having curved boundary segments. Both pyroxenes are unzoned, and the clinopyroxenes sometimes show sub-solidus exsolution of a Ca-poor pyroxene (Plate 8.4). Rarely, they are strained, showing undulose extinction. The polyonal microstructure is

equivocal as to their origin, which may be magmatic (e.g. cumulate) or as a metamorphic tectonite.

3. Basic granulite

Two samples of probable deep crustal origin have been brought to the surface as inclusions within Plio-Pleistocene mafic alkaline lavas. Both consist of an anhydrous mineral assemblage consisting of plagioclase, olivine, spinel, orthopyroxene and clinopyroxene. A gneissose foliation, on a mm scale, is defined by alternating mafic and felsic bands. This may reflect an original igneous layering, or metamorphic differentiation, or a combination of the two. There are no visible reaction relationships between the constituent minerals, although the most noteworthy petrographic feature is a symplectic intergrowth of dark green hercynitic spinel and clinopyroxene. This may be the result of exsolution of spinel and pyroxene from an original Ca-rich garnet at high pressure. Plagioclase ($\lesssim$ 1 mm) is unzoned, and has a granoblastic texture, which implies annealing during metamorphic differentiation. 120° grain boundary intersections are abundant in the felsic bands.

4. Discrete megacrysts

Clinopyroxene megacrysts ($\lesssim$ 2 cm) are black and vitreous in hand specimen. They are variably corroded, and show evidence for syn-eruptive partial melting and re-equilibration with the host lava (Plate 8.5).

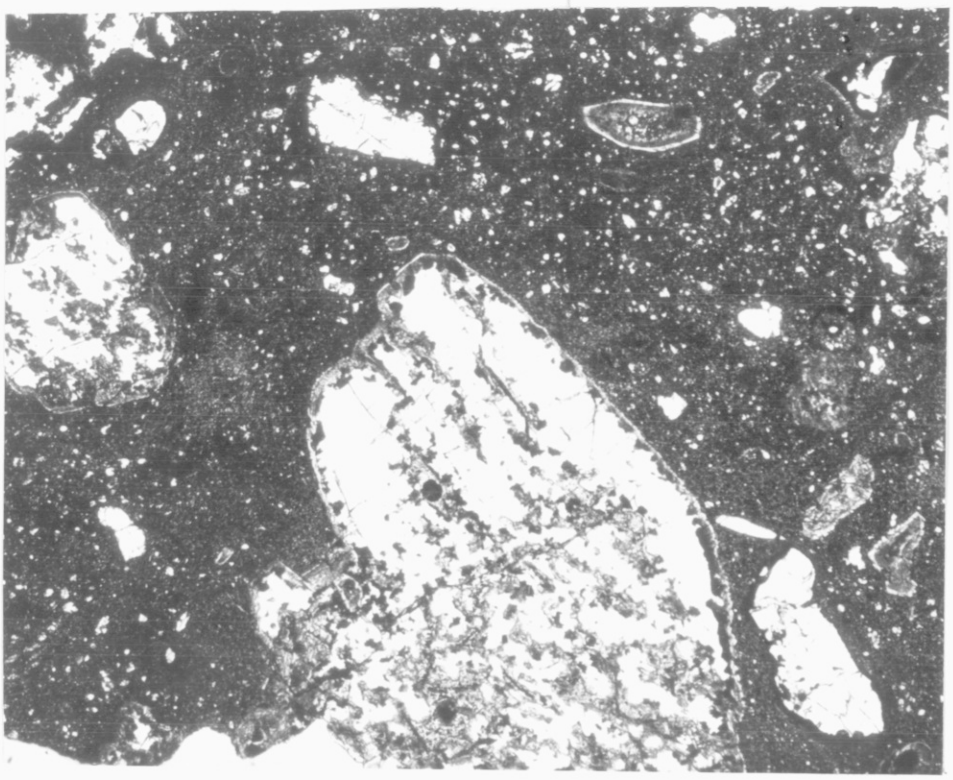

Plate 8.5

Clinopyroxene megacryst (bottom centre left) in hawaiite (K162)
Sieve texture is probably due to incipient
partial melting.
Field of view represents 5 cm.

5. Petrographic features of lava-inclusion reaction

Except where there has been pervasive melt entry into the xenolith, reaction is confined to the margins of xenoliths and megacrysts. Clinopyroxenes often develop spongy border zones in contact with the host basalts, which has been interpreted in terms of small degree partial melting induced by the high temperature of the magma and a reduction in pressure during magma ascent and involving Na loss from the pyroxene (White, 1966). Brown, Cr-rich spinel reacts with the magma to form a more Fe-rich black magnetite rim, up to 0.5 mm thick. Orthopyroxene generally reacts to form a rind ($<$ 1 mm thick) of fine-grained rounded olivines. Olivines are slightly zoned, being more Fe-rich adjacent to the lava.

8.3 Mineral chemistry

Mineral compositions in each xenolith were determined using a Cambridge Instruments Microscan V electron microprobe. Operating conditions are given in Appendix A. Representative point analyses of minerals are given in Appendix D. Compositional variation between similar minerals within individual xenoliths is negligible, and the variations discussed here are between one xenolith and another.

1. Magnesian peridotites

The olivines have a restricted compositional range, varying from Fo 89.1 to Fo 91.3 (ave. Fo 90.2; Figure 8.2). Slight zoning occurs towards a more Fe-rich rim only where they are in contact with the host lava (see above). Ni contents are high (NiO $<$ 0.54 wt. %), and comparable

Figure 8.2

Forsterite content of olivines in spinel peridotites

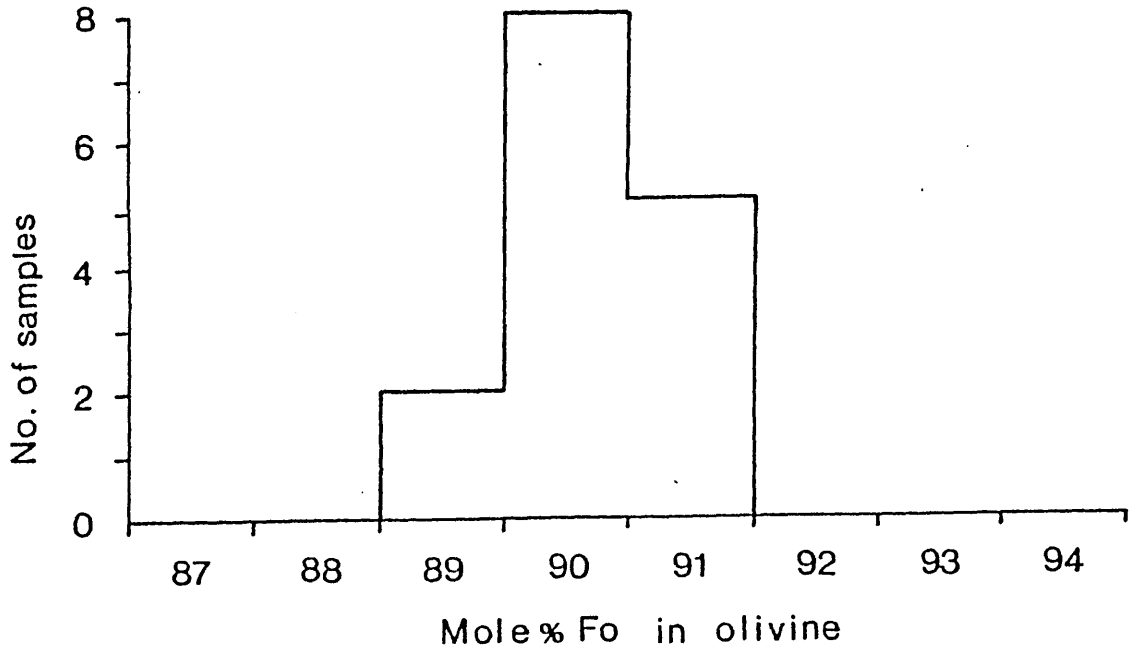

to values reported for olivines from other spinel peridotites (e.g. Brown et al, 1982).

The orthopyroxenes are unzoned and Mg-rich (MgO = 31.7 - 33.6 wt. %), with an average end-member composition of En 89.0 Fs 9.5 Wo 1.5. Compositions are shown in the pyroxene quadrilateral in Figure 8.3. Exsolution of a Ca-rich component was not observed, either optically or by back-scattered electron imagery. They are relatively homogeneous with respect to their CaO, FeO and MgO contents, but show considerable inter-xenolith variations in alumina (Al_2O_3 = 2.6 - 5.4 wt. %). This is related to the Cr : Al ratio in co-existing spinel (Figure 8.4).

Clinopyroxene compositions are also shown in Figure 8.3. Their diopsidic composition clusters closely around an average of En 48.5 Fs 4.9 Wo 46.5. Characterised by low TiO_2 ($TiO_2 \leqslant$ 0.51 wt. %) and high Cr_2O_3 ($Cr_2O_3 \geqslant$ 0.65 wt. %) contents, they are similar to Group 1 inclusions from San Carlos, Arizona (Frey and Prinz, 1978). The alumina content varies from xenolith to xenolith (Al_2O_3 = 3.6 - 6.9 wt. %), correlated with the Cr : Al ratio in co-existing spinel (Figure 8.4), as with the orthopyroxenes. The chemistry of co-existing pyroxenes varies sympathetically from one xenolith to another (Figure 8.5). Clinopyroxenes from spinel peridotites can be distinguished from those occurring in pyroxenites, and as megacrysts, on the basis of their higher Cr content (Figure 8.6).

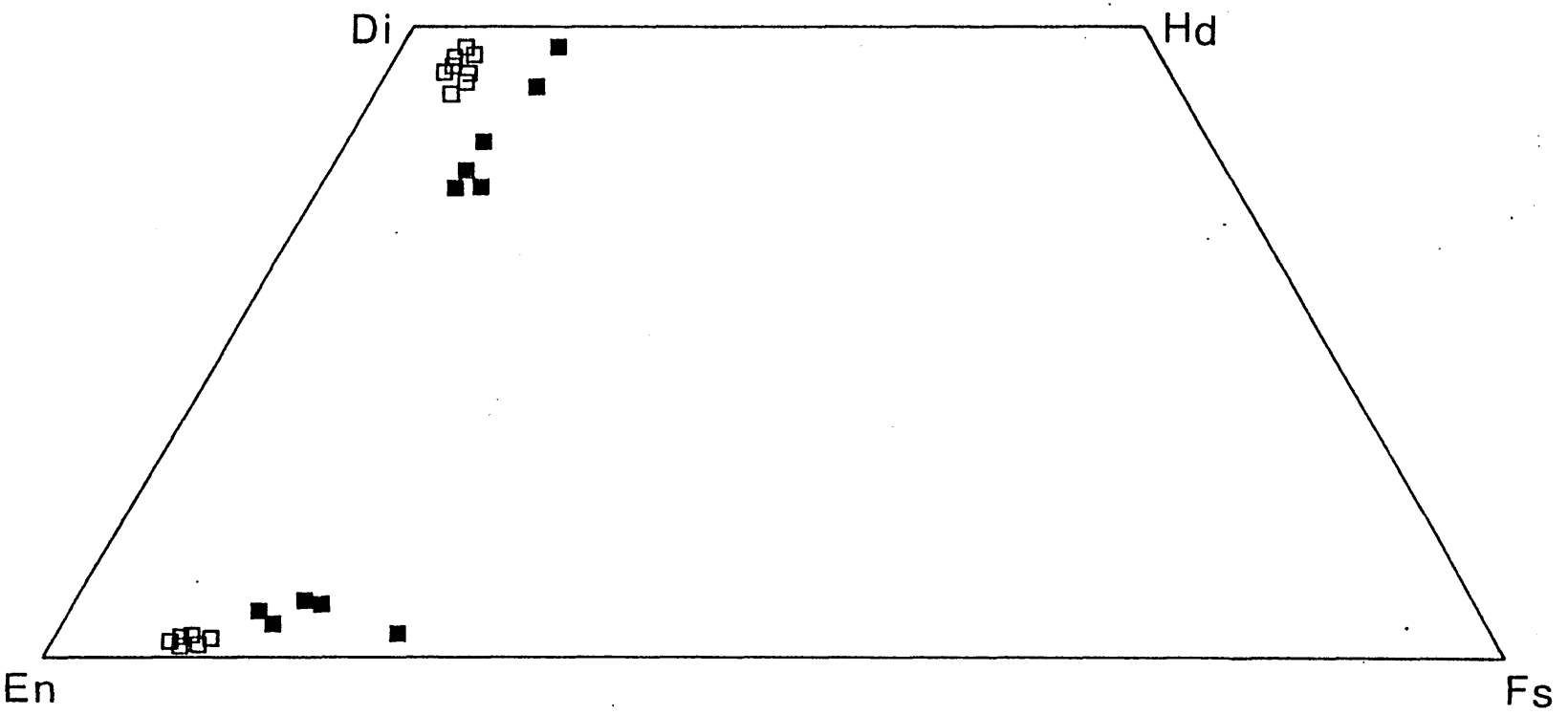

Figure 8.3

Compositional variation of pyroxenes in mantle inclusions. Open squares = spinel peridotite; filled squares = pyroxenes and megacrysts.

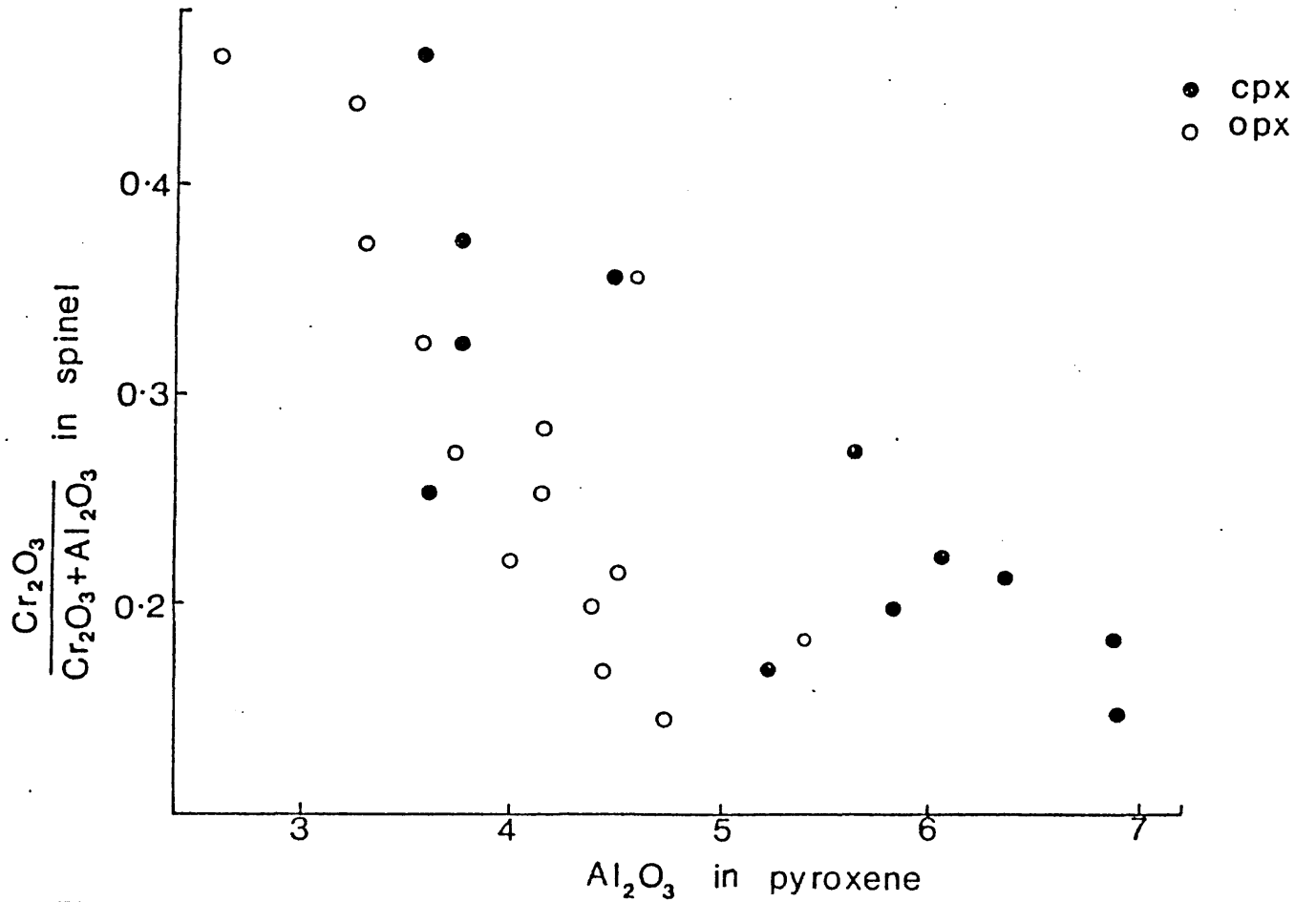

Figure 8.4

Variation of Al_2O_3 in pyroxenes against $Cr_2O_3/Cr_2O_3 + Al_2O_3$ in coexisting spinels

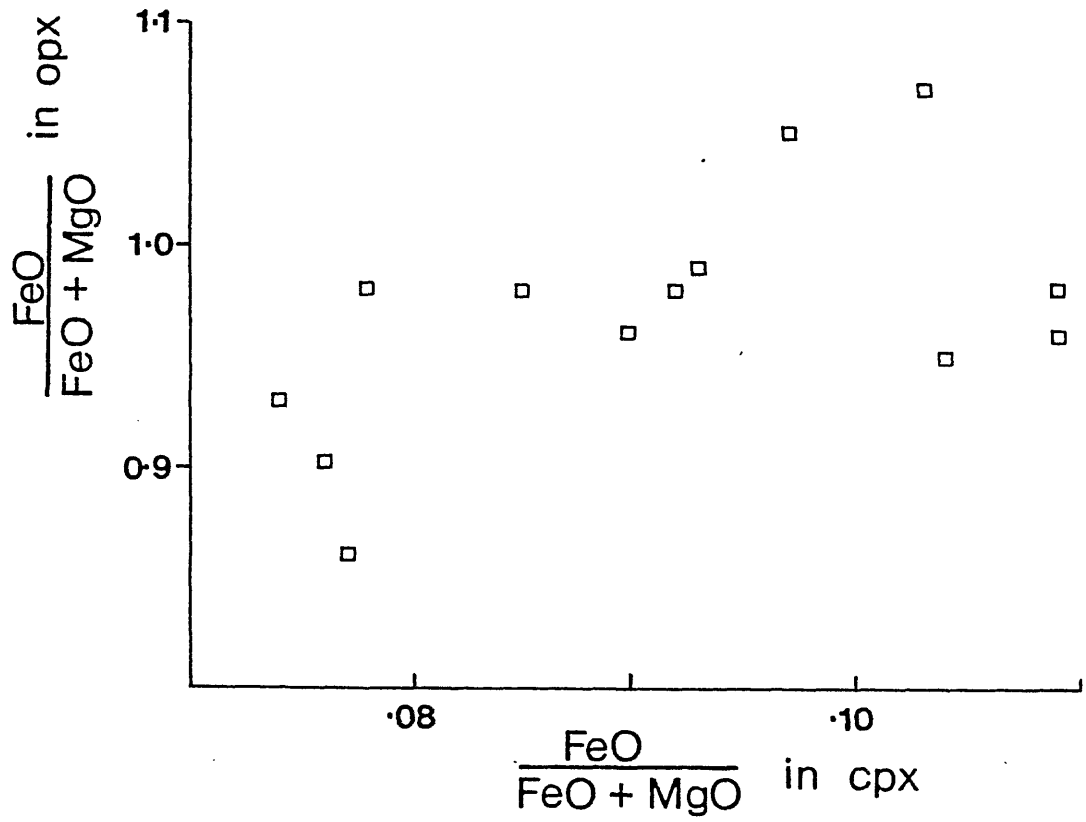

Figure 8.5

Fe/Mg ratios in co-existing pyroxenes from spinel peridotite inclusions.

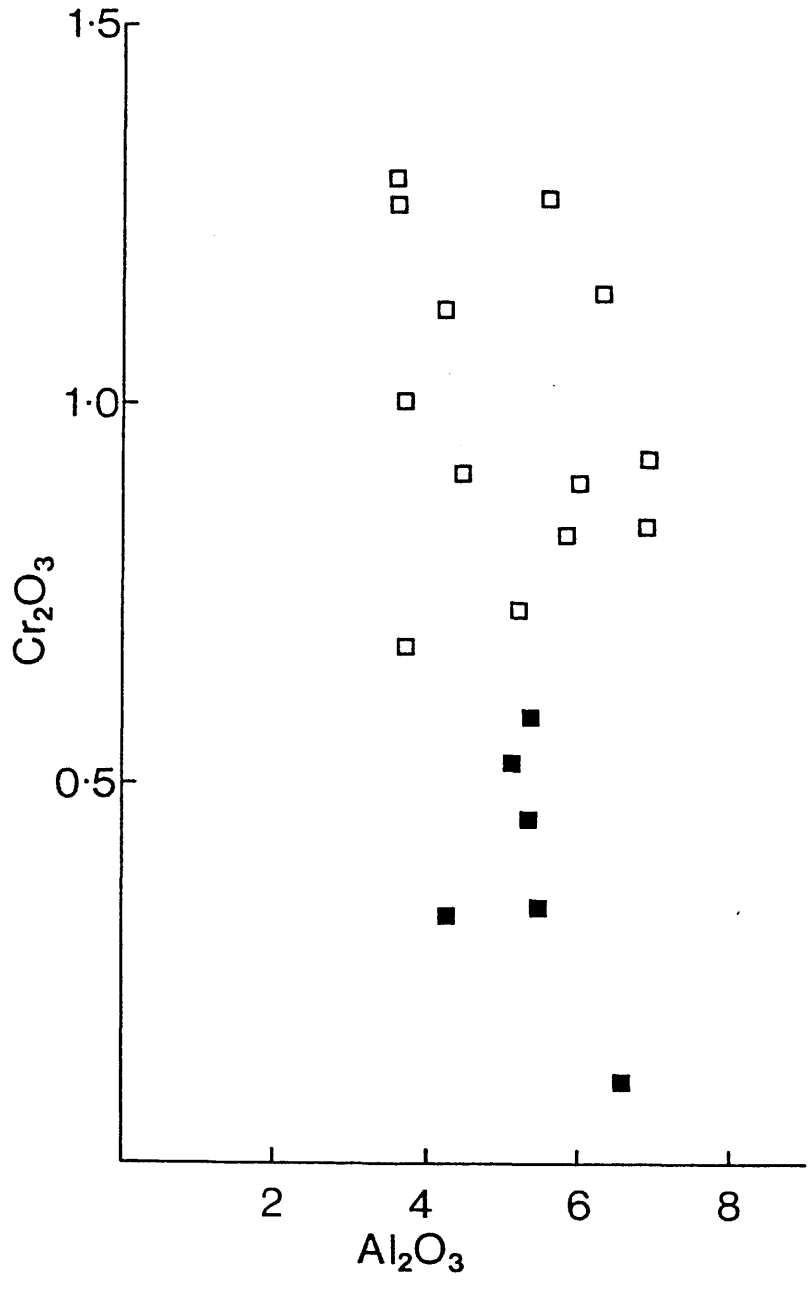

Figure 8.6

Plot of Cr_2O_3 against Al_2O_3 in clinopyroxenes
Open squares represent magnesian peridotites, and filled squares represent megacrysts and pyroxenites

Since the spinels are all Cr-rich (after the classification of Carswell, 1980), the peridotites can be classed as Cr-spinel peridotites. There is considerable variability in their alumina (Al_2O_3 = 9.8 - 31.7 wt. %) and Cr (Cr_2O_3 = 36.6 - 57.4 wt. %) contents from xenolith to xenolith. The Cr : Al ratio is related to the alumina content of co-existing pyroxenes (Figure 8.4), and their Cr/Cr + Al ratio decreases with increasing Mg/Mg + Fe (Figure 8.7). Zoning occurs only where spinel is in contact with the host lava (see above). Estimated temperatures of equilibration, derived using the two-pyroxene geothermometer of Wells (1977), calculated for peridotite xenoliths of contrasting mineral chemistry, lie within the estimated error limit for this geothermometer (see below). Therefore these systematic and sympathetic between-xenolith variations in mineral chemistry are probably related to variations in bulk rock chemical composition rather than to different physical conditions of equilibration.

2. Anhydrous pyroxenites

Rocks of pyroxenite mineralogy contain black, Fe-Ti rich clinopyroxenes, and are similar to the Group II pyroxene-bearing nodules of Frey and Prinz (1978). Ca-rich pyroxenes are augitic, with an average end-member composition of En 41.0 Fs 10.8 Wo 48.2. They are unzoned, and have a lower Cr : Al ratio than diopsidic pyroxenes from spinel peridotites (Figure 8.6). Pyroxene compositions are shown in Figure 8.2. The augites are characterised by higher

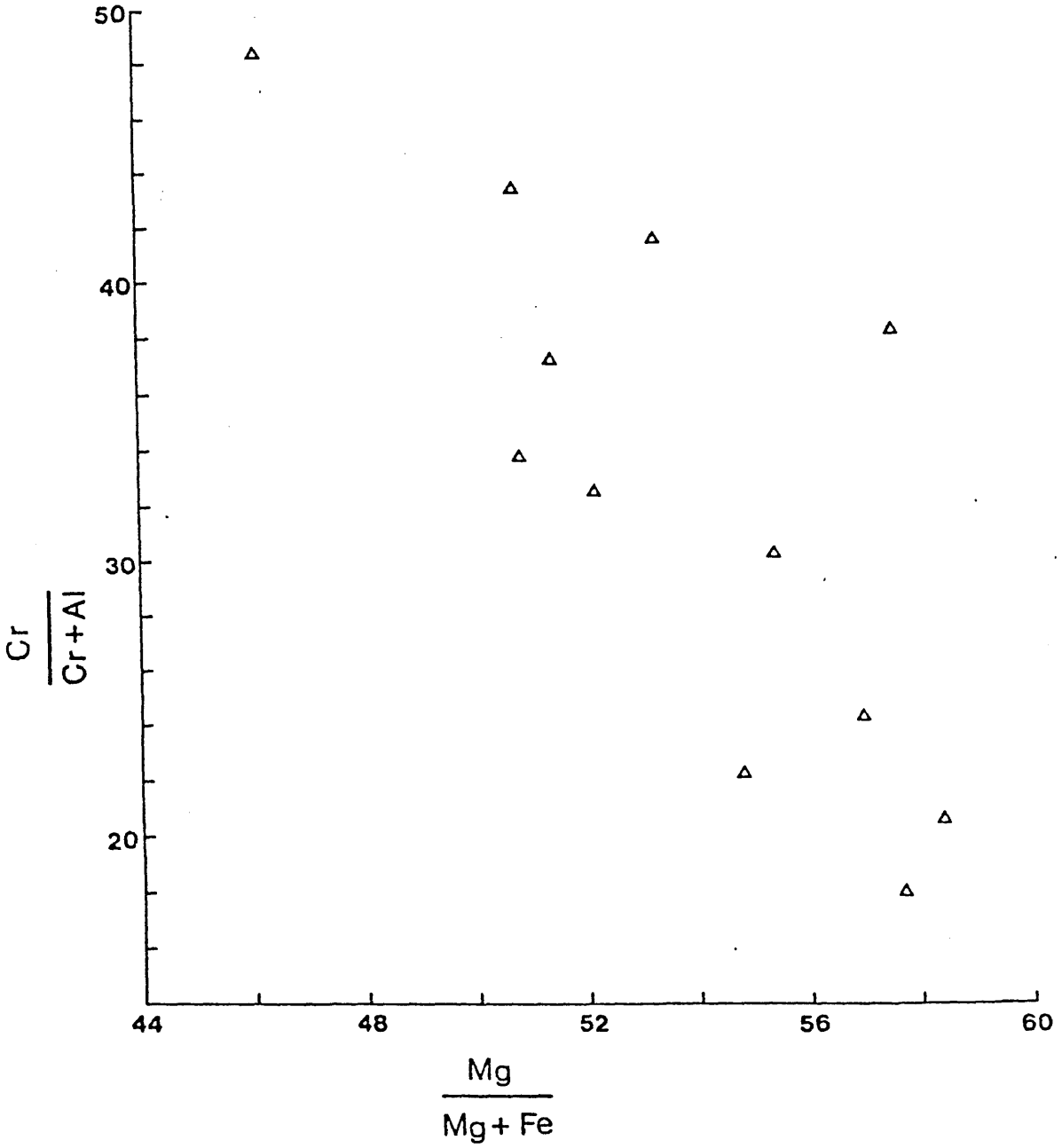

Figure 8.7

Decreasing Cr/Cr + Al with increasing Mg/Mg + Fe in spinels

FeO/FeO + MgO (0.15 - 0.21) ratios than the diopsides. They also have higher Ti ($TiO_2 \geq$ 0.4 wt. %) and Al ($Al_2O_3 \geq$ 4.2 wt. %) abundances. Orthopyroxenes are characterised by high alumina (Al_2O_3 = 4.0 - 4.8 wt. %) and low calcium (CaO = 0.7 - 1.5 wt. %) contents, which is consistent with a relatively high pressure origin (Thompson, 1974). They vary in composition from one xenolith to another, ranging in chemistry from En 83.4 Fs 13.8 Wo 2.8 to En 75.3 Fs 23.3 Wo 1.4.

3. Basic granulites

The olivine of the basic granulites is more Fe-rich than those from the spinel peridotites, having an end-member composition of Fo 78.6 Fa 21.4. The spinels are dark green, Fe-rich hercynites, with higher ferrous iron (FeO $\geq$ 18.9 wt. %), lower Cr ($Cr_2O_3 \sim$ 0.05 wt. %) and higher alumina ($Al_2O_3 \sim$ 61.5 wt. %) than the spinels from the magnesian peridotites. The spinel forms a symplectic intergrowth with Ca-rich pyroxene (En 42.6 Fs 7.9 Wo 49.5). The enstatitic orthopyroxene (En 78.2 Fs 20.5 Wo 1.3) is more Fe-rich than those in the spinel peridotites. The high Al_2O_3 content of both pyroxenes, and the low Ca abundance of the enstatite (CaO $\leq$ 0.65 wt. %) are characteristic of high grade pyroxene granulites.

4. Clinopyroxene megacrysts

Augitic clinopyroxene megacrysts (average composition = En 44.4 Fs 10.7 Wo 44.9) are chemically similar to the Ca-rich pyroxenes of the anhydrous pyroxenites. They are characterised by higher Al ($Al_2O_3 \gg$ 4.2 wt. %) and lower Cr ($Cr_2O_3 \leq$ 0.33 wt. %) than diopsides from spinel peridotites

(Figure 8.5). Their high Al_2O_3 and high Na (Na_2O = 0.52 - 0.77 wt. %) contents are consistent with a moderate to high pressure origin. They are compositionally similar to near-liquidus clinopyroxenes experimentally synthesised from alkali basalt (Thompson, 1974) and hawaiite (Knutson and Green, 1975) lavas. Comparative data are given in Table 8.1. TiO_2 decreases, but Al_2O_3 and Na_2O increase, with increasing pressure and temperature (Thompson, 1974). Trace element and isotopic data also support the hypothesis that pyroxene megacrysts may have been in equilibrium with their host magmas at relatively high pressures (Irving and Frey, 1984).

8.4 Geothermometry of magnesian peridotites and anhydrous pyroxenites

Spinel peridotite and pyroxenite inclusions probably represent fragments of mantle wall-rock which have become accidentally entrained within rising mafic alkaline magmas (Menzies, 1983). Estimates for their equilibration temperatures have been calculated using a variety of thermodynamic models. Mineral compositions were obtained by electron microprobe analysis, taking care to avoid both the edges of grains, and those grains which were in contact with the host lava.

The two-pyroxene geothermometer is based on the width of the diopside-enstatite miscibility gap, using experimental data on the pyroxene solvus in the simple system $Ca_2Si_2O_6$ - $Mg_2Si_2O_6$ (Davis and Boyd, 1966; Nehru and Wyllie, 1974; Mori and Green, 1975; 1978; Lindsley and Dixon, 1976). Numerical formulations

TABLE 8.1

COMPARATIVE MINERAL CHEMISTRY FOR PYROXENES EXPERIMENTALLY SYNTHESISED AT RELATIVELY HIGH PRESSURES, AND CLINOPYROXENE MEGACRYSTS FROM NORTHWESTERN SARDINIA

	1	2	3	4
SiO_2	49.40	50.70	51.37	52.18
TiO_2	1.93	0.85	1.40	0.67
Al_2O_3	6.55	5.64	4.22	5.40
FeO	9.13	8.73	6.27	6.33
MnO	0.48	0.20	0.07	0.14
MgO	13.62	18.60	14.70	17.26
CaO	17.89	13.60	20.68	16.99
Na_2O	0.76	0.56	0.52	0.77
K_2O	0.06	0.02	-	-
Cr_2O_3	0.18	1.05	0.33	0.23
SUM	100.00	99.95	99.56	99.97

1. Clinopyroxene in equilibrium with hawaiite at 10 kb, 1120°C and 2% H_2O (Knutson and Green, 1975).

2. Clinopyroxene in equilibrium with alkali basalt at 10 kb and 1225°C.

3. Clinopyroxene megacryst, N.W. Sardinia.

4. Clinopyroxene megacryst, N.W. Sardinia.

of the pyroxene solvus, derived from this experimental data, have been calculated by several authors (Wood and Banno, 1973; Wells, 1977; Mori and Green, 1978), and are given in Appendix E. Temperatures of equilibration for 15 spinel peridotite and pyroxenite inclusions are presented in Table 8.2. Temperature estimates have also been calculated, based on the distribution of octahedrally-co-ordinated aluminium and chromium between orthopyroxene and clinopyroxene (Mysen and Boettcher, 1975; Table 8.2). Comparative equilibration temperatures for some spinel peridotites from world-wide localities, calculated using the Wells (1977) geothermometer, are given in Table 8.3. Equilibration temperatures for Sardinian spinel peridotites lie within the range defined by these. They have an average value of 956 $\pm$ 34^{o}C (1s error). The estimated error limit for this geothermometer is $\pm$ 50^{o}C (Fuji and Scarfe, 1982), and the low 1s error for Sardinian peridotites implies that they have been derived from a restricted portion of the upper mantle. Temperatures derived using the equation of Mori and Green (1978) have an average value of 990 $\pm$ 39^{o}C which is slightly higher than, but within the 1s error for the Wells (1977) formulation. Equilibration temperatures calculated using the equation of Mysen and Boettcher (1975) are variable, which may be due to the low Cr content of the orthopyroxenes, which is close to the detection limit of the electron microprobe technique in use.

TABLE 8.2

TEMPERATURES OF EQUILIBRATION FOR SPINEL LHERZOLITE XENOLITHS CALCULATED FROM PUBLISHED GEOTHERMOMETERS

	Wood and Banno (1973)	Mysen and Boettcher (1975)	Wells (1977)	Mori and Green (1978)
N9	1111	1216	898	921[2]
POZZ-2[1]	905	779	861	947[2]
POZZ-12	1185	1061	996	1035
N1	1198	1188	978	1020
POZZ-10	1042	1019	936	969
POZZ-3	1033	965	923	953
POZZ-9	1071	1187	975	1016
N5	1074	784	973	1010
N3	1041	1033	931	960
N4	1018	1027	907	935
POZZ-4	1067	1046	961	995
POZZ-5	1101	1053	1004	1044
POZZ-1	1077	927	971	1005
POZZ-14	1085	987	979	1012[2]
TH-I[1,3]	-	-	1071	1149[2]
TH-I[1,4]	-	-	1091	1172[2]

1 Pyroxenite.

2 Temperature too high because the bulk rock is too iron-rich (Carswell, 1980).

3 Temperature calculated from co-existing clino- and orthopyroxene.

4 Temperature calculated from exsolved Ca-poor pyroxene and host clinopyroxene.

TABLE 8.3

TEMPERATURE OF EQUILIBRATION, CALCULATED USING THE WELLS (1977) GEOTHERMOMETER, OF SPINEL LHERZOLITES FROM WORLD-WIDE LOCALITIES

Temperature (°C)	Locality	Reference
940-1010	Calton Hill, Derbyshire	Donaldson, 1978
1050-1150	Summit Lake, British Columbia	Brearley et al, 1984
900-1040	West Kettle River, British Columbia	Fuji and Scarfe, 1982
1150-1165	Dreiser Weiher, West Germany	Sachtleben and Seck, 1981
794- 974	Massif Central, France	Brown et al, 1980
925-1050	Saudi Arabia	Ghent et al, 1980
898-1004	Northwestern Sardinia	This work

8.5 Major element whole-rock chemistry of spinel peridotites

The whole-rock major element chemical composition of two spinel peridotites from northwestern Sardinia, and comparative data for some spinel peridotites from other localities, are given in Table 8.4. POZZ-3 was analysed by XRF. The major element chemistry of N7 was calculated from its mineral chemistry, combined with its modal composition.

CaO, MgO and Al_2O_3 contents are shown in the ternary diagram in Figure 8.8. POZZ-3 and N7 are characterised by low alumina and calcium relative to a model pyrolite composition (Ringwood, 1975). They also have low TiO_2, Na_2O and K_2O abundances, and high MgO and Cr/Cr + Al relative to this model pyrolite. They are, therefore, depleted in the most fusible "basaltic" components, and may be residues after varying degrees of extraction of basalt magma by partial melting (Ringwood, 1975). A continuous range of depletion, towards the MgO apex, is apparent from the data given for world-wide spinel peridotite xenoliths in Figure 8.8. High MgO ($>$ 43.4 wt. %) in POZZ-3 and N7 is reflected in their high modal olivine content. Clinopyroxene is the major host for Na_2O, K_2O and CaO in rocks of spinel peridotite mineralogy, and low modal clinopyroxene abundances are reflected in the low concentrations of these elements. MgO/MgO + FeOT ratios are high ($\geqslant$ 0.85) and comparable to similar ratios reported for spinel peridotites from other localities (see review by Carswell, 1980). Sardinian spinel peridotites are poorer in FeOT, Na_2O, K_2O, TiO_2 and Al_2O_3 than some Fe-rich lherzolite xenoliths described from New South Wales, Australia (Wilkinson and Binns, 1977),

TABLE 8.4

MAJOR ELEMENT CHEMICAL COMPOSITION OF PERIDOTITE XENOLITHS FROM NORTHWESTERN SARDINIA, AND DATA FOR OTHER PERIDOTITES FROM WORLD-WIDE LOCALITIES

	Spinel lherzolite POZZ-3[1]	Harzburgite N7[2]	Lizard Peninsula (Green, 1964)	Spring Mount, New South Wales (Wilkinson & Binns, 1977)	Pyrolite (Ringwood, 1966)
SiO_2	45.32	43.68	44.77	43.48	45.16
TiO_2	0.03	0.01	0.19	0.13	0.71
Al_2O_3	1.69	1.89	4.16	2.65	3.54
Fe_2O_3T	7.90	8.54	8.21	16.22	8.45
MnO	0.18	0.06	0.11	0.25	0.14
MgO	43.43	45.23	39.22	29.40	37.47
CaO	1.38	0.23	2.42	2.95	3.08
Na_2O	-	-	0.22	0.40	0.57
K_2O	-	-	0.05	0.13	0.13
P_2O_5	0.01	-	0.01	0.04	0.06
NiO	0.34	0.37	0.24	0.22	-
Cr_2O_3	0.38	0.43	0.40	0.25	0.43

	San Carlos, Arizona (Frey & Prinz, 1978)	Victoria, Australia (Frey & Green, 1974)	Hawaii (Kuno & Aoki, 1970)
SiO_2	43.82	43.58	44.08
TiO_2	0.03	0.03	-
Al_2O_3	2.55	1.02	0.47
Fe_2O_3T	8.09	10.00	8.41
MnO	0.13	0.15	0.13
MgO	43.52	43.68	45.32
CaO	1.18	0.97	0.76
Na_2O	0.35	0.12	0.14
K_2O	0.14	0.02	< 0.05
P_2O_5	0.03	0.006	< 0.05
NiO	-	0.30	-
Cr_2O_3	0.28	0.32	0.32

1 XRF analysis.

2 Major element chemical composition calculated from mineral compositions and modal analysis. Fe_2O_3T denotes total iron expressed as Fe_2O_3. All values are given in weight percent oxide.

Figure 8.8

Whole-rock chemical compositions of spinel peridotites from Sardinia and other world-wide localities projected onto $MgO-Al_2O_3-CaO$. Sources of the data are:
1. chromite lherzolite (Carswell et al, 1979);
2. chromite lherzolite (Rhodes and Dawson, 1975);
3. Cr-spinel lherzolite (Suwa et al, 1975);
4. spinel lherzolite (Hutchinson and Gass, 1971);
5. spinel harzburgite (Dawson et al, 1970);
6. spinel lherzolite (Dawson et al, 1970);
7. spinel lherzolite (Maaloe and Aoki, 1977);
8. Al-spinel lherzolite (Hamad, 1963);
9. Al-spinel lherzolite (Griffin, 1973);
10. spinel lherzolite (Hutchinson et al, 1970);
11. Fe-rich spinel lherzolite (Wilkinson and Binns, 1977);
12. Pyrolite (Ringwood, 1966);
13. Pyrolite (Ringwood, 1975)

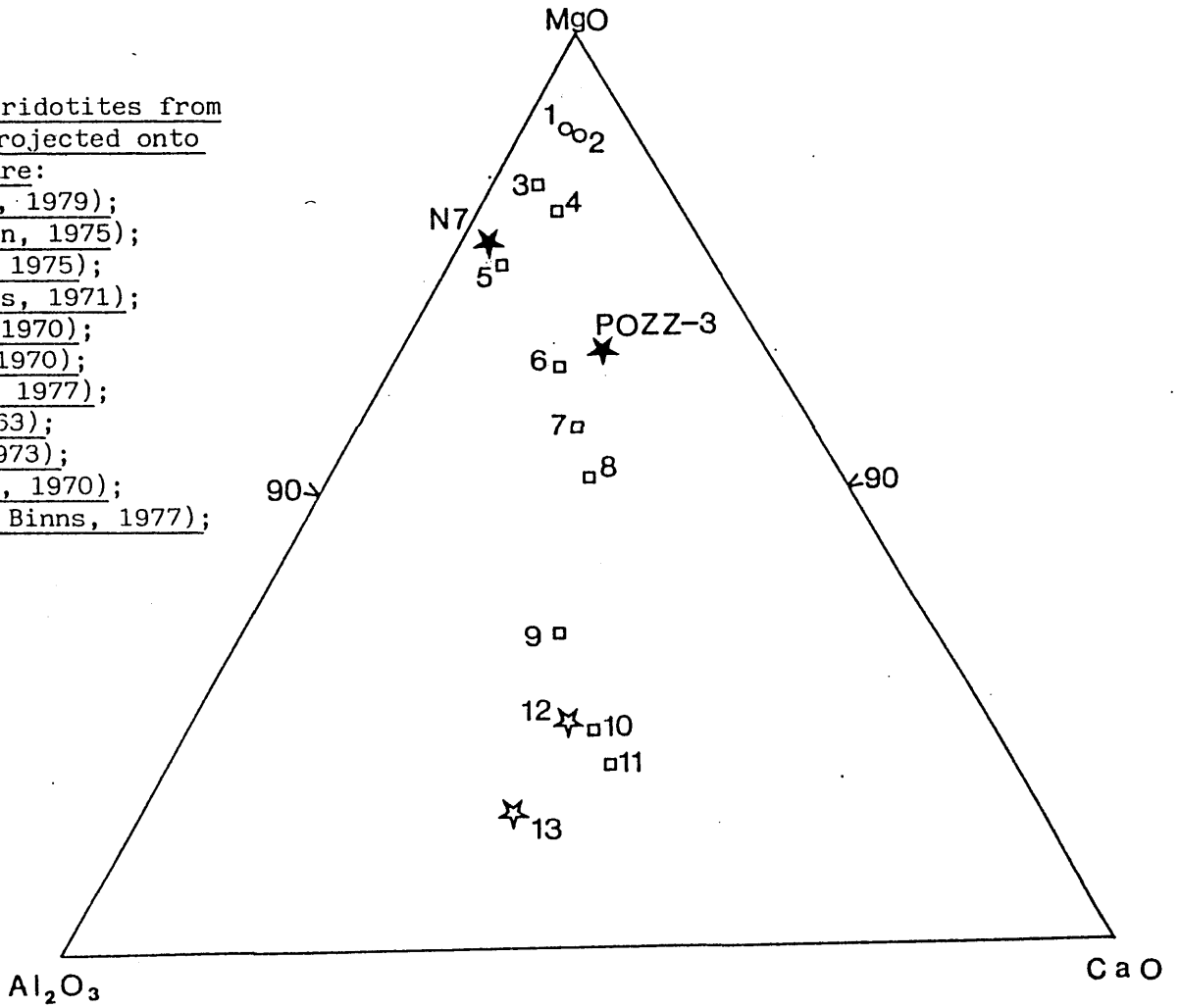

and which have been suggested as possible source rocks for continental anorogenic magmas.

8.6 Rare-earth element (REE) geochemistry of spinel peridotites

(a) Whole-rock REE content of POZZ-3

REE data are given in Appendix B. Abundances of the middle REE (MREE) in POZZ-3, with the exception of europium, are close to the detection limits for the analytical proceedure (see Appendix A). The chondrite-normalised REE pattern is given in Figure 8.9, together with that of an anhydrous spinel peridotite from Dreiser Weiher in West Germany (Stosch and Seck, 1980). They are characterised by a concave upwards-profile, with both light REE (LREE) and heavy REE (HREE) enriched relative to the MREE. This results, for POZZ-3, in high chondrite-normalised ratios of La/Eu_N = 8.7 and Yb/Eu_N = 4.2. The moderately high LREE/HREE enrichment results in La/Yb_N = 2.1. Such whole-rock REE concentrations in spinel peridotite xenoliths may suffer contamination from the host basalt, even in the absence of pervasive melt infiltration (Shimizu, 1975). However, in rocks of spinel peridotite mineralogy, only the M2 site in clinopyroxenes is sufficiently large to accommodate the REE. Therefore, to minimise the possibility of contamination, clinopyroxene grains were separated from two freshly crushed spinel peridotites, and cleaned using an acid etching technique (Appendix A).

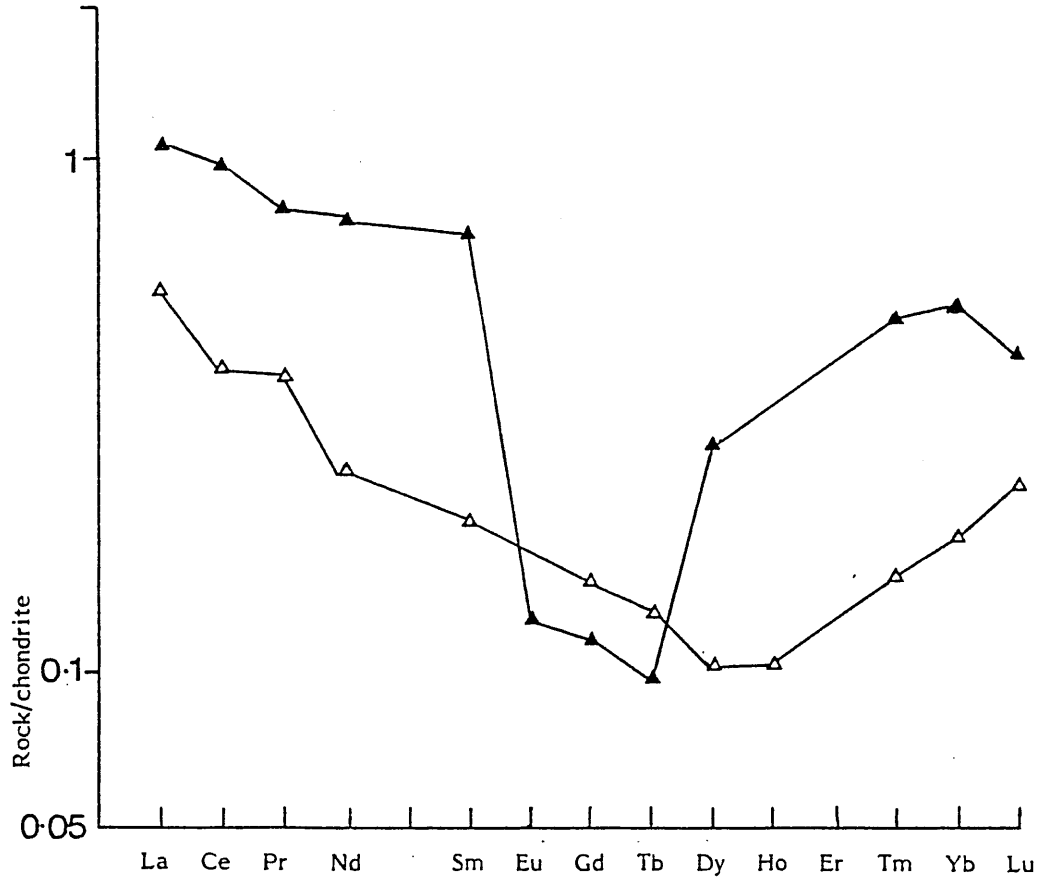

Figure 8.9

Whole-rock chondrite-normalised REE data for a Sardinian spinel peridotite (Pozz-3; filled triangles) and a spinel peridotite from Dreiser Weiher (Stosch and Seck, 1980; open triangles).

(b) REE abundances in Cr-diopsides from two spinel peridotites

REE abundances, obtained on POZZ-8 and POZZ-1, are given in Table 8.5, and the data are plotted on a chondrite-normalised diagram in Figure 8.10. The diopsides are characterised by LREE concentrations which are 3-7 times chondritic, and HREE concentrations of 2-3 times chondrite. This moderate LREE-enrichment results in La/Yb_N = 1.3-1.6. The MREE have above-chondritic REE abundances, although they are depleted relative to both the LREE and HREE. Such a "U-shaped" REE pattern (similar to that of the whole-rock) has La/Eu_N = 2.2-5.0, and Yb/Eu_N = 1.4-2.1. La/Yb_N ratios in diopsides from northwestern Sardinia are lower than those reported from Dreiser Weiher (Stosch and Seck, 1980).

8.7 Sr-isotopic composition of Cr-diopsides from Sardinian spinel peridotites

$^{87}Sr/^{86}Sr$ ratios were determined on the same clinopyroxene separates using techniques detailed in Appendix A, and the results are given in Table 8.5 The Sr content of POZZ-1 was too low for the determination of a satisfactory Sr-isotope ratio. $^{87}Sr/^{86}Sr$ = 0.70362 for POZZ-8 lies within the range obtained on clinopyroxene mineral separates from other peridotites (0.702-0.706, Menzies, 1983).

TABLE 8.5

RARE-EARTH ELEMENT AND STRONTIUM ISOTOPIC COMPOSITION OF CHROME DIOPSIDES FROM 2 SPINEL LHERZOLITE XENOLITHS

	POZZ-1	POZZ-8
La	1.32	2.35
Ce	3.02	5.88
Pr	0.56	1.01
Nd	2.15	3.44
Sm	0.63	0.62
Eu	0.14	0.11
Gd	0.47	0.43
Dy	0.68	0.85
Ho	0.14	0.18
Er	0.52	0.68
Yb	0.55	0.67
Lu	0.08	0.10
$^{87}Sr/^{86}Sr$	-	0.70362 ± 5

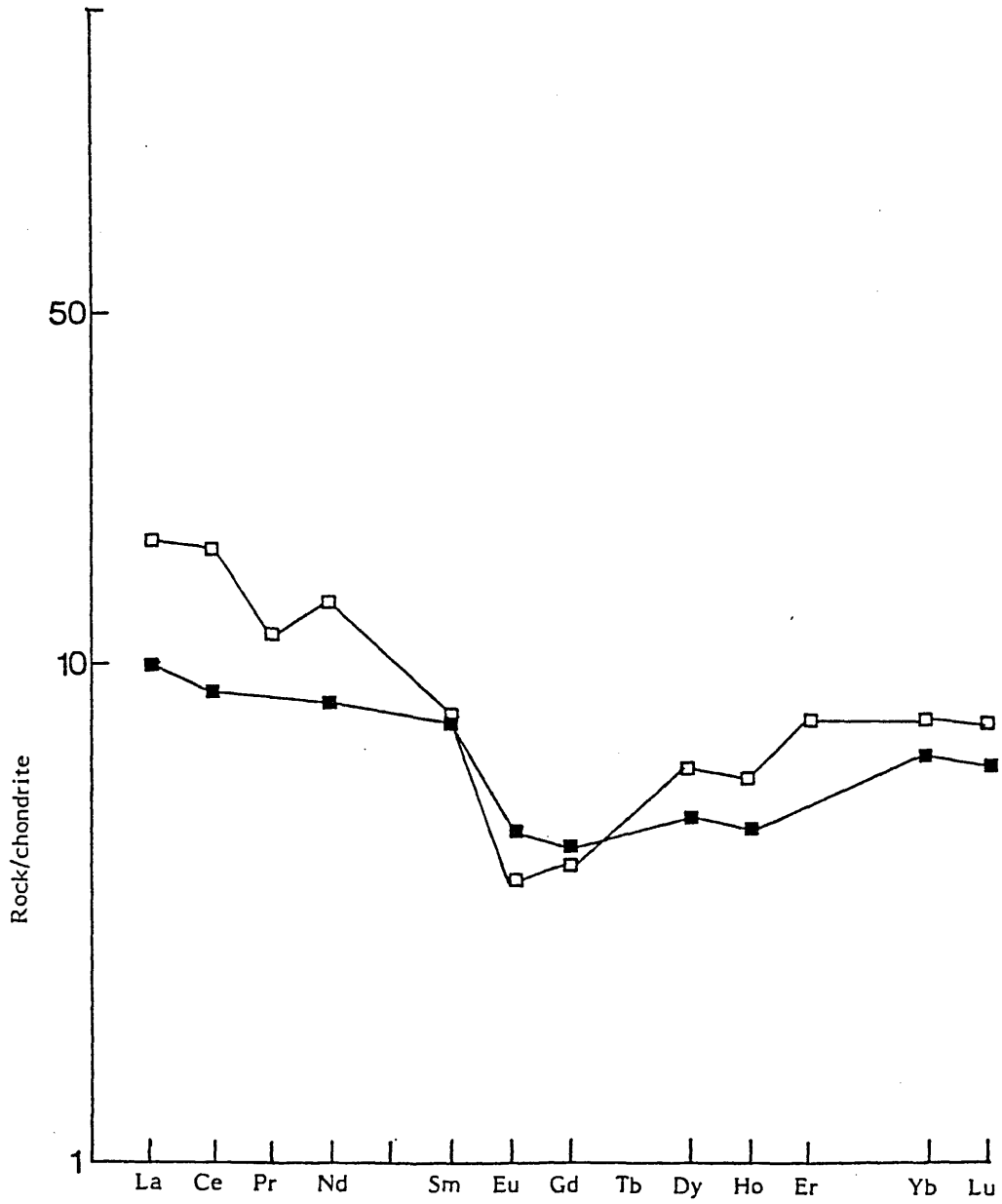

Figure 8.10

Chondrite-normalised REE patterns for clinopyroxenes from magnesium peridotites. Open squares = Pozz-8; filled squares = Pozz-1.

8.8 Origin of Sardinian spinel peridotites

The petrogenesis of spinel peridotite inclusions, which are found as xenoliths in mafic alkaline magmas, has been the subject of much controversy (Frey and Green, 1974); Menzies, 1983). Hypotheses put forward to explain their origin include:-

1. Parental upper mantle which is capable of producing basaltic magma by partial melting (Wilkinson and Binns, 1977);
2. Upper mantle which has been variably depleted by basalt magma extraction, possibly during the formation of the continental crust (Ringwood, 1975);
3. Cumulates, representing the petrogenetic pathway from hypersthene- to nepheline-normative basalts by fractional crystallisation at moderate to high pressures (O'Hara, 1967);
4. Older cumulates, within the deep crust or upper mantle.

A cumulate origin, with a genetic relationship to the host basalt, has previously been suggested to explain the occurrence of spinel peridotite xenoliths in Sardinian Plio-Pleistocene magmas (Brotzu et al, 1969). This seems unlikely, however, for the following reasons:-

1. Estimated temperatures of equilibration are well below the liquidus temperature for basaltic magma at 10 kb within the spinel lherzolite stability field;
2. The $^{87}Sr/^{86}Sr$ ratio in separated diopsides from a spinel peridotite is too low to have been in equilibrium with the host magma, in the absence of significant sialic contamination of the magma.

3. Petrographic studies indicate that most Sardinian spinel peridotites are metamorphic tectonites, which have undergone deformation and re-crystallisation within the upper mantle;
4. Trace element geochemistry precludes the derivation of nepheline-normative from hypersthene-normative basalts by plausible crystal fractionation mechanisms.

Further, the whole-rock FeOT/FeOT + MgO ratio in analysed Sardinian peridotites is much lower than in peridotite xenoliths from Australia, which have been suggested as possible source rocks for continental tholeiitic basalts (Wilkinson and Binns, 1977). The major element chemistry of Sardinian ultrabasic xenoliths is consistent with an origin by variable degrees of basalt magma extraction from a pyrolite model composition, by partial melting. Accordingly, a batch melting model (Shaw, 1970) has been applied in order to model the petrogenesis of a spinel lherzolite, POZZ-3, by variable degrees of partial melting of a pyrolite source mantle (cf. Frey and Green, 1974; Stosch and Seck, 1980).

Geochemical modelling of peridotite genesis

An equilibrium batch melting equation (Shaw, 1970) has been used to model the Sc and Yb abundances determined in POZZ-3, to the Sc and Yb contents of a model pyrolite composition (Jagoutz, 1979), by variable degrees of partial melting.

A starting composition of 49% olivine, 21% clinopyroxene and 30% orthopyroxene (Schilling, 1975) was used, with melting proportions of 55% clinopyroxene, 30% orthopyroxene and 15% olivine (Stosch and Seck, 1980). Spinel was disregarded in the calculations, both because of its low modal abundance, and because

of its very low concentrations of Yb and Sc. Partition coefficients for Yb and Sc in ultrabasic systems are poorly constrained, and are pressure, temperature and composition-dependent (Henderson, 1981). Those used in this study are given in Table 8.6. Yb and Sc contents in POZZ-3 are lower than in the model pyrolite mantle composition, and can be modelled in terms of a 20% batch melt of the pyrolite starting composition (Figure 8.11).

However, the depleted geochemical composition of POZZ-3 relative to a model pyrolite composition, implied by both the major element chemistry and some trace elements, is inconsistent with the observed LREE-enrichment relative to the HREE in the separated diopsides. $La/Yb_N > 1$ ratios cannot reasonably be related to the residues of a single stage partial melting event, because of the higher melt/mineral partition coefficients of the LREE relative to the HREE in pyroxene-dominated mineral assemblages. Thus the "U-shaped" REE distribution pattern is best interpreted in terms of a mixture of two chemically distinct components (Frey and Green, 1974). Component A is a LREE-depleted residue after basalt magma extraction as discussed above. Component B may be a LREE-enriched fluid or melt ascending from within the garnet stability-field. Garnet preferentially incorporates the HREE relative to the LREE, and might thereby affect fractionation of the LREE from the HREE in a co-existing fluid or melt.

TABLE 8.6

PARTITION COEFFICIENTS USED IN THE GEOCHEMICAL MODELLING OF SPINEL PERIDOTITE PETROGENESIS

	OL/CPX	OPX/CPX	CPX/L
Sc	0.066[1]	0.385[1]	0.8[2]
Yb	0.019[1]	0.200[1]	0.28[3]

1 Stosch, 1981.

2 Lindstrom, 1976.

3 Grutzeck et al, 1974.

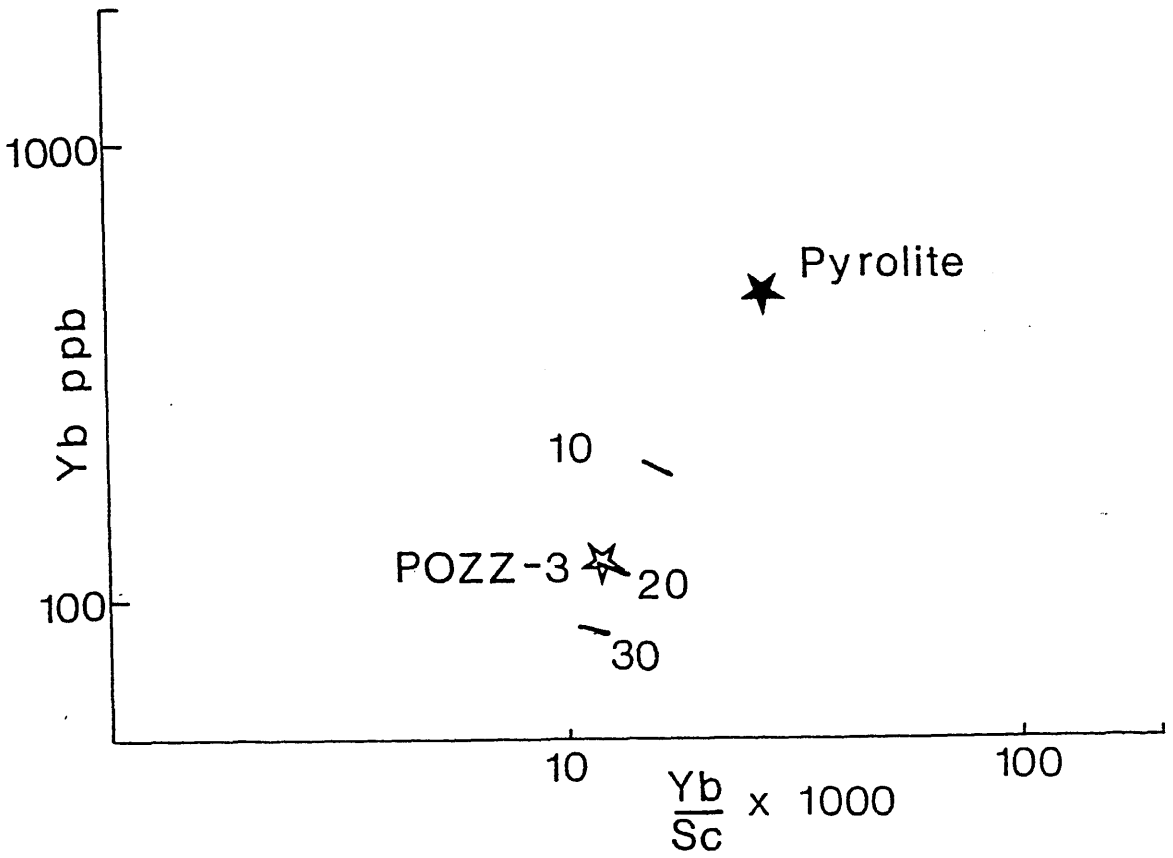

Figure 8.11

Yb vs. Yb/Sc batch melting model.
Pyrolite represents upper mantle peridotite starting composition.
10, 20 and 30 represent % partial melting of pyrolite

8.9 The nature of the lower crust beaneath Sardinia

Felsic granulites are rare as inclusions in mafic alkaline lavas (Kay and Kay, 1981), although the average chemical composition of the lower continental crust is probably tonalitic, with about 61 wt. % SiO_2 (Weaver and Tarney, 1980). Two basic granulite-facies gneisses have been collected from a basanite flow in N.W. Sardinia. In the absence of any unequivocal lower crustal rocks exposed at the surface they provide our only sample of the Sardinian deep crust. Various hypotheses put forward to explain the nature and origin of the lower continental crust are summarised below:-

1. Lower crustal rocks are cumulates, derived by fractional crystallisation of mantle-derived magmas.
2. Lower crustal rocks are residues after the extraction of a partial melt (Pride and Muecke, 1980). These authors suggest that the low contents of K, Rb, Th and U observed in granulite-facies rocks is due to their removal in a melt phase during partial melting.
3. Lower crustal rocks may represent a primary melt composition.
4. Low abundances of LILE may be the result of the removal of these elements in a H_2O-rich (Fowler, 1985) or CO_2-rich (Tarney and Windley, 1977) fluid.

Geochemistry of Sardinian granulite-facies geneiss (GR-P)

The major element chemical composition of GR-P is dominated by high contents of Mg(MgO = 17.1 wt. %) and Al(Al_2O_3 = 20.1 wt. %), but low Si (SiO_2 = 42.2 wt. %). Abundances of P, Ti, K and Na are abnormally low, and such a rock composition is unlikely to represent a liquid composition. Multi-element data are plotted on a chondrite-normalised diagram in Figure 8.12. Excepting high Sr abundances (Sr = 377 ppm), all the elements are present at anomalously low concentrations. Low Y = 1 ppm and Zr = 28 ppm also suggest that GR-P is not a liquid composition. The most noteworthy feature of the REE chondrite-normalised pattern (Figure 8.13) is the obvious positive Eu anomaly. High Sr and Eu values in GR-P reflect the influence of plagioclase, either as a cumulate phase, or as a residual phase during partial melting. The LREE-enriched pattern (Figure 8.13) is difficult to reconcile with a single stage partial melting model, because the LREE would preferentially be enriched in the melt phase in pyroxene-bearing assemblages. An estimated temperature of equilibration of 748^{o}C has been calculated for GR-P using the geothermometer of Wells (1977). Such a temperature is well below the basalt liquidus temperature, but is comparable with temperature estimates for Norwegian granulite-facies rocks (Obata et al, 1974) and Scourian rocks from Gruinard Bay (Fowler, 1985). Textural evidence, including annealed plagioclase, and the sympletic intergrowth of spinel and clinopyroxene, implies some degree of re-equilibration, and possibly metamorphic differentiation.

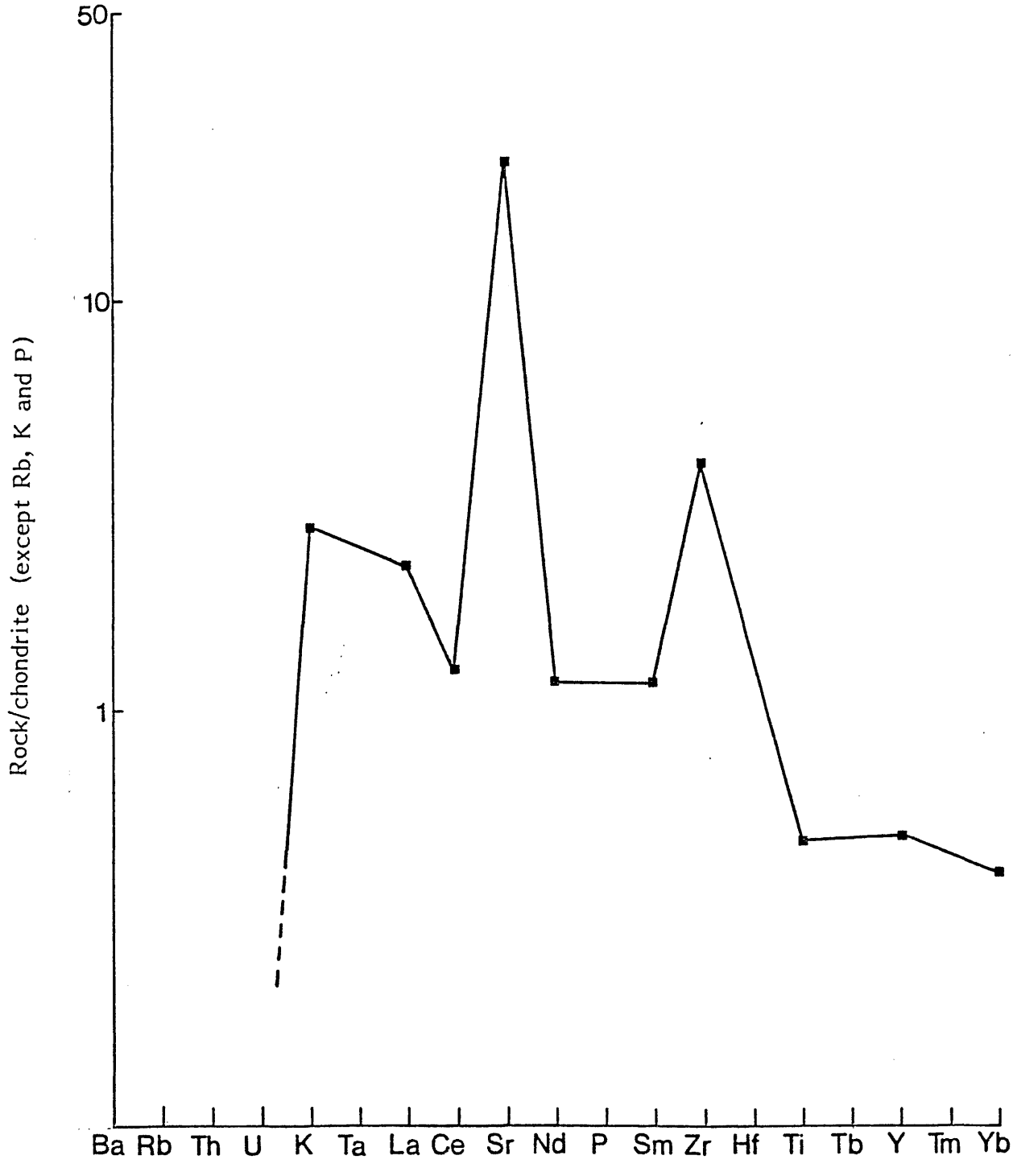

Figure 8.12

Chondrite-normalised multi-element plot of a mafic granulite-facies gneiss (GR-P)

Figure 8.13

Chondrite-normalised REE pattern for a mafic granulite-facies gneiss (GR-P)

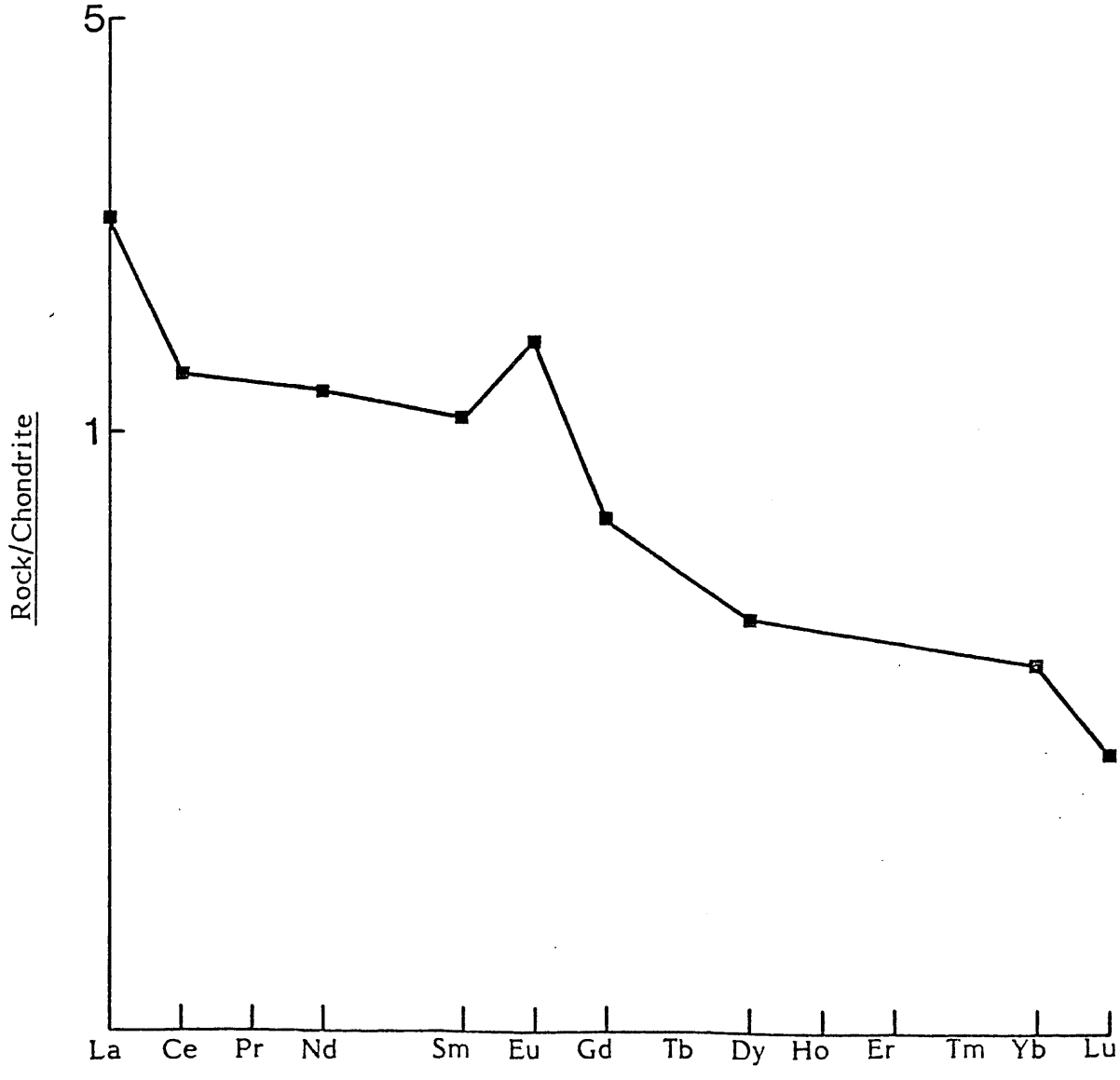

It is envisaged that GR-P was originally a gabbroic cumulate within the lower crust. A moderately high Ni (Ni = 115 ppm) content suggests that olivine was a minor cumulate phase, together with pyroxene and plagioclase. Subsequent metamorphic re-crystallisation may have exaggerated an initial igneous layering. High LREE/HREE ratios imply that garnet was not a primary cumulate phase. Low abundances of K, Rb, Th and U, and low Rb/Sr may reflect this cumulate origin, rather than removal of these elements by fluids or melts.

8.10 Synthesis

A schematic cross-section through the Sardinian upper lithosphere is shown in Figure 8.14, based on data presented in this Chapter.

Figure 8.14

Hypothetical lithospheric structure beneath Sardinia.

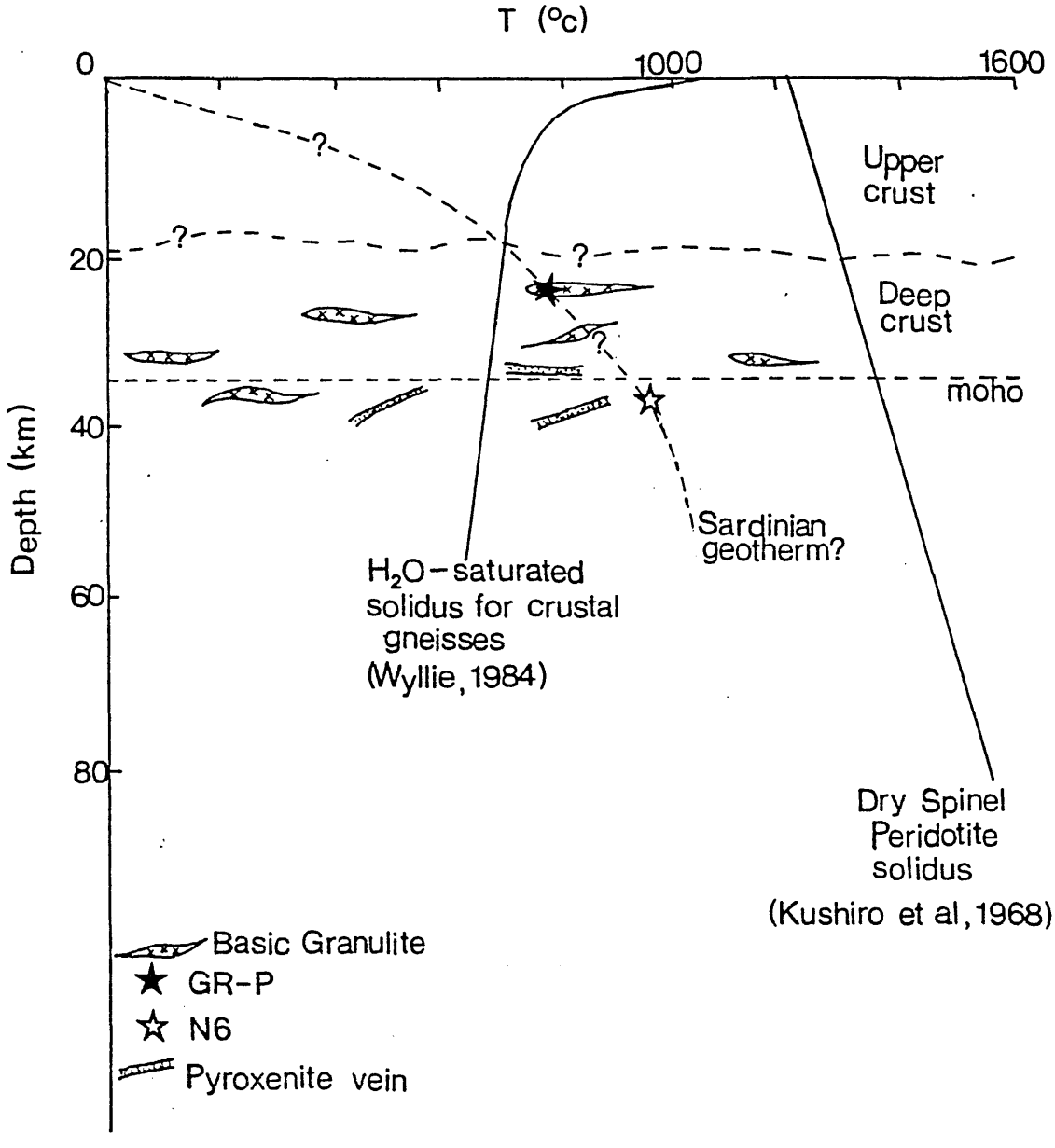

Since no reliable geobarometers are available for rocks of spinel peridotite mineralogy, a depth of about 40 km has been estimated from the P-T grid of Carswell (1980)

BIBLIOGRAPHY

ABBEY, S., 1980. Studies in "Standard samples" for use in the general analysis of silicate rocks and minerals. Part 6. 1979 Edition of "useable" values. Can. Geo.1. Surv. Prof. Pap. 80-14, pp 1-30.

AHREN, J.L. and TURCOTTE, D.L., 1979. Magma migration beneath an ocean ridge. Earth Planet. Sci. Lett., 45, pp 115-122.

ALLÈGRE, C.J., DUPRÉ, B., LAMBRET, B. and RICHARD P., 1981. The sub-continental versus sub-oceanic debate, 1. Lead-neodymium-strontium isotopes in primary alkali basalts from a shield area: Ahaggar volcanic suite. Earth Planet. Sci. Lett., 52, pp 85-92.

ALVAREZ, W., 1972. Rotation of the Corsica-Sardinia microplate. Nat. Phys. Sci., 235, pp 103-105.

ALVAREZ, W., 1976. A former continuation of the Alps. Geol. Soc. Am. Bull., 87, pp 891-896.

ALVAREZ, W., COCOZZA, T., and WEZEL, F.C., 1974. Fragmentation of the Alpine orogenic belt by microplate dispersal. Nature, 248, pp 309-314.

BAILEY, D.K., 1982. Mantle metasomatism - continuing chemical change within the Earth, Nature, 296, pp 525-530.

BAKER, P.E., 1984. Geochemical evolution of St. Kitts and Montserrat, Lesser Antilles. J. Geol. Soc. London, 141, pp 401-411.

BARBERI, F., BORSI, S., FERRARA, G. and INNOCENTI, F., 1969. Strontium isotopic composition of some recent basic volcanites of the Southern Tyrrhenian Sea and Sicily Channel. Contrib. Mineral, Pet., 23, pp 157-172.

BARBERI, F., BIZOUARD, H., CAPALDI, G., FERRARA, G., GASPARINI, P., INNOCENTI, F., JORON, J.L., LAMBRET, B., TREUIL, M., and ALLEGRE, C., 1978. Age and nature of basalts from the Tyrrhenian abyssal plain. Init. Rep. D.S.D.P., XLII(1), pp 509-514.

BARREIRO, B., 1983. Lead isotopic compositions of South Sandwich Island volcanic rocks and their bearing on magmagenesis in intra-oceanic island arcs. Geochim. Cosmo. Acta, 47, pp 817-822.

BECCALUVA, L., MACCIOTTA, G., SAVELLI, C., CANTONI, M. and VENTURELLI, G., 1977. Geochronology and magmatic character of the Plio-Pleistocene volcanism in Sardinia (Italy). Bull. Volc., 40(3), pp 1-16.

BELLON, H., and BROUSSE, R., 1977. Le magmatisme periméditerranéan occidental Essai de synthèse. Bull. Soc. Geol. France 7, pp 469-480.

BOCCALETTI, M., ELTER, P., and GUAZZONE, G., 1971. Plate tectonic models for the development of the western Alps and northern Apennines. Nature Phys. Sci., 234, pp 108-111.

BOETTCHER, A. and WYLLIE, P.J., 1969. Phase relationships in the system $NaAlSiO_4$-SiO_2-H_2O to 35 kb pressure. Am. J. Sci., 267, pp 875-909.

BREARLEY, M., SCARFE, C.M., and FUJI, T., 1984. The petrology of ultramafic xenoliths from Summit Lake, near Prince George, British Columbia. Contrib. Mineral Petrol., 88, pp 53-63.

BROTZU, P., Di SABATINO, B., and MORBIDELLI, L., 1969. Contributo alla conoscenza delle vulcaniti post-elveziane dei Monti ferru. Nota VII: Caratteri mineralogici di un nodulo spinello-lerzolitico ospitato nelle lave basaltiche del settore di M. te Urtigu. Quatderni, 1st Petrog. Roma, 7.

BROTZU, P., Di SABATINO, B. and MORBIDELLI, L., 1970. Sui minerali di aggregati nodulari ultrafemici presenti nelle lava basaltiche del settore Orosei-Dorgali. Per. Mineral, Vol. Speciale.

BROWN, G.M., PINSENT, R.H. and COISY, P., 1980. The petrology of spinel peridotite xenoliths from the Massif Central, France. Am. Journ. Sci., 280-A, pp 471-498.

BROWN, L., KLEIN, J., MIDDLETON, R., SACKS, I. and TERA, F., 1982. ^{10}Be in island-arc volcanoes and implications for subduction. Nature, 299, pp 718-720.

BURHOLT, G.D., CAESAR, E.A.Y., and JONES T.C., 1982. The fast cyclic activation system for neutron activation analysis in the University of London Reactor. Nuclear Instruments and Methods, 204, No. 1, pp 231-234.

CARLSON, R.W., LUGMAIR, G.W. and MacDOUGALL, J.D., 1981. Columbia River volcanism: the question of mantle heterogeneity or crustal contamination. Geochim. Cosmo. Acta, 45, pp 2483-2499.

CARMICHAEL, I., TURNER, F. and VERHOOGEN, J., 1974. Igneous Petrology. McGraw-Hill.

CARSWELL, D.A., 1980. Mantle derived lherzolite nodules associated with kimberlite, carbonatite and basalt magmatism: A review. Lithos, 13, pp 121-138.

CHEN, C. and FREY, F.A., 1983. Origin of Hawaiian tholeiite and alkalic basalt. Nature, 302, pp 785-789.

CHERCHI, A. and MONTADERT, L., 1982. Oligo-Miocene rift of Sardinia and the early history of the Western Mediterranean Basin. Nature, 298, pp. 736-739.

CHURCH, S.E., 1981. Multi-element analysis of 54 geochemical reference samples using inductively coupled plasma-atomic emission spectrometry. Geostandards Newsletter, 5, pp 133-160.

CIONI, R., CLOCCHIATTI, R., Di PAOLA, G., SANTACROCE, R. and TONARINI, S., 1982. Miocene calc-alkaline heritage in the Pliocene post-collisional volcanism of Monte Arci (Sardinia, Italy). Jour. Volc. Geoth. Res., 14, pp 133-167.

COLES, G.G., 1977. In : Physical Methods in Determinative Mineralogy (Ed. Zussman, J.), pp 343-370.

COULON, C., DEMANT, A. and BELLON, H., 1974. Premieres datations par la methode K/Ar de quelques laves Cenozoiques et Quaternaires de Sardaige nord-occidentale. Tectonophysics, 22, pp 41-57.

COULON, C., DOSTAL, J. and DUPUY, C., 1978. Petrology and geochemistry of the ignimbrites and associated lava domes from N.W. Sardinia. Contrib. Mineral, Petrol., 68, pp 89-98.

COULON, C. and DUPUY. C., 1977. Caracteres mineralogiques et geochimiques de la suite andesitique de Sardaigne: le probleme de la zonation spatiale. Bull. Soc. Geol. Frange, 7(4), pp 857-863.

COX, K.G., 1972. The Karroo volcanic cycle. J. Geol. Soc. London, 128, pp 311-336.

COX, K.G., 1980. A model for flood basalt vulcanism. Journ. of Petrol., 21(4), pp 629-650.

COX, K.G., BELL, J.D. and PANKHURST, R.J., 1979. The interpretation of igneous rocks. London: George Allen and Unwin.

COX, K.G. and HAWKESWORTH, C.J., 1984. Relative contribution of crust and mantle to flood basalt magmatism, Mahabaleshwar area, Deccan Traps. Phil. Trans. R. Soc. Lond., A 310, pp 627-642.

CRONAN, D.S., 1969. Average abundances of Mn, Fe, Ni, Co, cU, Pb, Mo, U, Cr, Ti and P in Pacific pelagic clays. Geochim. Cosmochim. Acta, 33, pp 1562-1565.

DAVIS, B.T.C. and BOYD, F.E. 1966. The join $Mg_2Si_2O_6$-$CaMgSi_2O_6$ at 30 kilobars pressure and its application to pyroxenes from kimberlites. J. Geophys. Res., 71, pp 3507-3576.

De JONG, K.A., MANZONI, M., STAVENGA, T., Van DIJK, F., Van der VOO, R., and ZIJDERVELD, J., 1973. Palaeomagnetic evidence for rotation of Sardinia during the arly Miocene. Nature, 243, pp 281-283.

De PAOLO, D.J., 1981. Trace element and isotopic effects of combined wallrock assimilation and fractional crystallisation Earth. Planet. Sci. Lett., 53, pp 189-202.

De PAOLO, D.J. and JOHNSON, R.W., 1979. Magma genesis in the New Britain island arc: Constrains from Nd and Sr isotopes and trace element patterns. Contrib. Min. Pet., 70, pp 367-380.

DIETRICH, V., EMMERMANN, R., PUCHELT, H. and KELLER, J., 1977. Oceanic basalts from the Tyrrhenian Basin, D.S.D.P. Leg 42A, Hole 373A. Init. rep. D.S.D.P., XLII(1), pp 515-530.

DONALDSON, C.H., 1978. Petrology of the uppermost upper mantle deduced from spinel-lherzolite and harzburgite nodules at Calton Hill, Derbyshire. Contrib. Mineral, Petrol., 65, pp 363-377.

DOSTAL, J., COULON, C. and DUPUY, C. 1982. Cainozoic andesitic rocks of Sardinia (Italy), In: Andesites, Ed., R.S. Thorpe, pp 353-370.

DUPUY, C., DOSTAL, J. and COULON, C., 1979. Geochemistry and origin of andesitic rocks from northwestern Sardinia. Jour. Volc. Geoth. Res., 6, pp 375-389.

FERRARA, G., RICCI, C.A., and RITA, F., 1978. Isotopic ages and tectono-metamorphic history of the metamorphic basement of northeastern Sardinia. Contrib. Mineral. Petrol., 68, pp 99-106.

FITTON, J.G. and DUNLOP, H.M., 1985. The Cameroon Line, West Africa, and its bearing on the origin of oceanic and continental alkali basalt. Earth Planet. Sci. Lett., 72, pp 23-38.

FLEET, M.E., 1974. Distortions in the co-ordination polyhedra of M site atoms in olivines, clinopyroxenes, and amphiboles. Am. Mineral, 59, pp 1083-1093.

FODEN, J.D., 1983. The petrology of the calcalkaline lavas of Rindjani volcano, East Sunda arc: a model for island arc petrogenesis. Jour. Pet., 24(1), pp 98-130.

FRASER, D.J., WATT, F., GRIME, G.W., and TAKACS, J., 1984. Direct determination of strontium enrichment on grain boundaries in a garnet lhorzolite xenolith by proton microprobe analysis. Nature, 312, pp 352-354.

FREY, F.A. and GREEN, D.H., 1974. the mineralogy, geochemistry and origin of lherzolite inclusions in Victorian basanites. Geochim. Cosmochim. Acta, 38 pp 1023-1059.

FREY, F.A. and PRINZ, M., 1978. Ultramafic inclusions from San Carlos, Arizona: Petrologic and geochemical data bearing on their petrogenesis. Earth Plant. Sci. Lett., 38, pp 129-176.

FREY, F.A., GREEN, D.H., and ROY, S.D., 1978. Integrated models of basalt petrogenesis: A study of quartz-tholeiites to olivine melilitites from southeastern Australia utilising geochemical and experimental petrological data. Jour. of Pet., 19(3), pp 463-513.

FUJII, T. and SCARFE, C.M., 1982. Petrology of ultramafic nodules from West Kettle River, near Kelowna, southern British Columbia. Contrib. Mineral Petrol., 80, pp 297-306.

GAST, P.W., 1968. Trace element fractionation and the origin of tholeiitic and alkaline magma types. Geochim. Cosmochim. Acta, 32, pp 1057-1086.

GILL, J.B., 1976. From island arc to oceanic islands. Fiji, southwestern Pacific. Geology 4, pp 123-126.

GILL, J.B., 1984. Sr-Pb-Nd isotopic evidence that both MORB and OIB sources contribute to oceanic island arc magmas in Fiji. Earth Planet., Sci. Lett., 68, pp 443-458.

GHENT, E.D., COLEMAN, R.G. and HADLEY, D.G., 1980. Ultramafic inclusions and host alkali olivine basalts of the southern coastal plain of the Red Sea, Saudi Arabia. Am. Journ. Sci., 280-A, pp 499-527.

GIESE, P., MORELLI, C. and NICOLIC, R., 1978. Review of the crustal structure of the northern Apennines, the Ligurian sea and Corsica. In : H. Class, D. Roeder and K. Schmidt (Editors), Alps, Apennines, Hellenides. Inter-Union Commission on Geodynamics, Scientific Report No. 38, pp 221-225.

GOGUEL, R., 1981. Flame emission for accurate cesium determination in geostandards. Geostandards Newsletter, 5, pp 95-99.

GORDON, G.E., RANDLE, K., COLES, G.G., CORLIS, J.B., BEESON, M.H. and OXLEY, S.S., 1968. Instrumental activation analysis of standard rocks with high-resolution γ-ray detectors. Geochim. Cosmochim. Acta, 32, pp 369-396.

GOVINDARAJU, K., 1980. Report (1980) on three GIT-IWG rock reference samples: Anorthosite from Greenland, AN-G; Basalte d'Essey-là - Côte, BE-N; Granite de Beauvoir, MN-N, Geostandards Newsletter, 4, pp 49-138.

GRUTZECK, M., KRIDELBAUGH, S. and WEIIL, D., 1974. The distribution of Sr and REE between diopside and silicate liquid. Geophys. Res. Lett., 1, pp 273-275.

HAFNER, S.S., VIRGO, D. and WARBURTON, D., 1971. Cation distribution and cooling history of clinopyroxenes from Oceanus Procellarum. In: Lunar Science Conference, 2nd Proc., Vol. 1, Geochim. Cosmochim. Acta. Suppl. No. 2, pp 91-108.

HAMAD, S. et D., 1963. The chemistry and mineralogy of the olivine nodules of Calton Hill, Derbyshire. Mineral. Mag. 33, pp 483-497.

HAWKESWORTH, C.J. and POWELL, M., 1980. Magma genesis in the Lesser Antilles Island arc. Earth Planet. Sci. Lett., 51, pp 297-308.

HAWKESWORTH, C.J., ERLANK, A.J., MARSH, J.S. MENZIES, M., and VAN CALSTEREN, P., 1983. Evolution of the continental lithosphere: evidence from volcanics and xenoliths in southern Africa. In: Continental Basalts and Mantle Xenoliths, Ed. Hawkesworth, C. and Norry, M. Shiva Geology Press.

HENDERSON, P., 1981. Inorganic Geochemistry, 353 pp Pergamon Press.

HENDERSON, P. and WILLIAMS, C.T., 1981. Application of intrinsic Ge detectors to the instrumental neutron activation analysis for rare earth elements in rocks and minerals. Journal of Radioanalytical Chemistry, 67, No. 2, pp 445-452.

HENRY, D.T. and MEDARIS, L.G., 1980. Application of pyroxene and olivine-spinel geothermometers to spinel peridotites in southwestern Oregon. Am.J. Sci., 280A, pp 211-231.

HIRN, A. and SAPIN, M., 1976. La croûte terrestre sous la Corse: données sismiques. Bull. Soc. Géol. France, 7(5), pp 1195-1199.

HOFFMAN, A.W. and WHITE, W.M., 1982. Mantle plumes from ancient oceanic crust. Earth Planet. Sci. Lett., 57, pp 421-436.

HOLE, H.J., SAUNDERS, A.D., MARRINER, G.F., and TARNEY, J., 1984. Subduction of pelagic sediments: implications for the origin of Ce-anomalous basalts from the Mariana Islands. J. Geol. Soc. London, 141, pp 453-472.

HOLM, P.M. and MUNKSGAARD, N.C., 1982. Evidence for mantle metasomatism: an oxygen and strontium isotope study of the Vulsinian District, Central Italy. Earth Planet. Sci. Lett.60, pp 376-388.

HUANG, W.L. and WYLLIE, P.J., 1975. Melting reactions in the system $NaAlSi_3O_8$-$KAlSi_3O_8$-SiO_2 to 35 kilobars, dry and with excess water. J. Geol., 83, pp 737-748.

HUPPERT, H. and SPARKS, R.S., 1985. Cooling and contamination of mafic and ultramafic magmas during ascent through continental crust. Earth Planet. Sci. Lett. 74, pp 371-386.

HUTCHINSON, I., VON HERZEN, R.P., LOUDEN, K.E., SCLATER, J.G. and JEMSEK, J., 1985. Heat flow in the Balearic and Tyrrhenian Basins, Western Mediterranean. Journ. Geophy. Res., 90, pp 685-701.

HUTCHINSON, R. and DAWSON, J.B., 1970. Rb, Sr and $^{87}Sr/^{86}Sr$ in ultrabasic xenoliths and host-rocks, Lashaine volcano, Tanzania. Earth Planet. Sci. Lett., 9, pp 87-92.

IRVING, A.J., 1978. A reivew of crystal/liquid partitioning. Geochim. Cosmochim. Acta, 42, pp 743-770.

JOHANNES, W., 1984. Beginning of melting in the granite system Qz-Or-Ab-An-H_2O. Contrib. Mineral. Petrol., 86, pp 264-273.

KAY, R.W., 1984. Elemental abundances relative to identification of magma sources. Phil. Trans. R. Soc. London, A310, pp 535-548.

KAY, S.M. and KAY, R.W., 1982. Tectonic controls on tholeiitic and calc-alkaline magmatism in the Aleutian Arc. Journ. Geophys. Res., 87, pp 4051-4072.

KELLER, J., 1981. Alkali basalts from the Tyrrhenian Sea Basin: Magmatic and Geodynamic significance. Bull. Vol., 44(3), pp 327-337.

KNUTSON, J. and GREEN T.H., 1975. Experimental duplication of a high-pressure megacryst/cumulate assemblage in a near-saturated hawaiite. Contrib. Mineral. Pet., 52, pp 121-132.

KRAMAR, U. and PUCHELT, H., 1982. Reproducibility tests for INNA determinations with AGV-1, BCR-1 and GSP-1 and new data for 17 geochemical reference materials. Geostandards Newsletter, 6, pp 221227.

Le MAITRE, R.W., 1979. A new generalised petrological mixing model. Contrib. Mineral, Pet., 71, pp 133-137.

LETZ, H., REICHERT, C., WIGGER, P. and GIESE, P., 1978. Seismic refraction measurements in the Ligurian Sea and in the northern Apennines. In: H. Closs, D. Roeder and K. Schmidt (Editors), Alps, Apennines, Hellenides. Inter-Union Commission on Geodynamics, Scientific Report No. 38, pp 215-220.

LINDSLEY, D.H. and DIXON, S.A., 1976. Diopside-enstatite equilibria at 850° to 1400°C, 5-35 kb. Am. J. Sci., 276, pp 1285-1301.

LINDSTROM, D.J., 1976. Experimental study of the partitioning of the transition metals between clinopyroxene and co-existing silicate liquids. Ph. D. thesis, University of Oregon, 188 pp.

LUHR, J.F. and CARMICHAEL, I.S., 1981. The Colima Volcanic Complex, Mexico: Part 11. Late-Quaternary Cinder Cones. Contrib. Mineral. Petrol., 76, pp 127-147.

LUTH, W.C., JAHNS, R.H. and TUTTLE, O.F., 1964. The granite system at pressure of 4 to 10 kilobars. J. Geophys. Res., 69, pp 759-773.

MACCIOTTA, G., VENTURELLI, G. and BECCALUVA, L., 1978. Geochemistry of mafic Cainozoic volcanic rocks from Sardinia. Bull. Volc., 41 (1), pp 56-77.

MacDONALD, R., GASS, K.N., THORPE, R.S. and GASS, I.G., 1984. Geochemistry and petrogenesis of the Derbyshire Carboniferous basalts. Jour. Geol. Soc., 141 (1), pp 147-159.

MAHONEY, J.J., MacDOUGALL, J.D., LUGMAIR, G.W., GOPALAN, K., and KRISHNAMURTHY, P., 1985. Origin of contemporaneous tholeiitic and K-rich alkalic lavas: a case study from the northern Deccan Plateau, India. Earth Planet. Sci. Lett., 72, pp 39-53.

MANN, A.C., 1983. Trace element geochemistry of high alumina basalt-andesite-dacite-rhyodacite lavas of the Main Volcanic Series of Santorini Volcano, Greece. Contrib. Mineral. Petrol., 84, pp 43-57.

MATTHEY, D.P., CARR, R.H., WRIGHT, I.P. and PILLINGER, C.T., 1984. Carbon isotopes in submarine basalts. Earth Planet, Sci. Lett., 70, pp 196-206.

MAUFFRET, A., FAIL, J.P., MONTADERT, L., SANCHO, J., and WINNOCK, E., 1973. Northwestern Mediterranean sedimentary basin from seismic reflection profile. Am. Assoc. Pet. Geol. Bull. V., 57 (11), pp 2245-2262.

McKENZIE, D., 1984. The generation and compaction of partially molten rock. Jour. Pet., 25 (3), pp 713-765.

McKENZIE, D.P., 1985. ^{230}Th-^{238}U disequilibrium and the melting processes beneath ridge axes. Earth Plant. Sci., Lett., 72, pp 149-157.

MENZIES, M., 1983. Mantle ultramafic xenoliths in alkaline magmas: evidence for mantle heterogeneity modified by magmatic activity. In: Continental Basalts and Mantle Xenoliths. Ed. Hawkesworth, C.J. and Norry, M.J., Shiva Geology Press.

MERRIER, J-C., 1972. Structures des péridotites en enclaves dans quelques basaltes d'Europe et d'Hawai. Regards sur la constitution du manteau superieur. These Doct. 3^{e} Cycle, Nantes, pp 1-227.

MERCIER, J-C, and NICOLAS, A., 1975. Textures and fabrics of upper mantle peridotites as illustrated by xenoliths from basalts. Journal of Petrology, 16, pp 454-487.

MIYASHIRO, A., 1974. Volcanic rock series in island arcs and active continental margins, Am. J. Sci., 274, pp 321-355.

MONTIGNY, R., EDEL, J.B., and thuizat, R., 1981. Oligo-Miocene rotation of Sardinia: K-Ar ages and palaeo-magnetic data of Tertiary volcanics. Earth Planet. Sci. Lett., 54, pp 261-271.

MORI, T., 1977. Geothermometry of spinel lherzolites. Contrib. Mineral. Petrol., 59, pp 261-279.

MORI, T. and GREEN, D.H., 1975. Pyroxenes in the system $Mg_2Si_2O_6$-$CaMgSi_2O_6$. Earth Planet. Sci. Lett., 26, pp 277-286.

MORI, T. and GREEN, D.H., 1978. Laboratory duplication of phase equilibria observed in natural garnet lherzolites. Journal of Geology, 86, pp 83-97.

MORRIS, J.D. and HART, S.R., 1983. Isotopic and incompatible element constraints on the genesis of island arc volcanics from Cold Bay and Amak Island, Aleutians, and implications for mantle structure. Geochim. Cosmochim. Acta., 47, pp 2015-2030.

MURPHY, K. and DYMOND, J., 1984. Rare earth element fluxes and geochemical budget in the eastern equatorial Pacific. Nature, 307, pp 444-447.

NAKAMURA, N., 1974. Determination of REE, Ba, Fe, Mg, Na and K in carbonaceous and ordinary chondrites. Geochim. Cosmo. Acta, 38, pp 757-775.

NAKAMURA, E., CAMPBELL, I.H. and SUN, S.S., 1985. The influence of subduction processes on the geochemistry of Japanese alkaline basalts. Nature, 316, pp 55-58.

NEHRU, C.E. and WYLLIE, P.J., 1974. Electron-microprobe measurements of pyroxenes co-existing with H_2O under-saturated liquid in the join $CaMgSi_2O_6$-$Mg_2Si_2O_6$-H_2O, at 30 kilobars with application to geothermometry. Contrib. Mineral. Petrol., 48, pp 221-228.

NICOLAS, A., BOUCHEZ, J-L., BOUDIER, F. and MERCIER, J-C., 1971. Textures, structures and fabrics due to solid state flow in some European lherzolites. Tectonophysics, 12, pp 55-86.

NIELSON PIKE, J.E. and SCHWARZMAN, E.C., 1977. Classification of textures in ultramafic xenoliths. Journal of Petrology, 85, pp 49-61.

NORRISH, K. and CHAPPELL, B.W., 1977. In: Physical Methods in Determinative Mineralogy (Ed. Zussman, J.), pp 201-272.

NORRISH, K. and HUTTON, J.T., 1969. An accurate X-ray spectrographic method for the analysis of a wide range of geological samples. Geochim. Cosmochim. Acta, 33, pp 431-453.

O'HARA, M.J., 1967. Mineral parageneses in ultrabasic rocks. In: Ultramafic and Related Rocks (Ed. P.J. Wyllie), pp 393-403.

OLSON, P., YUEN, D. and BALSIGER, D., 1984. Convective mixing and the fine structure of mantle heterogeneities. Phys. Earth. Planet. Int., 36, pp 291-304.

O'NIONS, R.K., 1984. Isotopic abundances relevant to the identification of magma sources. Phil. Trans. Roy. Soc. Lond. A 310, pp 591-603.

PARKER, R.J., 1977. Factors affecting the quality of major element rock analysis by X-ray fluorescene combined with flux-fusion sample preparation. Tech. Report XRF-2B, Dept. Geol., Imperial College, 35 pp.

PARKER, R.J., 1979. A computer-based system of XRF analysis and its application to a study of volcanic rocks from Vulsini, Central Italy. Ph. D. thesis, Univ. of London.

PARKER, R.J., 1980. Computer processing and evaluation of XRF analytical data for silicate rock samples. Tech. Report. XRF-4, Dept. Geol., Imperial College.

PARRY, S.J., 1982. Epithermal neutron activation analysis of short-lived nuclides in geological material. Journal of Radioanalytical Chemistry, 72, No. 1-2, pp 195-207.

PATCHETT, P.J., 1980. Thermal effects of basalt on continental crust and crustal contamination of magmas. Nature, 283, pp 559-561.

PEARCE, J. and NORRY, M.J., 1979. Petrogenetic implications of Ti, Zr, Y and Nb variations in volcanic rocks. Contrib. Mineral. Petrol., 69, pp 33-47.

PEARCE, J.A., 1982. Trace element characteristics of lavas from destructive plate boundaries. In: Andesites, Ed. R.S. Thorpe, pp 525-548.

PECCERILLO, A. and TAYLOR, S.R., 1976. Geochemistry of Eocene calc-alkaline volcanic rocks from the Kastamonu area, northern Turkey. Contrib. Miner. Pet., 58, pp 63-81.

PERFIT, M.R., BRUECKNER, H., LAWRENCE, J.R. and KAY, R.W., 1980. Trace element and isotopic variations in a zoned pluton and associated rocks, Unalaska Island, Alaska: a model for fractionation in the Aleutian calc-alkaline suite. Contrib. Mineral. pet., 73, pp 69-87.

POIRIER, J.P. and NICOLAS, A., 1975. Deformation induced recrystallisation due to progressive misorientation of sub-grains, with special reference to mantle peridotites. Journal of Geology, 83, pp 707-720.

POTTS, D.J., THORPE, O.W. and WATSON, J.S., 1981). Determination of the rare-earth element abundances in 29 international rock standards by instrumental neutron activation analysis: a critical appraisal of calibration errors. Chemical Geology, 34, No. 3-4, pp 331-352.

REUTTER, K-J., GÜNTHER, K. and GROSCURTH, J., 1978. An approach to the Geodynamics of the Corsica-Northern Apennines double orogene. In: H. Closs, D. Roeder and K. Schmidt (Editors), Alps, Apennines and Hellenides, Inter-Union Commision on Geodynamics, Scientific Report No. 38, pp 299-311.

RINGWOOD, A.E., 1982. Phase transformations and differentiation in subducted lithosphere: implications for mantle dynamics, basalt petrogenesis, and crustal evolution. Jour. of Geol., 90 (6), pp 611-643.

ROGERS, N.W., HAWKESWORTH, C.J., PARKER, R.J. and MARSH, J.S., 1985. The geochemistry of ptassic lavas from Vulsini, Central Italy and implications for mantle enrichment processes beneath the Roman region. Contrib. Mineral. Petrol., 90, pp 244-257.

ROUX, J. and HAMILTON, D.L., 1976. Primary igneous analcite - an experimental study. J. Petrol., 17 (2), pp 244-257.

SHAW, D.M., 1970. Trace element fractionation during anatexis. Geochim. Cosmochim. Acta, 34, pp 237-243.

SHIMIZU, N., 1975. Rare earth elements in garnets and clinopyroxenes from garnet lherzolite nodules in kimberlites. Earth Planet. Sci. Lett., 25, pp 26-32.

SPARKS, R.S.J., PINKERTON, H., and MacDONALD, R., 1977. The transport of xenoliths in magmas. Earth Planet. Sci. Lett., 35, pp 234-238.

STEELE, T.W., WILSON, A., GOUDVIS, R., ELLIS, P.J. and RADFORD, A.J., 1978. Analysis of the NIMROC reference samples for minor and trace elements. National Institute of Metallurgy, S.A., Report No. 1945; Geostandards Newsletter, 2: pp 71-106.

STOSCH, H-G., 1981. Sc, Cr, Co and Ni partitioning between minerals from spinel peridotite xenoliths. Contrib. Mineral. Petrol., 78, pp 166-174.

STOSCH, H-G., 1982. Rare earth element partitioning between minerals from anhydrous spinel peridotite xenoliths. Geochim. Cosmochim. Acta, 46, pp 793-811.

STOSCH, H-G. and SECK, H.A., 1980. Geochemistry and mineralogy of two spinel peridotite suites from Dreiser Weiher, West Germany. Geochim. Cosmochim. Acta, 44, pp 457-470.

STROH, J.M., 1976. Solubility of alumina in orthopyroxene and spinel as a geobarometer in complex systems. Applications to spinel bearing Alpine-type peridotites. Contrib. Mineral, Petrol. 54, pp 173-188.

STECKLER, M.S., 1985. Uplift and extension at the Gulf of Suez; indications of induced mantle convection. Nature, 317, pp 135-139.

STUEBER, A.M. and LKRAMUDDIN, M., 1974. Rubidium, strontium and the isotopic composition of strontium in ultramafic nodule minerals and host basalts. Geochim. Cosmochim. Acta, 38, pp 207-216.

SUN, S-S., 1980. Lead isotopic study of young volcanic rocks from mid-ocean ridges, ocean islands and island arcs. Philos. Trans. R. Soc. Lond. A297, pp 409-445.

SUN, S-S., NESBITT, R.W. and SHARASKIN, A., 1979. Geochemical characteristics of mid-ocean ridge basalts. Earth Planet. Sci. Lett., 44, pp 119-138.

TATSUMI, Y., 1981. Melting experiments on a high-magnesian andesite. Earth Planet. Sci. Lett., 54, pp 357-365.

THIRLWALL, M.F. and JONES, N.W., 1983. Isotope geochemistry and contamination mechanics of Tertiary lavas from Skye, northwest Scotland. In: Continental Basalts and Mantle Xenoliths. Ed: Hawkesworth, C.J. and Norry, M.J., Shiva Geology Press.

THIRLWALL, M.F., and GRAHAM, A.M., 1984. Evolution of high-Ca, high-Sr, C-series basalts from Grenada, Lesser Antilles: the effects of intra-crustal contamination. J. Geol. Soc. Lond., 141, pp 427-445.

THOMPSON, R.N., 1974. Some high-pressure pyroxenes. Min. Mag., 39, pp 768-787.

THOMPSON, R.N., 1982. Magmatism of the British Tertiary Volcanic Province. Scott. J. Geol., 18, pp 50-107.

THOMPSON, R.N., DICKIN, A.P., GIBSON, I.L. and MORRISON, M.A., 1982. Elemental fingerprints of isotopic contamination of Hebridean Palaeocene mantle-derived magmas by Archaean sial. Contrib. Min. Pet., 79, pp 159-168.

THOMPSON, R.N., MORRISON, M.A., DICKIN, A.P. and HENDRY, G.L., 1983. Continental flood basalts ... Arachnids Rule O.K.? In: Continental Basalts and Mantle Xenoliths, Ed. Hawkesworth, C.J. and Norry, M.J. Shiva Geology Press.

THOMPSON, E.N., MORRISON, M.A., HENDRY, G.L. and PARRY, S.J., 1984. As assessment of the relative roles of crust and mantle in magma genesis: an elemental approach. Phil. Trans. R. Soc. London, A310, pp 549-590.

THOMPSON, R.N., 1985. Asthenospheric source of Ugandan ultra-potassic magma? Jour. of Geol. (in press).

THORPE, R.S., FRANCIS, P.W., and O'CALLAGHAN, L., 1984. Relative roles of source composition, fractional crystallisation and crustal contamination in the petrogenesis of Andean volcanic rocks. Phil. Trans. R. Soc. London, A310, pp 675-692.

VANNIMAN, D.T., CROWE, B.M., and GLADNEY, E.S., 1982. Petrology and geochemistry of hawaiite lavas from Crater Flat, Nevada. Contrib. Mineral. Petrol., 80, pp 341-357.

WALKER, G.P., 1973. Explosive volcanic eruptions - A new classification scheme. Geol. Rundsch., 62, pp 431-446.

WALKER, G.P. and CROASDALE, R., 1972. Characteristics of some basaltic pyroclastics. Bull. Volc., 35, pp 303-317.

WALSH, J.N., BUCKLEY, F. and BARKER, J., 1981. The simultaneous determination of rare earth elements in rocks using inductively coupled plasma source spectrometry. Chem. Geol. 33, pp 141-153.

WATKINS, P.J., 1980. Analysis of silicates using a single solution proceedure. Technical Report Number 8, Geology Department, Imperial College University of London, 50 pp.

WATKINS, P.J. and THOMPSON, M., 1983. Determination of Be and Zr in 45 geochemical reference samples by inductively coupled plasma emission spectrometry. Geostandards Newsletter 7, No. 2, pp 273-277.

WEAVER, B.L. and TARNEY, J., 1980. Rare earth geochemistry of Lewisian granulite-facies gneisses, northwest Scotland: implications for the petrogenesis of the Archaean lower continental crust. Earth Planet. Sci. Lett. 51, pp 279-296.

WELLS, P.R.A., 1977. Pyroxene thermometry in simple and complex systems. Contrib. Mineral. Petrol., 62, pp 129-139.

WESTPHAL, M., BARDON, C., BOSSERT, A. and HAMZEH, R., 1973. A computer fit of Corsica and Sardinia against southern France. Earth Planet. Sci. Lett., 18, pp 137-140.

WHITE, R.W., 1966. Ultramafic inclusions in basaltic rocks from Hawaii. Contrib. Mineral. Petrol., 12, pp 245-314.

WHITE, W.M. and PATCHETT, P.J., 1984. Hf-Nd-Sr isotopes and incompatible element abundances in island arcs: implications for magma origins and crust-mantle evolution. Earth Planet. Sci. Lett., 67, pp 167-185.

WILKINSON, J.F.G. and BINNS, R.A., 1977. Relatively iron-rich lherzolite xenoliths of the Cr-diopside suite: A guide to the primary nature of anorogenic tholeiitic andesite magmas. Contrib. Mineral. Petrol., 65, pp 199-212.

WILLIAMS, S.N. 1983. Plinian airfall deposits of basaltic composition. Geology, 11 (4), pp 211-214.

WILSON, M. and DAVIDSON, P., 1984. The relative roles of crust and upper mantle in the generation of oceanic island arc magmas. Phil. Trans. R. Soc. Lond., A310, pp 661-674.

WOOD, B.J. and BANNO, S., 1973. Garnet-orthopyroxene and orthopyroxene-clinopyroxene relationships in simple and complex systems. Contrib. Mineral. Petrol., 42, pp 109-142.

WOOD, D.A., GIBSON, I.L. and THOMPSON, R.N., 1976. Elemental mobility during zeolite facies metamorphism of the Tertiary basalts of eastern Iceland. Contrib. Mineral. Pet., 55, pp 241-254.

WOOD, D.A., JORON, J-L., TREUIL, M., NORRY, M. and TARNEY, J., 1979. Elemental and strontium isotope variations in basic lavas from Iceland and the surrounding ocean floor. Earth Planet. Sci. Lett., 70, pp 319-339.

WYLLIE, P.J., 1977. Crustal anatexis: an experimental review. Tectonophy., 43, pp 41-71.

WYLLIE, P.J., 1984. Constraints imposed by experimental petrology on possible and impossible magma sources and products. Phil. Trans. R.Soc. London, A310, pp 439-456.

APPENDIX A

ANALYTICAL TECHNIQUES

Bulk rock chemical analysis

(a) Sample preparation

Weathered surfaces were removed from each rock sample using a mechanical splitter. The rocks were then split into approximately 3 centimetre cubes, and crushed in a steel jaw-crusher. Care was taken to ensure complete collection of the finest grain size material. The possibility of inter-sample contamination was minimised by scrupulous cleaning of the jaw-crusher with deionised water and alcohol between samples, and by the successive crushing of rocks of similar bulk chemical composition. A representative proportion of each rock sample was then powdered in a tungsten carbide tema mill. Grinding times of 30-60 seconds were sufficient to produce a suitable grain size ($<$ 200 mesh) for analytical work. Grinding in a tungsten carbide tema mill produces tantalum and cobalt contamination of the sample, and some samples were therefore also ground in agate. Tantalum values, obtained by instrumental neutron activation analysis, of rock samples ground in both tungsten carbide and agate, are given in Table A1.

(b) Major element analysis by X-Ray Fluorescence Spectrometry (XRF)

The concentrations of major element oxides, SiO_2, TiO_2, Al_2O_3, FeO_3T, MnO, MgO, CaO, K_2O, Na_2O and P_2O_5 were determined on a Philips PW 1212 semi-automated XRF spectrometer, using a chromium tube at 60 mV and 32 mA.

TABLE A1

TANTALUM VALUES OBTAINED BY I.N.A.A.
FOR SAMPLES GROUND IN TUNGSTEN CARBIDE
AND IN AGATE
(ALL VALUES IN PPM)

	Agate	Tungsten carbide
K83	1.13	1.30
K106	2.80	3.24
MR17	0.25	0.32

TABLE A2

ANALYSES OF TWO INTERNATIONAL GEOCHEMICAL
REFERENCE STANDARDS ON A DRY BASIS
(110°C) BY XRF

	BR		GA	
	This work	Literature value (Abbey, 1980)	This work	Literature value (Abbey, 1980)
SiO_2	39.16	38.39	70.56	69.96
TiO_2	2.63	2.61	0.36	0.38
Al_2O_3	10.14	10.25	14.69	14.51
Fe_2O_3T	12.83	12.90	2.78	2.77
MnO	0.23	0.20	0.11	0.09
MgO	13.35	13.35	0.93	0.95
CaO	13.80	13.87	2.48	2.45
Na_2O	3.01	3.07	3.75	3.55
K_2O	1.41	1.41	4.18	4.03
P_2O_5	1.10	1.05	0.15	0.12

All values given as weight percent oxide

Fe_2O_3T denotes total iron expressed as Fe_2O_3

Samples were prepared according to the method of Norrish and Hutton (1969). About 5g of finely ground rock powder was dried at 110°C for more than 12 hours. The powders were then ignited to a constant weight at 950°C. The weight loss (or gain) on ignition gives an estimate of the total volatile content, having corrected for the oxidation of FeO to Fe_2O_3. About 0.280g of ignited sample powder, accurately weighed to four decimal places, was thoroughly mixed with 1.500g of Johnson Matthey Spectroflux 105, previously dried at 400°C for 4 hours. The flux/powder mixture was fused in a platinum-gold crucible at about 1000°C. Ten minutes was found to be adequate for fusion and complete homogenisation. The melt was then poured on to a mould and pressed under a plunger to form a glass disc suitable for XRF analysis. The small weight loss in the flux during the fusion process was corrected for by adjusting the flux/sample ratio by an appropriate amount.

All XRF data was corrected for machine drift and dead time. Rock standards, run before and after the samples, were used to calculate a calibration line. The data was processed using programs CHECK, SORD and PWMAJ (Parker, 1977; 1979; 1980). Two international rock standards (BR and GA) were run as unknowns, and the data obtained for these rocks, together with their accepted literature values, are given in Table A2. Precision data obtained for 9 separate preparations of a hawaiite (K33) is presented in Table A3. Replicate analyses of 5 samples, with varying chemical compositions, were determined by inductively-coupled plasma atomic emission spectrometry (ICP) by comparison with a calibration line obtained from the analysis

TABLE A3

NINE SEPARATE ANALYSES OF A HAWAIITE (K33) BY XRF

All values given as weight percent oxide

	Mean	Standard deviation (1s)
SiO_2	50.44	0.20
TiO_2	2.05	0.01
Al_2O_3	15.38	0.08
Fe_2O_3T	10.36	0.19
MnO	0.18	0.03
MgO	7.47	0.15
CaO	7.91	0.05
Na_2O	4.04	0.13
K_2O	2.50	0.02
P_2O_5	0.55	0.01

of 10 international standard rocks. The ICP data is in good agreement with that obtained by XRF (Table A4).

(c) Trace element analysis by XRF

The concentration of some trace elements (Cu, Ni, V, Cr, Nb, Zr, Y, Th, Sr, Rb, Zn and Ba) were determined by XRF on a Philips PW 1212 semi-automated XRF spectrometer at Imperial College. Ba ($L\beta_2$ peak) was analysed using a chromium tube at 600 mV and 32 mA; Nb, Zr, Cr, Cu, Ni, Zn and V (all $K\alpha$ peaks) were analysed using a tungsten tube at 60 kV and 32 mA; Y, Sr, Th and Rb (all $K\alpha$ peaks), were analysed using a molybdenum tube at 90 mV and 20 mA.
5.0g of rock powder was mixed with 6-8 drops of 20% polyvinyl alcohol. Boric acid powder was used to give the briquettes strong side walls. The briquettes were then pressed under a hydraulic press at a pressure of 8 tons per square inch for 30 seconds. Immediately prior to analysis the briquettes were dried for more than 8 hours at $50^{o}C$.
The data was processed using programs TRANS and PTRAC (Parker, 1977). Matrix corrections, tube contamination corrections and peak interference (Sr on Zr; Rb on Y; Ti on V; Y on Nb; and V on Cr) corrections were made. Trace element concentrations obtained for 4 U.S.G.S. standard rocks, together with their concensus values, are given in Table A5. Precision data, obtained on 10 trace element briquettes of a hawaiite (K33) is given in Table A6. Detection limits (D.L.) for this method were calculated from 4 U.S.G.S. standard rocks, using the formula (Norrish and Chappell, 1977):

$$\text{D.L. (in ppm)} = \frac{6}{m}\sqrt{\frac{Rb}{Tb}}$$

TABLE A4

COMPARATIVE MAJOR ELEMENT DATA FOR FIVE SAMPLES OF VARYING CHEMICAL COMPOSITION ANALYSED BY XRF AND ICP

	K34[1]		GR-P[2]		MR20[3]		POZZ-3[4]		U120[5]	
	X.R.F.	I.C.P.	X.R.F.	I.C.P.	X.R.F.	I.C.P.	X.R.F.	I.C.P.	X.R.F.	I.C.P.
SiO_2	50.56	50.36	42.16	41.98	44.74	44.58	45.32	45.01	13.92	13.93
Al_2O_3	15.71	15.59	20.09	20.56	18.26	18.02	1.69	1.73	3.47	3.46
Fe_2O_3T	10.55	10.24	10.53	9.90	13.74	13.47	8.78	8.66	2.32	2.32
MgO	7.08	7.08	17.09	16.58	6.81	6.84	43.43	43.47	1.06	1.05
CaO	7.71	7.71	11.26	11.37	12.22	12.32	1.38	1.38	41.76	41.02
Na_2O	3.90	4.17	0.05	0.19	2.54	2.61	0.00	0.01	2.44	2.43
K_2O	2.62	2.56	0.00	0.00	0.35	0.32	0.00	0.00	0.29	0.29
P_2O_5	0.57	0.56	0.05	0.02	0.20	0.19	0.01	0.02	0.12	0.12
TiO_2	2.12	2.13	0.05	0.06	1.28	1.30	0.03	0.04	9,12	0.11
MnO	0.16	0.13	0.14	0.12	0.22	0.19	0.18	0.13	0.19	0.19

1 Alkali basalt

2 Basic granulite facies gneiss

3 High-Al basalt

4 Spinel lherzolite

5 Pelagic calcareous marl

TABLE A5

TRACE ELEMENT ANALYSES OF U.S.G.S. STANDARD ROCKS BY XRF

		G-2	AGV	BCR	W-1
Ba	1	1885	1234	726	138
	2	1880 ± 20	1221 ± 16	678 ± 16	162 ± 5
Nb	1	10.4	14.8	13.8	9.9
	2	13 ± 4	15 ± 3	14 ± 3	8 ± 2
V	1	37	123	375	266
	2	36 ± 5	123 ± 12	404 ± 40	260 ± 25
G	1	12	14	18	120
	2	9 ± 2	12 ± 3	16 ± 4	120 ± 14
Ni	1	8	18	12	73
	2	4.9 ± 2.3	17 ± 4	13 ± 4	75 ± 9
Cu	1	20	61	26	117
	2	11 ± 3	60 ± 6	19 ± 4	114 ± 10
Zn	1	91	87	125	87
	2	85 ± 7	88 ± 2	129 ± 1	84 ± 6
Th	1	24	6	4	0
	2	24.6 ± 1.5	6.5 ± 0.37	6.4 ± 0.6	2.4 ± 9.4
Rb	1	166	67	49	23
	2	170 ± 3	67 ± 1	47.1 ± 0.6	21.4 ± 0.3
Sr	1	472	670	340	190
	2	478 ± 3	662 ± 9	330 ± 5	187 ± 7
Y	1	6	20	38	23
	2	11.4 ± 2.3	21 ± 6	39 ± 7	26 ± 4
Zr	1	309	218	186	94
	2	300 ± 30	225 ± 18	191 ± 5	100 ± 9

1 This work
2 U.S.G.S. consensus values (1982)
All values given in ppm

TABLE A6

PRECISION DATA FOR TRACE ELEMENT ANALYSIS OF A HAWAIITE (K33) BY XRF

	Mean	1s
V	164	4
Cr	177	10
Ni	108	3
Cu	35	4
Zn	104	2
Th	9.6	5.9
Rb	59	6
Sr	827	8
Y	20.5	2.6
Zr	241	5
Nb	58.4	3.9
Ba	964	10

All values given in ppm

TABLE A7

AVERAGE DETECTION LIMITS FOR SOME TRACE ELEMENTS DETERMINED BY XRF

	Detection limit
Cr	6.4
Zn	9.0
Ba	51.0
Rb	6.2
Cu	7.8
Ni	5.6
V	10.0
Sr	5.4
Th	10.2
Y	3.4
Zr	12.0

All values given in ppm

where $m = \frac{Rp - Rb}{\text{standard concentration}}$

and Rp = Peak counting rate, counts/sec.

Rb = Background counting rate, counts/sec.

Tb = Background counting time, sec.

Standard concentration is given in ppm.

Calculated average detection limits are given in Table A7.

CIPW norms, using major and trace element data, were calculated using the program AGNORM (Parker, 1977).

(d) Ferrous iron determination

FeO was determined in several samples using a cold HF decomposition procedure with subsequent titration of the liberated ferrous iron with potassium dichromate (Whipple, 1974).

(e) Rare earth element analysis

The rare earth elements (REE) were determined by inductively-coupled plasma atomic emission spectrometry (ICP) at King's College, London. After dissolution, the REE were separated using ion exchange column separation techniques (Walsh et al, 1981). 0.500g of finely ground (< 200 mesh) rock powder was mixed with 1.500g of lithium metaborate in a clean porcelain crucible. The mixture was transferred to a platinum dish and fused at 1000°C for 30 minutes. The fused bead was dissolved, using a magnetic stirrer, in a glass beaker containing 60 ml of 2N HCl and 40 ml of water.

This solution was then passed through an ion exchange column containing Bio-Rad AG50W-X8 resin. The unwanted elements were eluted with 500 ml of 1.75 N HCl. The REE were then eluted with

600 ml of 4.0 N HCl. The solution was then evaporated to dryness on a hot plate. 10 ml of concentrated HNO_3 were then added, and the solution was again evaporated to dryness. Immediately prior to analysis, the REE salts were dissolved in 5.0 ml of 2N HNO_3.

The REE were analysed on a Philips PV 8210 spectrometer at King's College, London. Machine drift was monitored using a composite REE solution. Line interferences produced by residual Ba, Fe, Ca and Zr and by some REE on other REE, were corrected manually using chemical interference standards. International rock standards were run as unknowns. Values obtained for BE-N and NIM-G are given in Table A8. A hawaiite (K33) was fused seven times and the REE determined for each preparation. This data was used to test the precision of the dissolution and separation procedures (Table A9).

Six reagent blank solutions were also analysed in order to determine an approximate detection limit for the procedure used. The detection limit is taken as three times the standard deviation on the reagent blank solution, and this data is also given in Table A9.

(f) Mass spectrometry

87 Sr/86 Sr ratios in 43 samples were determined by mass spectrometry in the Age Laboratory, at the University of Oxford. Strontium was separated out using ion exchange column techniques.

About 200 mg of finely ground rock powder was weighed into a Teflon beaker, and 4 ml of HF and 1 ml of concentrated HNO_3 were added. The solution was evaporated to dryness. A further

TABLE A8

REE ANALYSES OF INTERNATIONAL STANDARD ROCKS BY ICP

	BE-N		NIM-G	
	This work	Lit. value[1]	This work	Lit. value[1]
La	81	81	108	114
Ce	153	154	203	210
Pr	16.0	17	19.5	21
Nd	69.4	66	74.6	76
Sm	11.7	12	15.0	16
Eu	3.65	3.8	0.37	0.35
Gd	10.40	9.3	15.6	16
Dy	6.26	6.9	17.9	18
Ho	1.15	1.3	4.25	4.2
Er	2.83	2.9	14.0	13
Yb	1.87	1.8	14.5	14
Lu	0.24	0.19	2.0	2.2

1 Potts, P.J. et al., (1981)

All values given in ppm

TABLE A9

REE ANALYSES BY ICP.
MEAN AND STANDARD DEVIATIONS (1s) FOR SEVEN SEPARATE PREPARATIONS OF A HAWAIITE (K33) AND FOR SIX REAGENT BLANK SOLUTIONS

	K33		Reagent Blank		Calculated Detection limit
	Mean	1s	Mean	1s	
La	37.4	1.7	0.8	0.2	0.6
Ce	77.2	3.4	0.6	0.1	0.3
Pr	8.4	0.1	-	-	-
Nd	36.7	0.3	0.09	0.02	0.06
Sm	7.23	0.15	0.10	0.02	0.06
Eu	2.11	0.05	-	-	-
Gd	5.78	0.31	0.03	0.04	0.12
Dy	3.94	0.04	0.01	0.05	0.15
Ho	0.79	0.01	0.01	0.003	0.009
Er	1.84	0.04	0.125	0.019	0.057
Yb	1.20	0.04	0.026	0.005	0.015
Lu	0.17	0.01	0.024	0.005	0.015

All values given in ppm

2 ml of concentrated HNO_3 was added, and the solution evaporated to incipient dryness. About 4 ml of 2.5 M HCl was then added, and the suspension was transferred to a centrifuge tube. 1 ml of each sample was pipetted onto each column, and the unwanted elements eluted with a previously calibrated amount of 2.5 M HCl. The Sr fraction was then eluted and collected with a further calibrated amount of 2.5 M HCl. Having evaporated to a small volume, the solutions were transferred to microbeakers and evaporated to dryness. To minimise inter-sample contamination, the evaporations were carried out within separate Teflon covers which were not open to the air. A stream of filtered air was passed over the samples in order to remove the fumes quickly. The Sr samples were loaded onto single tantalum filaments for mass spectrometry using a V.G. Micromass 30. $^{87}Sr/^{86}Sr$ values obtained were normalised to an Eimer and Amend Sr CO_3 solution of $^{87}Sr/^{86}Sr = 0.70800$.

(g) Determination of Sc, Be and Ba by ICP

The concentrations of Be and Ba in some samples were determined by ICP at Imperial College, London. Sc was analysed by ICP at King's College, London.

0.2500g of finely ground rock powder was mixed with 0.750g of $LiBO_2$. The mixture was fused in a pre-ignited graphite crucible at 1000°C for 20 minutes. The molten bead was dissolved in a plastic beaker containing 25 ml of 2N HNO_3 and 150 ml of deionised water. Care was taken to ensure that all the melt was transferred from the graphite crucible into the beaker. The solution was made up to 250 ml with dionised water and filtered into a plastic bottle (Watkins, 1980).

Sample concentrations were calculated using a calibration line calculated from international rock standards. Machine drift was monitored by running the same solution after every 10 samples. Line interferences (V on Be; Ti on V) were corrected manually using chemical interference standards. Sc, Be and Ba data for standard rocks is presented in Table A10. Comparative scandium data for samples analysed by both ICP and instrumental neutron activation analysis is given in Table A11. Detection limits of 0.1 ppm (Be) and 36 ppm (Ba) were calculated.

(h) Instrumental neutron activation analysis (I.N.A.A.)

I.N.A.A. (Gordon et al., 1968), is a particularly useful analytical method for determining the concentrations of some geologically important trace elements down to the ppm and sub-ppm level. Irradiations during the course of this work were undertaken at the University of London Reactor Centre at Silwood Park. Counting for some samples, for a restricted number of elements (U, Th and Hf), was performed on a lithium-drifted germanium (Ge-Li) detector at the University Reactor Centre. More complete analyses, including the REE, Ta, Co, Rb and Sc as well as U, Th and Hf were undertaken in the Department of Mineralogy at the British Museum on both Ge-Li and high purity germanium detectors. Nine samples were analysed for Hf by epithermal neutron activation analysis (Parry, 1981).

(i) Thermal I.N.A.A.

100 mg of finely ground rock powder were irradiated for 5 days in sealed polythene capsules within a thermal neutron flux. Short-lived nuclides were allowed to decay for four days prior to counting.

Synethetic chemical standards were used for calibration. These were prepared by pipetting 1 ml of a standard solution onto a filter paper, inside a polythene capsule, and evaporating to dryness. Three standards were included in each run of 12 samples. The 12 samples are stacked in an outer polythene irradiation tube. One sample (REE standard) was placed at each end of the irradiation tube, and another standard (other elements) in the centre of the tube. This enables any variations in the neutron flux during irradiation along the length of the containers to be monitored. Data processing utilised nuclear data software involving a peak search routine, correction for decay time, and correction for spectral interferences. Matrix corrections are minimal because neutrons penetrate deeply into the target (Coles, 1977) and are disregarded.

A high-purity germanium detector was used forNd, Sm, Ho, Lu, Eu and U (Henderson & Williams, 1981), and a lithium-drifted germanium detector for La, Ce, Tb, Yb, Th, Sc, Co, Cr, Ni, Zn, Hf, Ta, Rb, Cs and Sb. An international rock standard (GA) was run with each batch of 11 standards and samples. Three separate analyses of GA are presented in Table A12.

TABLE A10

DETERMINATION OF Sc, Be AND Ba IN INTERNATIONAL ROCK STANDARDS BY ICP

(i) Scandium values in ppm

	This work	Literature value
BE-N	22.2	22.0[1]
UB-N	9.2	13.1
JB-1	27.6	28.0
GS-N	7.0	7.5
GA	6.0	8.0

(ii) Beryllium values in ppm

	This work	Literature value
GH	5.3	6?, 5.54[2]
W-1	0.6	0.8?, 0.65[2]
G-Z	2.3	2.4, 2.33[2]
BE-N	1.7	1.96[2]
SY-3	22.5	22, 22.4[2]

(iii) Barium values in ppm

	This work	Literature value
GH	26	22
BE-N	1048	1025[1]
JB-1	496	490
GS-N	1373	1400
W-1	155	160
G-Z	1836	1900

All literature values are from Abbey (1980) except:

1 Govindaraju (1980)

2 Watkins and Thompson (1983)

TABLE A11

COMPARATIVE SCANDIUM DATA FOR SAMPLES ANALYSED BY ICP AND I.N.A.A.

	I.C.P.	I.N.A.A.
K33	15.6	16.2
K111	17.0	15.7
K83	14.9	15.7
K110	15.1	16.1
K90	6.3	6.9
K59	15.5	14.5
MR14	29.7	32.8
K58	13.0	10.1
K102	24.6	24.5
K62	13.6	14.6

All values given in ppm

TABLE A12

ANALYSES OF GA BY I.N.A.A.

	1	2	3	Literature values
La	43	41	47	40[1]
Ce	74	70	85	77[1]
Nd	28.2	27.0	31.1	29.0[1]
Sm	5.27	5.08	5.58	5.20[1]
Eu	0.99	0.99	1.08	1.05[1]
Tb	0.61	0.52	0.72	0.66[1]
Ho*	1.1	0.86	1.07	0.8[1]
Yb	2.56	1.99	2.24	2.03[1]
Lu	0.28	0.28	0.34	0.31[1]
Th	15.7	14.5	16.3	16.9[1]
U	5.8	4.4	5.4	5.1[2]
Sc	6.9	6.7	7.5	6.8[2]
Co	4.3	4.1	5.1	4.61
Cr	8.5	8.0	13.5	8.8[2]
Ni	<9	<9	11.8	8.2[3]
Zn	114	110	123	80[3]
Hf	4.00	3.77	4.69	4.2[1]
Ta	1.18	1.14	1.34	1.3[1]
Rb	165	158	173	164[2]
Cs	6.2	6.0	6.7	6.0[2]
Sb	0.32	0.30	0.62	0.18[2]

All values given in ppm

* Values obtained for Ho are consistently high due to a U interference on Ho which is difficult to correct (Williams, pers. comm.)

1 Potts, P.J., Thorpe, O.W., Watson, J.S. (1981);

2 Kramar U and Puchelt H. (1982);

3 Church S.E. (1981).

Epithermal neutron activation analysis

The determination of Hf by epithermal neutron activation analysis has been previously described (Parry, 1981), and will only be summarised here. A nuclear reactor contains three types of neutrons with different energies. Fast (high energy) neutrons interact with the target and produce nuclides with too short half-lives. Thermal (slow) neutrons are in equilibrium at the reactor temperature. Epithermal neutrons have an intermediate energy. Epithermal neutron activation analysis utilises a cadmium-lined tube to filter out low energy thermal neutrons. This lowers the background by decreasing the activity of nuclides such as ^{27}Mg and ^{28}Al, and therefore enhances the ^{179m}Hf peak ($T_{1/2}$ = 18.7 seconds) at 217 keV relative to the background. Hf was counted on a Ge-Li detector for 30 seconds, after a 30 second irradiation, followed by a 30 second decay. Chemical standards (1 ppm Hf) were used for calibration. Powdered samples were irradiated in polythene capsules in a fast pneumatic transfer system (Burholt et al., 1982).

Cesium analysis by flame emission spectrometry

Encouraging results from preliminary work on the determination of Cs by flame emission spectrometry were obtained using the method proposed by Goguel (1981). The Cs value determined for geochemical reference standard NIM-S (6.1 ppm) is in good agreement with it's literature values (6.33 ppm[1]; 5.7-10.1 ppm[2]). Cs values obtained by emission spectrometry and I.N.A.A. for a hawaiite (K33) show close agreement (0.7/0.7 ppm and 0.68 ppm, respectively).

1 Goguel, 1981; 2 Abbey, 1980.

Clinopyroxene separation proceedure

In order to minimise the possibility of REE contamination from the host basalt to spinel peridotite inclusion, diopsides were separated from freshly crushed peridotite xenoliths by several stages of hand-picking under a binocular microscope. Care was taken to avoid grains which showed evidence of silicate or fluid inclusions. The pyroxenes were carefully ground to a finer grain size in an agate mortar, followed by a further stage of hand-picking. The separates were then washed in a PTFE beaker, with 20 ml of ZN HCl for 15 minutes using a magnetic stirrer. Subsequently, they were washed several times in deionised water, and then allowed to stand in cold 5% HF solution for 15 minutes. Such an etching proceedure has been found to be effective in removing grain surface contamination (Shimizu, 1975). Finally, any remaining liquid was allowed to evaporate.

Mineral analyses

Mineral analyses were performed at Imperial College using a Cambridge Instruments Microscan 5 fitted with a Link Systems energy dispersive detector. Operating conditions used were an accelerating voltage of 15 kV and a specimen current of 4.0 nA (2.5 nA for alkali feldspar and analcite to minimise Na loss from the specimen). Counting times of 100 seconds, with the electron beam focused into a spot, were used. Metal oxides, pure metals and end-member minerals were used for calibration purposes, Replicate analyses of standard minerals analysed during the course of this work are presented in Table A13.

TABLE A13

MULTIPLE PROBE ANALYSES OF OLIVINE STANDARD

	1	2	3	4	5	6	7	8	9	10	11	12
SiO_2	40.01	40.48	40.27	39.88	39.89	40.67	40.57	40.59	40.05	40.29	40.24	41.50
FeO	9.05	8.73	8.73	9.16	8.76	9.17	9.16	9.08	8.63	8.12	8.89	9.08
MnO	.08	.08	.20	.11	.18	.13	.13	0	.05	.27	.23	.21
MgO	49.63	50.09	49.62	49.70	49.38	48.44	48.77	50.17	49.29	50.01	49.14	49.62
CaO	.10	.13	.12	.03	.12	.04	.09	.04	.10	.03	.06	.06
NiO	.60	.45	.39	.40	.57	.24	.36	.60	.36	.54	.33	.69
SUM	99.47	99.91	99.33	99.28	98.90	98.69	99.08	100.48	98.48	99.26	98.89	101.16
FO	90.64	91.06	90.83	90.53	90.78	90.27	90.34	90.78	91.01	91.39	90.57	90.49
FA	9.36	8.94	9.17	9.47	9.22	9.73	9.66	9.22	8.99	8.61	9.43	9.51
F/M	.103	.098	.101	.105	.102	.108	.107	.102	.099	.094	.104	.105
F/FM	.094	.089	.092	.095	.092	.097	.097	.092	.090	.086	.094	.095

1 OL STD10
2 OL STD10
3 OL STD10
4 OL STD10
5 OL STD10
6 OL STD10
7 OL STD10
8 OL STD10
9 OL STD10
10 OL STD10
11 OL STD10
12 OL STD10

TABLE A13 (Cont'd.)

	13	14	15	16	17	18	19	20	21
SiO_2	41.02	40.72	40.58	41.28	41.23	41.13	40.76	40.67	39.89
FeO	8.91	9.13	9.12	9.21	9.69	9.15	8.84	9.38	9.00
MnO	.14	.15	.13	.20	.04	.13	.19	.13	.10
MgO	49.28	49.04	49.03	49.53	49.01	49.97	49.33	49.30	49.76
CaO	.08	.10	.14	.04	.01	0	0	.14	.10
NiO	.40	.23	.44	.21	.41	.40	.33	.35	.36
SUM	99.83	99.37	99.44	100.47	100.39	100.78	99.45	99.97	99.21
FO	90.66	90.40	90.43		89.98	90.56	90.68	90.23	90.69
FA	9.34	9.60	9.57	9.64	10.02	9.44	9.32	9.77	9.31
F/M	.103	.106	.106	.107	.111	.104	.103	.108	.103
F/FM	.093	.096	.096	.096	.100	.094	.093	.098	.093

13 OL STD10
14 OL STD10
15 OL STD10
16 OL STD10
17 OL STD10
18 OL STD10
19 OL STD10
20 OL STD10
21 OL STD10

APPENDIX B

MAJOR AND TRACE ELEMENT DATA

	K1	K3	K4	K5	K7	K9
SiO_2	51.32	51.12	49.51	51.43	48.45	53.97
TiO_2	0.89	0.87	2.46	0.89	2.56	2.37
Al_2O_3	18.70	18.94	15.12	18.74	15.32	16.58
Fe_2O_3T	10.22	10.17	9.40	10.00	10.02	9.46
MnO	0.20	0.24	0.14	0.20	0.16	0.12
MgO	4.74	4.80	7.95	4.97	8.36	3.16
CaO	9.68	10.29	7.32	9.93	7.92	5.34
Na_2O	2.70	3.56	3.48	2.46	3.98	4.35
K_2O	1.11	0.93	3.30	0.88	1.61	3.85
P_2O_5	0.29	0.24	0.70	0.31	0.70	0.82
LoI	0.53	0.57	0.71	0.59	1.72	0.33
Total	100.38	101.73	100.09	100.40	100.80	100.35
V	192	194	211	192	198	142
Cr	48	28	238	38	263	43
Ni	23	18	167	23	211	53
Cu	87	80	43	77	44	23
Zn	82	77	92	93	83	117
Rb	22	14	60	20	14	75
Sr	619	695	986	616	996	1103
Y	24	26	17	27	21	-
Zr	110	99	237	116	274	319
Nb	5	5	52	11	66	71
Ba	204	160	1379[1]	213[1]	1808	1906
Th	2.34	-	-	-	-	-
Hf	3.00	-	-	-	-	-
U	0.51	-	-	-	-	-
Ta	-	-	-	-	-	-
Be	1.0	-	2.2	1.3	-	-
Sc	26.7	-	14.8	-	-	-
Cs	1.02	-	-	-	-	-

	K10	K11	K12	K13	K14	K15
SiO_2	53.09	49.89	52.48	52.21	52.46	53.20
TiO_2	2.36	2.46	2.17	2.12	2.20	2.25
Al_2O_3	16.73	17.38	17.44	16.47	16.37	16.02
Fe_2O_3T	10.27	10.71	7.45	10.37	9.95	9.46
MnO	0.23	0.13	0.08	0.13	0.13	0.12
MgO	3.67	4.18	3.09	4.80	4.49	4.14
CaO	6.31	6.21	3.82	6.50	6.38	6.45
Na_2O	4.22	3.88	3.25	4.67	4.47	5.02
K_2O	2.47	2.31	4.53	1.84	2.46	2.68
P_2O_5	0.54	1.19	0.87	0.52	0.62	0.69
LoI	0.62	1.91	4.48	1.06	0.85	0.36
Total	100.51	100.25	99.66	100.69	100.38	100.39
V	171	180	116	168	157	172
Cr	73	66	98	144	102	98
Ni	64	63	93	97	84	66
Cu	26	24	33	30	19	26
Zn	115	110	86	112	130	116
Rb	74	28	79	22	50	54
Sr	1008	1153	1026	800	955	919
Y	17	23	17	25	30	21
Zr	260	256	379	221	274	279
Nb	54	53[1]	71[1]	43	56	52[1]
Ba	1003	1084[1]	1527[1]	766	1029	1044[1]
Th	-	-	-	-	-	-
Hf	-	-	-	-	-	-
U	-	-	-	-	-	-
Ta	-	-	-	-	-	-
Be	-	1.3	2.5	-	-	1.7
Sc	-	14.1	-	-	-	12.2
Cs	-	-	-	-	-	-

	K16	K18	K19	K20	K21	K22
SiO_2	53.12	51.63	53.79	54.49	53.73	50.41
TiO_2	2.28	2.35	2.10	2.01	2.06	2.05
Al_2O_3	16.46	16.26	15.90	15.46	15.65	15.32
Fe_2O_3T	9.92	10.52	9.66	9.48	9.67	10.17
MnO	0.15	0.15	0.13	0.14	0.13	0.14
MgO	3.63	4.99	4.00	5.18	5.52	7.24
CaO	6.14	6.74	6.01	6.87	7.03	7.76
Na_2O	4.70	4.24	4.67	4.17	4.23	3.79
K_2O	2.74	2.15	2.35	1.71	1.82	2.41
P_2O_5	0.72	0.63	0.56	0.45	0.44	0.53
LOI	0.48	0.43	0.97	0.59	0.19	0.09
Total	100.34	100.09	100.14	100.55	100.47	99.91
V	153	161	176	160	169	182
Cr	101	97	117	148	162	160
Ni	74	80	68	87	86	108
Cu	29	24	30	16	29	29
Zn	123	124	120	114	111	110
Rb	55	29	52	42	32	46
Sr	1002	1021	890	769	800	831
Y	25	27	29	20	20	19
Zr	300	274	237	207	203	228
Nb	69	59	46[1]	37[1]	39[1]	49[1]
Ba	1115	1021	860[1]	679[1]	687[1]	943[1]
Th	-	-	-	-	-	-
Hf	-	-	-	-	-	-
U	-	-	-	-	-	-
Ta	-	-	-	-	-	-
Be	-	-	2.4	2.0	1.4	1.3
Sc	-	-	12.2	13.9	14.4	15.3
Cs	-	-	-	-	-	-

	K28	K30	K32	K33	K34	K35
SiO_2	50.45	53.33	52.47	50.44	50.56	50.09
TiO_2	2.12	2.03	2.38	2.05	2.12	2.43
Al_2O_3	15.56	16.16	15.93	15.38	15.71	15.20
Fe_2O_3T	10.08	11.05	9.02	10.36	10.55	9.21
MnO	0.19	0.13	0.10	0.18	0.16	0.14
MgO	7.11	4.70	4.86	7.47	7.08	7.98
CaO	7.64	7.07	6.06	7.91	7.71	7.30
Na_2O	4.22	4.49	3.98	4.04	3.90	3.35
K_2O	2.58	1.22	3.58	2.50	2.62	3.59
P_2O_5	0.58	0.37	0.75	0.55	0.57	0.69
LoI	0.02	0.22	1.30	0.00	-0.23	0.79
Total	100.55	100.77	100.43	100.88	100.74	100.77
V	178	182	169	165	159	180
Cr	137	98	75	177	141	238
Ni	100	65	65	108	106	136
Cu	43	34	29	35	36	42
Zn	101	124	103	104	104	87
Rb	65	27	72	59	58	71
Sr	891	631	979	827	873	994
Y	16	17	23	21	19	19
Zr	235	154	279	241	249	252
Nb	48[1]	30[1]	63	58[1]	52[1]	50[1]
Ba	989[1]	489[1]	1390[1]	951[1]	997[1]	1350[1]
Th	-	-	-	5.20	-	-
Hf	-	-	-	5.29	-	-
U	-	-	-	1.16	-	-
Ta	-	-	-	2.96	-	-
Be	1.8	1.2	1.9	1.9	1.6	2.2
Sc	14.9	12.8	11.0	15.6	14.4	15.6
Cs	-	-	-	0.68	-	-

	K36	K37	K40	K43	K44	K47
SiO_2	49.77	51.54	58.71	56.40	50.00	46.87
TiO_2	2.34	2.22	0.76	1.52	2.36	2.28
Al_2O_3	15.17	15.09	17.31	15.42	15.05	14.11
Fe_2O_3T	9.28	9.63	8.19	8.74	9.26	10.27
MnO	0.15	0.15	0.16	0.10	0.17	0.13
MgO	7.79	7.25	2.84	4.29	8.43	11.03
CaO	7.47	7.64	6.66	7.71	7.58	9.48
Na_2O	4.71	4.01	2.71	3.85	3.33	2.26
K_2O	1.37	2.20	2.54	0.82	2.59	1.40
P_2O_5	0.74	0.65	0.17	0.19	0.71	0.84
LoI	1.27	1.03	0.62	1.03	0.95	2.21
Total	100.06	101.40	100.68	100.07	100.41	100.88
V	167	180	116	144	187	229
Cr	225	241	12	230	241	338
Ni	145	175	7	147	181	317
Cu	46	38	42	38	36	23
Zn	71	80	52	100	81	91
Rb	73	-	86	19	56	35
Sr	1036	1047	395	458	1071	832
Y	16	22	34	15	23	23
Zr	247	289	187	98	311	257
Nb	58	57	10	17	70	52
Ba	1380[1]	1477	294	293[1]	1583	1247[1]
Th	-	-	-	-	-	-
Hf	-	-	4.77	2.50	-	-
U	-	-	-	-	-	-
Ta	-	-	-	-	-	-
Be	1.5	-	1.2	0.7	-	1.4
Sc	16.7	-	-	13.2	-	20.2
Cs	-	-	-	-	-	-

	K51	K52	K53	K55	K56	K57
SiO_2	46.59	45.28	52.58	53.11	52.98	52.85
TiO_2	2.65	2.99	2.14	2.23	2.30	2.37
Al_2O_3	14.15	14.09	15.77	16.22	15.88	16.19
Fe_2O_3T	9.89	10.11	10.92	10.83	9.24	9.52
MnO	0.13	0.16	0.17	0.18	0.11	0.14
MgO	10.42	9.46	5.50	5.54	4.29	3.55
CaO	8.30	10.06	7.05	7.00	6.74	6.11
Na_2O	4.62	5.23	3.90	4.06	4.29	4.09
K_2O	1.20	0.56	1.65	1.65	3.54	3.58
P_2O_5	0.82	0.98	0.47	0.48	0.80	0.82
LoI	1.77	2.04	0.00	-0.35	0.41	1.00
Total	100.54	100.96	100.15	100.95	100.58	100.22
V	196	279	161	191	151	176
Cr	294	227	131	117	117	111
Ni	203	-	91	97	66	70
Cu	41	36	36	37	23	31
Zn	63	73	105	113	105	114
Rb	45	89	36	30	71	71
Sr	1124	1055	749	766	1047	1077
Y	24	22	19	23	19	18
Zr	329	335	179	147	266	271
Nb	84	75	40	28	57	59
Ba	1457	1595[1]	638[1]	671[1]	1382[1]	1402
Th	-	-	4.65	-	-	-
Hf	-	7.27	-	-	-	-
U	-	-	0.96	-	-	-
Ta	-	-	-	-	-	-
Be	-	1.9	1.3	1.3	2.05	1.7
Sc	-	23.4	13.2	13.2	12.2	12.9
Cs	-	-	-	-	-	-

	K58	K59	K61	K62	K63	K64
SiO_2	53.55	50.06	49.73	54.47	53.66	53.45
TiO_2	2.03	2.30	2.24	1.66	1.66	1.67
Al_2O_3	16.23	16.00	15.46	15.62	15.62	15.64
Fe_2O_3T	10.83	10.10	10.36	10.75	10.67	10.75
MnO	0.14	0.14	0.14	0.11	0.12	0.13
MgO	4.99	6.52	7.74	5.61	5.39	5.62
CaO	6.94	7.52	8.11	7.36	7.34	7.32
Na_2O	4.58	3.67	3.76	4.28	4.33	3.93
K_2O	1.47	2.91	2.46	0.96	0.98	1.01
P_2O_5	0.40	0.64	0.57	0.21	0.22	0.25
LoI	-0.29	0.74	-0.19	0.15	0.10	0.04
Total	100.87	100.60	100.38	101.18	100.09	99.81
V	158	183	171	179	165	152
Cr	81	114	160	163	151	148
Ni	57	92	111	92	91	84
Cu	35	33	36	37	36	31
Zn	112	114	104	124	120	108
Rb	31	62	54	27	28	22
Sr	690	935	848	454	449	479
Y	18	20	24	16	17	23
Zr	169	281	252	126	129	143
Nb	33[1]	68[1]	62[1]	16[1]	14[1]	18[1]
Ba	567[1]	1153[1]	990[1]	311[1]	312[1]	341[1]
Th	2.18	6.02	-	2.46	-	2.48
Hf	3.05	6.12	-	3.28	-	3.55
U	0.42	1.70	-	0.51	-	0.69
Ta	1.34	3.31	-	0.94	-	1.07
Be	1.0	1.8	1.8	0.5	0.8	0.9[2]
Sc	13.0	15.5	-	13.6	13.2	14.7[2]
Cs	0.26	0.43	-	0.64	-	0.67

	K65	K66	K68	K69	K71	K72
SiO_2	49.02	51.46	52.84	50.21	50.91	51.27
TiO_2	2.82	2.66	2.39	2.81	2.77	2.37
Al_2O_3	18.90	17.50	16.39	17.39	16.91	15.90
Fe_2O_3T	10.89	10.26	9.87	10.63	10.46	9.36
MnO	0.12	0.14	0.10	0.12	0.14	0.13
MgO	3.73	3.95	4.42	4.48	4.96	5.97
CaO	6.89	6.41	6.34	6.35	6.55	6.56
Na_2O	4.19	4.40	4.32	4.10	3.94	3.60
K_2O	1.73	2.47	2.66	2.39	2.50	3.87
P_2O_5	0.68	0.64	0.61	0.63	0.63	0.72
LoI	1.54	0.67	0.59	1.40	0.75	0.76
Total	100.51	100.56	100.53	100.49	100.52	100.51
V	130	177	154	214	181	180
Cr	29	29	61	70	55	211
Ni	33	33	58	61	58	129
Cu	24	-	27	29	22	31
Zn	124	120	126	117	120	94
Rb	-	43	55	28	37	69
Sr	1319	1260	1094	1279	1294	1081
Y	31	22	22	23	22	21
Zr	284	251	314	267	280	322
Nb	60	51	55	60	69	65
Ba	1249	1120[1]	1142[1]	1418[1]	1436	1548[1]
Th	-	-	5.38	-	-	8.95
Hf	-	-	5.97	-	-	7.38
U	-	-	1.14	-	-	-
Ta	-	-	3.01	-	-	-
Be	-	1.4	1.8	1.5	-	2.2
Sc	-	11.8	11.6[2]	13.1	-	15.3
Cs	-	-	0.91	-	-	0.65

	K73	K75	K76	K77	K78	K80
SiO_2	50.95	50.43	51.14	50.40	49.22	52.45
TiO_2	2.54	2.37	2.33	2.49	2.55	1.73
Al_2O_3	16.57	15.50	15.73	16.72	16.63	16.06
Fe_2O_3T	10.41	9.36	9.26	9.83	10.09	10.25
MnO	0.16	0.13	0.18	0.12	0.13	0.14
MgO	3.53	7.18	7.46	5.07	6.60	6.04
CaO	5.85	7.13	7.00	5.48	6.35	7.50
Na_2O	3.90	2.94	3.59	3.29	2.75	3.98
K_2O	3.46	3.59	3.05	4.03	3.35	1.46
P_2O_5	0.74	0.75	0.79	0.77	0.76	0.34
LoI	1.56	1.18	0.43	1.85	1.89	0.38
Total	99.67	100.56	100.96	100.05	100.32	100.33
V	207	177	158	162	202	170
Cr	107	250	196	193	245	234
Ni	91	152	137	151	143	147
Cu	32	36	34	37	36	45
Zn	116	101	86	105	100	104
Rb	59	68	45	76	41	20
Sr	952	1051	1072	954	1044	664
Y	23	24	22	34	20	17
Zr	299	304	299	321	320	153
Nb	62	59	67	71	73	29
Ba	1437[1]	1679	1661	1643	1983	544[1]
Th	-	-	-	-	-	-
Hf	-	-	-	-	-	-
U	-	-	-	-	-	-
Ta	-	-	-	-	-	-
Be	1.6	-	-	-	1.9	1.2
Sc	12.7	-	-	-	16.8	14.7
Cs	-	-	-	-	-	-

	K81	K82	K83	K84	K85	K88
SiO_2	54.36	54.64	54.76	54.61	54.83	46.67
TiO_2	1.67	1.57	1.51	1.66	1.55	2.32
Al_2O_3	15.65	15.69	15.78	15.76	15.27	14.10
Fe_2O_3T	9.78	9.68	9.47	9.51	9.70	10.68
MnO	0.10	0.16	0.13	0.10	0.15	0.15
MgO	6.52	6.07	6.11	6.19	6.76	9.59
CaO	7.39	7.44	7.26	6.65	7.44	9.60
Na_2O	3.60	3.40	3.98	4.19	3.90	3.74
K_2O	1.56	0.50	1.19	1.80	1.26	0.87
P_2O_5	0.33	0.19	0.28	0.38	0.26	0.79
LoI	0.00	0.62	0.35	0.03	0.04	1.58
Total	100.96	99.96	100.82	100.88	101.16	100.09
V	156	145	160	161	157	219
Cr	201	175	181	197	214	277
Ni	123	129	70	76	22	189
Cu	44	39	29	30	43	59
Zn	94	100	96	95	91	78
Rb	31	6	25	36	26	66
Sr	641	505	544	654	561	883
Y	18	19	20	20	18	21
Zr	161	113	133	172	133	256
Nb	26	14	25	36	17	64
Ba	499[1]	422[1]	410[1]	618[1]	365[1]	1049[1]
Th	-	-	2.40	-	2.44	-
Hf	-	-	3.21	-	3.42	-
U	-	-	0.51	-	0.67	-
Ta	-	-	1.12	-	0.89	-
Be	1.4	0.8	0.9	1.4	1.1	1.9
Sc	15.6	-	14.9	14.4	14.3	22.3
Cs	-	-	0.40	-	-	-

	K89	K90	K92	K93	K94	K100
SiO_2	63.43	64.05	51.02	51.03	50.99	68.77
TiO_2	0.43	0.50	0.98	0.95	0.98	0.54
Al_2O_3	15.63	17.31	18.81	18.85	18.87	16.08
Fe_2O_3T	4.06	4.66	10.91	10.36	10.47	3.43
MnO	0.17	0.09	0.23	0.27	0.26	0.03
MgO	0.88	1.14	3.67	3.99	4.03	0.36
CaO	6.62	4.79	9.56	9.53	9.54	3.49
Na_2O	3.55	3.65	3.00	2.75	2.90	3.36
K_2O	2.76	2.87	1.27	1.25	1.28	4.00
P_2O_5	0.22	0.25	0.28	0.29	0.28	0.14
LoI	2.94	0.87	0.70	1.41	1.16	0.70
Total	100.69	100.18	100.61	100.68	100.76	100.89
V	61	72	203	188	197	49
Cr	11	14	17	11	9	19
Ni	5	3	7	13	7	9
Cu	32	22	112	118	139	21
Zn	55	72	79	78	78	51
Rb	43	68	20	19	23	147
Sr	849	887	725	733	727	243
Y	24	25	26	25	23	34
Zr	161	165	102	103	81	229
Nb	10	12	5	4	5	12
Ba	391[1]	429[1]	169	162	188[1]	670[1]
Th	12.87	11.94	-	3.08	2.77	15.04
Hf	4.11	4.03	-	2.02	2.62	5.93
U	0.96	4.91	-	-	0.50	-
Ta	0.65	0.54	-	-	-	-
Be	1.9	2.15	-	-	1.6	2.0
Sc	6.4	6.3	-	-	26.7	-
Cs	2.30[3]	1.58	-	-	0.96	3.98

	K101	K102	K104	K105	K106	K107
SiO_2	51.21	57.00	52.90	52.13	51.22	52.22
TiO_2	0.86	0.72	2.29	2.32	2.18	2.51
Al_2O_3	20.15	17.34	16.70	16.47	15.73	17.88
Fe_2O_3T	10.71	8.07	9.95	9.92	10.29	10.61
MnO	0.21	0.22	0.11	0.12	0.15	0.12
MgO	3.12	3.46	3.79	3.71	6.25	1.81
CaO	10.22	7.81	5.86	6.45	7.80	4.86
Na_2O	2.39	2.78	4.69	4.65	3.72	4.10
K_2O	1.07	1.67	3.14	3.02	2.68	3.31
P_2O_5	0.14	0.14	0.66	0.64	0.55	0.65
LoI	0.64	1.41	0.50	0.91	0.68	1.68
Total	100.72	100.62	100.59	100.34	101.25	99.75
V	223	157	136	155	162	155
Cr	18	13	108	114	165	120
Ni	7	4	56	75	124	75
Cu	65	38	28	24	45	23
Zn	77	59	84	117	80	122
Rb	29	59	68	62	62	61
Sr	354	325	999	1009	832	1001
Y	20	18	23	26	22	25
Zr	69	96	269	264	226	302
Nb	3[1]	5[1]	52[1]	59[1]	47[1]	64[1]
Ba	211[1]	241[1]	1101[1]	1078[1]	891[1]	1220[1]
Th	-	3.75	-	-	5.48	5.51
Hf	-	2.46	-	-	5.98	6.30
U	-	1.10	-	-	1.28	1.52
Ta	-	0.35	-	-	2.80	3.08
Be	0.8	1.02	1.9	-	1.8	1.9
Sc	-	24.6	13.8	-	15.8	14.4
Cs	-	2.80	-	-	0.65	< 0.2

	K108	K109	K110	K111	K112	K114
SiO_2	53.03	53.04	54.76	54.77	54.19	51.18
TiO_2	2.19	2.29	1.60	1.63	1.68	2.59
Al_2O_3	16.39	16.09	15.61	15.63	16.18	16.41
Fe_2O_3T	9.70	9.45	9.62	10.03	10.26	9.88
MnO	0.14	0.13	0.15	0.15	0.11	0.14
MgO	4.25	4.81	5.72	5.76	5.15	4.84
CaO	6.22	6.85	7.01	6.99	7.00	6.82
Na_2O	4.25	4.30	3.46	3.81	3.77	4.13
K_2O	3.10	2.95	1.06	1.20	1.07	2.76
P_2O_5	0.60	0.59	0.30	0.31	0.30	0.63
LoI	0.77	0.44	0.79	0.47	0.87	0.64
Total	100.63	100.94	100.07	100.75	100.58	100.02
V	148	163	146	144	161	189
Cr	130	94	206	204	230	60
Ni	74	62	77	74	80	53
Cu	29	31	29	18	25	26
Zn	105	96	99	101	103	109
Rb	62	61	26	21	13	53
Sr	940	1017	593	592	638	1240
Y	28	18	20	23	21	18
Zr	314	235	153	159	153	246
Nb	62	49	29	18	22	67
Ba	1035	1037[1]	444[1]	456[1]	518[1]	1201[1]
Th	-	-	2.38	2.33	-	-
Hf	-	-	3.83	3.65	-	-
U	-	-	0.46	0.64	-	-
Ta	-	-	1.25	1.24	-	-
Be	-	1.3	1.0	-	0.8	1.95
Sc	-	12.4	15.1	17.0	16.0	11.5
Cs	-	-	0.43	< 0.14	-	-

	K115	K117	K118	K121	K122	K123
SiO_2	50.98	51.66	52.90	51.84	52.39	52.36
TiO_2	2.69	2.63	2.37	2.22	2.22	2.17
Al_2O_3	17.21	16.72	16.48	15.06	15.52	15.52
Fe_2O_3T	10.41	10.09	10.41	9.80	9.90	9.47
MnO	0.13	0.14	0.16	0.16	0.12	0.15
MgO	4.57	5.06	4.53	6.19	5.97	6.41
CaO	6.37	6.85	6.60	6.69	6.16	6.34
Na_2O	3.79	4.09	4.40	4.21	3.76	3.82
K_2O	2.86	2.66	2.03	2.79	2.85	2.72
P_2O_5	0.63	0.59	0.49	0.69	0.71	0.66
LoI	0.62	0.01	0.27	0.54	0.82	0.93
Total	100.25	100.50	100.64	100.19	100.42	100.55
V	167	178	153	181	148	176
Cr	47	47	62	281	209	235
Ni	52	42	58	192	182	159
Cu	27	25	31	31	29	29
Zn	114	96	103	108	116	105
Rb	57	51	27	57	58	58
Sr	1201	1277	1009	1043	1010	995
Y	23	22	19	21	31	19
Zr	274	236	208	261	278	259
Nb	71	65	45	58	59	59
Ba	1272	1088[1]	838	1034[1]	1075	1067[1]
Th	-	6.15	-	-	-	-
Hf	-	5.22	-	-	-	-
U	-	-	-	-	-	-
Ta	-	-	-	-	-	-
Be	-	1.7	1.3	1.8	-	1.7
Sc	-	11.6	11.1	14.4	-	13.7
Cs	-	-	-	-	-	-

	K126	K127	K129	K130	K134	K135
SiO_2	53.07	53.39	53.48	62.34	45.78	53.51
TiO_2	2.43	2.43	2.37	0.50	2.27	2.20
Al_2O_3	16.58	16.55	16.16	17.14	13.85	15.74
Fe_2O_3T	9.73	9.86	9.43	5.14	10.89	9.75
MnO	0.18	0.12	0.14	0.13	0.16	0.15
MgO	3.63	3.65	4.29	1.58	10.06	5.09
CaO	6.61	6.38	6.42	5.37	8.98	6.63
Na_2O	4.27	4.62	3.92	4.04	3.32	4.18
K_2O	2.56	2.57	3.50	2.31	3.87	2.31
P_2O_5	0.59	0.58	0.78	0.24	0.84	0.68
LoI	0.36	0.44	0.12	2.05	1.63	0.20
Total	100.01	100.59	100.63	100.84	100.85	100.44
V	187	185	136	74	173	148
Cr	63	68	86	9	301	97
Ni	47	58	63	5	206	72
Cu	27	25	29	20	47	32
Zn	106	103	90	73	89	116
Rb	49	53	78	71	49	
Sr	1092	1092	1078	882	977	980
Y	21	21	21	20	24	20
Zr	237	247	280	171	292	252
Nb	49	50	59	10	97	51
Ba	1084[1]	1058[1]	1493	405[1]	1308	940
Th	6.26	-	-	-	-	-
Hf	5.52	-	-	-	-	-
U	-	-	-	-	-	-
Ta	-	-	-	-	-	-
Be	1.4	1.3	-	1.9	-	-
Sc	11.7	12.7	-	7.1	-	-
Cs	-	-	-	-	-	-

	K136	K138	K139	K140	K141	K142
SiO_2	52.03	53.51	51.81	51.68	51.39	47.83
TiO_2	2.33	2.13	0.79	0.82	2.10	2.37
Al_2O_3	16.45	17.09	20.59	19.61	16.17	14.71
Fe_2O_3T	10.36	7.51	9.19	10.13	9.45	9.88
MnO	0.17	0.07	0.22	0.17	0.16	0.17
MgO	4.81	4.27	3.39	3.87	5.05	9.38
CaO	6.55	5.30	10.45	9.80	6.32	7.93
Na_2O	4.52	4.19	2.43	3.32	3.69	5.28
K_2O	2.09	4.44	1.02	1.03	3.10	1.58
P_2O_5	0.58	0.88	0.16	0.17	0.83	0.79
LoI	0.93	0.95	0.48	0.72	1.57	0.85
Total	100.82	100.34	100.53	100.32	99.83	100.77
V	159	140	179	169	163	180
Cr	110	76	16	13	71	258
Ni	80	73	6	6	58	203
Cu	23	26	49	47	32	35
Zn	118	79	65	74	97	78
Rb	33	74	31	34	64	49
Sr	1012	1279	392	360	968	1102
Y	25	21	17	17	22	23
Zr	261	280	59	70	250	336
Nb	48	47	4	5	52	81
Ba	1015	1467	166[1]	170[1]	1239[1]	1181[1]
Th	-	-	-	-	6.46	-
Hf	-	-	-	-	7.64	-
U	-	-	-	-	-	-
Ta	-	-	-	-	-	-
Be	-	2.6	0.8	1.05	1.6	1.9
Sc	-	8.3	25.4	-	10.4	-
Cs	-	-	-	-	-	-

	K143	K160	K165	MR1	MR4	MR13
SiO_2	48.59	52.80	47.18	49.84	49.76	51.65
TiO_2	2.80	2.60	2.47	2.08	2.09	2.24
Al_2O_3	14.44	16.44	13.22	15.53	15.51	15.63
Fe_2O_3T	9.45	9.60	10.27	10.56	10.49	8.93
MnO	0.11	0.13	0.18	0.15	0.15	0.13
MgO	9.55	4.72	11.02	7.69	7.19	6.61
CaO	8.07	5.81	9.45	8.17	7.87	6.95
Na_2O	4.49	4.12	2.48	4.09	4.08	4.93
K_2O	1.84	2.82	2.20	2.35	2.48	1.87
P_2O_5	0.68	0.68	0.50	0.55	0.56	0.77
LoI	1.46	1.24	1.48	-0.19	0.00	0.72
Total	101.48	100.96	100.45	100.82	100.18	100.43
V	237	166	195	200	199	188
Cr	254	51	305	153	144	213
Ni	159	47	218	107	100	136
Cu	47	24	58	45	37	43
Zn	72	106	77	103	99	87
Rb	73	59	55	54	62	39
Sr	1006	1109	783	802	809	1059
Y	19	15	23	20	14	18
Zr	241	228	203	213	220	286
Nb	61[1]	59[1]	49	53[1]	54	61
Ba	1708[1]	1116[1]	1179	935[1]	948	1408
Th	-	5.76	5.63	6.43	-	-
Hf	-	5.44	5.71	6.49	-	-
U	-	3.23	-	1.75	-	-
Ta	-	-	-	-	-	-
Be	1.6	2.1	-	1.5	-	-
Sc	19.7	8.5	-	-	-	-
Cs	-	-	-	0.59	-	-

	MR14	MR16	MR17	MR18	MR20	MR21
SiO_2	50.47	52.81	48.18	53.18	44.74	52.27
TiO_2	0.88	2.56	1.02	1.69	1.28	2.17
Al_2O_3	18.19	16.63	18.82	15.57	18.26	15.84
Fe_2O_3T	10.80	9.97	12.04	10.68	13.74	10.77
MnO	0.23	0.12	0.22	0.15	0.22	0.17
MgO	5.67	3.95	5.55	5.29	6.81	5.09
CaO	10.29	6.24	11.13	7.21	12.22	6.96
Na_2O	2.53	5.11	2.53	4.08	2.54	4.35
K_2O	0.96	2.57	0.81	1.26	0.35	1.61
P_2O_5	0.22	0.62	0.21	0.26	0.20	0.46
LoI	0.10	0.00	0.61	0.16	0.52	0.12
Total	100.34	100.58	101.12	99.53	100.88	99.81
V	253	180	217	175	354	181
Cr	61	23	22	148	33	150
Ni	24	34	22	85	31	93
Cu	182	17	65	43	64	33
Zn	78	108	81	117	80	129
Rb	22	50	18	34	4	30
Sr	767	1209	526	495	512	746
Y	19	22	24	17	23	22
Zr	75	231	70	166	67	166
Nb	2	52	6	20	4	41
Ba	149[1]	1074[1]	109[1]	406	90[1]	673
Th	259	-	1.14	-	0.79	5.17
Hf	1.95	5.86	2.05	-	1.40	5.83
U	0.77	-	-	-	<0.2	0.97
Ta	0.18	-	-	-	0.16	-
Be	0.9	1.3	1.7	-	0.7	-
Sc	29.7	-	31.9	-	53.7	-
Cs	0.67	-	-	-	< 0.22	-

	MR22	MR23	MR24	MR25	MR26	MR27
SiO_2	50.47	44.93	44.08	55.75	50.48	50.17
TiO_2	2.09	2.66	2.94	1.49	2.08	2.06
Al_2O_3	15.95	12.98	13.79	15.18	15.80	15.65
Fe_2O_3T	10.34	10.59	10.83	9.65	10.40	10.42
MnO	0.15	0.31	0.21	0.14	0.16	0.20
MgO	6.85	12.46	9.74	6.11	6.75	7.65
CaO	7.61	8.82	9.41	7.15	7.55	7.94
Na_2O	4.20	4.38	5.48	3.95	4.26	3.91
K_2O	2.58	1.87	0.54	0.84	2.54	2.38
P_2O_5	0.59	0.92	1.01	0.19	0.57	0.54
LoI	0.02	0.74	1.67	0.07	0.02	-0.24
Total	100.85	100.66	99.70	100.52	100.61	100.66
V	192	215	264	190	190	150
Cr	134	375	267	214	129	158
Ni	95	291	171	100	98	123
Cu	39	40	43	39	35	48
Zn	100	72	82	97	110	102
Rb	61	57	92	44	66	53
Sr	831	1065	1121	687	856	745
Y	19	30	24	17	15	19
Zr	227	361	388	71	225	213
Nb	55	94	96	11	58	52
Ba	1013	1361[1]	1227	297[1]	984	879
Th	-	-	11.04	1.81	-	-
Hf	-	-	10.27	2.70	-	-
U	-	-	-	0.51	-	-
Ta	-	-	-	0.68	-	-
Be	-	2.2	-	0.8	-	-
Sc	-	-	-	14.6	-	-
Cs	-	-	-	0.34	-	-

	POZZ3	GR-P	PS1	PS2	PS3	PS4
SiO_2	45.32	42.16	54.78	53.70	49.83	49.98
TiO_2	0.03	0.05	1.48	1.60	1.85	1.91
Al_2O_3	1.69	20.09	15.85	15.33	15.26	14.83
Fe_2O_3T	8.78	10.53	9.93	10.11	10.53	10.40
MnO	0.18	0.14	0.16	0.18	0.16	0.19
MgO	43.43	17.09	5.84	6.26	7.47	9.38
CaO	1.38	11.26	7.68	7.62	8.90	8.09
Na_2O	0.00	0.05	3.71	3.66	3.59	3.35
K_2O	0.00	0.00	0.56	0.92	1.48	2.09
P_2O_5	0.01	0.05	0.20	0.25	0.42	0.46
LoI	-0.14	0.13	0.24	0.25	0.96	0.00
Total	100.68	101.55	100.44	99.89	100.45	100.68
V	-[2]	24	127	145	163	172
Cr	2589[2]	29	197	180	211	281
Ni	2638[2]	115	119	128	158	200
Cu	-	22	31	38	39	38
Zn	882	45	94	101	80	84
Rb	<5[2]	<6	14	17	24	42
Sr	-	377	506	522	669	738
Y	-	1	18	19	22	19
Zr	-	28	100	126	163	192
Nb	-	1	12	38	32	43
Ba	-	11[1]	266[1]	366[1]	559[1]	720
Th	<0.12	-	1.69	2.33	3.97	5.49
Hf	<0.12	-	2.69	3.27	4.24	5.00
U	<0.12	-	-	-	0.89	-
Ta	<0.07	-	-	-	-	-
Be	-	0.2	0.5	0.7	0.9	1.3
Sc	10.8[2]	-	-	-	-	17.9
Cs	< 0.12	-	-	-	-	0.47

	PS5	PS7	U120	ARC-1	C1	C5
SiO_2	49.91	56.65	13.92	51.77	75.29	70.20
TiO_2	1.96	1.46	0.12	0.64	0.14	0.58
Al_2O_3	14.66	15.39	3.47	13.76	14.00	14.66
Fe_2O_3T	10.41	9.46	2.32	9.51	1.63	4.82
MnO	0.13	0.10	0.19	0.15	0.01	0.06
MgO	8.14	5.70	1.06	11.09	0.19	1.74
CaO	8.80	7.23	41.76	9.60	0.25	0.79
Na_2O	3.63	3.65	2.44	1.43	2.97	1.90
K_2O	2.11	0.60	0.29	0.55	5.16	2.97
P_2O_5	0.53	0.18	0.12	0.10	0.07	0.23
LoI	0.24	0.05	-	2.25	1.22	2.90
Total	100.52	100.47	65.69	100.85	100.93	100.85
V	157	125	25	170	21	102
Cr	214	210	11	402	14	81
Ni	156	124	16	222	7	41
Cu	44	44	37	74	9	28
Zn	84	92	18	74	31	82
Rb	41	21	nd*	12	162	121
Sr	757	454	1102	168	115	187
Y	21	25	18	23	45	30
Zr	209	95	49	69	84	177
Nb	60	10[1]	nd*	5[1]	10[1]	21
Ba	962	236[1]	647[1]	186[1]	693[1]	704
Th	-	-	0.28	-	13.48	-
Hf	-	1.95	0.64	-	3.36	-
U	-	-	nd*	-	1.35	-
Ta	-	-	0.01	-	-	-
Be	-	0.6	0.3	0.8	3.4	-
Sc	-	-	-	-	-	-
Cs	-	-	-	-	-	-

*nd = not detectable

	C6	C11	C13	C14	C15	C16
SiO_2	65.23	71.26	52.25	69.10	50.62	69.01
TiO_2	0.44	0.50	2.19	0.47	2.05	0.60
Al_2O_3	16.54	13.77	16.39	14.87	15.17	15.23
Fe_2O_3T	4.00	4.15	10.58	4.39	10.52	4.27
MnO	0.08	0.10	0.18	0.13	0.13	0.06
MgO	1.60	0.10	4.66	0.21	7.65	1.40
CaO	3.84	1.51	7.21	2.06	7.91	1.20
Na_2O	3.37	4.03	4.02	3.89	3.39	3.53
K_2O	2.95	4.13	2.10	4.78	2.37	4.01
P_2O_5	0.19	0.12	0.53	0.13	0.54	0.30
LoI	1.75	1.08	0.79	0.69	0.00	0.96
Total	99.99	100.75	100.88	100.70	100.35	100.57
V	61	72	193	26	183	81
Cr	29	10	140	7	212	57
Ni	10	8	87	4	164	21
Cu	10	14	29	21	56	24
Zn	72	59	114	62	91	78
Rb	101	136	23	143	41	162
Sr	386	136	851	157	761	142
Y	15	42	22	39	23	27
Zr	136	220	209	232	221	185
Nb	23	22	37	15	46	13
Ba	967[1]	559	920[1]	600	885[1]	683
Th	5.97	11.7	-	-	5.2	-
Hf	4.28	6.73	5.14	-	5.14	-
U	1.48	-	-	-	1.28	-
Ta	-	0.73	-	-	-	-
Be	2.2	2.05	1.3	-	1.3	-
Sc	-	-	-	-	-	-
Cs	-	-	-	-	-	-

	C18	C19	C20	C21	C22
SiO_2	75.45	85.18	77.65	68.02	46.53
TiO_2	0.02	0.59	0.05	0.49	2.15
Al_2O_3	13.64	7.79	12.52	16.02	16.35
Fe_2O_3T	0.58	2.36	0.97	4.17	11.51
MnO	0.14	0.03	0.03	0.08	0.20
MgO	0.14	0.42	0.03	1.05	6.44
CaO	0.37	0.61	0.41	3.82	3.32
Na_2O	4.16	1.14	3.12	3.29	2.82
K_2O	4.82	1.47	5.22	3.15	1.97
P_2O_5	0.20	0.09	0.01	0.12	0.40
LoI	0.73	0.90	0.63	0.40	3.85
Total	100.25	100.58	100.64	100.61	100.54
V	5	50	1	54	225
Cr	13	44	14	17	136
Ni	7	15	5	8	60
Cu	18	17	8	13	26
Zn	5	29	32	61	114
Rb	198	71	351	106	115
Sr	39	155	16	206	326
Y	3	16	108	26	43
Zr	28	445	77	185	218
Nb	12	12	24	13	13
Ba	113[1]	330[1]	74[1] 3	757	268[1]
Th	-	12.58	35	-	-
Hf	-	13.49	-	-	-
U	-	3.09	-	-	-
Ta	-	-	-	-	-
Be	8.3	1.2	4.0	-	1.4
Sc	-	-	-	-	-
Cs	-	-	-	-	-

	C23	C26	C31	QF-0
SiO_2	74.43	71.47	72.51	71.96
TiO_2	0.28	0.35	0.24	0.45
Al_2O_3	13.59	15.12	14.69	14.87
Fe_2O_3T	2.29	2.85	2.02	3.71
MnO	0.02	0.12	0.09	0.11
MgO	0.30	0.95	0.56	0.27
CaO	0.32	2.84	2.21	1.21
Na_2O	2.57	3.51	3.57	2.80
K_2O	5.48	3.49	4.27	4.41
P_2O_5	0.12	0.12	0.09	0.12
LoI	1.33	0.25	0.26	0.99
Total	100.73	101.05	100.49	100.89
V	29	32	22	-[2]
Cr	16	15	15	10[2]
Ni	9	3	5	<14[2]
Cu	47	15	10	-[2]
Zn	84	46	35	161[2]
Rb	170	103	147	118[2]
Sr	93	234	164	91[1]
Y	36	18	18	-[1]
Zr	123	111	102	185[1]
Nb	9	10	16	-[1]
Ba	643[3]	726	451[3]	465[1]
Th	21[3]	-	26[3]	8.30
Hf	-	-	-	5.79
U	-	-	-	2.55
Ta	-	-	-	0.88
Be	-	-	1.9	1.8[2]
Sc	-	-	-	7.9[2]
Cs			-	3.52

RARE-EARTH ELEMENT DATA

	K1	K3	K4	K11	K12	K13	K15
La	21	15	49	37	61	33	46
Ce	43	35	88	75	113	70	81
Pr	5.5	4.5	9.9	9.1	12.7	8.0	9.6
Nd	24.7	20.5	42.6	42.1	53.1	36.4	48.0
Sm	5.0	4.5	7.3	8.2	8.8	7.9	8.6
Eu	1.45	1.21	2.25	2.55	2.46	2.29	2.69
Gd	4.40	4.03	5.90	6.55	5.90	6.43	7.20
Tb	-	-	-	-	-	-	-
Dy	3.96	3.63	3.92	4.41	3.77	4.41	4.47
Ho	0.81	0.88	0.69	0.78	0.72	0.92	0.86
Er	2.20	2.30	1.62	1.80	1.55	2.21	1.98
Tm	-	-	-	-	-	-	-
Yb	2.26	2.07	1.13	1.34	0.87	1.50	1.37
Lu	0.35	0.28	0.15	0.18	0.12	0.21	0.18

	K19	K20	K21	K22	K28	K30	K31
La	41	31	30	36	43	21	50
Ce	80	54	57	69	74	44	97
Pr	9.4	6.9	7.3	8.0	8.4	5.4	11.1
Nd	43.6	36.0	33.9	36.1	39.0	26.4	49.1
Sm	8.9	6.8	7.0	6.9	7.0	5.9	8.7
Eu	2.57	2.20	2.26	2.17	2.22	2.05	2.68
Gd	7.49	5.70	5.80	5.70	5.90	5.78	6.60
Tb	-	-	-	-	-	-	-
Dy	4.85	4.04	4.20	3.98	3.91	4.02	4.52
Ho	1.03	0.74	0.76	0.71	0.73	0.76	0.80
Er	2.31	1.71	1.72	1.64	1.68	1.88	1.90
Tm	-	-	-	-	-	-	-
Yb	1.59	1.30	1.34	1.25	1.14	1.33	1.36
Lu	0.21	0.19	0.18	0.17	0.15	0.17	0.18

	K32	K33	K34	K35	K36	K40	K43
La	59	37	41	47	50	27	12
Ce	105	77	87	86	92	59	24
Pr	11.7	8.4	8.2	9.6	10.2	6.9	3.3
Nd	-	36.7	37.3	41.4	44.0	29.5	17.5
Sm	9.0	7.2	6.8	7.1	7.6	6.3	4.2
Eu	2.76	2.11	2.19	2.19	2.28	1.37	1.53
Gd	7.10	5.78	5.70	5.60	5.81	5.73	4.00
Tb	-	0.86	-	-	-	-	-
Dy	4.47	3.94	3.90	3.16	3.98	4.91	2.98
Ho	0.80	0.79	0.72	0.67	0.71	1.17	0.55
Er	1.87	1.84	1.66	1.55	1.65	2.06	1.25
Tm	-	0.34	-	-	-	-	-
Yb	1.25	1.20	1.22	1.07	1.19	2.01	1.03
Lu	0.16	0.17	0.16	0.14	0.15	0.43	0.14

	K44	K47	K52	K53	K55	K56	K57
La	53	59	70	25	28	57	57
Ce	118	99	133	53	58	105	106
Pr	6.8	10.8	14.4	6.5	6.9	11.8	12.0
Nd	24.5	48.2	60.3	31.6	32.6	52.1	53.0
Sm	6.8	7.7	9.3	6.7	7.3	8.7	9.0
Eu	1.98	2.37	2.68	2.23	2.22	2.64	2.71
Gd	6.19	6.80	7.22	5.70	6.07	6.55	6.90
Tb	-	-	-	0.96	-	-	-
Dy	2.67	4.72	5.15	4.04	4.27	4.28	4.44
Ho	0.62	0.95	0.98	0.72	0.88	0.75	0.79
Er	1.31	2.38	2.42	1.68	2.04	1.70	1.85
Tm	-	-	-	-	-	-	-
Yb	1.11	1.76	1.86	1.25	1.40	1.15	1.17
Lu	0.26	0.25	0.26	0.17	0.19	0.15	0.15

	K58	K59	K62	K64	K66	K68	K69
La	21	50	13	15	39	38	45
Ce	44	94	26	31	75	79	81
Pr	5.7	10.6	3.4	3.9	9.3	9.3	10.0
Nd	27.5	46.2	17.4	19.2	43.1	43.1	45.9
Sm	6.1	8.3	4.5	4.64	8.6	8.7	8.6
Eu	2.09	2.59	1.61	1.67	2.77	2.55	2.76
Gd	5.31	6.61	4.30	4.71	6.80	6.59	6.80
Tb	0.68	0.98	0.65	0.70	-	0.95	-
Dy	3.91	4.47	3.28	3.44	4.71	4.27	4.61
Ho	0.71	0.77	0.61	0.66	0.82	0.84	0.79
Er	1.56	1.79	1.40	1.77	1.90	1.85	1.83
Tm	0.24	0.21	0.24	-	-	0.32	-
Yb	1.20	1.25	1.14	1.25	1.41	1.18	1.26
Lu	0.15	0.16	0.15	0.18	0.19	0.14	0.16

	K72	K73	K75	K78	K79	K81	K82
La	60	61	63	66	37	25	12
Ce	111	107	126	114	69	42	25
Pr	12.2	12.6	12.3	12.5	8.5	5.2	3.5
Nd	51.6	56.0	50.7	51.7	40.4	24.1	18.3
Sm	8.5	9.7	8.8	8.5	7.8	4.9	4.5
Eu	2.55	2.92	2.30	2.56	2.43	1.66	1.60
Gd	6.70	7.60	6.74	6.50	6.30	4.41	4.55
Tb	-	-	-	-	-	-	-
Dy	4.49	5.10	4.40	4.41	4.24	3.18	3.21
Ho	0.81	0.92	0.90	0.81	0.77	0.60	0.63
Er	1.94	2.17	2.03	1.88	1.78	1.38	1.62
Tm	-	-	-	-	-	-	-
Yb	1.39	1.47	1.42	1.35	1.28	1.11	1.14
Lu	0.19	0.20	0.21	0.18	0.17	0.15	0.15

	K83	K84	K85	K88	K89	K90	K92
La	22	22	18	54	34	41	15
Ce	36	41	33	98	61	73	37
Pr	4.8	5.2	4.1	9.7	6.8	8.4	4.7
Nd	22.5	26.2	20.1	42.7	28.3	33.8	21.4
Sm	5.1	5.9	4.5	7.8	4.7	5.7	4.5
Eu	1.70	2.05	1.59	2.31	1.27	1.48	1.27
Gd	4.71	5.41	4.11	6.31	3.65	4.97	4.09
Tb	0.70	-	0.60	-	0.49	0.76	-
Dy	3.83	3.87	3.09	4.60	3.15	3.89	3.65
Ho	0.72	0.71	0.56	0.85	0.67	0.85	0.87
Er	1.70	1.64	1.29	2.10	1.88	2.54	2.34
Tm	0.31	-	-	-	-	0.30	-
Yb	1.44	1.26	1.08	1.61	1.99	2.39	2.07
Lu	0.20	0.17	0.14	0.22	0.32	0.36	0.28

	K94	K100	K101	K102	K104	K106	K107
La	18	32	9	14	50	40	45
Ce	36	69	20	26	90	78	101
Pr	4.8	7.9	2.6	3.1	10.9	9.0	10.8
Nd	21.1	30.3	11.9	13.7	47.2	38.3	47.6
Sm	4.8	6.1	3.2	3.0	8.8	7.2	8.8
Eu	1.42	1.17	0.90	0.91	2.65	2.19	2.48
Gd	3.90	4.91	3.41	3.01	6.82	5.70	6.43
Tb	-	-	-	0.54	-	0.81	1.00
Dy	3.83	4.61	3.28	3.01	4.82	4.25	4.75
Ho	0.78	1.18	0.78	0.65	0.85	0.75	0.96
Er	2.73	3.19	2.20	1.80	2.00	1.82	2.15
Tm	-	-	-	0.20	-	-	0.24
Yb	2.03	2.95	1.96	1.94	1.49	1.39	1.43
Lu	0.33	0.41	0.29	0.30	0.20	0.18	0.18

	K109	K110	K111	K112	K114	K118	K121
La	45	22	22	22	42	31	41
Ce	83	44	41	43	78	59	81
Pr	9.4	5.8	5.3	5.7	9.2	7.2	96
Nd	42.2	26.8	25.5	25.8	42.6	34.2	44.4
Sm	7.7	5.9	5.4	5.8	8.0	6.9	8.1
Eu	2.41	1.94	1.80	1.88	2.60	2.30	2.51
Gd	6.20	5.10	4.90	4.80	6.40	5.71	6.45
Tb	-	0.54	0.80	-	-	-	-
Dy	4.27	4.18	3.77	4.02	4.31	3.95	4.31
Ho	0.77	0.76	0.73	0.74	0.80	0.73	0.81
Er	1.87	1.84	1.74	1.75	1.83	1.59	1.91
Tm	-	0.32	-	-	-	-	-
Yb	1.38	1.57	1.48	1.50	1.29	1.14	1.38
Lu	0.19	0.22	0.22	0.21	0.18	0.15	0.19

	K123	K126	K129	K138	K139	K140	K141
La	44	40	52	66	9	10	47
Ce	83	76	103	112	18	22	89
Pr	10.0	9.5	11.4	11.9	2.6	2.7	10.3
Nd	46.9	4.30	49.4	52.2	11.8	12.5	46.4
Sm	8.6	8.5	8.1	8.4	2.9	3.23	8.1
Eu	2.60	2.70	2.56	2.53	0.91	0.96	2.54
Gd	6.52	6.82	6.84	6.50	2.70	3.31	6.51
Tb	-	-	-	-	-	-	-
Dy	4.55	4.64	4.08	3.94	3.00	3.30	4.38
Ho	0.81	0.80	0.74	0.71	0.65	0.81	0.79
Er	1.90	1.78	1.85	1.64	1.78	2.21	1.83
Tm	-	-	-	-	-	-	-
Yb	1.43	1.31	1.18	1.06	1.81	2.01	1.34
Lu	0.20	0.16	0.15	0.13	0.29	0.30	0.17

	K142	K143	K160	MR1	MR4	MR13	MR14
La	60	52	39	39	39	59	15
Ce	117	88	82	69	71	104	31
Pr	12.4	9.8	9.3	8.0	8.1	11.2	4.0
Nd	50.4	42.9	42.6	35.8	36.8	47.7	19.2
Sm	7.3	6.9	8.2	6.7	6.7	7.9	3.9
Eu	2.28	2.09	2.28	2.17	2.14	2.41	1.20
Gd	6.06	5.60	6.25	5.82	5.80	6.60	3.71
Tb	-	-	-	-	-	-	0.96
Dy	4.25	3.69	3.94	3.98	3.94	4.29	3.28
Ho	0.86	0.69	0.76	0.73	0.74	0.80	0.72
Er	2.05	1.64	1.65	1.61	1.59	1.77	1.75
Tm	-	-	-	-	-	-	0.16
Yb	1.40	1.15	0.93	1.21	1.21	1.39	1.87
Lu	0.20	0.16	0.12	0.16	0.17	0.19	0.29

	MR16	MR17	MR18	MR20	MR21	MR22	MR23
La	40	10	19	7	34	43	81
Ce	67	21	34	18	52	70	150
Pr	8.8	3.0	4.3	2.6	6.6	8.8	15.1
Nd	41.9	14.6	20.9	12.6	31.9	40.0	64.8
Sm	8.1	3.5	4.8	3.51	6.7	7.3	10.0
Eu	2.67	1.12	1.70	0.99	2.28	2.31	2.73
Gd	6.90	3.90	4.70	3.91	6.20	6.12	8.00
Tb	-	0.63	-	0.55	0.65	-	-
Dy	4.56	3.78	3.47	3.49	4.25	4.10	5.48
Ho	0.86	0.84	0.67	0.89	0.79	-	1.06
Er	1.87	2.07	1.42	2.40	1.73	1.61	2.51
Tm	-	-	-	0.17	-	-	-
Yb	1.48	2.23	1.20	2.00	1.39	1.18	2.03
Lu	0.20	0.36	0.17	0.26	0.20	0.16	0.31

	MR24	MR25	MR26	MR27	POZZ-3	GR-P	PS1
La	87	12	42	40	0.37	0.8	11
Ce	164	25	77	74	0.86	1.1	23
Pr	16.4	3.3	8.7	8.3	0.09	0.09	3.1
Nd	71.4	17.2	39.6	37.5	0.52	0.75	16.2
Sm	10.8	4.1	7.1	7.0	0.14	0.22	3.9
Eu	3.06	1.49	2.24	2.23	0.01	0.11	1.46
Gd	8.60	4.20	6.10	6.00	-	-	4.16
Tb	1.19	0.60	-	-	-	-	0.67
Dy	5.93	3.03	4.03	4.14	0.10	0.17	3.20
Ho	1.19	0.57	0.74	0.77	0.04	0.05	0.63
Er	2.88	1.49	1.60	1.67	-	0.13	1.68
Tm	-	0.22	-	-	-	-	-
Yb	2.22	1.07	1.17	1.28	0.12	0.09	1.21
Lu	0.33	0.15	0.15	0.17	0.02	0.01	0.17

	PS2	PS3	PS4	PS7	U120	ARC-1	C1
La	16	23	33	11	6.3	10	30
Ce	33	48	63	23	6.8	21	64
Pr	4.1	5.6	7.5	3.1	1.5	2.8	7.1
Nd	19.0	25.1	32.1	16.5	7.3	12.0	29.2
Sm	4.3	5.3	5.9	4.3	1.83	2.9	6.5
Eu	1.55	1.61	1.86	1.55	0.46	0.68	0.85
Gd	4.51	4.73	4.95	4.44	2.22	3.13	6.75
Tb	0.64	0.86	-	-	0.33	-	0.95
Dy	3.10	3.62	3.93	3.28	2.28	2.93	6.51
Ho	0.64	0.78	0.74	0.64	0.61	0.72	1.40
Er	1.72	1.94	1.79	1.64	1.69	1.98	4.13
Tm	-	-	-	-	-	-	-
Yb	1.30	1.48	1.45	1.27	1.58	1.78	3.63
Lu	0.18	0.20	0.20	0.17	0.22	0.25	0.52

	C6	C11	C13	C15	C18	C19	C20
La	17	27	33	35	2	19	15
Ce	38	55	70	74	4	43	37
Pr	4.4	6.6	7.6	8.4	0.4	4.8	5.2
Nd	19.7	29.0	35.0	36.6	1.9	19.3	23.9
Sm	4.1	6.2	7.2	7.0	0.7	3.7	9.4
Eu	1.11	1.32	2.10	1.99	0.13	0.65	0.22
Gd	3.42	6.39	5.56	5.42	0.70	2.03	12.00
Tb	0.45	1.02	-	0.66	-	0.36	-
Dy	2.50	6.38	4.02	4.04	0.91	2.66	14.5
Ho	0.57	1.44	0.84	0.84	0.18	0.68	3.23
Er	1.38	4.38	1.95	1.96	0.47	2.03	10.1
Tm	-	-	-	-	-	-	-
Yb	1.12	4.22	1.34	1.40	0.62	2.21	10.2
Lu	0.16	0.63	0.17	0.18	0.09	0.31	1.40

	C22	C31	U64	U66	U69	QF-D
La	19	19	5.9	10.4	10.9	22^2_2
Ce	50	40	8	7	10	51^2
Pr	6.5	4.8	1.7	2.0	2.3	-
Nd	31.3	19.5	9.4	10.7	11.2	24.3^2
Sm	7.7	3.6	2.8	2.36	2.45	5.8^2
Eu	2.03	0.73	0.89	0.64	0.66	1.08^2
Gd	7.42	3.23	3.77	2.93	3.01	5.56^2
Tb	-	-	-	-	-	0.87^2
Dy	6.88	2.93	4.22	3.15	3.14	-
Ho	1.65	0.62	0.99	0.75	0.76	1.07^2
Er	4.43	1.93	3.07	2.38	2.28	-
Tm	-	-	-	-	-	0.40^2
Yb	3.77	1.94	2.91	2.13	2.13	3.80^2
Lu	0.51	0.30	0.44	0.32	0.32	0.50^2

PRESENT DAY 87 Sr/86 Sr[1] RATIOS FOR 43 SAMPLES

Sample	87 Sr/86 Sr (2S error)
K59	0.70449 ± 6
K58	0.70478 ± 6
K100	0.70923 ± 3
K11	0.70540 ± 5
K109	0.70514 ± 5
K118	0.70476 ± 6
K89	0.70530 ± 3
K1	0.70610 ± 3
6R-P	0.70608 ± 4
C19	0.72504 ± 4
MR25	0.70477 ± 4
C11	0.70726 ± 6
K94	0.70487 ± 4
K43	0.70478 ± 5
MR17	0.70472 ± 3
C1	0.72527 ± 5
K72	0.70472 ± 6
C31	0.71789 ± 5
MR16	0.70461 ± 5
K107	0.70500 ± 4
POZZ-8	0.70362 ± 5
C6	0.71040 ± 6
C13	0.70473 ± 3
K111	0.70546 ± 2
K33	0.70442 ± 6
C12	0.70507 ± 3
K160	0.70463 ± 4
MR20	0.70440 ± 3
K142	0.70445 ± 3
C15	0.70460 ± 6
P54	0.70449 ± 3
MR1	0.70437 ± 4
K138	0.70493 ± 5
K102	0.70631 ± 5
K112	0.70552 ± 6
K69	0.70470 ± 5
K62	0.70469 ± 6
P57	0.70465 ± 5
P53	0.70458 ± 5
K64	0.70455 ± 9
K110	0.70558 ± 8
K20	0.70498 ± 6

All values are expressed relative to an Eimer and Amend $SrCO_3$ standard of 0.70800

[1]Strontium isotopic values were determined at the Department of Geology and Mineralogy, University of Oxford

Notes:

Major elements calculated on a dry basis.

All Fe reported as Fe_2O_3.

Most samples crushed in tungsten carbide, except those for which Ta data is quoted which were crushed in agate.

Major elements analysed by X.R.F.; Th, U, Hf, Ta, Cs and Tb by I.N.A.A.; Be and Sc by I.C.P.; REE (except Tb) by I.C.P.; other trace elements by X.R.F.

1. Ba, Be analysed by I.C.P. at Imperial College;
2. Trace elements analysed by I.N.A.A. at the British Museum.
3. Cs determined by emission spectrometry.
4. Sc analysed by I.C.P. at King's College, London.

FeO in some samples was determined by wet chemical methods. The results obtained are given below:-

MR13	4.88
MR16	5.62
MR17	4.72
MR18	3.02
MR21	4.32
MR25	6.88
MR25	6.88

FeO valves given as weight % oxide.
All major elements given as weight % oxide.
All trace elements given in ppm.

NORMATIVE COMPOSITIONS CALCULATED ASSUMING $Fe_2O_3/Feo = 0.15$

	C5	K130	K89	K90	C6	C21	K100	C16	C14
QZ	41.55	14.61	17.78	18.00	22.05	25.14	22.99	27.09	19.67
CO	7.43	0	0	.09	1.28	.54	0	3.62	0
OR	17.55	13.65	16.31	16.96	17.43	18.61	23.81	23.70	28.07
PL	18.49	56.00	48.60	53.02	46.32	46.01	46.12	33.86	43.78
AB	16.08	34.19	30.04	30.89	28.52	27.84	31.05	29.87	36.47
AN	2.42	21.81	18.56	22.13	17.81	18.17	15.06	3.99	7.31
NE	0	0	0	0	0	0	0	0	0
DI	0	2.74	10.93	0	0	0	1.13	0	1.81
WO	0	1.36	5.36	0	0	0	.54	0	.86
EN	0	.53	1.67	0	0	0	.10	0	.08
FS	0	.85	3.90	0	0	0	.49	0	.87
HY	10.03	8.94	1.75	8.50	8.83	7.62	4.10	8.39	4.92
EN	4.33	3.41	.52	2.84	3.98	2.62	.70	3.49	.42
FS	5.70	5.53	1.22	5.66	4.85	5.00	3.41	4.91	4.50
OL	0	0	0	0	0	0	0	0	0
FO	0	0	0	0	0	0	0	0	0
FA	0	0	0	0	0	0	0	0	0
MT	.83	.88	.70	.80	.70	.72	.59	.74	.75
IL	1.10	.95	.82	.95	.84	.93	1.03	1.14	.89
AP	.54	.57	.52	.59	.45	.28	.31	.71	.31

	GR-P	MR24	MR20	MR23	POZZ-3	K52	K134	C22	K51
OR	0	3.19	2.07	11.05	0	3.31	18.14	11.64	7.09
PL	55.02	27.97	51.11	19.52	4.58	31.52	21.18	49.14	36.17
AB	.42	16.53	13.72	9.29	0	18.21	7.36	23.00	21.84
AN	54.59	11.43	37.39	10.23	4.58	13.32	13.82	26.14	14.33
NE	0	16.16	4.21	15.05	0	14.11	11.23	.47	9.35
KP	0	0	0	0	0	0	0	0	0
AC	0	0	0	0	0	0	0	0	0
NS	0	0	0	0	0	0	0	0	0
DI	.75	23.09	18.14	22.06	1.73	24.28	20.38	10.28	17.25
WO	.39	11.96	9.16	11.49	.92	12.61	10.54	5.23	8.97
EN	.27	7.82	4.50	7.88	.73	8.42	6.78	2.84	6.10
FS	.09	3.30	4.49	2.69	.08	3.25	3.06	2.21	2.18
HY	6.94	0	0	0	22.62	0	0	0	0
EN	5.18	0	0	0	20.36	0	0	0	0
FS	1.76	0	0	0	2.26	0	0	0	0
OL	35.76	16.88	18.35	22.31	70.13	15.12	19.19	17.16	19.40
FO	26.01	11.52	8.74	16.22	62.50	10.61	12.81	9.25	13.91
FA	9.75	5.36	9.62	6.09	7.63	4.51	6.38	7.92	5.49
CS	0	0	0	0	0	0	0	0	0
MT	1.81	1.87	2.36	1.83	1.52	1.74	1.88	1.99	1.71
IL	.09	5.58	2.43	5.05	.06	5.68	4.31	4.08	5.03
AP	.12	2.39	.47	2.18	.02	2.32	1.99	.95	1.94

	K53	K160	K55	MR16	K68	K57	K104	K118	K56
OR	9.75	16.66	9.81	15.19	15.72	21.16	18.56	12.00	20.92
PL	53.65	54.11	55.95	53.33	54.03	49.85	52.42	56.45	46.94
AB	33.00	37.15	36.05	38.48	36.55	34.61	37.17	37.23	33.32
AN	20.65	16.96	19.91	14.85	17.47	15.24	15.24	19.22	13.62
NE	0	0	0	2.58	0	0	1.36	0	1.62
DI	9.26	6.19	9.57	9.97	8.23	8.05	7.89	8.52	12.00
WO	4.70	3.15	4.87	5.03	4.17	4.05	3.97	4.31	6.09
EN	2.47	1.70	2.60	2.51	2.16	1.95	1.91	2.18	3.21
FS	2.09	1.34	2.11	2.42	1.89	2.04	2.01	2.03	2.70
HY	16.04	4.10	9.28	0	4.74	3.32	0	8.02	0
EN	8.68	2.29	5.13	0	2.53	1.62	0	4.15	0
FS	7.36	1.81	4.15	0	2.21	1.70	0	3.87	0
OL	3.46	9.62	8.31	10.62	8.69	7.97	11.40	7.03	10.07
FO	1.79	5.14	4.39	5.14	4.43	3.70	5.28	3.47	5.23
FA	1.67	4.47	3.91	5.48	4.27	4.27	6.12	3.56	4.84
MT	1.88	1.67	1.87	1.73	1.70	1.64	1.71	1.80	1.59
IL	4.06	5.01	4.24	4.86	4.54	4.50	4.35	4.50	4.37
AP	1.11	1.59	1.11	1.47	1.44	1.94	1.56	1.16	1.89

	K7	K143	K65	K78	K4	MR4	K36	P53	MR1	K61
CO	0	0	0	0	0	0	0	0	0	0
OR	9.51	10.87	10.22	19.80	19.50	14.65	8.10	8.75	13.89	14.48
PL	47.16	37.35	63.11	46.41	38.09	41.15	49.69	50.21	40.71	38.20
AB	27.98	23.54	35.45	23.27	22.20	24.47	33.49	29.06	23.64	22.67
AN	19.18	13.81	27.65	23.14	15.89	16.68	16.20	21.15	17.08	15.53
NE	3.09	7.83	0	0	3.93	5.45	3.45	.72	5.94	7.52
DI	12.55	17.48	1.73	2.76	12.80	15.24	12.94	16.50	16.15	16.92
WO	6.49	9.09	.87	1.42	6.62	7.81	6.69	8.46	8.29	8.70
EN	4.14	6.19	.41	.85	4.26	4.59	4.27	4.97	4.96	5.28
FS	1.92	2.19	.45	.50	1.92	2.84	1.99	3.08	2.90	2.94
HY	0	0	1.05	7.97	0	0	0	0	0	0
EN	0	0	.49	5.01	0	0	0	0	0	0
FS	0	0	.55	2.97	0	0	0	0	0	0
OL	17.67	17.13	13.09	12.25	16.32	15.69	16.04	16.08	16.33	16.01
FO	11.69	12.33	5.88	7.42	10.89	9.33	10.60	9.56	9.94	9.93
FA	5.98	4.80	7.21	4.84	5.43	6.36	5.43	6.52	6.39	6.08
MT	1.73	1.62	1.88	1.74	1.62	1.81	1.59	1.81	1.83	1.80
IL	4.86	5.32	5.36	4.84	4.67	3.97	4.44	3.51	3.95	4.22
AP	1.66	1.61	1.61	1.80	1.66	1.33	1.75	.99	1.30	1.35

	K109	K126	K10	K16	K108	MR18	K11	PS5	PS4
OR	17.43	15.13	14.60	16.19	18.14	7.45	13.65	12.47	12.35
PL	51.32	54.64	55.12	55.49	49.14	54.97	55.68	42.11	45.03
AB	35.43	36.13	35.71	39.77	35.37	34.52	32.58	24.63	25.77
AN	15.89	18.51	19.41	15.72	13.78	20.45	23.10	17.48	19.26
NE	.52	0	0	0	3.21	0	0	3.30	1.40
DI	11.68	8.64	6.95	8.33	10.76	11.23	.30	18.44	14.46
WO	5.95	4.35	3.49	4.19	5.45	5.69	.15	9.49	7.46
EN	3.23	2.09	1.61	1.97	2.78	2.90	.07	5.78	4.71
FS	2.51	2.20	1.85	2.17	2.53	2.64	.07	3.17	2.28
HY	0	8.34	11.02	1.06	0	17.75	13.58	0	0
EN	0	4.06	5.14	.51	0	9.29	6.85	0	0
FS	0	4.28	5.89	.56	0	8.46	6.72	0	0
OL	11.37	4.38	3.79	10.20	11.55	1.37	5.08	16.30	20.05
FO	6.13	2.03	1.67	4.60	5.76	.68	2.44	10.15	13.07
FA	5.24	2.35	2.11	5.59	5.78	.69	2.64	6.14	6.98
MT	1.62	1.68	1.77	1.71	1.70	1.84	1.78	1.80	1.80
IL	4.35	4.62	4.48	4.33	4.14	3.21	4.71	3.72	3.63
AP	1.40	1.40	1.28	1.71	1.44	.62	2.77	1.26	1.09

	C11	C26	C31	C23	C1	K66	K18	K37	MR13	K117
QZ	26.69	25.63	27.70	36.49	36.74	0	0	0	0	0
CO	.21	0	0	3.14	3.24	0	0	0	0	0
OR	24.41	20.51	25.41	32.38	30.49	14.60	12.70	12.88	11.05	15.72
PL	40.81	47.11	42.54	22.55	25.91	57.94	54.86	47.43	51.82	53.74
AB	34.10	35.62	32.58	21.75	25.13	37.23	35.88	32.47	36.83	34.33
AN	6.71	11.48	9.97	.80	.78	20.71	18.98	14.96	15.00	19.41
NE	0	0	0	0	0	0	0	2.21	2.65	.15
DI	0	1.46	.40	0	0	5.72	8.51	15.10	11.72	8.79
WO	0	.73	.20	0	0	2.89	4.32	7.77	6.03	4.48
EN	0	.28	.07	0	0	1.42	2.26	4.75	3.72	2.45
FS	0	.46	.14	0	0	1.41	1.94	2.58	1.96	1.87
HY	5.25	4.77	3.62	3.44	2.47	.22	3.91	0	0	0
EN	.25	1.81	1.18	.75	.47	.11	2.10	0	0	0
FS	5.00	2.96	2.44	2.69	2.00	.11	1.81	0	0	0
OL	0	0	0	0	0	12.20	11.01	14.67	14.11	13.10
FO	0	0	0	0	0	5.82	5.66	9.18	8.93	7.12
FA	0	0	0	0	0	6.38	5.36	5.49	5.18	5.98
MT	.71	.49	.36	.39	.28	1.77	1.81	1.67	1.54	1.74
IL	.95	.63	.47	.53	.27	5.05	4.46	4.20	4.25	4.99
AP	.28	.26	.19	.28	.17	1.52	1.49	1.59	1.82	1.40

	K21	K19	K58	K9	K112	K80	K14	K32	K12	K122
QZ	0	0	0	0	3.05	0	0	0	2.86	0
CO	0	0	0	0	0	0	0	0	2.33	0
OR	10.75	13.89	8.75	22.75	6.32	8.63	14.54	21.16	26.77	16.84
PL	54.13	55.00	57.82	51.15	55.97	55.32	55.16	48.71	40.77	50.10
AB	35.79	39.52	37.74	36.81	31.90	33.68	37.82	33.68	27.50	33.85
AN	18.34	15.48	20.09	14.34	24.07	21.64	17.34	15.03	13.27	16.25
NE	0	0	0	0	0	0	0	0	0	0
DI	11.18	8.83	10.08	5.65	7.17	10.94	8.46	8.29	0	7.64
WO	5.70	4.46	5.10	2.84	3.63	5.57	4.29	4.23	0	3.91
EN	3.18	2.19	2.58	1.30	1.88	3.06	2.19	2.38	0	2.25
FS	2.30	2.18	2.39	1.51	1.66	2.30	1.98	1.67	0	1.49
HY	12.74	8.55	12.10	4.21	20.64	11.03	2.20	1.06	14.38	5.39
EN	7.38	4.29	6.28	1.95	10.95	6.29	1.16	.62	7.70	3.24
FS	5.36	4.26	5.82	2.27	9.69	4.74	1.05	.44	6.68	2.15
OL	4.02	5.10	5.26	7.39	0	7.30	10.95	11.31	0	11.74
FO	2.24	2.44	2.60	3.24	0	3.99	5.49	6.37	0	6.78
FA	1.79	2.66	2.66	4.15	0	3.31	5.46	4.93	0	4.95
MT	1.67	1.67	1.87	1.62	1.77	1.77	1.71	1.55	1.29	1.71
IL	3.91	3.99	3.87	4.50	3.19	3.29	4.18	4.52	4.12	4.20
AP	1.04	1.33	.90	1.94	.71	.81	1.47	1.78	2.06	1.78

	K81	K62	K20	K84	K82	K83	K111	K85	PS1
QZ	.67	.02	.80	0	5.63	1.05	2.53	.27	2.38
OR	9.22	5.67	10.10	10.64	2.95	7.03	7.09	7.45	3.25
PL	52.40	56.79	53.70	54.33	54.84	55.35	54.24	53.44	57.02
AB	30.46	36.22	35.29	35.45	28.77	33.68	32.24	33.00	34.02
AN	21.94	20.57	18.42	18.88	26.07	21.68	22.00	20.44	23.01
DI	10.26	11.99	10.44	9.50	7.85	10.23	8.74	12.05	11.19
WO	5.25	6.08	5.31	4.86	4.01	5.22	4.45	6.17	5.70
EN	3.02	3.17	2.91	2.78	2.24	2.95	2.41	3.57	3.13
FS	1.99	2.74	2.21	1.87	1.61	2.06	1.88	2.31	2.36
HY	21.93	20.11	17.60	16.48	22.11	20.82	21.25	21.84	21.05
EN	13.22	10.80	9.99	9.85	12.88	12.27	11.93	13.26	12.01
FS	8.71	9.31	7.60	6.62	9.23	8.55	9.32	8.58	9.04
OL	0	0	0	3.40	0	0	0	0	0
FO	0	0	0	1.95	0	0	0	0	0
FA	0	0	0	1.44	0	0	0	0	0
MT	1.68	1.86	1.64	1.64	1.67	1.64	1.73	1.67	1.73
IL	3.17	3.15	3.82	3.15	2.98	2.87	3.10	2.94	2.81
AP	.78	.50	1.07	.90	.45	.66	.73	.62	.52

	K59	K35	K44	MR27	K77	K22	K75	K34	K28	MR22
OR	17.20	21.21	15.42	14.12	23.81	14.24	21.21	15.48	15.25	15.25
PL	44.54	37.52	44.38	39.93	46.79	45.50	43.37	40.89	41.93	43.34
AB	25.95	21.68	26.95	24.09	27.84	27.83	24.88	24.68	26.03	26.30
AN	18.59	15.83	17.43	15.84	18.95	17.67	18.49	16.21	15.89	17.05
NE	2.76	3.61	1.22	6.89	0	2.30	0	6.06	5.24	5.01
DI	11.85	12.81	12.87	16.22	2.63	14.13	9.70	14.68	14.82	13.74
WO	6.07	6.63	6.67	8.34	1.34	7.25	5.00	7.53	7.61	7.04
EN	3.55	4.29	4.38	5.05	.74	4.32	3.12	4.43	4.53	4.10
FS	2.23	1.89	1.82	2.83	.55	2.56	1.58	2.72	2.69	2.61
HY	0	0	0	0	2.56	0	1.14	0	0	0
EN	0	0	0	0	1.46	0	.76	0	0	0
FS	0	0	0	0	1.09	0	.38	0	0	0
OL	15.03	16.21	17.62	16.47	13.34	15.88	15.28	16.10	15.29	15.46
FO	8.89	10.92	12.08	10.18	7.31	9.61	9.81	9.60	9.24	9.09
FA	6.14	5.29	5.54	6.29	6.03	6.27	5.47	6.50	6.06	6.38
MT	1.74	1.59	1.61	1.78	1.70	1.75	1.61	1.83	1.74	1.78
IL	4.37	4.62	4.48	3.93	4.73	3.89	4.50	3.99	4.03	3.97
AP	1.52	1.63	1.61	1.28	1.82	1.26	1.78	1.35	1.37	1.40

	K76	K114	K106	K92	K101	K72	K1	K141	K5
QZ	0	0	0	0	2.78	0	.83	0	2.36
OR	18.02	16.31	15.90	7.50	6.32	22.87	6.56	18.32	5.20
PL	47.01	51.44	45.97	59.49	61.32	42.52	58.47	49.63	58.31
AB	29.21	33.35	28.75	25.39	20.22	26.73	22.85	31.22	20.82
AN	17.80	18.09	17.22	34.11	41.09	15.80	35.63	18.40	37.49
NE	.63	.87	2.17	0	0	2.02	0	0	0
DI	9.52	9.55	14.64	9.64	7.33	9.81	8.71	6.17	8.07
WO	4.91	4.86	7.47	4.80	3.63	5.03	4.38	3.14	4.07
EN	3.10	2.63	4.19	1.94	1.35	2.97	2.08	1.71	1.99
FS	1.51	2.05	2.98	2.90	2.35	1.81	2.25	1.32	2.01
HY	0	0	0	17.92	17.58	0	20.25	6.39	20.86
EN	0	0	0	7.20	6.42	0	9.73	3.61	10.39
FS	0	0	0	10.72	11.16	0	10.52	2.77	10.47
OL	16.68	12.27	13.71	0	0	13.92	0	9.38	0
FO	10.85	6.60	7.69	0	0	8.34	0	5.08	0
FA	5.83	5.67	6.02	0	0	5.58	0	4.30	0
MT	1.59	1.70	1.78	1.88	1.84	1.61	1.77	1.62	1.73
IL	4.43	4.92	4.14	1.86	1.63	4.50	1.69	3.99	1.69
AP	1.87	1.49	1.28	.66	.33	1.71	.69	1.97	.73

	K88	K47	K165	K142	MR17
OR	5.14	8.27	13.00	9.34	4.79
PL	42.31	43.34	34.37	33.54	59.01
AB	23.19	19.12	15.92	21.77	21.41
AN	19.12	24.22	18.44	11.77	37.60
NE	4.58	0	2.74	12.41	0
KP	0	0	0	0	0
AC	0	0	0	0	0
NS	0	0	0	0	0
PI	18.86	13.92	20.22	18.06	13.48
WO	9.75	7.23	10.51	9.36	6.78
EN	6.25	4.85	7.08	6.13	3.20
FS	2.86	1.84	2.63	2.57	3.49
HY	0	6.09	0	0	4.93
EN	0	4.41	0	0	2.36
FS	0	1.67	0	0	2.57
OL	18.61	18.09	20.11	17.67	12.75
FO	12.36	12.76	14.27	12.08	5.79
FA	6.25	5.33	5.84	5.59	6.96
CS	0	0	0	0	0
MT	1.84	1.77	1.77	1.70	2.07
IL	4.41	4.33	4.69	4.50	1.94
AP	1.87	1.99	1.18	1.87	.50

	K15	K30	K129	K127	K64	K138	K135	P52	K63
QZ	0	0	0	0	.60	0	0	1.65	0
CO	0	0	0	0	0	0	0	0	0
OR	15.84	7.21	20.80	15.19	5.97	26.24	13.65	5.44	5.79
PL	51.79	58.33	42.29	55.92	55.31	48.36	52.73	53.65	56.93
AB	38.53	37.99	32.22	39.09	33.25	33.65	35.37	30.97	36.64
AN	13.26	20.34	10.07	16.83	22.05	14.71	17.36	22.68	20.29
NE	2.14	0	6.06	0	0	.98	0	0	0
DI	11.73	10.20	13.91	9.14	10.40	4.76	9.10	11.05	12.10
WO	5.94	5.14	7.06	4.61	5.27	2.44	4.63	5.63	6.13
EN	3.04	2.51	3.70	2.21	2.75	1.42	2.51	3.12	3.16
FS	2.76	2.55	3.15	2.33	2.37	.91	1.96	2.29	2.82
HY	0	13.52	0	3.55	20.94	0	12.03	21.61	16.80
EN	0	6.71	0	1.73	11.25	0	6.76	12.47	8.88
FS	0	6.81	0	1.82	9.70	0	5.27	9.14	7.92
OL	10.19	3.70	9.67	7.82	0	11.02	4.44	0	1.93
FO	5.10	1.75	4.98	3.61	0	6.46	2.39	0	.97
FA	5.10	1.96	4.69	4.21	0	4.55	2.05	0	.95
MT	1.62	1.90	1.64	1.70	1.86	1.29	1.68	1.74	1.84
IL	4.27	3.86	4.50	4.62	3.17	4.05	4.18	3.04	3.15
AP	1.63	.88	1.82	1.37	.59	2.08	1.61	.59	.52

	K110	MR25	K43	PS7	K102	K40
QZ	3.13	3.52	7.30	7.15	10.02	11.78
OR	6.44	4.96	4.85	3.55	9.87	15.01
PL	55.04	54.63	54.95	54.72	53.43	50.49
AB	32.15	33.42	32.58	30.89	23.52	22.68
AN	22.89	21.21	22.37	23.84	29.90	27.81
DI	8.42	10.66	12.06	8.90	6.60	2.97
WO	4.29	5.44	6.11	4.53	3.31	1.48
EN	2.38	3.04	3.14	2.50	1.51	.63
FS	1.75	2.18	2.81	1.87	1.78	.86
HY	21.31	20.90	14.27	20.45	15.51	16.19
EN	12.27	12.18	7.54	11.70	7.11	6.84
FS	9.04	8.72	6.73	8.75	8.40	9.35
OL	0	0	0	0	0	0
FO	0	0	0	0	0	0
FA	0	0	0	0	0	0
MT	1.68	1.67	1.51	1.62	1.39	1.42
IL	3.10	2.83	2.89	2.77	1.37	1.44
AP	.71	.45	.45	.43	.33	.59

	ARC-1	K139	K121	K136	K105	K13	K107	MR21	C13	K123
QZ	2.78	3.34	0	0	0	0	0	0	0	0
CO	0	0	0	0	0	0	.27	0	0	0
OR	3.25	6.03	16.49	12.35	17.85	10.87	19.56	9.51	12.47	16.07
PL	41.60	62.82	47.40	56.67	49.85	58.06	54.56	55.75	56.20	49.49
AB	12.10	20.56	33.45	38.25	34.70	39.52	34.69	36.81	36.72	32.32
AN	29.50	42.26	13.96	18.42	15.15	18.54	19.86	18.94	19.47	17.17
NE	0	0	1.18	0	2.52	0	0	0	0	0
DI	14.10	7.14	12.01	8.47	10.50	8.50	0	10.37	10.15	8.12
WO	7.29	3.56	6.15	4.29	5.29	4.30	0	5.25	5.13	4.16
EN	4.72	1.51	3.57	2.22	2.52	2.20	0	2.70	2.57	2.47
FS	2.08	2.07	2.30	1.95	2.69	1.99	0	2.42	2.45	1.48
HY	32.95	16.46	0	1.77	0	2.32	13.60	8.17	1.87	7.83
EN	22.90	6.94	0	.94	0	1.22	4.09	4.31	.96	4.90
FS	10.06	9.52	0	.83	0	1.10	9.51	3.86	.91	2.93
OL	0	0	14.20	12.16	10.24	11.94	1.04	7.89	11.80	9.99
FO	0	0	8.30	6.18	4.71	5.98	.29	3.97	5.76	6.02
FA	0	0	5.90	5.98	5.53	5.96	.75	3.92	6.04	3.97
MT	1.64	1.58	1.70	1.78	1.71	1.78	1.83	1.86	1.84	1.64
IL	1.22	1.50	4.22	4.43	4.41	4.03	4.77	4.12	4.14	4.12
AP	.24	.38	1.63	1.37	1.52	1.23	1.54	1.09	1.26	1.56

	C18	C20	C19
QZ	31.91	35.55	70.20
CO	1.39	.22	3.43
OR	28.48	30.85	8.69
PL	35.73	32.18	12.08
AB	35.20	30.21	9.65
AN	.53	1.97	2.44
HY	1.36	1.36	3.33
EN	.35	0	1.05
FS	1.01	1.36	2.28
MT	.10	.17	.41
IL	.04	.08	1.12
AP	.47	.02	.21

	K71	K73	K115	K94	K93	K3	K140	C15
QZ	0	0	0	0	.94	0	3.77	0
OR	14.77	20.45	16.90	7.56	7.39	5.50	6.09	14.00
PL	54.41	50.49	53.57	59.23	58.67	63.08	59.68	47.76
AB	33.34	33.00	32.07	24.54	23.27	30.12	19.63	28.58
AN	21.07	17.49	21.50	34.69	35.40	32.95	40.05	19.18
NE	0	0	0	0	0	0	0	.05
DI	6.00	5.57	4.89	9.02	8.34	13.71	6.23	13.45
WO	3.05	2.80	2.48	4.51	4.17	6.90	3.11	6.90
EN	1.64	1.28	1.29	1.96	1.81	3.29	1.34	4.13
FS	1.31	1.49	1.12	2.55	2.36	3.52	1.77	2.41
HY	3.77	1.30	4.19	18.38	18.76	2.94	19.24	0
EN	2.10	.60	2.24	7.98	8.13	1.42	8.30	0
FS	1.68	.70	1.95	10.40	10.63	1.52	10.94	0
OL	11.37	11.05	10.79	.16	0	11.08	0	17.19
FO	6.04	4.84	5.50	.07	0	5.08	0	10.46
FA	5.33	6.21	5.29	.09	0	6.00	0	6.74
MT	1.80	1.80	1.80	1.81	1.78	1.75	1.74	1.81
IL	5.26	4.82	5.11	1.86	1.80	1.65	1.56	3.89
AP	1.49	1.75	1.49	.66	.69	.57	.40	1.28

	MR14	MR26	K69	K33
QZ	0	0	0	0
OR	5.67	15.01	14.06	14.83
PL	56.85	43.24	55.47	42.89
AB	21.41	26.75	31.99	25.90
AN	35.44	16.49	23.48	17.00
NE	0	5.04	0	4.26
DI	11.71	14.07	3.96	14.98
WO	5.92	7.20	2.01	7.67
EN	2.95	4.16	1.05	4.47
FS	2.85	2.72	.90	2.83
HY	18.37	0	7.20	0
EN	9.34	0	3.87	0
FS	9.02	0	3.33	0
OL	2.65	15.26	9.25	16.14
FO	1.28	8.87	4.74	9.50
FA	1.36	6.39	4.51	6.64
MT	1.86	1.80	1.84	1.86
IL	1.67	3.95	5.36	3.91
AP	.52	1.35	1.40	1.28

SAMPLE LOCALITIES

Sample	Rock Type	Location
K1	Basalt	Mte. Castanza, north of Cossoine (729776)
K3	Basalt	Mte. Castanza, north of Cossoine (742819)
K4	Hawaiite	Lava flow outcropping near cross, just to west of Cossoine
K5	Basalt	Mte. Castanza, north of Cossoine (727776)
K7	Basalt*	Roadside exposure 1 km SW of Cossoine on road to Pozzomaggiore
K9	Trachybasalt	500m further along road from K7, towards Pozzomaggiore
K10	Hawaiite	Roadside outcrop 400m NE of Nuarghe Caspiana (815945)
K11	Hawaiite	1.2 km SE of Case. Paule (819954)
K12	Trachybasalt	Dyke, S of Mte. Ruiu (781952)
K13	Hawaiite	Dyke, 200m E of K12 (783954)
K14	Hawaiite	Agglutinated scoria. Summit of Mte. Ruiu (781958)
K15	Trachybasalt	Scoria. Mte. Sa Pescia (783963)
K16	Trachybasalt	Scoria. Mte. Sa Pescia (783963)
K18	Hawaiite	Scoria. Mte. Sa Pescia (783964)
K19	Trachybasalt	Dyke. Mte. Pubulena (776977)
K20	Basaltic abdesite	Summit of Mte. Pubulena (776978)
K21	Basaltic andesite	Scoria. Mte. Pubulena (776978)
K22	Hawaiite	Scoria. Roadstone quarry, Mte. Lisir, near Ittireddu
K28	Hawaiite	Scoria. Roadstone quarry, Mte. Lisir near Ittireddu
K30	Basaltic andesite	Roadstone outcrop, 1 km N of Staz.di Torralba
K31	Hawaiite	Lava exposed by road, on northern outskirts of Giave
K32	Trachybasalt	Lava flow at Giave, near to S Cosimo
K33	Hawaiite	Scoria. Mte. Lisir, near Ittireddu
K34	Hawaiite	Scoria. Mte. Lisir, near Ittireddu
K35	Hawaiite	Lava flow exposed on Cossoine-Pozzomaggiore road by Nghe. Alvu
K36	Hawaiite	Roadside outcrop, 3 km NE of Pozzomaggiore by road to Cossoine
K37	Hawaiite	Roadside exposure on road from Cossoine to Pozzomaggiore (717727)
K40	Andesite	4 km SW of Pozzomaggiore (694694)
K43	Andesite	1 km S of Padria (713689)
K44	Hawaiite	1 km SE of Pozzomaggiore, by road to Semestene (722718)
K47	Basalt*	Lava flow lying above crystal tuff on Pozzomaggiore-Semestene road
K51	Basalt*	Roadside outcrop, 1 km NE of Semestene, 500m after hairpin bend

K52	Basalt*	Lava flow by railway track at Cantra Cadrèas, 1.5 km SW of Bonorva
K53	Hawaiite	At junction of S.S.131 and Rui Mannu, 2 km N of Giave
K55	Basaltic andesite	Mte. Amaru, 1.5 km N of Giave
K56,K57	Trachybasalt	Lava from plateau, 1 km W of Cheremule
K58	Basaltic andesite	In valley of Rui Mannu, by road heading SW from Staz. di Torralba
K59	Hawaiite	Scoria. Mte. Cujaru, 10 km NW of Foresta Burgos
K61	Hawaiite	Lava flow. 1 km SW of Mte. Cujaru
K62,K63	Basaltic andesite	Scoria. Mte. Austidu. Roadstone quarry
K64	Basaltic andesite	Lava flow, 500 m E of summit of Mte. Austidu
K65,K66	Hawaiite	Scoria. Mte. Austu, 500 m NE of Torralba
K68	Hawaiite	Scoria. Mte. Mannu (778940)
K69	Hawaiite	Scoria. Mte. Meddaris (779998)
K71,K72	Hawaiite	Lava flow 1.5 km S of summit of Mte. Pelao
K73	Trachybasalt	Lava flow. 600 m S of Mte. Pelao summit
K75	Hawaiite	Scoria. Mte. Pelao
K76	Hawaiite	Lava flow, 1 km NE of Mte. Pelao
K77	Mugearite	Lava flow, margin of lava plateau, 1 km NE of Mte. Pelao
K78	Hawaiite	Lava flow. Summitof Mte. Pelao
K79	Hawaiite	Lava flow at junction of flow from Mte. Ruiu and S.S.131 (754950)
K80,K81	Basaltic andesite	Lava flow. Roadside outcrop 2 km S of Bonorva, just to E of S.S.131
K82	Basaltic andesite	1 km W of Padru Mannu, next to S.S.131
K83	Basaltic andesite	Lava flow 2 km E of Padru Mannu
K84	Basaltic andesite	Lava flow 3 km W of Badde Salighes on road to S.S.131
K85	Basaltic andesite	Lava flow in disused roadside quarry, 2 km S of Bonorva next to S.S.131
K88	Basalt*	Lava flow near Pozzomaggiore (708722)
K89	Dacite	Lava flow, Mte. Pizzinnu (694750)
K90	Dacite	Lava flow, Mte. Pizzinnu, showing columnar jointing
K92	Basalt	Mte. Seda Oro (740818)
K93,K94	Basalt	Mte. Seda Oro (742819)
K100	Dacite	2 km S of Ittiri, next to S.S.131b
K101	Basalt	Lava flow exposed by road S.S.131b near Cantra, Pianu
K102	Andesite	Lava flow. 400 m S of Mte. Ozzastru next to road from Theisi-Ittiri road to S.S.131

* These compositions do not represent liquid compositions since they contain abundant olivine xenocrysts.

K104	Trachybasalt	Lava flow, Mte. Santo
K105	Trachybasalt	Lava flow, Mte. Santo
K106	Hawaiite	Lava flow, Mte. Santo
K107	Trachybasalt	Lava flow, Mte. Santo
K108	Trachybasalt	Lava flow, Mte. Santo
K109	Trachybasalt	Lava flow, Mte. Santo
K110	Basaltic andesite	Lava flow, 2 km W of Foresta Burgos
K111	Basaltic andesite	Roadside outcrop, 2.5 km N of Foresta Burgos on Pranu Mannu
K112	Basaltic andesite	On Pranu Mannu lava plateau, by road 3 km N of Foresta Burgos
K114,K115	Hawaiite	Lava flow exposed 1 km W of summit of Mte. Massa, 10 km W of Chiaramonti
K117	Hawaiite	Lava flow outcropping near Nghe. Iscala Reales, 6 km NW of Ploaghe
K118	Hawaiite	400 m S of S. Michele, 2 km W of Ploaghe (761007)
K121,K122, K123	Hawaiite	Scoria. Mte. Fruiscu, near Ardara (842985)
K126,K127	Hawaiite	Scoria. Mte. Fruiscu, near Ardara
K129	Trachybasalt	Lava flow from N-S trending promontory of plateau above Cheremule
K130	Dacite	Lava, Mte. Pizzinnu, 1 km NW of Mara
K134	Hawaiite	Lava exposed in valley of Rui Cannas de Cheggia, 3 km SW of Pozzomaggiore
K135,K136	Hawaiite	Agglutinated scoria, Mte. Sa Pescia (783963)
K138	Mugearite	Lava flow on N slopes of Mte. Sa da Figu (783948)
K139	Basalt	Thin lava flow (1m) on hillside, 1 km NE of Nghe Runara
K140	Basalt	Roadside outcrop on S.S.131b near Cant. ra Pianu
K141	Hawaiite	Lava exposed by road 2 km W of Pozzomaggiore (695714)
K142	Hawaiite	Lava flow from summit of Mte. Benalzosu, near Semestene
K143	Hawaiite	Lava from roadstone quarry, 2 km W of Theisi
K160	Hawaiite	Lava flow above ignimbrite, close to Na. Sar. di Saccargia
K165	Basalt	Volcanic plug of Mte. Elias di Bonarva, 3 km SW of Bonorva
MR1,MR4	Hawaiite	Scoria. Mte. Cuccuruddu, near Cheremule
MR13	Hawaiite	Lava exposed 400m E of summit of Mte. Pelao
MR14	Basalt	Mte. Seda Oro (744825)
MR16	Mugearite	Lava flow exposed on S flank of Mte. Oes, 1 km SE of Torralba
U66,U64, U69	Calcareous marl	Pelagic calcareous oozes, Pacific

MR17	Basalt	Lava flow from W slopes of Pte. Cuguttada
MR18	Basaltic andesite	Scoria. Mte. Austidu, roadstone quarry
MR20	Basalt	Lava flow from W slopes of Pte. Cuguttada
MR21	Basaltic andesite	Lava exposed in river, 500 m N of Mte. Annaru
MR22	Hawaiite	Scoria. Mte. Cuccuruddu, near Cheremule
MR23	Basanite	Lava flow exposed in a cliff next to Rui Puttu, 2.5 km E of Pozzomaggiore
MR24	Basanite	Xenolith-bearing flow, 3 km E of Pozzomaggiore
MR25	Basaltic andesite	Nghe. de Iscolca, 2 km SW of Semestene
MR26,MR27	Hawaiite	Scoria. Mte. Cuccuruddu, near Cheremule
POZZ-3	Spinel lherzolite	Xenolith in basanite lava flow
GR-P	Granulite	Xenolith in basanite lava flow
PS1	Basaltic andesite	Roadside exposure on S.S.125, 2 km W of Cala Liberotto
PS2	Basaltic andesite	Lava outcrop on S.S.125, 3 km SW of Cala Liberotto
PS3	Alkali basalt	Roadside exposure, 11 km SW of Orosei by S.S.125
PS4	Alkali basalt	Lava flow, outcropping 9 km SW of Orosei on S.S.125
PS5	Alkali basalt	Lava exposed 3 km SW of Orosei on S.S.125
PS7	Andesite	Lava flow exposed by road, 3 km NE of Orosei
QF-O	Acid xenolith	Acid xenolith incorporated in scoria, Mte. Cujaru
U120	Calcareous ooze	Pelagic calcareous ooze, Pacific Ocean
ARC-1	Gabbro	Intrusion to W of Mte. Arcuentu, NW of Guspini
C1	Quartzo-feldspathic gneiss	1 km N of Ozieri, next to S. Nicola
C5	Mica-schist	Roadside exposure, 7 km W of Pattada
C6	Granodiorite	Hillside exposure, just outside Pattada
C11	Rhyolite	Basal flow, 2 km N of Macomer, next to old road into Macomer
C13	Hawaiite	Lava flow stratigraphically above C11
C14	Dacite	Lava flow, 1 km N of Macomer by railway track
C15	Hawaiite	Immediately S of Macomer, cliff exposure on old road by hairpin bend
C16	Mica-schist	Roadside exposure near Budoni
C18	Granite pegmatite	Vein cutting C16
C19	Mica-schist	Roadside outcrop, S. Lucia, on S.S.125 6 km E of Siniscola
C20	Granite	Road-cutting, 2 km W of Cala Liberotto
C21	Granodiorite	Intrusion exposed 12 km E of Monti by road to Olbia
C22	Basalt	Dyke cutting gneisses, 6 km W of Siniscola on road to Buddoso
C23	Granite	Intrusion of Siniscola
C26	Granite	5 km NW of S. Teodoro on road to Padru
C31	Granite	Quarry near Olbia, just off the S.S.127 by I.P. Petrol Station

APPENDIX C

REPRESENTATIVE MICROPROBE POINT ANALYSES OF OLIVINES

	K106 p/c		K106 g/m		MR25 p/c		MR25 p/c		MR24 p/c		MR14 p/c	
MgO	42.09		30.29		40.30		43.35		42.81		35.19	
SiO_2	39.06		36.84		38.76		40.01		39.70		37.43	
CaO	.23		.33		.29		.17		.35		.17	
MnO	.21		.55		.30		.20		.32		.59	
FeO	17.78		32.04		19.80		16.89		16.23		27.44	
NiO	.38		.15		.29		.32		.02		0	
Al_2O_3	0		0		.22		.01		.78		0	
SuM	99.75		100.20		99.96		100.95		100.21		100.82	
Si	.999	.999	1.005	1.005	.998	.998	1.004	1.004	1.000	1.000	.992	.992
Mg	1.604		1.232		1.547		1.622		1.607		1.390	
Ca	.006		.010		.008		.005		.009		.005	
Mn	.005		.013		.007		.004		.007		.013	
Fe	.380		.731		.426		.354		.342		.608	
Ni	.008		.003		.006		.006		.000		0	
Al	0	2.003	0	1.989	.007	2.000	.000	1.992	.023	1.989	0	2.016
O	4.000		4.000		4.000		4.000		4.000		4.000	
FO	80.65		62.35		78.13		81.88		82.17		69.11	
FA	19.35		37.65		21.87		18.12		17.83		30.89	
F/M	.240		.604		.280		.221		.217		.447	
F/FM	.193		.376		.219		.181		.178		.309	

PROBE ANALYSES OF OLIVINES

	N12(L) p/c		K83 p/c		MR20 p/c		K108 p/c		GR-P		N12 x/c		MR24 x/c	
MgO	40.15		41.41		30.78		38.00		38.17		47.19		47.80	
SiO_2	38.27		38.67		36.14		37.96		37.61		40.32		41.18	
CaO	.34		.21		.36		.15		.49		.02		.19	
MnO	.29		.12		.79		.58		.22		.15		.04	
FeO	21.29		19.18		30.98		23.59		18.25		11.97		11.11	
NiO	.08		.25		0		.06		0		.37		.19	
Al_2O_3	0		0		.16		.07		2.12		0		.20	
SuM	100.42		99.84		99.21		100.41		96.86		100.02		100.71	
Si	.988	.988	.994	.994	.994	.994	.992	,992	,991	,991	.999	.999	1.007	1.007
Mg	1.546		1.586		1.262		1.480		1.499		1.743		1.742	
Ca	.009		.006		.011		.004		.014		.001		.005	
Mn	.006		.003		.018		.013		.005		.003		.001	
Fe	.460		.412		.713		.515		.402		.248		.227	
Ni	.002		.005		0		.001		0		.007		.004	
Al	0	2.023	0	2.012	.005	2.009	.002	2.016	.066	1.985	0	2.002	.006	1.984
O	4.000		4.000		4.000		4.000		4.000		4.000		4.000	
FO	76.83		79.27		63.32		73.69		78.64		87.40		88.43	
FA	23.17		20.73		36.68		26.31		21.36		12.60		11.57	
F/M	.302		.262		.579		.357		.272		.144		.131	
F/FM	.232		.207		.367		.263		.214		.126		.116	

REPRESENTATIVE MICROPROBE POINT ANALYSES OF PYROXENES

Sample No.	MR14		K85		K106		K1		MR24	
SiO_2	51.57		49.97		47.48		51.99		50.86	
Al_2O_3	2.20		2.47		3.02		2.37		2.62	
TiO_2	0.42		1.89		3.06		0.42		0.36	
FeO	9.32		9.63		13.59		9.01		11.48	
MnO	0.30		0.28		0.21		0.48		0.48	
MgO	15.50		14.17		12.77		15.17		12.83	
CaO	19.84		19.86		19.93		21.05		19.79	
Na_2O	0.74		0.79		0.49		0.13		0.27	
Cr_2O_3	-		-		0.30		-		0.06	
SuM	99.89		99.06		100.85		100.62		98.75	
SI	1.924		1.887		1.807		1.925		1.936	
AL	0.076	2.000	0.110	1.997	0.135	1.942	0.075	2.000	0.064	2.000
AL	0.021		0		0		0.028		0.054	
TI	0.012		0.054		0.088		0.012		0.010	
FE	0.291		0.304		0.433		0.279		0.366	
MN	0.009		0.009		0.007		0.015		0.015	
MG	0.862		0.798		0.724		0.837		0.728	
CA	0.793		0.804		0.813		0.835		0.807	
CR	-		0.001		0.009		-		0.002	
NA	0.054	2.042	0.058	2.028	0.036	2.109	0.009	2.015	0.020	2.002
O	6.000		6.000		6.000		6.000		6.000	
EN	44.08		41.67		36.65		42.58		37.99	
FS	15.36		16.36		22.23		14.95		19.88	
WO	40.56		41.98		41.12		42.47		42.13	
F/M	0.348		0.393		0.606		0.351		0.523	
F/FM	0.258		0.282		0.378		0.260		0.344	

PROBE ANALYSES OF PYROXENES

Sample No.	C15 p/c		P57 p/c		C13 p/c		K43 p/c		P57 p/c	
SiO_2	51.91		54.16		51.70		53.70		52.58	
Al_2O_3	0.91		0.94		2.15		2.11		1.39	
TiO_2	0.88		0.32		1.09		0.33		0.82	
FeO	7.21		14.94		8.01		10.38		12.18	
MnO	0.18		0.24		0.15		0.12		0.20	
MgO	15.24		26.48		15.97		29.71		18.63	
CaO	21.73		2.22		20.46		1.57		14.06	
Na_2O	0.75		0.40		0.62		0.37		0.63	
Cr_2O_3	0.07		0.16		0.27		0.52		0.15	
SuM	98.88		99.86		100.42		98.81		100.64	
SI	1.948		1.963		1.911		1.923		1.937	
AL	0.040	1.988	0.037	2.000	0.089	2.000	0.077	2.000	0.061	1.998
AL	0		0.003		0.005		0.012		0	
TI	0.025		0.009		0.030		0.009		0.023	
FE	0.226		0.453		0.248		0.311		0.375	
MN	0.006		0.007		0.005		0.004		0.006	
MG	0.853		1.430		0.880		1.586		1.023	
CA	0.874		0.086		0.810		0.060		0.555	
CR	0.002		0.004		0.008		0.015		0.004	
NA	0.054	2.040	0.028		0.044	2.030	0.026	2.023	0.045	2.031
O	6.000		6.000		6.000		6.000		6.000	
EN	43.53		72.36		45.30		80.89		52.21	
FS	11.85		23.28		12.99		16.04		19.47	
WO	44.62		4.36		41.71		3.07		28.32	
F/M	0.272		0.322		0.287		0.198		0.373	
F/FM	0.214		0.243		0.223		0.165		0.272	

PROBE ANALYSES OF PYROXENES

Sample No.	K58		MR20[1]		MR20[2]	
SiO_2	48.81		47.51		49.48	
Al_2O_3	3.12		5.71		4.71	
TiO_2	2.85		1.32		0.89	
FeO	11.70		8.45		8.73	
MnO	0.17		0.14		0.08	
MgO	12.71		12.93		13.93	
CaO	20.55		22.77		22.22	
Na_2O	0.63		0.99		0.78	
Cr_2O_3	0.11		0.00		0.12	
SuM	100.65		99.82		100.82	
SI	1.841		1.791		1.838	
AL	0.138	1.979	0.209	2.000	0.162	2.000
AL	0		0.045		0.044	
TI	0.081		0.038		0.025	
FE	0.369		0.266		0.271	
MN	0.005		0.004		0.003	
MG	0.714		0.727		0.771	
CA	0.830		0.920		0.884	
CR	0.003		0.000		0.003	
NA	0.046		0.072		0.056	
O	6.000		6.000		6.000	
EN	37.23		37.90		39.98	
FS	19.51		14.13		14.19	
WO	43.26		47.97		45.84	
F/M	0.524		0.373		0.355	
F/FM	0.344		0.272		0.262	

1 Core composition

2 Rim composition

PROBE ANALYSES OF PYROXENES

Sample No.	MR20 p/c		MR25 p/c		N 12(L) p/c		MR25 p/c		GR-P	
SiO_2	48.46		52.03		49.15		54.07		50.88	
Al_2O_3	5.93		2.57		3.86		2.51		5.03	
TiO_2	1.37		0.98		2.20		0.28		0	
FeO	8.92		17.65		5.77		10.76		4.76	
MnO	0.18		0.35		0.04		0.20		0.07	
MgO	12.76		10.63		14.58		28.86		14.61	
CaO	23.01		14.26		22.99		1.81		23.67	
Na_2O	0.21		0.83		0.37		0		0.35	
Cr_2O_3	0.08		0.01		0.37		0.65		0.08	
SuM	100.92		99.31		99.33		99.14		99.45	
SI	1.805		1.983		1.837		1.932		1.881	
AL	0.195	2.000	0.017	2.000	0.163	2.000	0.068	2.000	0.119	2.000
AL	0.066		0.098		0.007		0.038		0.101	
TI	0.038		0.028		0.062		0.008		0	
FE	0.278		0.562		0.180		0.322		0.147	
MN	0.006		0.011		0.001		0.006		0.002	
MG	0.708		0.604		0.812		1.537		0.805	
CA	0.918		0.582		0.921		0.069		0.938	
CR	0.002		0		0.011		0.018		0.002	
NA	0.015	2.032	0.061	1.948	0.027	2.022	0	1.998	0.025	2.020
O	6.000		6.000		6.000		6.000		6.000	
EN	37.09		34.31		42.43		79.48		42.55	
FS	14.84		32.61		9.49		16.94		7.89	
WO	48.07		33.08		48.09		3.58		49.55	
F/M	0.400		0.950		0.224		0.213		0.186	
F/FM	0.286		0.487		0.183		0.176		0.156	

REPRESENTATIVE MICROPROBE POINT ANALYSES OF PLAGIOCLASE FELDSPARS

Sample No.	P57 p/c		P57 mp/c		K58 p/c		K43 p/c		K64 p/c	
SiO_2	53.88		57.67		60.27		54.08		54.30	
Al_2O_3	29.48		25.86		24.34		28.48		27.83	
FeO	0.45		0.73		0.68		0.49		0.63	
CaO	11.51		8.43		6.43		11.46		11.16	
Na_2O	4.87		6.64		7.03		4.86		4.93	
K_2O	0.13		0.31		0.79		0.09		0.18	
SUM	100.32		99.64		99.54		99.46		99.03	
SI	2.421		2.601		2.700		2.452		2.478	
AL	1.561	3.981	1.374	3.975	1.285	3.985	1.521	3.973	1.496	3.974
FE	0.017		0.028		0.025		0.019		0.024	
CA	0.554		0.407		0.309		0.557		0.546	
NA	0.424		0.581		0.611		0.427		0.436	
K	0.007	1.003	0.018	1.033	0.045	0.990	0.005	1.008	0.010	0.016
O	8.000		8.000		8.000		8.000		8.000	
AN	56.21		40.50		32.00		56.28		54.99	
AB	43.04		57.73		63.32		43.19		43.96	
OR	0.76		1.77		4.68		0.53		1.06	

	MR20 p/c		C15 p/c		K85 p/c		K104 p/c		MR25 p/c	
SiO_2	46.16		54.13		53.84		55.08		54.84	
Al_2O_3	33.84		28.16		27.64		27.59		27.95	
FeO	0.34		0.77		0.71		0.75		1.02	
CaO	17.94		10.95		11.44		10.18		11.87	
Na_2O	1.60		4.90		5.11		5.33		4.63	
K_2O	0.03		0.30		0.30		0.66		0.14	
SUM	99.91		99.29		99.04		99.59		100.45	
SI	2.129		2.466		2.461		2.496		2.473	
AL	1.839	3.968	1.512	3.977	1.489	3.950	1.473	3.970	1.485	3.958
FE	0.013		0.029		0.027		0.028		0.038	
CA	0.887		0.534		0.560		0.494		0.573	
NA	0.143		0.433		0.453		0.468		0.405	
K	0.002	1.054	0.022	1.018	0.017	1.058	0.038	1.029	0.008	1.024
O	8.000		8.000		8.000		8.000		8.000	
AN	85.96		54.02		54.36		49.39		58.14	
AB	13.87		43.75		43.94		46.80		41.04	
OR	0.17		2.23		1.70		3.81		0.82	

REPRESENTATIVE MICROPROBE POINT ANALYSES OF GROUNDMASS ALKALI FELDSPARS

	C15		K108		K106	
SiO_2	61.75		63.57		65.85	
Al_2O_3	22.25		19.77		20.17	
FeO	0.61		0.69		0.43	
CaO	4.35		3.21		1.53	
Na_2O	6.91		5.86		5.44	
K_2O	2.99		6.60		8.19	
SuM	98.86		99.70		101.61	
SI	2.797		2.882		2.923	
AL	1.188	3.985	1.056	3.938	1.055	3.978
FE	0.023		0.026		0.016	
CA	0.211		0.156		0.073	
NA	0.607		0.515		0.468	
K	0.179	1.014	0.382	1.079	0.464	1.021
O	8.000		8.000		8.000	
AN	21.31		14.81		7.24	
AB	61.25		48.93		46.60	
OR	17.44		36.26		46.16	

PROBE ANALYSIS OF ANALCITE

	g/m MR24
Na_2O	10.21
Al_2O_3	21.93
SiO_2	55.20
K_2O	0.35
CaO	0.85
FeO	0.85
	89.39

REPRESENTATIVE MICROPROBE POINT ANALYSES OF AMPHIBOLES

	K90	K130
Na_2O	1.972	2.132
MgO	13.591	14.068
Al_2O_3	11.602	14.174
SiO_2	43.407	40.469
K_2O	.702	.758
CaO	11.871	12.430
TiO_2	2.089	1.918
Cr_2O_3	.000	.092
MnO	.275	.028
FeO	12.732	9.758
NiO	.000	.020
SUM	98.241	95.846
Na	.561	.617
Mg	2.974	3.131
Al	2.007	2.495
Si	6.372	6.043
K	.132	.144
Ca	1.867	1.989
Ti	.231	.215
Cr	.000	.011
Mn	.034	.004
Fe	1.563	1.219
Ni	.000	.002
O	23.000	23.000

REPRESENTATIVE MICROPROBE POINT ANALYSES OF BIOTITES

	K108 p/c		K104 p/c		K104 p/c	
SiO_2	41.74		39.91		39.52	
TiO_2	5.25		5.03		6.36	
Al_2O_3	11.40		11.41		12.09	
FeO	6.76		9.13		8.84	
MnO	.08		0		.05	
MgO	21.03		19.25		18.60	
CaO	0		.27		.25	
Na_2O	.91		1.33		1.16	
K_2O	9.73		9.25		9.56	
SUM	96.90		95.58		96.43	
Si	5.898		5.801		5.696	
Al	1.898	7.796	1.954	7.755	2.053	7.750
Al	0		0		0	
Ti	.558		.550		.689	
Mn	.010		0		.006	
Mg	4.429		4.170		3.996	
Fe	.799	5.796	1.110	5.830	1.066	5.757
K	1.754		1.715		1.758	
Ca	0		.042		.039	
Na	.249	2.003	.375	2.132	.324	2.120
O	22.000		22.000		22.000	
ANN	15.43		21.02		21.05	
PHLG	84.57		78.98		78.95	
F/M	.183		.266		.268	
F/FM	.154		.210		.211	

PROBE ANALYSES OF BIOTITES

	C15		K100	
SiO_2	37.89		31.65	
TiO_2	8.75		5.22	
A_2O_3	12.77		11.83	
FeO	8.95		27.84	
MnO	.10		.09	
MgO	16.95		10.30	
CaO	.06		.10	
Na_2O	.89		.91	
K_2O	9.58		7.86	
SUM	95.94		95.80	
Si	5.506		5.090	
Al	2.187	7.693	2.242	7.333
Al	0.000		0.000	
Ti	.956		.631	
Mn	.012		.012	
Mg	3.671		2.469	
Fe	1.088	5.727	3.745	6.857
K	1.776		1.612	
Ca	.009		.017	
Na	.251	2.036	.284	1.913
O	22.000		22.000	
ANN	22.86		60.26	
PHLG	77.14		39.74	
F/M	.300		1.522	
F/FM	.231		.603	

APPENDIX D

REPRESENTATIVE MICROPROBE POINT ANALYSES OF CLINOPYROXENES FROM ULTRABASIC XENOLITHS

	N4		POZZ-4		POZZ-5		POZZ-1		POZZ-14		N1	
SiO_2	51.75		52.05		52.27		52.87		53.52		52.84	
TiO_2	.29		.42		.50		.10		.28		.51	
Al_2O_3	5.21		5.81		6.86		3.73		3.56		6.88	
FeO	2.59		2.88		3.29		2.24		2.40		2.87	
MnO	.05		.25		0		.12		.05		.13	
MgO	15.51		15.21		15.06		16.66		16.75		14.67	
CaO	21.60		20.14		19.97		22.57		22.06		19.46	
Cr_2O_3	.73		.83		.93		1.05		1.26		.84	
Na_2O	1.12		1.51		1.53		.36		.70		1.92	
SuM	98.85		99.10		100.41		99.70		100.58		100.12	
Si	1.898		1.901		1.882		1.992		1.928		1.902	
Al	.102	2.000	.099	2.000	.118	2.000	.078	2.000	.072	2.000	.098	2.000
Al	.123		.151		.174		.082		.079		.194	
Ti	.008		.012		.014		.003		.008		.014	
Fe	.079		.088		.099		.068		.072		.086	
Mn	.002		.008		0		.004		.002		.004	
Mg	.848		.828		.808		.903		.899		.787	
Ca	.849		.788		.771		.879		.851		.750	
Cr	.021		.024		.026		.030		.036		.024	
Na	.080	2.010	.107	2.004	.107	1.998	.025	1.993	.049	1.996	.134	1.993
O	6.000		6.000		6.000		6.000		6.000		6.000	
En	47.70		48.37		48.18		48.70		49.29		48.35	
Fs	4.56		5.59		5.90		3.87		4.05		5.55	
Wo	47.75		46.04		45.92		47.43		46.66		46.10	
F/M	.096		.116		.123		.080		.082		.115	
F/FM	.087		.104		.109		.074		.076		.103	

PROBE ANALYSES OF CLINOPYROXENES FROM ULTRABASIC XENOLITHS

	POZZ-2		K162		POZZ-12		POZZ-10		POZZ-3		POZZ-9	
SiO_2	50.74		51.64		52.43		52.87		52.91		53.03	
TiO_2	.40		.77		.22		.46		.17		.16	
Al_2O_3	5.46		5.42		6.34		6.04		4.17		5.62	
FeO	6.44		6.32		3.22		2.63		2.76		2.84	
MnO	.12		.10		.05		.12		.08		.07	
MgO	13.99		17.51		14.93		15.07		16.05		15.26	
CaO	22.90		16.64		19.64		21.01		22.27		20.57	
Cr_2O_3	.34		.59		1.15		.92		1.12		1.27	
Na_2O	.38		.98		1.53		1.42		.83		1.39	
SuM	100.77		99.97		99.51		100.54		100.36		100.21	
Si	1.863		1.878		1.903		1.901		1.915		1.913	
Al	.137	2.000	.122	2.000	.097	2.000	.099	2.000	.085	2.000	.087	2.000
Al	.100		.110		.175		.157		.093		.152	
Ti	.011		.021		.006		.012		.005		.004	
Fe	.198		.192		.098		.079		.084		.086	
Mn	.004		.003		.002		.004		.002		.002	
Mg	.766		.949		.808		.808		.866		.821	
Ca	.901		.648		.764		.809		.864		.795	
Cr	.010		.017		.033		.026		.032		.036	
Na	.027	2.016	.069	2.011	.108	1.992	.099	1.995	.058	2.004	.097	1.993
O	6.000		6.000		6.000		6.000		6.000		6.000	
En	40.99		52.94		48.34		47.51		47.69		48.17	
Fs	10.79		10.89		5.94		4.87		4.74		5.16	
Wo	48.23		36.17		45.71		47.62		47.57		46.67	
F/M	.263		.206		.123		.102		.099		.107	
F/FM	.208		.171		.109		.093		.090		.097	

PROBE ANALYSES OF CLINOPYROXENES FROM ULTRABASIC XENOLITHS

	N9		N5		N3		TH-I[1]		TH-I[2]	
SiO_2	52.51		52.87		51.90		51.59		51.41	
TiO_2	0		.38		.01		.65		.75	
Al_2O_3	3.74		3.61		4.45		5.14		5.29	
FeO	2.53		2.86		2.42		5.47		5.20	
MnO	.02		.20		.11		.08		.02	
MgO	17.20		17.03		16.90		17.24		16.51	
CaO	22.16		20.83		21.88		17.40		18.45	
Cr_2O_3	.68		1.31		.91		.53		.46	
Na_2O	1.04		1.34		.94		1.09		1.46	
SuM	99.88		100.43		99.52		99.19		99.55	
Si	1.910		1.913		1.894		1.888		1.881	
Al	.090	2.000	.087	2.000	.106	2.000	.112	2.000	.119	2.000
Al	.070		.067		.085		.110		.109	
Ti	0		.010		.000		.018		.021	
Fe	.077		.087		.074		.167		.159	
Mn	.001		.006		.003		.002		.001	
Mg	.932		.919		.919		.940		.900	
Ca	.864		.808		.855		.682		.723	
Cr	.020		.037		.026		.015		.013	
Na	.073	2.037	.094	2.028	.067	2.030	.077	2.013	.104	2.030
O	6.000		6.000		6.000		6.000		6.000	
En	49.77		50.50		49.64		52.46		50.49	
Fs	4.14		5.10		4.17		9.48		8.96	
Wo	46.09		44.40		46.19		38.06		40.56	
F/M	.083		.101		.084		.181		.177	
F/FM	.077		.092		.078		.153		.151	

1. Core composition.
2. Rim composition.

REPRESENTATIVE MICROPROBE POINT ANALYSES OF ORTHOPYROXENES FROM ULTRABASIC XENOLITHS

	N1		POZZ-9		POZZ-1		POZZ-5		POZZ-4	
SiO_2	54.83		56.28		55.74		55.45		54.96	
TiO_2	.13		.05		.10		.05		.11	
Al_2O_3	4.73		2.59		3.29		5.39		4.37	
FeO	6.60		5.68		5.78		6.16		5.93	
MnO	.17		.20		.25		.09		.20	
MgO	31.72		33.38		33.06		32.17		32.61	
CaO	.71		.85		.71		.83		.78	
Cr_2O_3	.43		.54		.46		.47		.35	
NiO	.35		.08		.06		.03		.17	
SuM	99.67		99.65		99.45		100.64		99.48	
Si	1.905		1.946		1.932		1.899		1.907	
Al	.095	2.000	.054	2.000	.068	2.000	.101	2.000	.093	2.000
Al	.098		.052		.066		.117		.086	
Ti	.003		.001		.003		.001		.003	
Fe	.192		.164		.168		.176		.172	
Mn	.005		.006		.007		.003		.006	
Mg	1.642		1.721		1.708		1.643		1.686	
Ca	.026		.031		.026		.030		.029	
Cr	.012		.015		.013		.013		.010	
Ni	.010	1.989	.002	1.992	.002	1.992	.001	1.984	.005	1.996
O	6.000		6.000		6.000		6.000		6.000	
EN	88.04		89.51		89.46		88.69		89.07	
FS	10.55		8.85		9.16		9.67		9.40	
WO	1.42		1.54		1.38		1.64		1.53	
F/M	.120		.090		.102		.109		.106	
F/FM	.107		.090		.093		.098		.095	

PROBE ANALYSES OF ORTHOPYROXENES FROM ULTRABASIC XENOLITHS

	N6		POZZ-7		POZZ-10		POZZ-12		POZZ-2	
SiO_2	54.39		56.34		56.09		54.69		52.72	
TiO_2	.15		.07		.04		.07		.12	
Al_2O_3	4.95		3.24		3.98		4.50		4.79	
FeO	6.36		6.04		6.28		6.03		14.42	
MnO	.14		.10		.12		.14		.43	
MgO	32.88		33.06		32.66		32.60		26.90	
CaO	.82		.82		.74		.74		.68	
Cr_2O_3	.40		.56		.37		.44		.10	
NiO	.14		.21		.10		.23		.14	
SuM	100.23		100.44		100.38		99.44		100.30	
Si	1.879		1.936		1.927		1.900		1.888	
Al	.121	2.000	.064	2.000	.073	2.000	.100	2.000	.112	2.000
Al	.081		.067		.088		.084		.090	
Ti	.004		.002		.001		.002		.003	
Fe	.184		.174		.180		.175		.432	
Mn	.004		.003		.003		.004		.013	
Mg	1.693		1.693		1.673		1.688		1.436	
Ca	.030		.030		.027		.028		.026	
Cr	.011		.015		.010		.012		.003	
Ni	.004	2.011	.006	1.989	.003	1.986	.006	2.000	.004	2.006
O	6.000		6.000		6.000		6.000		6.000	
EN	88.58		89.12		88.79		89.08		75.30	
FS	9.83		9.29		9.76		9.46		23.33	
WO	1.59		1.59		1.45		1.45		1.37	
F/M	.111		.104		.110		.106		.310	
F/FM	.100		.094		.099		.096		.237	

PROBE ANALYSES OF ORTHOPYROXENES FROM ULTRABASIC XENOLITHS

	N9		POZZ-9		POZZ-3		N4		N3	
SiO_2	55.03		55.50		55.72		55.25		53.67	
TiO_2	0		.12		.03		.08		0	
Al_2O_3	3.55		3.72		3.22		4.41		4.59	
FeO	5.57		6.58		6.07		6.15		5.99	
MnO	.08		.11		.12		.13		.38	
MgO	33.51		32.11		32.70		32.42		32.94	
CaO	.75		.74		.80		.73		.75	
Cr_2O_3	.63		.67		.51		.41		.53	
NiO	.19		.22		.09		.17		.02	
SuM	99.31		99.77		99.26		99.75		98.87	
Si	1.912		1.925		1.937		1.912		1.879	
Al	.088	2.000	.075	2.000	.063	2.000	.088	2.000	.121	2.000
Al	.057		.077		.068		.092		.069	
Ti	0		.003		.001		.002		0	
Fe	.162		.191		.176		.178		.175	
Mn	.002		.003		.004		.004		.011	
Mg	1.735		1.660		1.694		1.672		1.719	
Ca	.028		.028		.030		.027		.028	
Cr	.017		.018		.014		.011		.015	
Ni	.005	2.007	.006	1.986	.003	1.990	.005	1.991	.001	2.018
O	6.000		6.000		6.000		6.000		6.000	
EN	90.03		88.22		88.98		88.90		88.89	
FS	8.52		10.32		9.45		9.66		9.65	
WO	1.45		1.46		1.56		1.44		1.45	
F/M	.095		.117		.106		.109		.109	
F/FM	.086		.105		.096		.098		.098	

PROBE ANALYSES OF ORTHOPYROXENES FROM ULTRABASIC XENOLITHS

	N7		K162		N5		TH-I[1]	
SiO_2	54.97		52.89		54.65		54.33	
TiO_2	.04		.49		.08		.44	
Al_2O_3	4.14		6.02		4.12		3.95	
FeO	5.92		9.52		6.16		8.83	
MnO	.19		.18		.11		.19	
MgO	33.62		28.26		32.39		30.70	
CaO	.71		1.97		.75		1.46	
Cr_2O_3	.49		.08		.53		.35	
NiO	.25		.23		.02		.00	
SuM	100.33		99.64		98.81		100.29	
Si	1.895		1.869		1.910		1.894	
Al	.105	2.000	.131	2.000	.090	2.000	.106	2.000
Al	.063		.120		.080		.056	
Ti	.001		.013		.002		.012	
Fe	.171		.281		.180		.257	
Mn	.006		.005		.003		.006	
Mg	1.727		1.489		1.687		1.595	
Ca	.026		.075		.028		.055	
Cr	.013		.002		.015		.010	
Ni	.007	2.014	.007	1.991	.001	1.996	.000	1.990
O	6.000		6.000		6.000		6.000	
EN	89.51		80.47		88.87		83.40	
FS	9.13		15.50		9.65		13.75	
WO	1.36		4.03		1.48		2.85	
F/M	.102		.193		.109		.165	
F/FM	.093		.162		.098		.142	

[1] Ca-poor pyroxene exsolved from clinopyroxene host.

REPRESENTATIVE MICROPROBE POINT ANALYSES OF OLIVINES FROM ULTRABASIC XENOLITHS

	N7		POZZ-12		POZZ-10		POZZ-7		POZZ-3	
SiO_2	40.06		41.05		40.25		40.54		41.10	
Al_2O_3	.07		.10		.07		0		0	
TiO_2	0		0		0		.02		.06	
FeO	9.38		9.70		9.51		9.75		9.26	
MnO	.01		.12		.21		.11		.09	
MgO	49.79		49.00		48.85		48.11		49.04	
CaO	.05		.05		.05		.07		.04	
NiO	.41		.32		.31		.30		.15	
Cr_2O_3	.03		.04		0		.04		0	
SuM	99.80		100.38		99.25		98.94		99.74	
Si	.985	.985	1.002	1.002	.995	.995	1.005	1.005	1.006	1.006
Ti	0		0		0		0		.001	
Al	.002		.003		.002		0		0	
Mn	.000		.002		.004		.002		.002	
Mg	1.824		1.783		1.799		1.777		1.790	
Fe	.193		1.98		.197		.202		.190	
Ca	.001		.001		.001		.002		.001	
Ni	.008		.006		.006		.006		.003	
Cr	.001	2.029	.001	1.994	0	2.010	.001	1.990	0	1.986
O	4.000		4.000		4.000		4.000		4.000	
FO	90.44		90.00		90.15		89.79		90.42	
FA	9.56		10.00		9.85		10.21		9.58	
F/M	.106		.112		.112		.115		.107	
F/FM	.096		.101		.100		.103		.097	

PROBE ANALYSES OF OLIVINES FROM ULTRABASIC XENOLITHS

	N3		POZZ-9		N9		N5		POZZ-4	
SiO_2	40.30		40.85		40.14		40.02		40.90	
Al_2O_3	0		0		.03		.10		0	
TiO_2	.05		.03		0		.06		0	
FeO	9.00		10.54		9.00		9.61		9.65	
MnO	.16		.09		.03		.16		.14	
MgO	49.17		48.26		49.68		49.25		48.19	
CaO	0		.08		.07		.05		.10	
NiO	.17		.23		.30		.54		.45	
Cr_2O_3	0		.11		.06		.10		.04	
SuM	98.85		100.19		99.31		99.89		99.47	
Si	.997	.997	1.003	1.003	.989	.989	.985	.985	1.008	1.008
Ti	.001		.001		0		.001		0	
Al	0		0		.001		.003		0	
Mn	.003		.002		.001		.003		.003	
Mg	1.812		1.766		1.825		1.807		1.770	
Fe	.186		.216		.185		1.98		.199	
Ca	0		.002		.002		.001		.003	
Ni	.003		.005		.006		.011		.009	
Cr	0	2.006	.002	1.993	.001	2.021	.002	2.026	.001	1.984
O	4.000		4.000		4.000		4.000		4.000	
FO	90.56		89.08		90.77		90.13		89.90	
FA	9.31		10.92		9.23		9.87		10.10	
F/M	.105		.124		.102		.111		.114	
F/FM	.095		.110		.093		.100		.102	

PROBE ANALYSES OF OLIVINES FROM ULTRABASIC XENOLITHS

	POZZ-4		POZZ-5		POZZ-1		POZZ-14		N1	
SiO_2	41.29		40.57		41.39		41.25		39.96	
Al_2O_3	.22		.05		.19		0		0	
TiO_2	0		.04		0		.03		.04	
FeO	8.42		9.71		9.15		8.67		10.35	
MnO	.18		.14		.06		.20		.09	
MgO	49.60		49.18		49.24		49.36		47.83	
CaO	.10		.08		.05		.02		.03	
NiO	.48		.46		.44		.50		.48	
$Cr2O_3$	0		0		.02		.05		0	
SuM	100.29		100.23		100.54		100.08		98.78	
Si	1.003	1.003	.994	.994	1.006	1.006	1.006	1.006	.996	.996
Ti	0		.001		0		.001		.001	
Al	.006		.001		.005		0		0	
Mn	.004		.003		.001		.004		.002	
Mg	1.797		1.796		1.783		1.794		1.778	
Fe	.171		.199		.186		1.77		.216	
Ca	.003		.002		.001		.001		.001	
Ni	.009		.009		.009		.010		.010	
Cr	0	1.990	0	2.011	.000	1.986	.001	1.987	0	2.006
O	4.000		4.000		4.000		4.000		4.000	
FO	91.30		90.03		90.56		91.03		89.17	
FA	8.70		9.97		9.44		8.97		10.83	
F/M	.097		.112		.105		.101		.122	
F/FM	.089		.101		.095		.092		.109	

REPRESENTATIVE MICROPROBE POINT ANALYSES OF SPINELS FROM INCLUSIONS OF PROBABLE UPPER MANTLE OR DEEP CRUSTAL ORIGIN

	POZZ-5	POZZ-1	N7	POZZ-7	N1	N3	N4	GR-P
SiO_2	0.74	0.49	0.10	0.80	0.47	0.36	0.68	1.04
TiO_2	0.19	0.21	0.04	0.23	0.17	0.02	0.06	0.00
Al_2O_3	54.17	41.49	48.07	38.81	57.48	43.98	55.63	61.46
Cr_2O_3	12.11	24.71	18.94	28.14	9.82	23.56	11.21	0.05
FeO	12.83	13.58	12.65	15.24	11.34	12.66	11.34	19.17
MnO	0.03	0.09	0.15	0.07	0.09	0.00	0.20	0.09
MgO	20.05	18.10	19.79	16.79	19.91	19.28	20.49	17.23
SuM	100.12	98.67	99.74	100.08	99.28	99.86	99.61	99.04

PROBE ANALYSES OF SPINELS

	POZZ-3	POZZ-9	N9	N5	POZZ-14	POZZ-4
SiO_2	0.66	0.51	0.23	0.16	0.54	0.61
TiO_2	0.18	0.01	0.02	0.17	0.11	0.26
Al_2O_3	51.93	49.21	45.78	50.33	37.34	52.91
Cr_2O_3	14.71	18.38	22.03	17.03	31.98	13.22
FeO	12.08	12.90	11.12	12.43	13.99	12.05
MnO	0.00	0.14	0.00	0.00	0.14	0.12
MgO	19.62	18.19	19.44	19.89	17.16	20.58
SuM	99.18	99.34	98.62	100.01	101.26	99.75

REPRESENTATIVE MICROPROBE POINT ANALYSES OF CLINOPYROXENE MEGACRYSTS

Sample No.	K162a		K162b		K162c[1]	
SiO_2	52.18		51.37		52.13	
TiO_2	0.67		1.40		1.30	
Al_2O_3	5.40		4.22		2.73	
FeO	6.33		6.27		5.69	
MnO	0.14		0.07		0.07	
MgO	17.26		14.70		15.90	
CaO	16.99		20.68		22.42	
Cr_2O_3	0.23		0.33		0.49	
Na_2O	0.77		0.52		0.03	
SUM						
SI	1.894		1.893		1.905	
Al	0.106	2.000	0.107	2.000	0.095	2.000
Al	0.125		0.076		0.023	
TI	0.018		0.039		0.036	
Fe	0.192		0.193		0.174	
Mn	0.004		0.002		0.002	
Mg	0.934		0.807		0.866	
Ca	0.661		0.816		0.878	
Cr	0.007		0.010		0.014	
Na	0.054	1.890	0.037	1.981	0.002	1.994
O	6.000		6.000		6.000	
En	52.15		44.38		45.11	
Fs	10.94		10.74		9.17	
Wo	36.91		44.88		45.72	
F/M	0.206		0.242		0.203	
F/FM	0.171		0.195		0.169	

1 Reaction rim around clinopyroxene megacryst.

APPENDIX E

PROBLEMS AND ASSUMPTIONS INHERENT IN GEOTHERMOMETRY

Temperatures of equilibration for 15 ultramafic inclusions have been calculated using experiementally calibrated geothermometers (Table E.1). Such calculations require that certain assumptions are made, and it is also necessary to be aware of the limitations of each geothermometer. A brief discussion of these two related subjects is given below.

1. In all pyroxene geothermometry it is necessary to distribute the cations between the different available sites in the pyroxene lattice. In this study, all the Si is assigned to the tetrahedral site, and the deficiency in that site is made up with Al^{VI}. The remainder of the Al is assigned to Al^{VI} in the M1 site along with Ti and Cr.
   Some authors have arbitrarily taken Al/2 to be equal to the Al^{VI} and Al^{IV} values (Mysen and Boettcher, 1975), although there is some evidence of a preference of Al for the tetrahedral site (Stroh, 1976). Ca, Mn, Ni and Na are assigned to the octahedral M2 site. Fe^{2+} and Mg^{2+} are assumed to be randomly distributed between the M1 and M2 sites. Ideal mixing of cations on all sites is assumed.
2. The position of the pyroxene solvus is composition-dependent, and the effects of other components such as Cr^{3+}, Mn^{2+} and Ti^{4+} on the natural solvus curve is poorly constrained.

TABLE E1

NUMERICAL FORMULATIONS USED TO CALCULATE EQUILIBRATION TEMPERATURES OF SPINEL LHERZOLITES AND PYROXENITES

(a) Diopside-Enstatite Miscibility Gap

Wood and Banno (1973)

$$T = \frac{-10202}{-\ln K - 7.65\left(X_{Fe}^{opx}\right) + 3.88\ X_{Fe}^{opx\ 2} - 4.6}$$

Wells (1977)

$$T = \frac{7341}{3.355 + 2.44\left(X_{Fe}^{opx}\right) - \ln K}$$

Mori and Green (1978)

$$T = \frac{-6860}{\ln K - 3.03}$$

where,

$$\ln K = \frac{a_{Mg_2Si_2O_6}^{cpx}}{a_{Mg_2Si_2O_6}^{opx}} = \frac{\left[X_{Mg}^{M1} \cdot X_{Mg}^{M2}\right]^{cpx}}{\left[X_{Mg}^{M1} \cdot X_{Mg}^{M2}\right]^{opx}}$$

and,

X_{Fe}^{opx} = mole fraction of iron in orthopyroxene.

(b) Al^{VI} - Cr Distribution between orthopyroxene and clinopyroxene

Mysen and Boettcher (1975)

$$T = \frac{4091}{\ln K + 2.7898}$$

where,

$$\ln K = \frac{\left(X_{Al}^{VI} / X_{cr}\right)^{opx}}{\left(X_{Al}^{VI} / C_{cr}\right)^{cpx}}$$

3. Electron microprobe analysis determines total Fe as FeO. Although some of this Fe may be present as Fe_2O_3 in pyroxenes, in this study total Fe is assumed to be Fe^{2+}.
4. Thermodynamic models and equations assume solid-solid equilibrium, and no subsequent modification of element distribution by solid-state diffusion. The absence of reaction relationships between co-existing minerals, and the lack of zoning probably make this, at least, a reasonable assumption for Sardinian peridotites. Careful selection of core compositions for micro-analysis, avoiding those grains in contact with the host lava, is also important.
5. Some elements are present in concentrations which are close to the detection limit for electron probe energy dispersive spectrum analysis. Chromium contents in enstatite are low, and temperature estimates which depend on this parameter are therefore subject to large error. Detection limits for Cr, however, could be improved by use of a single crystal spectrometer.
6. Temperature estimates (see Table 8.2) calculated using the equation of Wood and Banno (1973) are consistently high with respect to those calculated using the geothermometers of Wells (1977), and Mori and Green (1978). Wood and Banno (1973) use the pyroxene solvus data at 30 kb of Davis and Boyd (1966), although it is now known that the diopside solvus is steeper than previously thought (Carswell, 1980).

7. Mori and Green (1978) use new experimental data at 30-40 kb on synthetic garnet lherzolite compositions, but their geothermometer is unsuitable for Fe-bearing systems. This explains the substantially higher temperatures of equilibration calculated using their equation for the pyroxenite, TH-1 (Table 8.2; FeO/MgO = 0.32).

APPENDIX F

NORMALISATION FACTORS

Details of the normalisation proceedure are given in Thompson (1982). The elements are arranged in a general order of increasing incompatibility from right to left of the diagram. This arrangement was chosen to give the smoothest elemental patterns for ocean-floor basalts from Iceland and the North Atlantic. An Yb normalising factor of 0.223 (White and Patchett, 1983) was used rather than the 0.22 from Nakamura (1974). Elemental data is normalised to chondritic (C1) meteorites except for Rb, K and Cs (volatile at the time of the Earth's formation) and P (partitioned into the core). Rb, K, Cs and U abundances are normalised to "undepleted" mantle (Sun, 1980). Other sources of data are given in Thompson (1982). Normalising factors are given below (all values in ppm):-

Ba	6.9	Ti	620
Rb	0.35	Tb	0.052
Th	0.042	Y	2.0
U	0.013	Tm	0.034
K	12.0	Yb	0.223
La	0.328	Pr	0.122
Ce	0.865	Eu	0.077
Sr	11.8	Gd	0.276
Nd	0.63	Dy	0.343
P	46	Ho	0.078
Sm	0.203	Er	0.225
Zr	6.84	Lu	0.0339
Hf	0.2	Cs	0.019